

https://dspace.org/

Characterization of the fibroblast growth factor receptor 2 splicing mechanism in triple-negative breast cancer

Moodley, Kiashanee

2016-10-28
http://hdl.handle.net/10539/21316

Downloaded from a DSpace repository. https://dspace.org/

Characterization of the Fibroblast Growth Factor Receptor 2 Splicing Mechanism In Triple-Negative Breast Cancer



Kiashanee Moodley

0707149W

Faculty of Health Sciences

Department of Internal Medicine

School of Clinical Medicine

A thesis submitted in fulfilment of the requirements

For the degree of Doctor of Philosophy in Medicine

Johannesburg, 2016

DECLARATION

I, Kiashanee Moodley, declare that the thesis, which I hereby submit for the degree of Doctor of Philosophy in Medicine at the University of the Witwatersrand, Johannesburg, South Africa, is my own work and has not been submitted by me or any other person for degree purposes at any other university.



Kiashanee Moodley

6th day of June 2016

ABSTRACT

Breast cancer is the second most frequently diagnosed cancer in the world and the most frequently diagnosed cancer in women. Triple-negative breast cancer (TNBC), a subtype of breast cancer, is characterised by the lack of expression of the oestrogen receptor, progesterone receptor and a lack of overexpression of the human epidermal growth factor receptor 2. Therapeutic options targeting TNBCs are limited, and since it can be more aggressive compared to other breast cancer subtypes, research into its progression is necessary. A number of genome-wide association studies have identified an association between the fibroblast growth factor receptor (FGFR) 2 and the risk of breast cancer. This receptor is alternatively spliced, and a switch in the mutually exclusive inclusion of either the *FGFR2 IIIb* or the *FGFR2 IIIc* exons is associated with epithelial-to-mesenchymal transition (EMT) and mesenchymal-to-epithelial transition (MET). A nuclear proteomic analysis comparing an epithelial TNBC cell line to a mesenchymal one revealed that the RNA binding protein, KH-type Splicing Regulatory Protein (KSRP), is overexpressed in the basal cell line compared to the mesenchymal cell line; these cell lines preferentially include *FGFR2 IIIb* and *FGFR2 IIIc*, respectively.

This project aimed to investigate the role of KSRP in the *FGFR2* splicing mechanism in the context of triple-negative breast cancer progression using epithelial and mesenchymal cell line models. In addition, this project aimed to discover the genome-wide consequences of KSRP knockdown.

The epithelial and mesenchymal phenotypes, preferential *FGFR2* isoform inclusion, differential expression of KSRP and alteration of *FGFR2* isoform expression in MDA-MB-468 (epithelial) and MDA-MB-436 (mesenchymal) cells were confirmed using fluorescent microscopy, semi-quantitative polymerase chain reaction, quantitative real-time PCR (qRT-PCR), and western blotting. qRT-PCR was used to determine whether the expression of *FGFR2 IIIb* and *FGFR2 IIIc* became altered in response to changes in the expression of KSRP (either up- or downregulation). Fluorescent microscopy was used to determine if changes in the phenotypes of the epithelial and mesenchymal cells were the consequence of the KSRP mediated changes in *FGFR2 IIIb* and *FGFR2 IIIc* expression. The

ultraviolet cross-linking and immunoprecipitation (UV-CLIP) technique was used to investigate whether KSRP binds directly to *FGFR2* mRNA in epithelial cells. We report that the role of KSRP in *FGFR2* splicing involves the tissue-specific control of the expression of *FGFR2 IIIb* and *FGFR2 IIIc*. KSRP up- and downregulation in MDA-MB-436 causes an upregulation of *FGFR2 IIIb* and *FGFR2 IIIc* expression. KSRP up- and downregulation in MDA-MB-468 cells causes a downregulation of *FGFR2 IIIb* and *FGFR2 IIIc* expression. The efficiency of the upregulation (in MDA-MB-436 cells) and downregulation (in MDA-MB-468 cells) in *FGFR2 IIIb* expression is different to that of *FGFR2 IIIc* expression, this is dependent on the level of KSRP expression. A clear switch from the splicing of *FGFR2 IIIb* to *FGFR2 IIIc*, or vice versa, in response to manipulation of KSRP expression, was not observed in epithelial and mesenchymal cells, indicating that this protein does not control the mutually exclusive splicing nature of this gene. We also show that KSRP does not control EMT or MET in epithelial or mesenchymal cells and that KSRP directly binds to *FGFR2* mRNA at exon 9 (*FGFR2 IIIb*) in epithelial cells. This role of KSRP in *FGFR2* isoform inclusion and the direct binding of KSRP to *FGFR2* mRNA have not been previously reported.

The Affymetrix GeneChip® Human Transcriptome Array 2.0 was used to identify the genome-wide consequences of KSRP knockdown in epithelial cells. Numerous significant changes in gene expression in response to KSRP knockdown were observed. In particular, three genes involved in the canonical Wnt pathway – namely *Cyclin D3* (*CCND3)*, *Dickkopf WNT Signaling Pathway Inhibitor 1* (*DKK1)* and *Protein Phosphatase 2, Regulatory Subunit A, Beta (PPP2R1B)* – were upregulated in response to KSRP downregulation, suggesting a regulatory role of KSRP in this pathway. *CCND3*, *DKK1* and *PPP2R1B* were chosen for further analysis and the change in their expression in response to KSRP downregulation was validated using qRT-PCR. A possible direct interaction between KSRP and the selected targets was predicted using STRING and investigated using confocal fluorescence microscopy. KSRP was not predicted to interact with any of these proteins but interestingly co-localises with DKK1. This suggests that KSRP and DKK1 directly interact and that KSRP could antagonise Wnt signalling. This link between KSRP, DKK1 and the Wnt pathway has not been previously reported.

To the One whose word
created the heavens, breath
made the stars and hands
formed my heart

ACKNOWLEDGEMENTS

I would like to thank the following people, without which, this work would not have been possible.

Those who have supervised me,

Dr Raquel Duarte, you have been such a great mentor to me and I will always be thankful for the faith you have shown in me. Thank you for guiding me scientifically and caring about me. Your trust and faith in my abilities and that I could do the things that I didn't think I could have been an immense encouragement, and I am so grateful.

Prof. Juan Valcárcel Juárez, thank you for accepting me into your research group and for making me feel welcome. Your continuous willingness to discuss research with me, celebrate good results and encourage me/calm me down when things didn't go the way I wanted has shaped me into the scientist I am and inspired me for the future. Thank you for investing in me.

Dr Caroline Dickens, for giving me scientific guidance and for always making time to assist me, especially with the statistical analysis and proofreading. This work would have many more mistakes if not for you.

The past and present members of my research groups,

The Oncology Research Group. Thérèse Dix-Peek, for being always willing to assist me with anything I need, from teaching me new techniques to helping me locate chemicals/reagents in the infamous –20 °C freezer. I appreciate your help and assistance so much. Dr Lerato Mpye and Dr Alex Kasembelli, thank you for being great colleagues and great friends. Thanks for encouraging me, helping me with research, keeping me company in the lab and advising me. I miss you so much!

The Regulation of Alternative pre-mRNA Splicing during Cell Differentiation, Development and Disease research group – Anna Ribó Rubio, Belen Miñana Gómez, Dr Camilla Iannone, Elena Martín Rodríguez, Dr Elisabeth Daguenet, Dr Gwendal Dujardin, Jordi Hernández Ribera, Luisa Vigevani, Dr

Panagiotis Papasaikas, Dr Ramòn Tejedor and Dr Sophie Bonnal. Thanks to every one of you for welcoming me into the lab, teaching me, advising me and assisting me in every way possible. A special thank you to Dr Gwendal Dujardin for assisting me with the UV-CLIP experiments and investing your knowledge in me.

Funding institutions,

The National Research Fund, for the financial support of the DAAD-NRF Joint Scholarship Award and the University of the Witwatersrand for the financial support of the Postgraduate Merit Award.

The CRG-Wits-Novartis mobility program,

To every person involved in making this program a reality - thank you for organising an amazing program and for being concerned about, and investing in, the next generation of scientists. The experiences I gained in this program have, and continue to, teach and inspired me.

The examiners of this thesis,

I am thankful to my examiners for their careful review of this thesis and for providing me with insightful comments and suggestions. These have much improved the quality of the thesis.

My Family,

Mum and Dad. You never said no to my dreams, and both encouraged me to pursue them and supported me through them. I would not be the person I am today if not for your love and guidance. Thanks for always being in my corner and being my greatest supporters and encouragers. Being able to chase my dreams, wherever they take me, is but one of the countless gifts you have given me, and I will always be thankful. I love you!

My brother. Thanks for always making an effort to understand what I'm doing and why I'm doing it, even though my field of interest is not yours. I appreciate your support, encouragement and pep talks more than you know.

My grandmothers and late grandfathers. Seeing happiness in your face is such a joy. Thanks for always being interested in what I am doing and encouraging me to move forward.

My church, RCA Shanti. Thanks for being the community I need. I always know I am supported and prayed for by you. Serving Jesus with you is such a treasure!

My Barcelona family,

I am so thankful I found The International Church of Barcelona. You were the church, the community and place I could serve that I prayed for before I landed in Barcelona. I will always remember the overwhelming feeling of "being home" at my very first service. I'm thankful for the community I found with you and the life-long friendships that have changed my life in so many ways. You made me fall in love with Barcelona and turned my scientific experience into the most amazing life experience. Family isn't always defined by blood, thank you for demonstrating Jesus' love the way you do!

Jesus,

None of this would be possible without you, and even if it were, I wouldn't want it. Knowing you is the greatest joy of my life and serving you is my greatest passion. The greatest gift that the journey of this Ph.D. has given me is that it brought me closer to you. I will always be amazed by your love and grace.

RESEARCH OUTPUTS

Title of Proceeding	**SASBMB Biennial Conference**
Contribution	Poster presentation
Title of Contribution	The Role of KSRP in the Alternative Splicing of the Fibroblast Growth Factor Receptor 2 in Triple-Negative Breast Cancer
All Authors	Moodley, K., Dujardin, G., Valcárcel, J. and Duarte, R.
Status	Published/produced
Year	2014
City/Country	Cape Town, South Africa

Title of Proceeding	**Faculty of Heath Sciences Research Day & Postgraduate Expo**
Contribution	Poster presentation
Title of Contribution	The Role of KSRP in the alternative splicing of the fibroblast growth factor receptor 2 in triple-negative breast cancer
Authors	Moodley, K., Dujardin, G., Valcárcel, J. and Duarte, R.
Status	Published/produced
Year	2014
City/Country	Johannesburg, South Africa

Title of Proceeding	**CRG-Novartis-Wits Mobility Program**
Contribution	Oral presentation
Title of Contribution	Alternative Splicing of the Fibroblast Growth Factor Receptor 2 in Triple-negative Breast Cancer
All Authors	Moodley, K.
Status	Delivered
Year	2014
City/Country	Barcelona, Spain

Title of Proceeding	**Genomics on the Move**
Contribution	Oral presentation
Title of Contribution	Mechanisms of Alternative Splicing in the Progression of Triple-negative Breast Cancer
All Authors	Moodley, K.
Status	Delivered
Year	2015
City/Country	Johannesburg, South Africa

TABLE OF CONTENTS

DECLARATION ii
ABSTRACT iii
ACKNOWLEDGEMENTS vi
RESEARCH OUTPUTS ix
TABLE OF CONTENTS xi
LIST OF FIGURES xiv
LIST OF TABLES xxiii
LIST OF ABBREVIATIONS xxiv
1. LITERATURE REVIEW 1
1.1. The Central Dogma of Molecular Biology 1
1.2. Alternative Splicing 11
1.3. Cancer 17
1.4. Fibroblast Growth Factors and Receptors 32
1.5. The KH-Type Splicing Regulatory Protein 41
2. HYPOTHESIS, AIMS & OBJECTIVES 44
2.1. Hypothesis 44
2.2. Aims 44
2.3. Objectives 45
3. MATERIALS & METHODS 47
3.1. Cell Lines and Cell Culture Maintenance 47
3.2. Plasmids and Plasmid Amplification 47
3.3. Primers 49
3.4. Antibodies 51
3.5. Knockdown and Overexpression of Proteins 52
3.6. RNA Extractions 52
3.7. Complementary DNA Synthesis 54
3.8. Semi-Quantitative Polymerase Chain Reaction 54
3.9. Polyacrylamide Gel Electrophoresis to Resolve DNA 55
3.10. Quantitative Real-Time Polymerase Chain Reaction 55
3.11. Total Protein Extraction 56
3.12. Protein Quantification 56
3.13. Sodium Dodecyl Sulphate Polyacrylamide Gel Electrophoresis to Resolve Proteins 57
3.14. Transfer of Proteins From the Resolved Gel to Membrane 57

3.15. Immunodectection 57
3.16. Confocal Fluorescence Microscopy 58
3.17. Ultra Violet Cross-Linking and Immunoprecipitation 59
3.18. Affymetrix GeneChip® Human Transcriptome Array 2.0 61
3.19. ImageJ Analysis 63
3.20. Statistical Analysis 64
4. RESULTS 65
4.1. Hypothesis-Based Approach 65
4.2. Discovery-Based Approach 98
5. DISCUSSION 119
5.1. Hypothesis-Based Approach 119
5.2. Discovery-Based Approach 135
6. FINDINGS, CONCLUSIONS & FUTURE WORK 142
6.1. Findings and Conclusions 142
6.2. Future Work 143
7. REFERENCES 145
8. APPENDIX A 160
8.1. Luria Broth 160
8.2. LB-Kanamycin Agar Plates 160
8.3. Buffer P1 160
8.4. Buffer P2 161
8.5. Buffer N3 161
8.6. Buffer PB 161
8.7. Buffer PE 161
8.8. Buffer EB 161
8.9. 10x PBS 162
8.10. RLT Buffer 162
8.11. RPE Buffer 162
8.12. 0,5 M EDTA 162
8.13. RIPA Buffer 162
8.14. 10% SDS 163
8.15. 10% APS 163
8.16. 10% Polyacrylamide Gel 163
8.17. 10x TBE 163
8.18. Stacking Gel Buffer (0,5 M Tris-HCl) 163
8.19. Separating Gel Buffer (1,5 M Tris-HCl) 163

8.20. 6x Loading Dye ____ 164
8.21. Sodium Dodecyl Sulphate Polyacrylamide Gel ____ 164
8.22. SDS Running Buffer ____ 165
8.23. Transfer Buffer ____ 165
8.24. 1X PBS-Tween ____ 165
8.25. 5% Non-Fat Milk in 1X PBS-Tween ____ 165
8.26. Lysis Buffer ____ 166
8.27. High-Salt Wash ____ 166
8.28. PNK Buffer ____ 166
8.29. Plasmid Maps ____ 167
9. APPENDIX B ____ 168
9.1. 2100 Bioanalyzer Results ____ 168
10. APPENDIX C ____ 169
10.1. Ethical Clearance Certificate ____ 169
11. APPENDIX D ____ 170
11.1. Turnitin Report ____ 170

LIST OF FIGURES

Figure 1.1 – The central dogma of molecular biology, describing the transfer of information from DNA to protein [2]. In the nucleus, DNA is transcribed into RNA and this RNA is post-transcriptionally processed. The processed RNA is then exported to the cytoplasm and finally translated into protein. **1**

Figure 1.2 – A simplified pre-mRNA splicing reaction [2]. 1) The splicing reaction involves the 5′ exon, the intron with the internal branch point adenosine and the 3′ exon. 2) The branch point adenosine in the intron attacks the 5′ splice site of the exon and cleaves the sugar-phosphate backbone at this site. 3) The 5′ end of the intron covalently binds the branch point adenosine, thereby forming a loop and the 3′ -OH end of the cleaved exon reacts with the 5′ end of the 3′ exon. 4) This causes the joining of the two exons and the release of the intron in the form of a lariat. **5**

Figure 1.3 – The location of the primary splicing signals in the pre-mRNA [13]. GU and AG nucleotides designate the location of the 5′ ss and the 3′ ss, respectively. The adenine residue in the intron designates the branch point and downstream from this is the location of the polypyrimidine tract. **6**

Figure 1.4 – The assembly of spliceosomal elements on pre-mRNA to achieve splicing [10]. Splicing of pre-mRNA is dependent on the activity of a number of components that assemble on the transcript through a series of steps. The binding of the U1-snRNP to the 5′ ss forms complex E and the U2-snRNP then binds the 3′ ss and interacts with the U1-snRNP, forming complex A. The addition of the U4-, U5- and U6-snRNPs (the tri-snRNP) to complex A forms complex B, which becomes activated through conformational and compositional changes. Active complex B catalyses the first step in splicing and forms complex C, which catalyses the second step in splicing and results in the formation of the post-spliceosomal complex. This complex releases the spliced exons as well as the lariat intron bound by the U2-, U5- and U6 snRNPs. The lariat intron and snRNPs are finally recycled. **8**

Figure 1.5 – Alternative splicing events describing the possible outcomes of each [25]. a) Exon inclusion/skipping results in the presence or absence of a particular exon in the final transcript. b) Alternative 3′ ss involves the usage of differential 3′ splice sites thereby altering the final transcript. c) Alternative 5′ ss involves the usage of differential 5′ splice sites thereby altering the final transcript. d) Mutually exclusive exons involve the exclusive inclusion of only one of two exons in the final transcript. e) Intron retention involves either the presence or absence of the intron sequence in the final transcript. f) Alternative promoters involve the use of different promoters thereby altering the final

transcript g) Alternative polyadenylation causes differences in the length of the poly(A) tail of the final transcript. **12**

Figure 1.6 – Hallmarks and enabling characteristics of cancer progression. The eight hallmarks and two enabling characteristics of cancer described by Hanahan and Weinberg in 2000 [61] and 2011 [3]. **19**

Figure 1.7 – The Wnt signalling pathway. This pathway consists of three major signalling branches – A) The canonical Wnt pathway in the absence and presence of Wnt B) The non-canonical planar cell polarity pathway and C) The non-canonical Wnt/Ca^{2+} pathway..... **22**

Figure 1.8 – Alternative splicing of the *FGFR* gene causes changes in the structure of the receptor [155]. The FGF receptor consists of an intracellular tyrosine kinase domain, a transmembrane domain and three extracellular Ig domains (Ig I-III). Ig III is responsible for ligand binding and corresponds to *FGFR2 IIIa* and either *FGFR2 IIIb* or *FGFR2 IIIc*. *FGFR2 IIIb* and *FGFR2 IIIc* are alternatively spliced in a mutually exclusive manner and the differential inclusion alters ligand specificity..... **33**

Figure 1.9 – *FGFR2* splicing mechanism in epithelial cells [160-173]. Red and green boxes indicate *cis*-acting splicing silencers and enhancers, respectively. Purple boxes indicate *cis*-acting elements that function to both silence and enhance splicing. Known *trans*-acting factors are illustrated bound to the appropriate *cis*-acting elements. Red and green lines indicate splicing silencing and activation, respectively, at the appropriate exon. **35**

Figure 1.10 – *FGFR2* splicing mechanism in mesenchymal cells [167, 169, 171, 178-180]. Red and green boxes indicate *cis*-acting splicing silencers and enhancers, respectively. Purple boxes indicate *cis*-acting elements that function to both silence and enhance splicing. Known *trans*-acting factors are illustrated bound to the appropriate *cis*-acting elements. Red and green lines indicate splicing silencing and activation, respectively, at the appropriate exon. **39**

Figure 1.11 – The structure of KSRP [189]. KSRP contains N- and C-terminal domains flanking four KH domains. This protein is post-translationally phosphorylated at Serine 132, 193, 274 and 670 as well as Threonine 692. ..... **41**

Figure 4.1 – Visualisation of epithelial and mesenchymal markers present in MDA-MB-436 cells. A) The epithelial marker, Cytokeratin 19, was not visible in MDA-MB-436 cells. B) The mesenchymal marker, Vimentin, was visible in MDA-MB-436 cells. The monoclonal rabbit anti-Cytokeratin 19 and monoclonal mouse anti-Vimentin primary antibodies as well as polyclonal goat anti-Rabbit IgG (H+L) Rhodamine Red and polyclonal goat anti-Mouse IgG DyLight 649 secondary antibodies were used. Images were captured using the Olympus IX71 Fluorescence Microscope. Included images are representative of similar ones obtained; n = 3..... **67**

Figure 4.2 - Visualisation of epithelial and mesenchymal markers present in MDA-MB-468 cells. A) The epithelial marker, Cytokeratin 19, was visible in MDA-MB-468 cells. B) The mesenchymal marker, Vimentin, was not visible in MDA-MB-468 cells. The monoclonal rabbit anti-Cytokeratin 19 and monoclonal mouse anti-Vimentin primary antibodies as well

as polyclonal goat anti-Rabbit IgG (H+L) Rhodamine Red and polyclonal goat anti-Mouse IgG DyLight 649 secondary antibodies were used. Images were captured using the Olympus IX71 Fluorescence Microscope. Included images are representative of similar ones obtained; n = 3. **68**

Figure 4.3 - Semi-qPCR primer design. One primer pair (FGFR2_e8e11) was designed to bind to either exon 8 (Fwd) or exon 11 (Rev). Because of the mutually exclusive inclusion of exon 9 (IIIb) and exon 10 (IIIc), and the differential sizes of these exons (IIIb – 147 nt and IIIc –144 nt), the resultant PCR products have distinct sizes. **70**

Figure 4.4 – Semi-quantitative analysis of preferential *FGFR2 IIIb* (IIIb) and *FGFR2 IIIc* (IIIc) inclusion in MDA-MB-436 and MDA-MB-468 cells. The *FGFR2 IIIb* transcript (exon 8, 9 and 11) is 412 bp while the *FGFR2 IIIc* transcript (exon 8, 10 and 11) is 464 bp. A) PCR product from each cell line resolved on a 10% polyacrylamide gel representing *FGFR2 IIIc* (top band) and *FGFR2 IIIb* (bottom band). B) ImageJ was used to quantify the intensity of the bands and this showed preferential expression of IIIc and IIIb in MDA-MB-436 and MDA-MB-468 cells, respectively. In MDA-MB-436 cells, the *FGFR2* isoforms consisted of 17% IIIb and 83% IIIc while in MDA-MB-468 cells, *FGFR2* isoforms consisted of 67% IIIb and 33% IIIc. Included image is representative of similar ones obtained; n = 3; standard deviations are shown. **71**

Figure 4.5 – *FGFR2 lllb* (IIIb) and *FGFR2 lllc* (IIIc) expression in MDA-MB-436 and MDA-MB-468. RNA expression levels of lllb and lllc were determined using absolute qRT-PCR quantification. The RNA levels of lllb and lllc in each cell line were expressed as a percentage of total *FGFR2* isoforms. In MDA-MB-436 cells, the *FGFR2* isoforms consisted of 3% *FGFR2 IIIb* and 97% *FGFR2 IIIc*, while in MDA-MB-468 cells, the *FGFR2* isoforms consisted of 66% *FGFR2 IIIb* and 34% *FGFR2 IIIc*. n = 3; standard deviations are shown. **72**

Figure 4.6 – KSRP protein expression level in MDA-MB-436 and MDA-MB-468 cells. A) Composite image of the western blot detection of KSRP and Histone-3 (loading control). B) ImageJ analysis of KSRP band density. KSRP band density in MDA-MB-468 cells was reported relative to KSRP band density in MDA-MB-436 cells, which was set at 100%. KSRP protein expression in MDA-MB-468 cells was 14% higher than KSRP protein expression in MDA-MB-436 cells. Included image is representative of similar ones obtained; n = 2; standard deviations are shown. **73**

Figure 4.7 – *FGFR2 IIIb* (IIIb) and *FGFR2 IIIc* (IIIc) expression is affected by ESRP1 and ESRP2 knockdown in MDA-MB-436 (436) and MDA-MB-468 (468) cells. mRNA expression levels of ESRP1, ESRP2, IIIb and IIIc in ESRP1&2 knockdown cells (siESRP1&2) were expressed relative to the mRNA expression levels of these genes in the transfection control cells (siScr). ESRP1 and ESRP2 were successfully downregulated in 436 and 468 cells and this downregulation resulted in decreases and increases in the expression of IIIb and IIIc, respectively. n = 3; standard deviations are shown. **74**

Figure 4.8 – KSRP knockdown (siKSRP) and overexpression (pKSRP) at the mRNA level in MDA-MB-436 (436) and MDA-MB-468 (468) cells. The mRNA expression levels of KSRP

when it was down- (siKSRP) or upregulated (pGFP) were expressed relative to the mRNA expression levels of KSRP in the knockdown (siScr) and overexpression (pGFP) transfection controls, respectively. n = 9; standard errors are shown; ** p ≤ 0,01; *** p ≤ 0,001. ..... **76**

Figure 4.9 – Confirmation of KSRP knockdown at the protein level in MDA-MB-436 (436) and MDA-MB-468 (468) cells. A) Western blots detecting KSRP and Histone-3 (loading control). B) ImageJ analysis of KSRP band density. For each cell line, siKSRP band density was reported as a percentage of siScr band density, which was set at 100%. In MDA-MB-436 KSRP knockdown cells, KSRP protein expression was decreased by 100% and in MDA-MB-468 KSRP knockdown cells, KSRP protein expression was decreased by 98%. Included image is representative of similar ones obtained; n = 3; standard deviations are shown. **77**

Figure 4.10 – Confirmation of KSRP overexpression at the protein level in MDA-MB-436 (436) and MDA-MB-468 (468) cells. A) Western blots detecting KSRP and Histone-3 (loading control). B) ImageJ analysis of KSRP band density. For each cell line, pKSRP band density was reported as a percentage of pGFP band density, which was set at 100%. In MDA-MB-436 KSRP overexpressed cells, KSRP protein expression was increased by 578% and in MDA-MB-468 KSRP overexpressed cells, KSRP protein expression was increased by 256%. Included image is representative of similar ones obtained; n = 3, standard deviations are shown. **78**

Figure 4.11 – The effect of *KSRP* knockdown (siKSRP) on *FGFR2 IIIb* (IIIb) and *FGFR2 IIIc* (IIIc) mRNA expression levels in MDA-MB-436 (436) cells. The mRNA expression level of *KSRP*, *FGFR2 IIIb* and *FGFR2 IIIc* when *KSRP* was downregulated (siKSRP) were expressed relative to the mRNA expression levels of these genes in the knockdown transfection control (siScr). n = 9; standard errors are shown; ** p ≤ 0,01. ..... **80**

Figure 4.12 – The effect of *KSRP* knockdown (siKSRP) on *FGFR2 IIIb* (IIIb) and *FGFR2 IIIc* (IIIc) mRNA expression levels in MDA-MB-468 (468) cells. The mRNA expression level of *KSRP*, *FGFR2 IIIb* and *FGFR2 IIIc* when *KSRP* was downregulated (siKSRP) were expressed relative to the mRNA expression levels of these genes in the knockdown transfection control (siScr). n = 9; standard errors are shown; *** p ≤ 0,001; * p ≤ 0,05. ..... **81**

Figure 4.13 – The effect of *KSRP* overexpression (pKSRP) on *FGFR2 IIIb* (IIIb) and *FGFR2 IIIc* (IIIc) mRNA expression levels in MDA-MB-436 (436) cells. The mRNA expression levels of *KSRP*, *FGFR2 IIIb* and *FGFR2 IIIc* when *KSRP* was upregulated (pKSRP) were expressed relative to the mRNA expression levels of these genes in the upregulation transfection control (pGFP). n = 9; standard errors are shown; *** p ≤ 0,001; ** p ≤ 0,01; * p ≤ 0,05. ..... **82**

Figure 4.14 – The effect of *KSRP* overexpression (pKSRP) on *FGFR2 IIIb* (IIIb) and *FGFR2 IIIc* (IIIc) mRNA expression levels in MDA-MB-468 (468) cells. The mRNA expression levels of *KSRP*, *FGFR2 IIIb* and *FGFR2 IIIc* when *KSRP* was upregulated (pKSRP) were expressed relative to the mRNA expression levels of these genes in the upregulation transfection control (pGFP). n = 9; standard errors are shown; *** p ≤ 0,001; * p ≤ 0,05. ..... **83**

Figure 4.15 – Comparing the effect of *KSRP* knockdown (siKSRP) on *FGFR2 IIIb* (IIIb) and *FGFR2 IIIc* (IIIc) mRNA expression levels between MDA-MB-436 (436) and MDA-MB-468 (468) cells. The mRNA expression levels of *KSRP*, *FGFR2 IIIb* and *FGFR2 IIIc* when *KSRP* was downregulated (siKSRP) were expressed relative to the mRNA expression levels of these genes in the knockdown transfection control (siScr). n = 9; standard errors are shown; ** p ≤ 0,01; *** p ≤ 0,001. ..... **84**

Figure 4.16 – Comparing the effect of *KSRP* overexpression (pKSRP) on *FGFR2 IIIb* (IIIb) and *FGFR2 IIIc* (IIIc) mRNA expression levels between MDA-MB-436 (436) and MDA-MB-468 (468) cells. The mRNA expression levels of *KSRP*, *FGFR2 IIIb* and *FGFR2 IIIc* when *KSRP* was upregulated (pKSRP) were expressed relative to the mRNA expression levels of these genes in the upregulation transfection control (pGFP). n = 9; standard errors are shown; ** p ≤ 0,01; *** p ≤ 0,001. ..... **85**

Figure 4.17 – Comparing the effect of *KSRP* knockdown (siKSRP) to the effect of *KSRP* overexpression (pKSRP) on the mRNA expression levels of *FGFR2 IIIb* (IIIb) and *FGFR2 IIIc* (IIIc) in MDA-MB-436 (436) cells. The mRNA expression levels of *KSRP*, *FGFR2 IIIb* and *FGFR2 IIIc* when *KSRP* was downregulated (siKSRP) and upregulated (pKSRP) were expressed relative to the mRNA expression levels of these genes in the knockdown (siScr) and upregulation (pGFP) transfection controls, respectively. n = 9; standard errors are shown; ns p > 0,05; *** p ≤ 0,001. ..... **86**

Figure 4.18 – Comparing the effect of *KSRP* knockdown (siKSRP) to the effect of *KSRP* overexpression (pKSRP) on the mRNA expression levels of *FGFR2 IIIb* (IIIb) and *FGFR2 IIIc* (IIIc) in MDA-MB-468 (468) cells. The mRNA expression levels of *KSRP*, *FGFR2 IIIb* and *FGFR2 IIIc* when *KSRP* was downregulated (siKSRP) and upregulated (pKSRP) were expressed relative to the mRNA expression levels of these genes in the knockdown (siScr) and upregulation (pGFP) transfection controls, respectively. n = 9; standard errors are shown; *** p ≤ 0,001; * p ≤ 0,05. ..... **87**

Figure 4.19 – Cytokeratin 19 visualisation in MDA-MB-436 cells expressing pEGFP-N1 (GFP) or pEGFPC1-6XHis-FLKSRP (GFP-KSRP). A) Cytokeratin 19 was not visible in MDA-MB-436 cells expressing GFP. B) Cytokeratin 19 was not visible in MDA-MB-436 cells expressing GFP-KSRP. The monoclonal rabbit anti-Cytokeratin 19 primary and polyclonal goat anti-Rabbit IgG (H+L) Rhodamine Red secondary antibodies were used. Images were captured using the Olympus IX71 Fluorescence Microscope. Included images are representative of similar ones obtained; n = 3. ..... **89**

Figure 4.20 – Vimentin visualisation in MDA-MB-436 cells expressing pEGFP-N1 (GFP) or pEGFPC1-6XHis-FLKSRP (GFP-KSRP). A) Vimentin was visible in MDA-MB-436 cells expressing GFP. B) Vimentin was visible in MDA-MB-436 cells expressing GFP-KSRP. The monoclonal mouse anti-Vimentin primary and polyclonal goat anti-Mouse IgG DyLight 649 secondary antibodies were used. Images were captured using the Olympus IX71 Fluorescence Microscope. Included images are representative of similar ones obtained; n = 3. ..... **90**

Figure 4.21 – Cytokeratin 19 visualisation in MDA-MB-468 cells expressing pEGFP-N1 (GFP) or pEGFPC1-6XHis-FLKSRP (GFP-KSRP). A) Cytokeratin 19 was visible in MDA-MB-468 cells expressing GFP. B) Cytokeratin 19 was visible in MDA-MB-468 cells expressing GFP-KSRP. The monoclonal rabbit anti-Cytokeratin 19 primary and polyclonal goat anti-Rabbit IgG (H+L) Rhodamine Red secondary antibodies were used. Images were captured using the Olympus IX71 Fluorescence Microscope. Included images are representative of similar ones obtained; n = 3. **91**

Figure 4.22 – Vimentin visualisation in MDA-MB-468 cells expressing pEGFP-N1 (GFP) or pEGFPC1-6XHis-FLKSRP (GFP-KSRP). A) Vimentin was not visible in MDA-MB-468 cells expressing GFP. B) Vimentin was not visible in MDA-MB-468 cells expressing GFP-KSRP. The monoclonal mouse anti-Vimentin primary and polyclonal goat anti-Mouse IgG DyLight 649 secondary antibodies were used. Images were captured using the Olympus IX71 Fluorescence Microscope. Included images are representative of similar ones obtained; n = 3. **92**

Figure 4.23 – UV-CLIP primers. The binding positions of the six designed UV-CLIP primers on *FGFR2* mRNA are illustrated on the top image. The primer sequences and the sequences of *FGFR2* mRNA they amplify are shown in the bottom image. **95**

Figure 4.24 – Gradient semi-qPCR analysis used to determine the optimal melting temperature of the six UV-CLIP primer pairs. Gradient semi-qPCR using A) FGFR2_i81 (primer pair 1) yielded a 195 bp PCR product; B) FGFR2_i82 (primer pair 2) yielded a 163 bp PCR product; c) FGFR2_i83 (primer pair 3) yielded a 166 bp PCR product; D) FGFR2_i8e9 (primer pair 4) yielded a 247 bp PCR product; E) FGFR2_e9 (primer pair 5) yielded a 197 bp PCR product; F) FGFR2_i9 (primer pair 6) yielded a 238 bp PCR product. A gradient of melting temperatures was used: lane 1) 55 °C; 2) 55,4 °C; 3) 56,3 °C; 4) 57,5 °C; 5) 59,2 °C; 6) 61,4 °C; 7) 63,9 °C; 8) 66,1 °C; 9) 67,7 °C; 10) 68,9 °C; 11) 69,7 °C. **96**

Figure 4.25 – UV cross-linking and immunoprecipitation of KSRP in MDA-MB-468 cells. MDA-MB-468 cells were UV cross-linked, lysed, the lysate incubated with an anti-KSRP antibody bound to magnetic beads (an anti-IgG antibody was used as a control), and the anti-KSRP antibody (with bound RNA) eluted. An aliquot of the input lysate (In), the flow-through (FT) and the elution (IP) was analysed using western blotting. The RNA bound to the eluted KSRP and IgG was extracted, reverse transcribed into cDNA and used for absolute qRT-PCR quantification. A) In the control samples, western blot analysis confirmed the presence of KSRP in the input (In) and flow-through (FT) fractions but the absence of KSRP in the immunoprecipitation (IP) fraction. In the KSRP samples, western blot analysis confirmed the presence of KSRP in the In, FT and IP fractions; U2AF65 was used as a loading control. B) 41% the mRNA bound to immunoprecipitated KSRP from the KSRP IP fraction belonged to *FGFR2* exon 9 (this was calculated relative to the amount of *FGFR2* exon 9 amplified in the control IP fraction). n = 3; standard deviations shown. **97**

Figure 4.26 – Hierarchical clustering of genes regulated in KSRP downregulated (siKSRP) MDA-MB-468 (468) cells compared to transfection control (siScr) 468 cells. Each row represents the relative expression levels of a single gene and each column represents the gene expression levels in a specific sample. Green and red colours represent relatively low and high gene expression, respectively. Hierarchical clustering was reported by A) Gene intensities and B) Distance to mean. n = 3. ..... **99**

Figure 4.27 – Venn diagrams summarising Affymetrix GeneChip® Human Transcriptome Array 2.0 data comparing MDA-MB-436 KSRP knockdown (siKSRP) cells to MDA-MB-468 transfection control (siScr) cells. A) Regulated genes overlapping regulated transcription factors with a fold change ≥ 1,5. B) No regulated genes overlapped regulated splicing factors with a fold change ≥ 1,5. C) Regulated genes that have regulated exons with a fold change ≥ 1,5. D) Regulated genes that also have regulated splicing patterns with a fold change ≥ 1,5. ..... **100**

Figure 4.28 – Wnt pathway adapted from KEGG. The positions of DKK (DKK1) and cyD (CCND3) – proteins regulated by KSRP – in the Wnt signalling pathway are bordered in red. The location of the TGF-β signalling pathway is bordered in blue. **107**

Figure 4.29 – TGF-β pathway adapted from KEGG. The position of PP2A (PPP2R1B) – a protein regulated by KSRP – in the TGF-β pathway is bordered in red. **108**

Figure 4.30 – Validation of the effect of *KSRP* knockdown (siKSRP) on *CCND3*, *DKK1* and *PPP2R1B* mRNA expression levels in MDA-MB-468 (468) cells. The mRNA expression levels of *KSRP*, *CCND3*, *DKK1* and *PPP2R1B* in MDA-MB-468 cells when *KSRP* was downregulated (siKSRP) were expressed relative to the mRNA expression levels of these genes in the knockdown transfection control (siScr). n = 9; standard errors are shown; *** p ≤ 0,001. ..... **109**

Figure 4.31 – STRING analysis of the possible interactions of A) KSRP and CCND3, B) KSRP and DKK1 as well as C) KSRP and PPP2R1B. No connection lines were observed in A, B or C, suggesting no direct interaction between these proteins. **110**

Figure 4.32 – STRING analysis predictions of protein interaction networks involving A) KSRP and CCND3, B) KSRP and DKK1 and C) KSRP and PPP2R1B. The proteins of interest are highlighted in yellow. **111**

Figure 4.33 – Co-localisation of GFP and KSRP as well as GFP-KSRP and KSRP in MDA-MB-468 cells expressing A) pEGFP-N1 and B) pEGFPC1-6xHis-FLKSRP. A) GFP did not co-localise with KSRP. B) GFP-KSRP co-localised with KSRP. The polyclonal rabbit anti-KSRP primary and polyclonal goat anti-Rabbit IgG (H+L) Rhodamine Red secondary antibodies were used. Images were captured using the Olympus IX71 Fluorescence Microscope. Included images are representative of similar ones obtained; n = 3. ..... **113**

Figure 4.34 – Co-localisation of GFP and CCND3 as well as GFP-KSRP and CCND3 in MDA-MB-468 cells expressing A) pEGFP-N1 and B) pEGFPC1-6xHis-FLKSRP. A) GFP did not co-localise with CCND3. B) GFP-KSRP did not co-localise with CCND3. The monoclonal

rabbit anti-Cyclin D3 primary and polyclonal goat anti-Rabbit IgG (H+L) Rhodamine Red secondary antibodies were used. Images were captured using the Olympus IX71 Fluorescence Microscope. Included images are representative of similar ones obtained; n = 3. ..... **114**

Figure 4.35 – Co-localisation of GFP and DKK1 as well as GFP-KSRP and DKK1 in MDA-MB-468 cells expressing A) pEGFP-N1 and B) pEGFPC1-6xHis-FLKSRP. A) GFP did not co-localise with DKK1. B) GFP-KSRP co-localised with DKK1. The monoclonal rabbit anti-DKK1 primary and polyclonal goat anti-Rabbit IgG (H+L) Rhodamine Red secondary antibodies were used. Images were captured using the Olympus IX71 Fluorescence Microscope. Included images are representative of similar ones obtained; n = 3. ..... **115**

Figure 4.36 – Co-localisation of GFP and PPP2R1B as well as GFP-KSRP and PPP2R1B in MDA-MB-468 cells expressing A) pEGFP-N1 and B) pEGFPC1-6xHis-FLKSRP. A) GFP did not co-localise with PPP2R1B. B) GFP-KSRP did not co-localise with PPP2R1B. The monoclonal rabbit anti-PPP2R1B primary and polyclonal goat anti-Rabbit IgG (H+L) Rhodamine Red secondary antibodies were used. Images were captured using the Olympus IX71 Fluorescence Microscope. Included images are representative of similar ones obtained; n = 3. ..... **116**

Figure 4.37 – 2D intensity histograms evidencing either positive or negative co-localisation events. Positive co-localisation of targets is indicated by a diagonal scatter pattern on the 2D intensity histogram. Positive co-localisation was seen between B) GFP-KSRP and KSRP and F) GFP-KSRP and DKK1. Negative co-localisation was seen between A) GFP and KSRP, C) GFP and CCND3, D) GFP-KSRP and CCND3, E) GFP and DKK1, G) GFP and PPP2R1B and H) GFP-KSRP and PPP2R1B. **117**

Figure 5.1 – *FGFR2* pre-mRNA illustrating the positions of *cis*-acting elements and indicating the position of KSRP binding in MDA-MB-468 cells. UV-CLIP findings revealed that KSRP directly binds to *FGFR2* pre-mRNA at exon 9 (*FGFR2 IIIb*) in MDA-MB-468 cells. **130**

Figure 5.2 – Known amplified *FGFR2* exon 9 (IIIb) sequence, indicating reported KSRP, hnRNP A1 and PTB binding sites. The reported KSRP binding sites (GGG, UGCAU, GGGU and AGGG) are highlighted in yellow. The reported hnRNP A1 binding site (UAGGG) is bordered in blue. The reported PTB binding site is indicated in red letters. **131**

Figure 5.3 – The proposed mechanism of KSRP action on *FGFR2 IIIb* and *FGFR2 IIIc* in epithelial and mesenchymal cells. A-1) in epithelial cells, abundant KSRP binding to *FGFR2 IIIb* causes a more efficient repression of *FGFR2 IIIc* expression compared to *FGFR2 IIIb* expression. A-2) in epithelial cells, scarce KSRP binding to *FGFR2 IIIb* causes a more efficient repression of *FGFR2 IIIb* expression compared to *FGFR2 IIIc* expression. B-1) in mesenchymal cells, abundant KSRP binding to *FGFR2 IIIc* causes a more efficient enhancement of *FGFR2 IIIb* expression compared to *FGFR2 IIIc* expression. B-2) in mesenchymal cells, scarce KSRP binding to *FGFR2 IIIc* causes a more efficient enhancement of *FGFR2 IIIc* expression compared to *FGFR2 IIIb* expression. * Denotes the exon that

becomes more efficiently upregulated (in mesenchymal cells - B) or downregulated (in epithelial cells - A) when KSRP is either upregulated (A-1 and B-1) or downregulated (A-2 and B2). **133**

Figure 8.1 – Plasmid maps. A) pEGFP-N1 plasmid map. B) pEGFPC1-6xHis-FLKSRP plasmid map. **167**

Figure 9.1 – 2100 Bioanalyzer results. RNA integrity was analysed using the 2100 Bioanalyzer. The top panel illustrates the electrophoretic trace of the 28S and 18S rRNA and the bottom panel displays the RINs for each sample. **168**

LIST OF TABLES

Table 1.1 - Assignment of TNBC cell lines to subtypes [110]. **28**
Table 3.1 – Table of Primer Information **50**
Table 3.2 – Table of Antibody Information **51**
Table 4.1 – Regulated Genes. The 49 genes identified as being regulated with a fold change ≥ 1,5 upon KSRP knockdown. **101**
Table 4.2 – Regulated genes involved in the Wnt signalling pathway. The three genes identified as being involved in the Wnt Signalling pathway and are upregulated with a fold change of ≥ 1,5 upon KSRP knockdown. **103**
Table 4.3 – Regulated genes that are transcription factors. The 8 transcription factors identified as being regulated with a fold change ≥ 1,5 upon KSRP knockdown..... **104**
Table 4.4 – Regulated genes that have regulated exons. The one regulated exon identified as being regulated with a fold change ≥ 1,5 upon KSRP knockdown. **104**
Table 4.5 – Regulated genes that have regulated splicing patterns. The 4 regulated splicing patterns identified as being regulated with a fold change ≥ 1,5 upon KSRP knockdown... **105**
Table 4.6 – Pearson's R Values for potential co-localisation events..... **118**

LIST OF ABBREVIATIONS

°C	Degree Celsius
2D	2 Dimensional
3′	3 prime
5′	5 prime
A	Adenosine
APC	Adenomatous Polyposis Coli
ARE	Adenylate-Uridine-Rich Element
ARE-BP	Adenylate-Uridine-Rich Element Binding Protein
ATP	Adenosine Triphosphate
BCA	Bicinchoninic Acid Assay
Bcl	B-Cell Lymphoma
BL1	Basal-Like 1
BL2	Basal-Like 2
BSA	Bovine Serum Albumin
C	Cytosine
C-terminal	Carboxyl-Terminal
Ca^{2+}	Calcium Ion
CaMKII	Ca^{2+}/Calmodulin-Dependent Protein Kinase II
CCND3	Cyclin D3
CDC42	Cell Division Control Protein 42
CDK	Cyclin Dependent Kinase
cDNA	Complementary Deoxyribonucleic Acid
CELF1	CUGBP, Elav-Like Family Member 1
ChIP	Chromatin Immunoprecipitation
ChIP-seq	Chromatin Immunoprecipitation With Sequencing
CK1	Casein Kinase-1
cm	Centi Meter
CO_2	Carbon Dioxide
CRC	Colorectal Cancers
Daam1	Dishevelled Associated Activator of Morphogenesis 1

DAG	Dystroglycan
DAPI	4′,6-diamidino-2-phenylindole
DCS	Downstream Control Sequence
dH_2O	Distilled Water
DISE	Downstream Intronic Splicing Enhancer
DISS	Downstream Intronic Splicing Silencer
Dkk	Dickkopf
DKK1	Dickkopf WNT Signaling Pathway Inhibitor 1
DMBA	7,12-Dimethylbenz[a]anthracene
DNA	Deoxyribonucleic Acid
dNTP	Deoxynucleotide Triphosphate
Dsh	Dishevelled
ECM	Extracellular Matrix
EDTA	Ethylenediaminetetraacetic Acid
EGF	Epidermal Growth Factor
eGFP	Enhanced Green Fluorescent Protein
EMT	Epithelial-to-Mesenchymal Transition
ER	Oestrogen Receptor
ESE	Exonic Splicing Enhancer
ESRP	Epithelial Splicing Regulatory Protein
ESS	Exonic Splicing Silencer
FAP	Familial Adenomatous Polyposis
FGF	Fibroblast Growth Factor
FGFR	Fibroblast Growth Factor Receptor
FIJI	FIJI Is Just ImageJ
FT	Flow-through
FUBP2	Far Upstream Element-Binding Protein 2
Fz	Frizzled
g	G-force
G	Guanosine
GAPDH	Glyceraldehyde-3-Phosphate Dehydrogenase
GBM	Glioblastoma Multiforme
GFP	Green Fluorescent Protein

GMP	Guanosine Monophosphate
GSK3-β	Glycogen Synthase Kinase 3 Beta
h	Hour
H_2O	Water
H3	Histone-3
HER2	Human Epidermal Growth Factor Receptor 2
HGF	Hepatocyte Growth Factor
hnRNP	Heterogeneous Nuclear Ribonucleoproteins
HPRT1	Hypoxanthine Phosphoribosyltransferase 1
hrs.	Hours
HSPG	Heparan Sulphate Proteoglycan
IAS	Intronic Activating Sequence
IDT	Integrated DNA Technologies
Ig	Immunoglobulin
IM	Immunomodulatory
In	Input
IP	Immunoprecipitate
IP3	Inositol Triphosphate
ISAR	Intronic Splicing Activator and Repressor
ISE	Intronic Splicing Enhancer
ISS	Intronic Splicing Silencer
JNK	c-Jun N-terminal Kinase
KEGG	Kyoto Encyclopedia of Genes and Genomes
KH	hnRNPK-homology
KSRP	KH-type Splicing Regulatory Protein
LAR	Luminal Androgen Receptor
LDH	Lactate Dehydrogenase
LRP-5/6	Lipoprotein Receptor-Related Protein 5/6
M	Mesenchymal
mA	Milli Ampere
MAPK	Mitogen Activated Protein Kinase
MET	Mesenchymal-to-Epithelial Transition
min	Minute

MIQE	Minimum Information for Publication of Quantitative Real-Time PCR Experiments
miRNA	micro RNA
mJ	Milli Joules
mL	Milli Litre
mRNA	Messenger RNA
mRNP	Messenger Ribonucleoprotein
MSL	Mesenchymal Stem-like
mTOR	Mechanistic Target of Rapamycin
N-terminal	Amino-terminal
NF-κB	Nuclear factor kappa-light-chain-enhancer of activated B cells
NFAT	Nuclear Factor of Activated T-cells
NLK	Nemo-Like Kinase
nm	Nano Meter
nM	Nano Molar
NMD	Nonsense-mediated Decay
NPC	Nuclear Pore Complexes
ns	Non-significant
nt	Nucleotide
OH	Hydroxide
p	P-value
PAB2	Polyadenylate-binding Protein 2
PAGE	Polyacrylamide Gel Electrophoresis
PARN	Poly(A)-Specific Ribonuclease
PBS	Phosphate Buffered Saline
PCR	Polymerase Chain Reaction
PDE	Phosphodiesterase
PDGF	Platelet-derived Growth Factor
PK	Pyruvate Kinase
PLC	Phospholipase C
PPP2R1B	Protein Phosphatase 2, Regulatory Subunit A, Beta
PR	Progesterone Receptor
pre-mRNA	Precursor mRNA

pri-miRNA	Primary Micro RNA
Prp	Pre-mRNA-splicing ATP-dependent RNA helicase
PTB	Polypyrimidine Tract Binding Protein
PVDF	Polyvinylidene Difluoride
qPCR	Quantitative PCR
qRT-PCR	Quantitative Reverse-transcriptase Polymerase Chain Reaction
Rac	Ras-Related C3 Botulinum Toxin Substrate 1
RISC	RNA-induced Silencing Complex
RNA	Ribonucleic Acid
RNP	Ribonucleoprotein
ROCK	Rho Kinase
rpm	Revolutions Per Minute
RS	Arginine-Serine
RT	Room Temperature
s	Second
Sam68	Src-Associated Substrate in Mitosis of 68 kDa
SDHA	Succinate Dehydrogenase Complex, Subunit A
SDS-PAGE	Sodium Dodecyl Sulphate Polyacrylamide Gel Electrophoresis
SF1	Splicing Factor 1
SFRP	Soluble Frizzled-related Protein
SIP1	Smad interacting protein 1
siRNA	Small Interfering RNA
SNP	Single Nucleotide Polymorphism
snRNP	Small Nuclear Ribonucleoprotein
SR	Serine-Arginine
ss	Splice Site
STRING	Search Tool for the Retrieval of Interacting Genes/Proteins
T	Threonine
TAC	Transcriptome Analysis Console
TAK	Transforming Growth Factor-Beta-Activated Kinase 1
TALS	Taybi-Linder syndrome
TBE	Tris/Borate/EDTA
TGF-β	Transforming Growth Factor Beta

TIA-1	T-Cell-Restricted Intracellular Antigen-1
TL	Terminal loop
TNBC	Triple-negative Breast Cancer
TP53	Tumour Suppressor 53
TPA	Tissue plasminogen activator
tRNA	Transfer RNA
TWIST	Twist Basic Helix-Loop-Helix Transcription Factor 1
U2AF	U2 Auxiliary Factor
UISS	Upstream Intronic Splicing Silencer
UTR	Untranslated Region
UV-CLIP	Ultra Violet Cross-linking and Immunoprecipitation
UV-Vis	Ultra Violet-visible
V	Volts
v/v	Volume/volume
WHO	World Health Organisation
WIF	Wnt-inhibitory factors
ZEB1	Zinc Finger E-Box Binding Homeobox 1
β-TrCP	Beta-Transducin Repeat Containing E3 Ubiquitin Protein Ligase
μg	Micro Gram
μL	Micro Litre
μM	Micro Molar

Chapter 1

1. LITERATURE REVIEW

1.1. The Central Dogma of Molecular Biology

"The central dogma of molecular biology" is a phrase first published in the 1970's by Francis Crick to define the relationship between Deoxyribonucleic Acid (DNA), Ribonucleic Acid (RNA) and proteins [1]. This phrase describes the process by which genetic information, contained in genomic DNA and located in the nucleus, ultimately encodes for protein (Figure 1.1) [2, 3]. RNA is synthesised from a DNA template strand through a process termed transcription and proteins are synthesised from the RNA strand through a process called translation [2, 3].

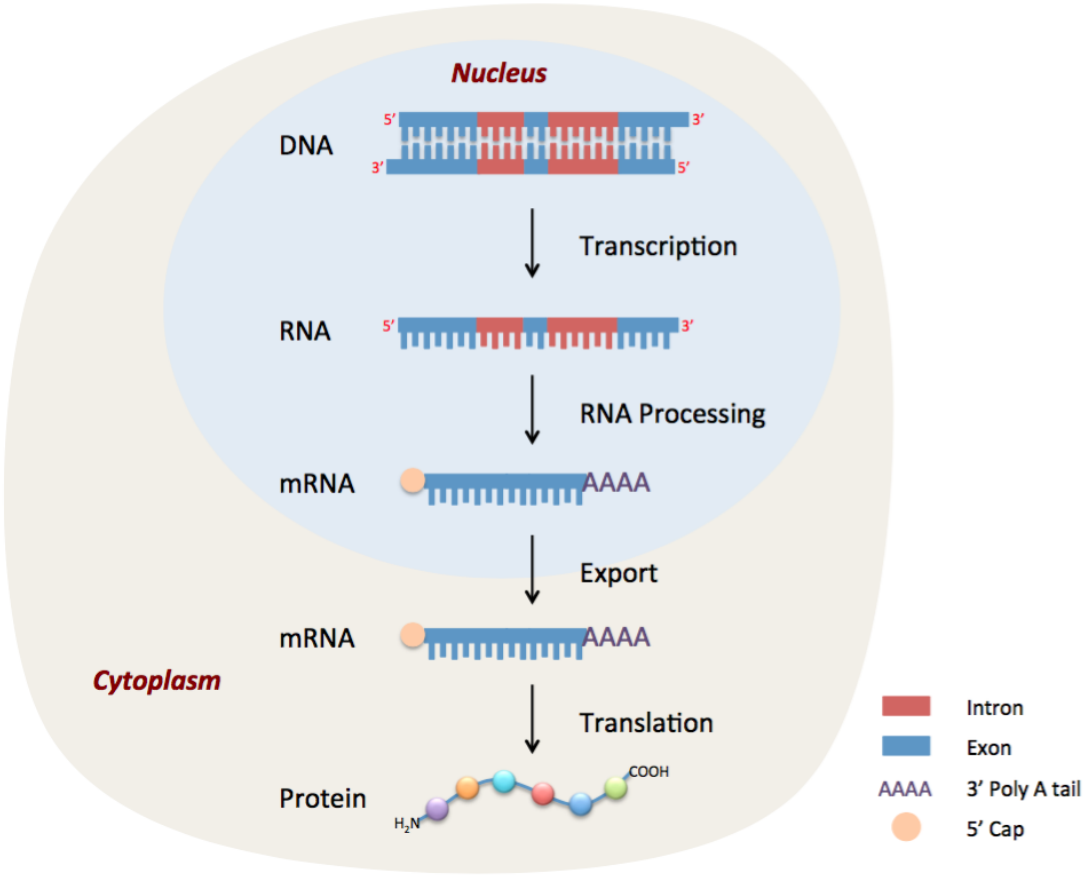

Figure 1.1 – The central dogma of molecular biology, describing the transfer of information from DNA to protein [2]. In the nucleus, DNA is transcribed into RNA and this RNA is post-transcriptionally processed. The processed RNA is then exported to the cytoplasm and finally translated into protein.

1.1.1. Transcription

Transcription is a term used to describe the process by which RNA is synthesised from DNA [2]. This process begins when RNA polymerases catalyse the unwinding of a portion of double-stranded DNA, allowing the exposure of individual nucleotide (nt) bases [2]. Once an opening in the DNA helix is achieved, the RNA chain is sequentially synthesised in a 5′-to-3′ direction through the addition of cytosine (C), guanine (G), uracil (U) or adenine (A) nucleotides by complementary base-pairing between the incoming nucleotide and the nucleotide on the DNA template [2]. The newly added nucleotide becomes covalently bound to the growing RNA chain through the formation of phosphodiester bonds [2]. These bonds are responsible for linking nucleotides together to form a linear chain and this process is catalysed by RNA polymerases [2]. Once each complementary nucleotide has been added, the growing RNA chain is progressively displaced from the DNA template strand and the helical conformation of DNA is re-established [2]. Therefore, the RNA strand is not covalently bound to the template DNA strand but is released as a single stranded molecule [2]. The almost immediate release of the RNA chain from the DNA template strand allows for multiple RNA chains to be synthesised in a relatively short period of time [2].

1.1.2. RNA Processing

In prokaryotes, once RNA is synthesised from the DNA template, it can immediately be used for protein synthesis, however, in eukaryotes, the synthesised RNA strand must undergo certain covalent and non-covalent modifications prior to its use as a template for protein synthesis [2]. In eukaryotes, prior to processing, RNA is known as precursor messenger RNA (pre-mRNA), and after processing, it is known as messenger RNA (mRNA). These processing steps (5′ processing, 3′ processing and splicing) function both to aid recognition of the strand by molecules responsible for translation and to rid the pre-mRNA strand of sequences that should not be translated into protein [2].

1.1.2.1. 5′ Processing

The modification of pre-mRNA at the 5′ end is called “capping” and aids the cell both in identifying mRNAs and distinguishing them from the other RNA molecules (e.g. tRNA, rRNA, snRNA etc.) present in the cell [2]. Additionally, capping is fundamental for the regulation of nuclear transport [4], the promotion of translation [5], and the promotion of 5′ proximal intron excision [6].

When the pre-mRNA chain being transcribed reaches a length of approximately 25 nucleotides, three sequentially functioning enzymes catalyse the “capping” process by the addition of covalent guanine nucleotides at the 5′ end of the pre-mRNA [2]. First, a phosphatase removes a phosphate group from the 5′ end of the pre-mRNA chain and secondly, a guanyl transferase adds a guanosine monophosphate (GMP) molecule to this end in a 5′-to-5′ direction instead of a 5′-to-3′ direction (this is known as reverse linkage). Finally, a methyl transferase adds a methyl group to the guanosine of the newly added GMP [2].

1.1.2.2. 3′ Processing

When the poly(A) signal added to the pre-mRNA transcript is recognised by complex cellular machinery, the transcript undergoes cleavage of its 3′ end [7]. Once the 3′ end of the pre-mRNA template is cleaved, polyadenylate polymerase removes adenosine monophosphate units from adenosine triphosphate, releasing the pyrophosphate and catalysing the addition of the adenosine monophosphate units to the 3′ end of the pre-mRNA strand, thus initiating the formation of the poly(A) tail [8]. Polyadenylate-binding protein 2 (PAB2) then binds to this poly(A) tail and in doing so, increases the affinity of the polyadenylate polymerase to the pre-mRNA strand [9]. When approximately 250 adenosine monophosphate units have been successfully added to the 3′ end of the pre-mRNA strand, polyadenylation is concluded [9]. The poly(A) tail promotes the transport of the mRNA transcripts from the nucleus to the cytoplasm and affects both their stability and their translation [7].

1.1.2.3. Splicing

While the genes from prokaryotic organisms characteristically consist of a continuous stretch of coding DNA, eukaryotic genes are comprised of short coding regions (called exons), interrupted by much longer non-coding sequences (called introns) [2]. In eukaryotes, both the non-coding intron and coding exon sequences are transcribed, however, before translation, the non-coding intron sequences are removed from the transcript through a process called RNA splicing [2]. Splicing is an active process, requiring the hydrolysis of a number of adenosine triphosphate (ATP) molecules and is controlled by many different proteins, highlighting its accuracy [2]. Approximately 60% of all human genes are spliced, causing the production of different mRNAs, and ultimately proteins, from the same gene transcript [2]. This observation emphasises the important role of splicing in increasing the coding potential of eukaryotic genomes [2]. Splicing removes introns from the pre-mRNA, joining flanking exons together, thereby producing mature mRNA. Each splicing reaction requires primary splicing signals, *cis*-acting regulatory elements and *trans*-acting factors [10].

Figure 1.2 illustrates a single splicing event involving the 5′ and 3′ exons (shown in orange) and the intron that separates them (shown in green). In each splicing reaction, a specific adenine nucleotide (called the branch point), located in the intron sequence, attacks the 5′ splice site and causes cleavage of the sugar-phosphate backbone. The cleaved 5′ end of the intron then becomes covalently bound to the adenine nucleotide forming an intron loop and the 3′-OH end of the cleaved exon reacts with the 5′ end of the 3′ exon. This causes the two previously separated exons to join and the intron to be released in the form of a lariat [2]. The two joined exons form a continuous coding sequence and the intron is degraded.

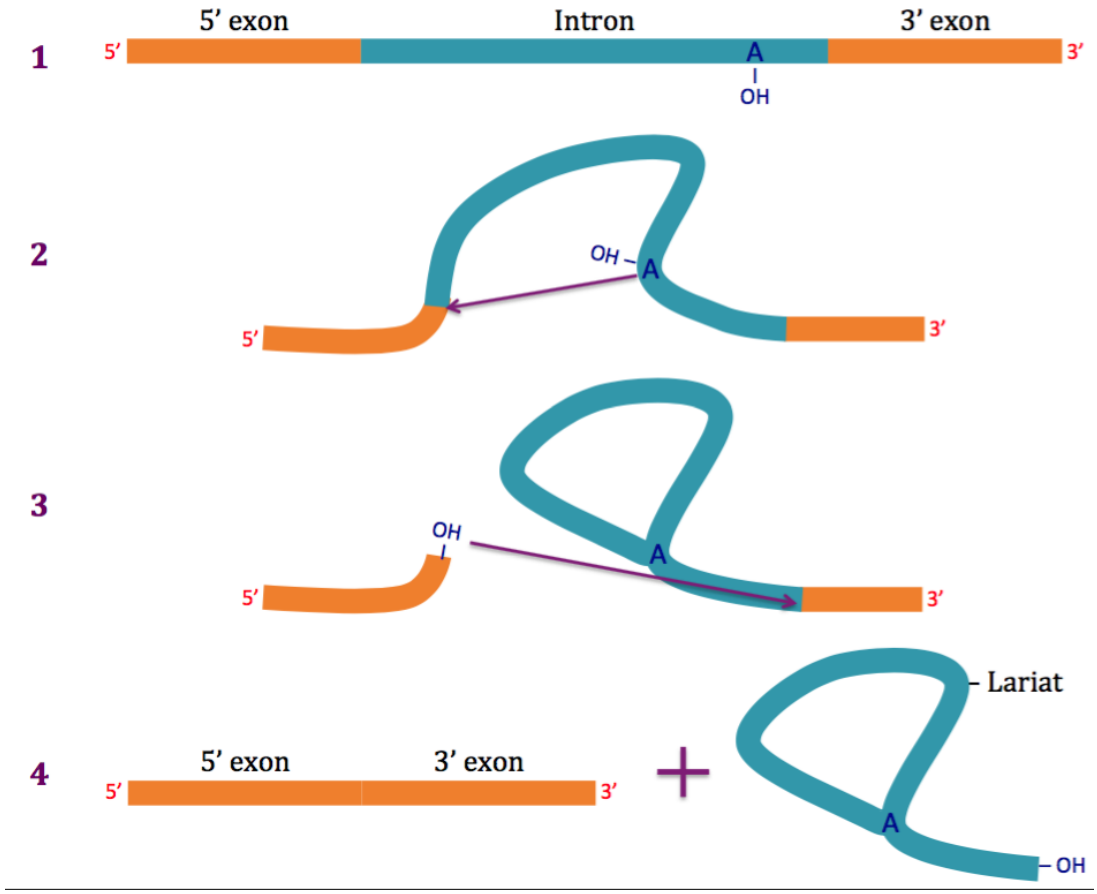

Figure 1.2 – A simplified pre-mRNA splicing reaction [2]. 1) The splicing reaction involves the 5′ exon, the intron with the internal branch point adenosine and the 3′ exon. 2) The branch point adenosine in the intron attacks the 5′ splice site of the exon and cleaves the sugar-phosphate backbone at this site. 3) The 5′ end of the intron covalently binds the branch point adenosine, thereby forming a loop and the 3′-OH end of the cleaved exon reacts with the 5′ end of the 3′ exon. 4) This causes the joining of the two exons and the release of the intron in the form of a lariat.

1.1.2.3.1. Primary Splicing Signals

The primary splicing signals consist of three highly conserved sequences, namely the 5′ splice site (5′ ss), 3′ splice site (3′ ss) and branch point. The 5′ ss and 3′ ss are located at the intron/exon junction and the branch point is located approximately 15-50 nucleotides upstream of the 3′ ss in the intron before the polypyrimidine tract (Figure 1.3) [10]. The 5′ ss is a sequence element consisting of 9 nucleotides where the GU dinucleotide designates the beginning of the intron [11] while the 3′ ss contains an invariant AG dinucleotide which designates the end of the intron [12]. These sequence elements are fundamental for the recruitment of *trans*-acting regulatory elements that catalyse the splicing reaction.

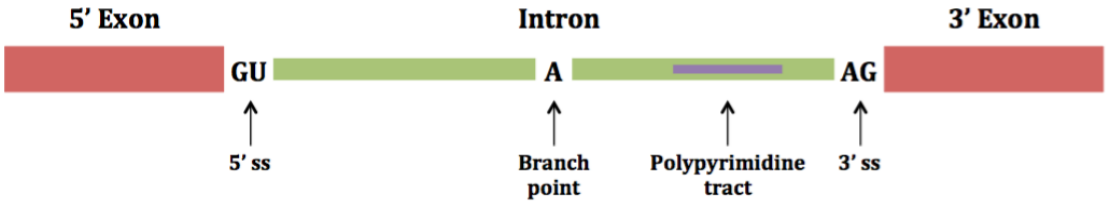

Figure 1.3 – The location of the primary splicing signals in the pre-mRNA [13]. GU and AG nucleotides designate the location of the 5′ ss and the 3′ ss, respectively. The adenine residue in the intron designates the branch point and downstream from this is the location of the polypyrimidine tract.

1.1.2.3.2. *Cis*-Acting Regulatory Elements

Cis-acting regulatory elements are sequence elements contained in the pre-mRNA that function to recruit *trans*-acting factors and to increase the accuracy of the splicing reaction [10]. Sequences that function to enhance splicing are known as exonic splicing enhancers (ESE) or intronic splicing enhancers (ISE), while those that function to silence splicing are known as exonic splicing silencers (ESS) or intronic splicing silencers (ISS), depending on where in the transcript they are located [14]. These sequences are not always clearly defined (do not have distinct consensus sequences) and often have overlapping functions [14].

1.1.2.3.3. *Trans*-Acting Regulatory Elements

Trans-acting regulatory elements are the proteins and ribonucleoproteins (RNPs) that are recruited by, and bind to the *cis*-acting factors in the pre-mRNA to catalyse the splicing reaction [10]. Five ribonucleoprotein (RNP) subunits and a large number of protein cofactors make up a dynamic macromolecular complex, known as the spliceosome [15]. This complex is responsible for catalysing the splicing reaction as it sequentially becomes assembled on the pre-mRNA [15, 16]. The sequential assembly of the spliceosome and how it accomplishes the splicing reaction is explained in the section below and is illustrated in Figure 1.4.

The 5′ ss is recognised by the U1 small nuclear ribonucleoprotein (snRNP), and once this factor binds (via nucleobase complementarity) to the mRNA at this point, the early complex (complex E) of the spliceosome is formed [10]. The formation of this complex is not dependent on ATP, and the interaction

of the 5′ ss with the U1 snRNP is weak but is stabilised by protein cofactors such as serine-arginine (SR) proteins [17, 18] and the cap-binding complex [19]. The 3′ ss is recognised and bound by the U2 snRNP as well as by splicing factor 1 (SF1) and U2 auxiliary factors (U2AFs), additional components of complex E [10]. The U2 snRNP then recognises specific sequences surrounding the branch point (adenine nucleotide) and interacts with the U1 snRNP, forming the pre-spliceosomal complex (complex A), which spans the intron [10]. Once complex A is formed, a pre-assembled tri-snRNP, consisting of U4-, U5- and U6-snRNPs, becomes recruited, and through a reaction catalysed by DExD/H helicase and Pre-mRNA-splicing ATP-dependent RNA helicase (Prp) 28, complex B is formed [10]. This complex B must, however, undergo a number of conformational and compositional changes, controlled by Brr2, 114kDa U5, Snu114 and Prp2, to become catalytically active [10]. Active complex B undergoes rearrangements that form the U2-U6 snRNP structure, responsible for catalysing the splicing reaction [20]. Active complex B then completes the first catalytic step in splicing, the formation of complex C, which contains the free exon 1 and the intron-exon 2 lariat intermediate [10]. After further active rearrangements in complex C, the second catalytic step of splicing (dependent on Prp8, Prp16 and Slu7) is completed, resulting in the formation of a post-spliceosomal complex, which contains the lariat intron and the spliced exons [10]. The U2, U5 and U6 snRNPs are released and these elements, as well as the lariat intron, are recycled.

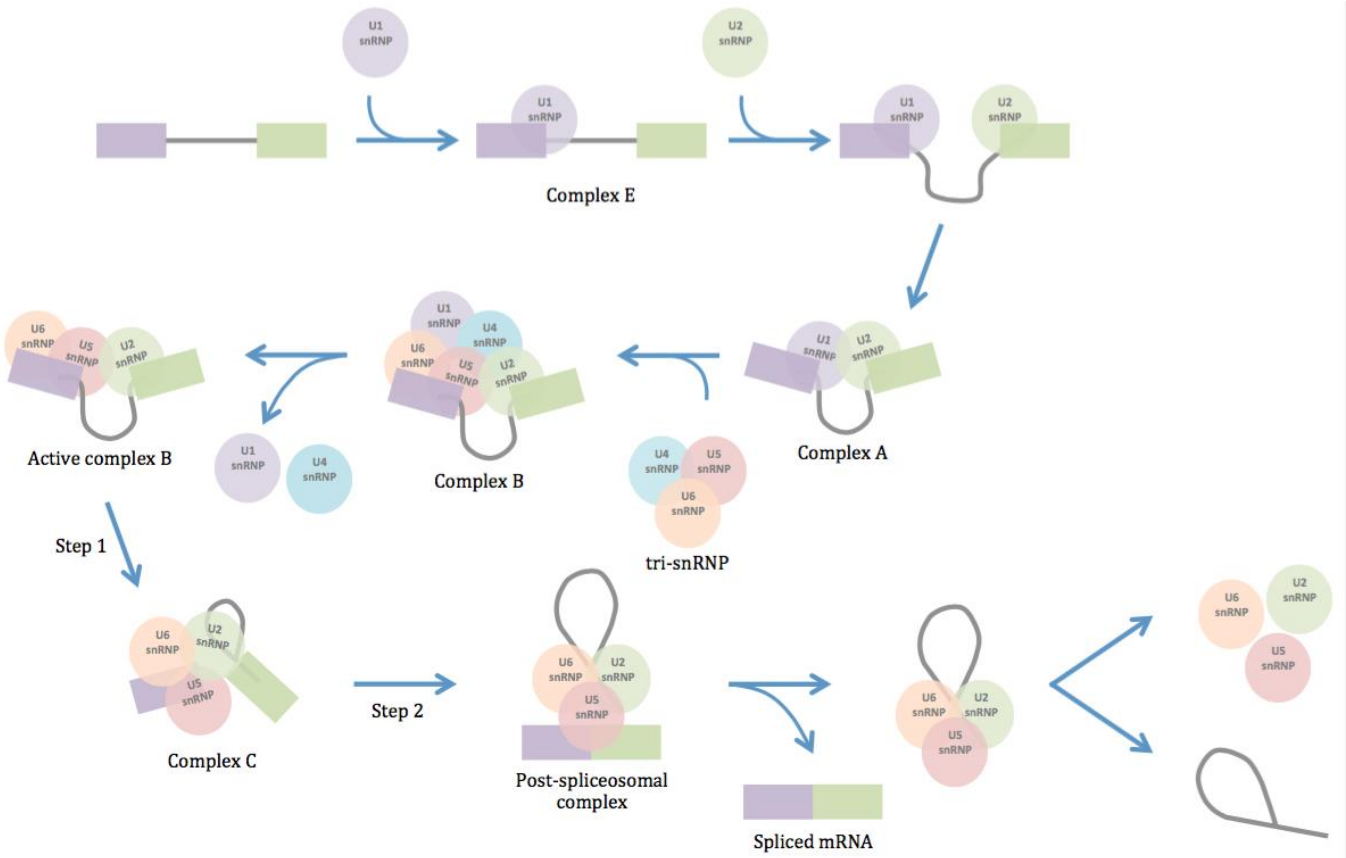

Figure 1.4 – The assembly of spliceosomal elements on pre-mRNA to achieve splicing [10]. Splicing of pre-mRNA is dependent on the activity of a number of components that assemble on the transcript through a series of steps. The binding of the U1-snRNP to the 5′ ss forms complex E and the U2-snRNP then binds the 3′ ss and interacts with the U1-snRNP, forming complex A. The addition of the U4-, U5- and U6-snRNPs (the tri-snRNP) to complex A forms complex B, which becomes activated through conformational and compositional changes. Active complex B catalyses the first step in splicing and forms complex C, which catalyses the second step in splicing and results in the formation of the post-spliceosomal complex. This complex releases the spliced exons as well as the lariat intron bound by the U2-, U5- and U6 snRNPs. The lariat intron and snRNPs are finally recycled.

The assembly of the major splicing machinery is reversible, and this observation in conjunction with the various catalytic steps involved in this process is strongly suggestive of the presence of proofreading in the splicing reaction [21] and further indicates the stringent control of splicing in the cell.

Alternative splicing is an additional level of complexity in this form of post-transcriptional processing and will be further discussed in sections to follow as it forms an integral part of the hypothesis of this study.

1.1.2.4. Export of mRNA From the Nucleus to the Cytoplasm

Once the synthesised pre-mRNA has been post-transcriptionally processed (5′ capping, 3′ polyadenylation and splicing), the resulting mRNA must be exported from the nucleus to the cytoplasm before it can be translated into protein [22]. The transport of mRNA between the nucleus and the cytoplasm occurs through macromolecular complexes called nuclear pore complexes (NPC) as these complexes connect the nuclear and cytoplasmic cellular compartments [23]. During the pre-mRNA processing steps, a number of RNA-binding and RNA-modifying proteins, called mature messenger ribonucleoproteins (mRNPs), become bound to the transcript [23]. When bound to the mRNA, these mRNPs diffuse from the transcription site in the nucleus to the NPC where they interact with the components of the complex [23]. The mRNA then moves through the NPC and is finally released into the cytoplasm [23]. Certain mRNPs are removed from the mRNA while it moves through the NPC while others are removed upon arrival of the mRNA in the cytoplasm [23].

1.1.3. Translation

Once the mRNA has been exported to the cytoplasm, translation can occur. This is the process by which the information contained in the mRNA transcript is decoded and used to synthesise proteins (macromolecules consisting of amino acids). Each successive group of 3 mRNA nucleotides, called a codon, hold the potential to signal the translational start site, code for one of the 20 amino acids commonly found in proteins or signal the termination of translation [2]. Ribosomes and transfer RNA (tRNA) molecules are two of the many factors involved in translation and have integral roles in this process. Ribosomes assemble around the mRNA, non-specifically bind codons and move along the

transcript [2]. tRNA molecules contain anticodon sequences that pair complementarily with the codon on the mRNA and bind the specific amino acid coded by the codon [2]. Translation is initiated when the ribosomal complex assembles around the mRNA, binds a codon and a tRNA molecule binds to this codon through nucleobase complementarity [2]. The ribosome then moves in a 5′ to 3′ direction to the next codon and binds the tRNA specific to that codon [2]. The first tRNA then transfers its amino acid to the second tRNAs amino acid, thus initiating the start of an amino acid chain, and this process is repeated until the ribosome reaches the stop codon [2]. Once the stop codon is reached, the ribosome releases both the mRNA transcript and the amino acid chain [2]. For the amino acid chain to be functional within the cell, it must form a unique three-dimensional structure, and this is accomplished through a folding process that begins during, and is completed after, synthesis [2]. After folding, some proteins are post-translationally modified through the action of protein-modifying enzymes, by the binding of co-factors or through their association with additional protein subunits [2]. Functional proteins are essential to accomplishing every molecular activity [2].

1.2. Alternative Splicing

As a result of splicing, only a few sequences from the primary RNA transcript are joined together to form mature mRNA [24]. There was, however, an additional level of complexity added to this process when it was discovered that most pre-mRNAs contained exons that could be either included in the final transcript or removed from it [24]. This decision of exon inclusion or removal is known as alternative splicing [24]. Alternative splicing functions to increase the diversity of mRNA transcribed from the genome by differentially combining selective exons contained in the pre-mRNA [24]. The pattern of alternative splicing can be altered in response to physiological conditions thus allowing the organism to respond to environmental changes [24]. There are currently seven recognised modes of alternative splicing, namely exon inclusion/skipping (Figure 1.5 a), an alternative 3′ ss (Figure 1.5 b), an alternative 5′ ss (Figure 1.5 c), mutually exclusive exons (Figure 1.5 d), intron retention (Figure 1.5 e), alternative promoters (Figure 1.5 f) and alternative polyadenylation (Figure 1.5 g) [25]. These modes of alternative splicing vary both in frequency and complexity, but it must be stressed that the alternative splicing pattern is not always a predetermined decision as it can vary in response to a number of environmental elements [26].

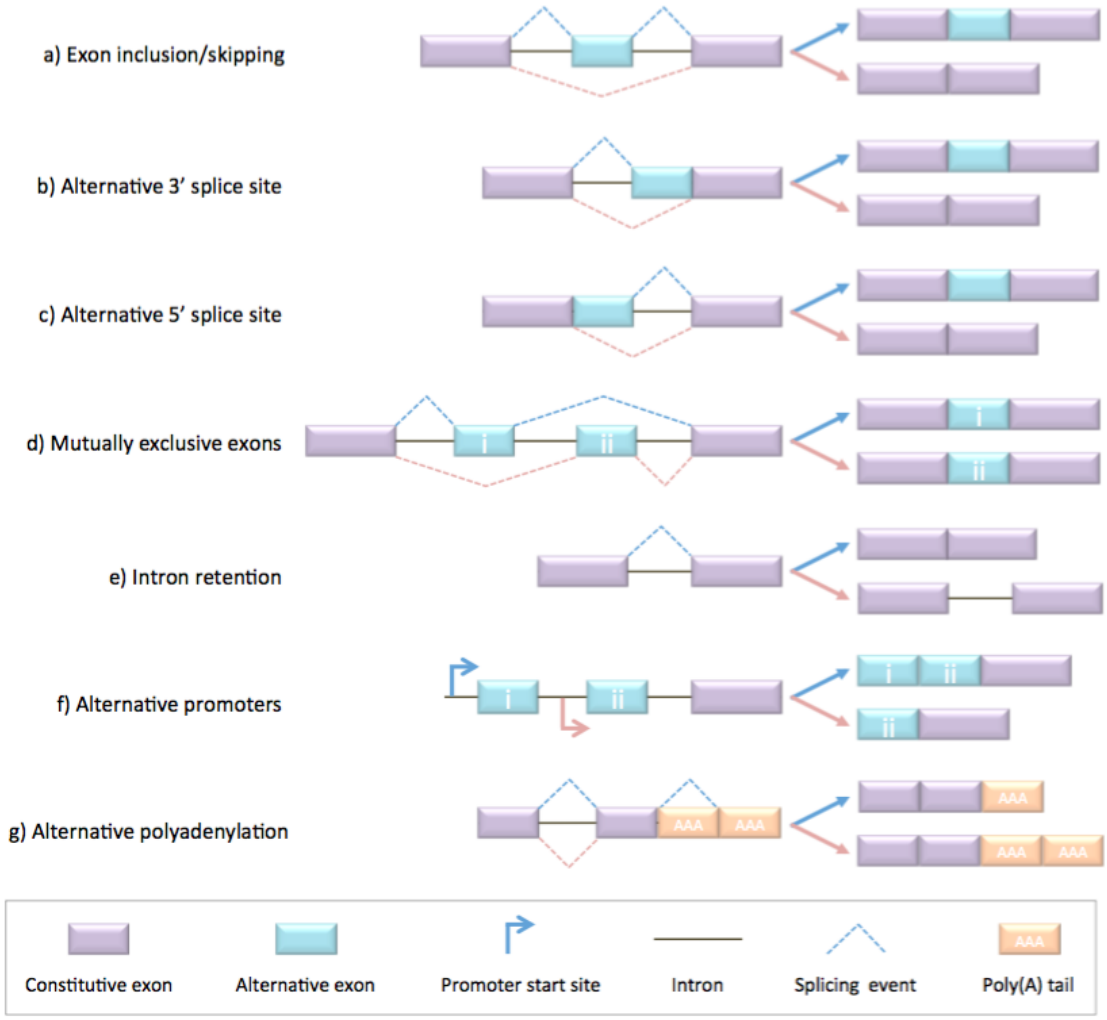

Figure 1.5 – Alternative splicing events describing the possible outcomes of each [25]. a) Exon inclusion/skipping results in the presence or absence of a particular exon in the final transcript. b) Alternative 3′ ss involves the usage of differential 3′ splice sites thereby altering the final transcript. c) Alternative 5′ ss involves the usage of differential 5′ splice sites thereby altering the final transcript. d) Mutually exclusive exons involve the exclusive inclusion of only one of two exons in the final transcript. e) Intron retention involves either the presence or absence of the intron sequence in the final transcript. f) Alternative promoters involve the use of different promoters thereby altering the final transcript g) Alternative polyadenylation causes differences in the length of the poly(A) tail of the final transcript.

1.2.1. Regulation of Alternative Splicing

Alternative splicing holds major importance in the control of protein expression and the increase of protein complexity from a limited genome [27, 28]. The control and regulation of the spliceosome as well as the interplay of *cis*- and *trans*-acting factors facilitates the control of alternative splicing. These control mechanisms will be further discussed in this section.

Regulatory sequence elements within intronic and exonic regions of the pre-mRNA can either stimulate (splicing enhancers) or disrupt (splicing silencers) spliceosomal assembly, which either promotes exon inclusion or causes exon skipping, respectively [26, 29]. In addition, the recruitment of the spliceosome, and thus splicing stimulation/silencing is also dependent on the strength or weakness of the 5′ ss and the 3′ ss [26, 29]. The majority of the regulatory sequence elements present in the pre-mRNA transcript act as binding sites for non-snRNP regulatory proteins, however, some possess the ability to alter splice site recognition through the generation of secondary RNA structures [29-32].

1.2.1.1. Exonic Elements

A family of proteins containing an RNA-binding domain as well as an Arginine-Serine dipeptide rich region (RS domain), known as SR proteins, bind ESEs and bring about splicing enhancement [33]. SR proteins are able to associate with spliceosomal factors important for splice site recognition (e.g. U1 snRNP and U2AF) [26, 33]. When bound to the ESEs, these spliceosomal factors become recruited to the exon to be spliced and are able to proceed with further spliceosomal assembly [26, 33]. In addition, the RS domains of SR proteins provide stability for the interaction of U2 snRNP and the branch point adenine, and in this way, further assist in enhancing splicing [34]. The interaction of the ESEs with the SR family of proteins is often weak, and thus can be blocked by proteins that regulate exon inclusion (e.g. heterogeneous nuclear ribonucleoproteins), further adding to the complexity of this mechanism [33].

ESSs and ISSs repress exon inclusion through the recruitment and binding of the heterogeneous nuclear ribonucleoprotein (hnRNP) family of proteins [33]. When bound to the ESSs or ISSs, these proteins sterically hinder spliceosomal binding to overlapping sequences, thereby inhibiting splicing and promoting exon inclusion [33].

Even though the SR and hnRNP protein families accomplish identified roles in splicing enhancement and repression, respectively, they are by no means the only proteins involved in this type of splicing regulation. Furthermore, a number of proteins that function similarly to SR proteins and hnRNPs, but are

not classified in these families, are involved in alternative splicing regulation [33].

1.2.1.2. Intronic Elements

Enhancing and silencing sequence elements located in the intronic regions of the pre-mRNA as well as the proteins that mediate their effects are not as well characterised as those located in exonic regions [33]. Intronic regulatory protein binding sites are located in the polypyrimidine tract, at the 5′ ss, adjacent to the branch point adenine as well as in sequences far away from the regulated exon [33]. Like ESEs, the function of some ISEs is dependent on SR protein binding [35, 36], while others do not bind this family of proteins [33]. A uridine-rich sequence found directly downstream from the 5′ ss, activates this splice site through the binding of the T-Cell-Restricted Intracellular Antigen-1 (TIA-1) protein [37, 38], which prompts U1 snRNP binding to the 5′ ss, thus initiating the splicing reaction [37]. Some members of the CUGBP, Elav-Like Family Member 1 (CELF1) family of proteins activate splicing by binding to intron enhancer elements [33]. The 5′-UGCAUG-3′ sequence is a common ISE element especially when duplicated [39-41], however, the protein mediating its effects is not definitively known [33]. These sequence duplications are often discovered downstream of the activated exon but have also been found >500 nucleotides from this exon [41]. The downstream control sequence (DCS) is made up of the 5′-GGGGG-3′ element (necessary for complete enhancer activity), the 5′-CUCUCU-3′ element (involved in splicing repression) and the 5′-UGCAUG-3′ element (essential for enhancer activity) [40, 42]. In addition, the DCS controls splicing through the assembly of a large RNP complex [43]. hnRNP H and F bind the 5′-GGGGG-3′ element, the polypyrimidine tract binding protein (PTB) binds the 5′-CUCUCU-3′ element and the KH-type Splicing Regulatory Protein (KSRP) binds the 5′-UGCAUG-3′ element [33]. The exact mechanisms by which these proteins affect splicing are not well defined.

The silencing of splicing can also be achieved through the action of regulatory elements located in the intronic sequences. These sequences are bound by SR proteins and hnRNP A1 to bring about splicing repression [33].

1.2.2. Splicing and Alternative Splicing in Human Disease

1.2.2.1. *Cis*-Acting Mutations

Cis-acting elements are components of the splicing code contained in the pre-mRNA sequence that function to recruit sequence-specific RNA binding factors that either suppress or induce splicing [44]. Mutations in these elements can be responsible for aberrant splicing.

Aberrant splicing most commonly leads to disease because of mutations found in the core splicing consensus sequences [12]. Mutations of the invariant sequences (GU or AG dinucleotides of the 5′ ss or the 3′ ss, respectively) can prevent the use of the appropriate splice site or cause the use of otherwise cryptic splice sites (sequences not normally used for splicing) [45], thereby causing improper intron skipping/retention [14, 46]. Mutations in non-invariant consensus sequences can reduce the strength of the splice site, causing either the partial or complete inhibition of its use [12]. Mutations in these sequences can also cause the formation of new splice sites that could lead to disease when used, and while branch point sequence mutations are less common, they too can impair splicing [12]. Aberrant alternative splicing has the potential to cause alterations in specific amino acid sequences, leading to modifications in the structure and potentially also the function of the proteins they collectively produce, thereby increasing the probability of disease induction [12]. Altered splicing can also cause changes in the mRNA reading frame (known as frame shifts), which could introduce premature stop codons into the transcript. In most cases, the introduction of these premature stop codons leads to a loss of protein function as these transcripts often become degraded through the nonsense-mediated decay (NMD) pathway [47]. Mutations in sequences responsible for either enhancing (ISEs and ESEs) or silencing (ISSs and ESSs) splicing are important for splicing regulation, and mutations in these elements can result in aberrant splicing, leading to disease [48]. This phenomenon is attributed as the causative factor in the development of Frontotemporal Dementia and Parkinsonism [49].

1.2.2.2. *Trans*-Acting Mutations

Trans-acting mutations refer to mutations in both spliceosomal and non-spliceosomal components responsible for the regulation of alternative splicing [50]. These *trans*-elements (proteins and snRNPs) bind *cis*-elements to enable splicing and alternative splicing.

Mutations causing increased activity of PRPF3, PRPF8, PRPF31 and SNRNP200, factors imperative for the proper assembly of the major spliceosome, are associated with autosomal dominant retinitis pigmentosa [50]. Additionally, mutations in the gene encoding *U4atac* (an RNA component of the minor spliceosome snRNP) causes Taybi-Linder syndrome (TALS), a disease characterised by growth retardation, abnormal bone morphology, brain malformation and mortality by the age of three [51, 52]. Whole genome or exome sequencing of a number of diseases e.g. myeloid neoplastic syndrome, acute myeloid leukaemia, chronic myelomonocytic leukaemia and chronic lymphocytic leukaemia, compared to matched normal controls, revealed somatic mutations in genes that encode components of the spliceosome [53-58].

Aberrant splicing and alternative splicing have also been implicated in cancer formation and progression and this will be discussed in upcoming sections.

1.3. Cancer

Cancer is a term used to describe a group of diseases in which cells in the body divide uncontrollably and spread to other tissues. In the body, cell growth and division are normal and necessary processes, however, when these cells divide uncontrollably, tumours are formed. Tumours that do not spread into surrounding tissues are called benign while those with the potential to invade nearby tissues are known as malignant.

In 2014, the World Health Organisation (WHO) reported that there were 14 million new cancer cases and 8.2 million cancer-related deaths in 2012, with the number of new cases expected to rise by 70% over the next 20 years [59]. The incidence rate of cancer is higher in more economically developed countries compared to developing countries; however, the mortality rates are higher in the latter compared to the former [59]. Cancer is the 9th highest contributor to the disease burden of South Africa [60], thus researching the progression of the disease is necessary.

1.3.1. Hallmarks of Cancer

In 2000, Hanahan and Weinberg suggested that all cancers share six common features (also known as hallmarks) that assist in promoting their progression [61] and eleven years later, the authors suggested two additional hallmarks and two enabling characteristics of the disease [3]. The hallmarks and enabling characteristics (depicted in Figure 1.6) were introduced as a means to better understand both the diversity and the complexity of cancers [61].

Sustaining proliferative signalling is the first hallmark of cancer, describing its ability to deregulate expression of the growth signals responsible for controlling cell growth and division, thereby allowing for the maintenance of chronic proliferation [3]. Evading growth suppressors is the second hallmark of cancer describing the ability of cancer cells to bypass the effect of certain tumour suppressive genes, which function in limiting cell growth and division, thereby regulating cell/tissue growth [3]. Activating invasion and metastasis collectively make up the third hallmark of cancer and describes the ability of cancer cells to disseminate from the primary tumour, travel to nearby or distant tissues or organs and initiate secondary tumours [3]. Enabling replicative immortality is

the fourth hallmark of cancer describing the ability of individual cancer cells to replicate unlimitedly, in stark contrast to the limited replicative potential of normal cells [3]. Inducing angiogenesis is the fifth hallmark of cancer describing the ability of these cancer cells to sustain blood vessel formation, providing the tumour with a continuous supply of oxygen and nutrients as well as continuous removal of metabolic waste and carbon dioxide [3]. Resisting cell death is the sixth hallmark of cancer describing the ability of cancer cells to resist apoptosis (programmed cell death), thus allowing for their continued propagation [3]. Reprogramming energy metabolism is the first emerging hallmark of cancer and describes the ability of these cells to preferentially metabolise energy by glycolysis, even in the presence of oxygen, leading to aerobic glycolysis, which aids cell growth and division [3]. Evading immune destruction is the second emerging hallmark of cancer and describes the ability of these cells to either evade detection by the immune system or limit the level of immunological killing, thus avoiding eradication [3]. Tumour-promoting inflammation is the first enabling characteristic of cancer and describes the ability of tumours to induce inflammation [3]. An increased presence of several molecules such as growth factors, survival factors and proangiogenic factors, which could perpetuate cancer forming capabilities of a number of hallmarks, are found in these regions of inflammation [3]. Finally, genome stability and mutation is the second enabling characteristic, describing cancer's increased sensitivity to mutagenic agents through the failure of one or more of the genomic maintenance machinery [3]. This increased sensitivity causes amplified rates of mutation that aid in orchestrating tumorigenesis in these cells [62, 63].

While these hallmarks and enabling characteristics aid in the conceptualisation of cancer and may provide convenient avenues for research and therapy, it must be noted that several additional features of cancer progression could potentially be added to the list.

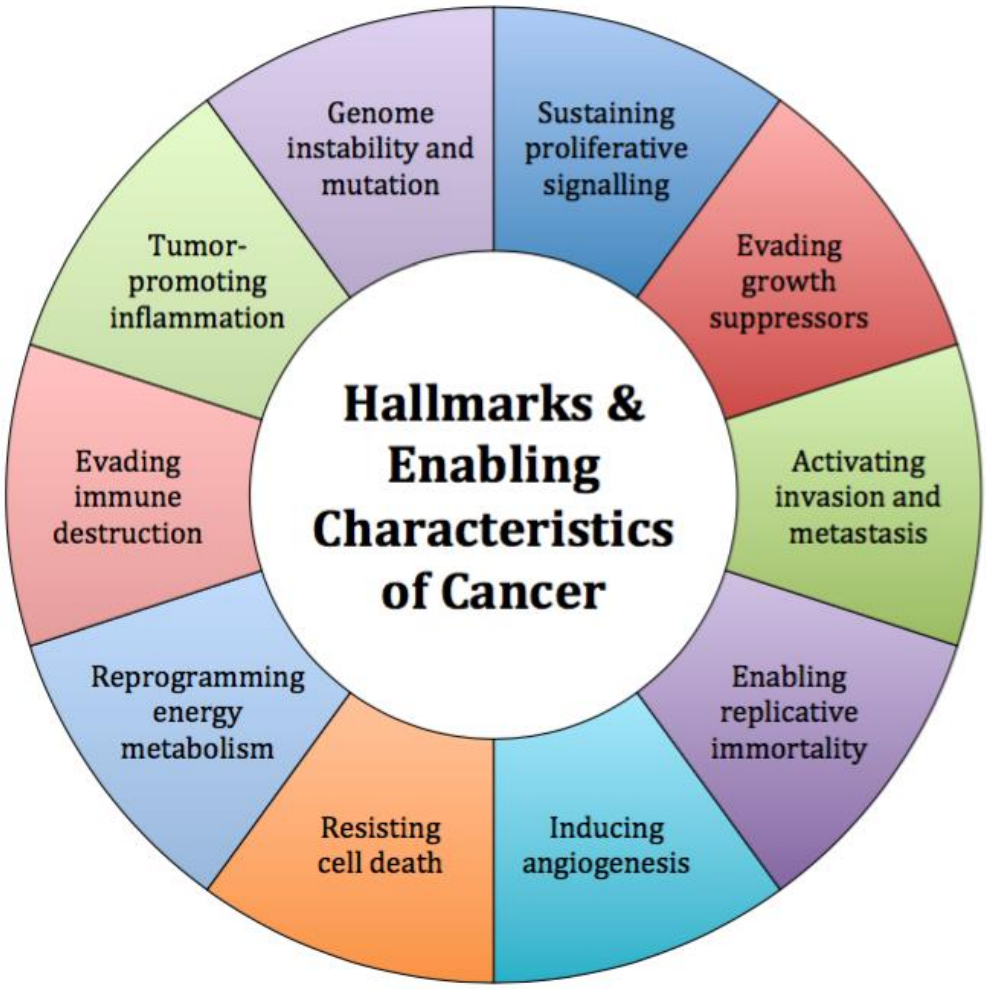

Figure 1.6 – Hallmarks and enabling characteristics of cancer progression. The eight hallmarks and two enabling characteristics of cancer described by Hanahan and Weinberg in 2000 [61] and 2011 [3].

1.3.2. Epithelial-to-Mesenchymal Transition and its Role in Cancer

Epithelial-to-mesenchymal transition (EMT) is a biological process in the cell where polarised epithelial cells, which usually interact with the basement membrane, undergo a number of biochemical changes and ultimately assume a mesenchymal phenotype [64]. In this mesenchymal phenotype, cells have an enhanced migratory capacity, an invasive nature, an increased resistance to apoptosis and an increased production of extracellular matrix (ECM) components [65]. Once the underlying basement membrane has been degraded and the mesenchymal cell is formed, EMT is complete, and the cell can then migrate away from the epithelial layer in which it originated [64]. The biochemical changes that take place to convert an epithelial cell to a

mesenchymal one include the activation of transcription factors, the expression of specific cell-surface proteins, the expression and reorganisation of cytoskeletal proteins, the production of enzymes that bring about ECM degradation as well as changes in the expression of specific microRNAs [64]. This process is reversible, i.e. mesenchymal cells can revert to epithelial cells. This process is known as the mesenchymal-to-epithelial transition (MET) and is distinct from neoplastic transformation [65].

Epithelial-to-mesenchymal transitions are observed in three specific biological settings (known as types 1-3), and facilitate different functional consequences [64]. Type-1 EMT is functional during embryonic implantation, embryogenesis and organ development while type-2 EMT is associated with tissue regeneration and organ fibrosis [64]. Type-3 EMT is associated with cancer progression and metastasis. Cells that undergo type-3 EMT are typically found at the invasive front of primary tumours and are thought to be the cells that will eventually intravasate into the blood stream, be transported through the circulatory system, extravasate out of the blood stream, form micrometastases and ultimately colonise to establish secondary tumours [66-68]. In a number of carcinomas, signalling molecules that induce EMT, e.g. hepatocyte growth factor (HGF), epidermal growth factor (EGF), platelet-derived growth factor (PDGF) and transforming growth factor beta (TGF-β) are thought to functionally activate EMT-inducing transcription factors (e.g. Snail, Slug, ZEB1, Twist, Goosecoid and FOXC2) in cancer cells [66, 69-73]. Once these transcription factors become expressed and are post-translationally activated, they function pleiotropically to accomplish the EMT programme. The internal cellular changes brought about by the EMT programme are accomplished through the action of signal-transducing proteins (e.g. ERK, MAPK, PI3K, Akt, Smads, RhoB, β-catenin, LEF, Ras and c-Fos), as well as cell surface proteins (such as the β4 integrins, the α5β1 integrin and the αVβ6 integrin) [74]. EMT activation is additionally facilitated by the disruption of cell-cell adherens/junctions as well as the cell-ECM adhesions mediated by integrins [75].

It is clear that EMT is a very involved and tightly controlled process. In particular, type-3 EMT and its regulation are of particular interest in tumour growth and cancer progression.

1.3.3. Signal Transduction Pathways and Cancer

Signal transduction pathways involve numerous proteins that function to transfer extracellular signals via transmembrane receptors to the cellular interior. These intracellular signals create specific responses inside the cell e.g. metabolism, growth, differentiation etc. [2]. There are many signal transduction pathways functioning in a cell, each with certain downstream cellular effects, although certain proteins can mediate numerous pathways [76]. The aberrant control of, and mutations in, proteins mediating these signal transduction pathways is often observed in cancers because of their fundamental role in the development of the cell [77].

The findings of the research to be presented and discussed focuses heavily on the Wnt signalling pathway, and therefore this signal transduction pathway will be elaborated on in the following section.

1.3.3.1. Wnt Pathway

Extracellular Wnt signals can stimulate the canonical Wnt pathway, the non-canonical planar cell polarity pathway or the non-canonical Wnt/Ca^{2+} pathway [78] (illustrated in Figure 1.7). Wnt proteins regulate cell fate determination, polarity, motility, primary axis formation, organogenesis and stem cell renewal [78], and the aberrant signalling of these proteins causes numerous diseases, including type II diabetes [79] and cancers of the colon, skin and breast [80].

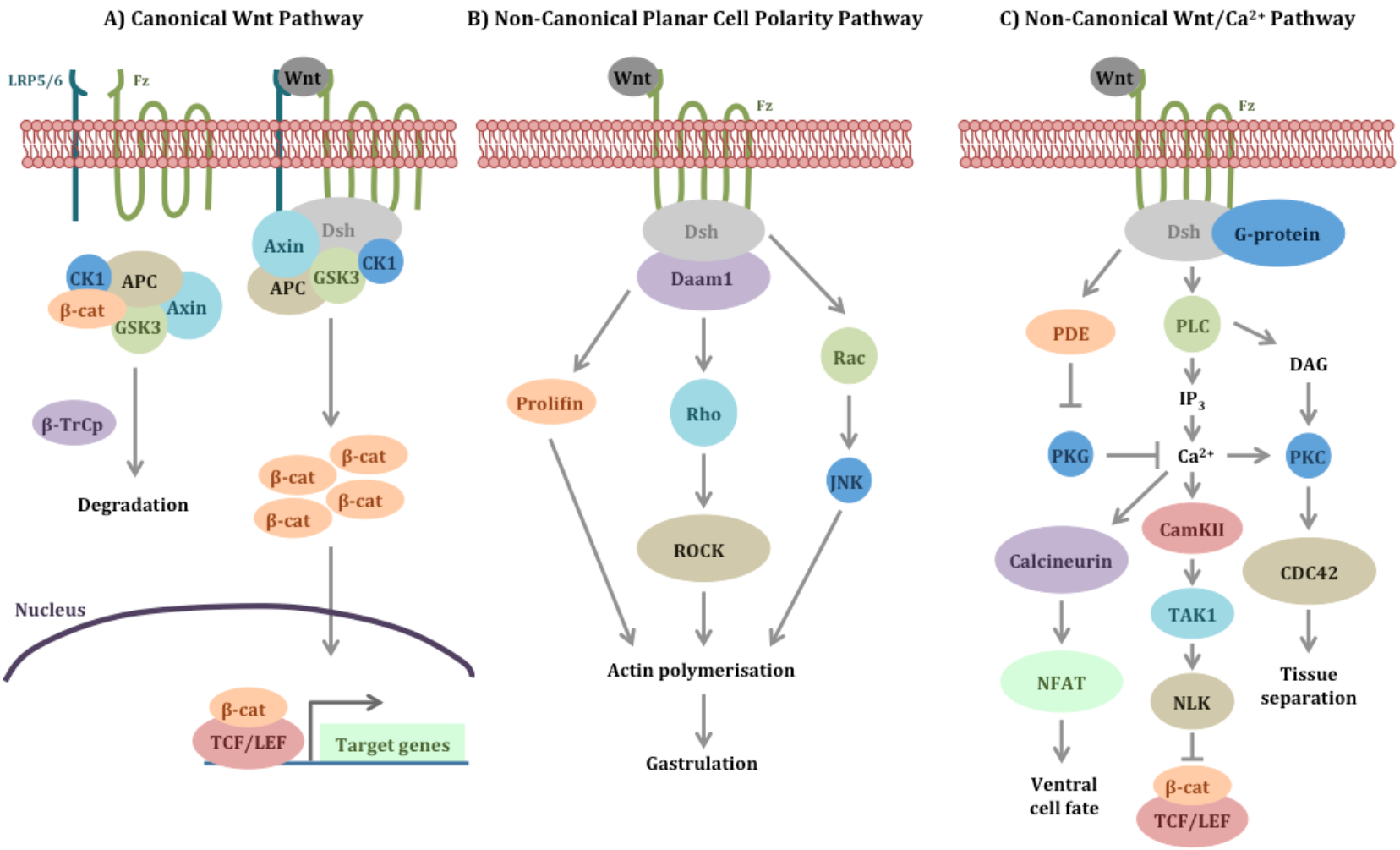

Figure 1.7 – The Wnt signalling pathway. This pathway consists of three major signalling branches – A) The canonical Wnt pathway in the absence and presence of Wnt B) The non-canonical planar cell polarity pathway and C) The non-canonical Wnt/Ca^{2+} pathway.

1.3.3.1.1. Canonical Wnt Pathway

Refer to Figure 1.7 A. A protein complex consisting of Axin, Adenomatous polyposis coli (APC), Glycogen Synthase Kinase 3 Beta (GSK3-β), Casein Kinase-1 (CK1) and β-catenin is present in the cytosol when Wnt ligands are either absent or not bound to the lipoprotein receptor-related protein (LRP)-5/6 and Frizzled (Fz) receptors [78]. In this complex, CK1 and GSK3-β dually phosphorylate β-catenin, thereby targeting it for degradation [78]. This degradation of β-catenin is accomplished through the activity of the proteasomal machinery, mediated by the beta-transducin repeat containing E3 Ubiquitin Ligase (β-TrCP) [78]. When Wnt ligands are present and bind the LRP5/6 and Fz receptors, LRP6 becomes dually phosphorylated by CK1 and GSK3-β, allowing for the translocation of the Axin, APC, GSK3-β, and CK1 protein complex from the cytosol to the plasma membrane [78]. Axin then becomes bound to the phosphorylated LRP5/6 receptor and Dishevelled (Dsh) is recruited and binds to the Fz receptor [78]. The formation of this protein complex at the plasma membrane stabilises cytosolic β-catenin, and once stable, it translocates to the nucleus [78]. In the nucleus, β-catenin forms protein complexes with members of the LEF/TCF family of transcription factors, and mediates the transcription of various target genes [78].

1.3.3.1.2. Non-canonical Planar Cell Polarity Pathway

In this pathway, the exclusive binding of Wnt ligands to the Fz receptor activates Dsh, which binds intracellularly to the Fz receptor at the plasma membrane [78].

Refer to Figure 1.7 B. Through the activity of Dishevelled Associated Activator Of Morphogenesis 1 (Daam1), Dsh activates Rho, which in turn activates Rho kinase (ROCK) [78]. Also through the activity of Daam1, Dsh activates the actin binding protein, Profilin [78]. Without Daam1 activity, Dsh mediates the activation of Ras-Related C3 Botulinum Toxin Substrate 1 (Rac), which activates c-Jun N-terminal kinase (JNK) [78]. ROCK, Profilin and JNK signalling become integrated and this results in the cytoskeletal alterations necessary for cell polarisation and cell motility during the process of gastrulation [78].

1.3.3.1.3. Non-canonical Wnt/Ca^{2+} Pathway

Refer to Figure 1.7 C. In this pathway, Wnt ligands bind to the Fz receptor, mediating the activation of Dsh via the activation of G-proteins. Dsh then activates a phosphodiesterase (PDE), which inhibits PKG, and this inhibition of PKG causes the inhibition of Ca^{2+} release [78]. Alternatively, activated Dsh can activate Inositol trisphosphate (IP3) through Phospholipase C (PLC), leading to the intracellular release of Ca^{2+}, which activates both calcineurin and the Ca^{2+}/calmodulin-dependent protein kinase II (CaMKII) [78]. Calcineurin activates the Nuclear factor of activated T-cells (NFAT) and brings about the regulation of ventral cell fates while CamK11 activates both the Transforming Growth Factor-Beta-Activated Kinase (TAK) 1 and the Nemo-Like Kinase (NLK) [78]. Activation of TAK and NLK inhibits the binding of β-catenin to members of the TCF family, thus negatively regulating the formation of the dorsal axis [78]. Additionally, Dsh activation of PLC causes the activation of Dystroglycan (DAG), which in turn activates the Cell division control protein 42 homolog (CDC42), which is responsible for the mediation of tissue separation and cell movement in the process of gastrulation [78].

1.3.3.1.4. Regulators of Wnt Secretion and Binding

Wnt proteins become glycosylated (addition of a carbohydrate) and palmitoylated (addition of fatty acids) prior to transportation to and release into the extracellular environment [81, 82]. After secretion into the extracellular environment, heparin sulphate proteoglycans (HSPGs) are able to bind Wnt proteins [78]. The binding of HSPGs to Wnt proteins stabilises them, limiting their diffusion and modulating their signalling abilities [83]. Additionally, secreted proteins such as the Dickkopf (Dkk) proteins, the Wnt-inhibitory factors (WIF) and the soluble Frizzled-related proteins (SFRP) bind to Wnt proteins, preventing their interaction with the Fz or LRP5/6 receptors, thus antagonising Wnt signalling.

1.3.3.1.5. Wnt Pathway in Cancer

Certain mutations that cause the constitutive activation of Wnt signalling can lead to the formation of various cancers [84]. Mutations leading to the formation of a truncated APC cause Familial Adenomatous Polyposis (FAP), a heritable

autosomal dominant disease resulting in the formation of colonic and rectal polyps [85, 86]. These polyps are caused by increased cellular proliferation resulting from the aberrant promotion of Wnt signalling, mediated by the truncated APC [84]. 90% of all colorectal cancers (CRC) are caused by mutations that activate Wnt signalling, e.g. mutations that cause the inactivation of APC or those that activate β-catenin [87]. In addition, mutations causing a loss of Axin functionality are observed in hepatocellular carcinomas [88]. The requirement of Wnt signalling for the maintenance of the stem cell compartment is evidenced by the observation that decreased TCF4 expression or Dkk overexpression causes stem cell loss in the colon crypt [89-91], and the established link between cancer and stem cells [92] further indicates a role for the Wnt pathway in colon cancer. These observances strongly suggest that aberrant Wnt signalling plays a significant role in cancer formation and progression.

1.3.4. Cancer Frequency

Among males, the most common sites of cancer diagnosis are lung, prostate, colorectum, stomach and liver while among women they are breast, colorectum, lung, cervix and stomach [59]. Globally, female breast cancer is the second most commonly diagnosed cancer, highlighting the frequency of its occurrence as well as the need for further research into novel treatment options.

1.3.5. Breast Cancer

Since 2008, there has been an alarmingly high increase in the incidence and mortality rates of breast cancer (20% and 14%, respectively) [93]. In 2012, 57% of the incidence and 65% of breast cancer mortality occurred in less developed regions of the world [94]. This is thought to be a consequence of lifestyle changes with these regions becoming more westernised and because, in some cases, clinical advances do not adequately reach the affected women [94].

Breast cancers are commonly divided into four molecular subtypes, i.e. Luminal A, Luminal B, HER2 and Triple-negative [95]. Luminal A tumours are oestrogen receptor (ER) and/or progesterone receptor (PR) positive, human epidermal growth factor (Her) 2 negative and have a low expression of Ki67 while Luminal B tumours are ER and/or PR positive and HER2 negative or ER and/or PR positive, HER2 positive and have a high expression of Ki67 [95]. HER2

tumours are ER negative, PR negative and HER2 positive while triple-negative tumours are ER negative, PR negative and lack HER2 overexpression. These subtypes have implication on both the prognostic outcome and treatment options for this disease [95].

In this study, we looked specifically at cell lines generated from TNBCs, and therefore, this breast cancer subtype will be further reviewed in the following sections.

1.3.5.1. Triple-Negative Breast Cancer

Triple-negative breast cancer (TNBC) is a subtype of breast cancer referring to breast cancer tumours that do not express the oestrogen receptor (ER) and progesterone receptor (PR) and lack the overexpression of the human epidermal growth factor receptor (HER2) [96, 97]. 10-15% of all breast cancer cases are triple-negative [98], although TNBCs are more common among women of African ancestry compared to other ethnic origins [99, 100]. This observation was confirmed in a South African study where 20,8% of black breast cancer patients had TNBC [101].

Compared to other breast cancer subtypes, TNBCs are often more aggressive and have higher associated mortalities [102]. In addition, TNBCs are characterised by increased cell proliferation, reduced cellular differentiation, recurring copy number imbalances and, in most cases, contain mutations in the *tumour suppressor 53* (*TP53)* gene [103, 104].

Hormone and HER2 receptor-positive breast cancer tumours are considered a favourable outcome for this disease due to their responsiveness to endocrine manipulations such as tamoxifen, aromatase inhibitors or ovarian ablation [105]. The non-expression of these receptors in TNBC tumours renders these treatment options non-viable. Patients with TNBCs receive chemotherapy as a mainstay treatment [106], however, these patients often exhibit poorer outcomes after chemotherapy compared to patients with other breast cancer subtypes [107, 108]. A number of targeted therapies, such as antiangiogenic factors, Poly-(adenosine diphosphate-ribose)-polymerase inhibitors, epidermal growth factor receptor inhibitors, Src tyrosine kinase inhibitors, Mechanistic Target of Rapamycin (mTOR) inhibitors and heat shock protein 90 inhibitors, are

under investigation to potentially treat TNBCs, however, much more research into these therapies is necessary before they can potentially be implicated [109]. Since the available treatment options for TNBC are limited, potential targeted therapy research is of much interest and importance.

1.3.5.1.1. Subtypes of TNBC

The heterogeneity of TNBC adds to the complexity of this breast cancer subtype and further complicates therapeutic interventions for the disease. In 2011, Brian Lehmann and a number of additional authors used gene expression profiling to investigate these tumours and defined six distinct subtypes of TNBC based on the characteristic set of genes expressed in each subtype [110]. These subtypes were named basal-like 1 (BL1), basal-like 2 (BL2), immunomodulatory (IM), mesenchymal (M), mesenchymal stem-like (MSL) and luminal androgen receptor (LAR) [110]. BL1 TNBC tumours are genetically enriched in components involved in cell cycle and cell division pathways while tumours of the BL2 subtype have enriched gene ontologies involved in growth factor signalling in addition to glycolysis and gluconeogenesis [110]. Gene ontologies in immune cell processes are enriched in TNBC tumours of the IM subtype while those in the M subtype are enriched in pathways involved in cell motility [110]. Tumours of the MSL subtype express low levels of genes involved in cell proliferation but are enriched in genes associated with stem cells as well as mesenchymal stem cell-specific markers, LAR tumours are the most differentiated, compared to the other TNBC subtypes, and contain gene ontologies enriched in hormonally regulated pathways [110].

The authors investigated these gene expression profiles, both in TNBC tumours and in immortalised TNBC cell lines. The gene expression profiles of the tumours were used to define the six TNBC subtypes, as described above, and investigation of the gene expression profiles of 30 TNBC cell lines revealed that 27 could be categorised into the aforementioned subtypes (these are recorded in Table 1.1) [110]. This finding is particularly relevant, as it allows for the use of cell lines as models for subtype specific preclinical TNBC experiments [110].

Table 1.1 - Assignment of TNBC cell lines to subtypes [110].

TNBC subtype	Cell line
BL1	HCC2157
	HCC1599
	HCC1937
	HCC1143
	HCC3153
	MDA-MB-468
	HCC38
BL2	SUM149PT
	CAL-851
	HCC70
	HCC1806
	HDQ-P1
IM	HCC1187
	DU4475
M	BT-549
	CAL-51
	CAL-120
MSL	HS578T
	MDA-MB-157
	SUM159PT
	MDA-MB-436
	MDA-MB-231
LAR	MDA-MB-453
	SUM185PE
	HCC2185
	CAL-148
	MFM-223

1.3.6. Alternative Splicing in Cancer

Cancer cells can cause the aberrant regulation of alternative splicing and use this to their advantage – genome-wide studies have led to the discovery of cancer-specific splicing patterns [111-113]. Developmental pathways controlling proliferation, apoptosis, cellular metabolism and epithelial-to-mesenchymal transition, are all themselves controlled by proteins, some arising from genes that are alternatively spliced [114]. Aberrant regulation of alternative splicing in theses developmental pathways can become exploited by cancer cells to aid their progression.

1.3.6.1. Alternative Splicing in the Regulation of Apoptosis

Alternative splicing of a substantial number of apoptosis-related genes often results in the production of protein isoforms which either promote or prevent cell death [115]. Alternative splicing at two competing 5′ splice sites in the B-cell lymphoma (Bcl)-x exon 2 pre-mRNA gives rise to either the anti-apoptotic Bcl-x(L) isoform or the pro-apoptotic Bcl-x(s) isoform [116]. High Bcl-x(L)/Bcl-x(s) ratios are observed in a number of cancers [117-119], and the use of antisense oligonucleotides complementary to the Bcl-x(L) 5′ ss caused splicing of Bcl-x to yield the Bcl-x(s) isoform instead of the Bcl-x(L) isoform. This accomplished the induction of apoptosis in a prostate cancer cell line [120]. These observations provide strong evidence for the role of the Bcl-x(L) isoform, and thus the alternative splicing mechanism controlling its expression, in the survival of cancer cells. Src-Associated Substrate in Mitosis of 68 kDa (Sam68) associates with Bcl-x mRNA and is thought to be involved in the regulation of Bcl-x alternative splicing, the overexpression of this protein increased the expression of the Bcl-x(s) isoform in Human Embryonic Kidney 293 (HEK293) cells [121], however, the phosphorylation of Sam68 by Fyn (a Src-like tyrosine kinase) reversed the effects of Sam68 overexpression [114].

Caspase-2 is a cysteine protease and a tumour suppressor [122, 123] whose mRNA is alternatively spliced, producing multiple isoforms [114]. Caspase-2L is the most prominent isoform found in the majority of tissues and produces a full-length protein with pro-apoptotic properties [124]. In brain and skeletal muscle tissues, the presence of a caspase-2 mRNA, containing an additional 61-nucleotide exon (exon 9), has been detected [124]. The inclusion of this exon in the transcript causes a shift in the reading frame, which introduces a premature termination codon, and results in the destruction of the substrate via the NMD pathway [125]. The loss of caspase-2 expression will undoubtedly result in the cell being less prone to pro-apoptotic signals. Overexpression of hnRNP A1 stimulated caspase-2 exon 9 inclusion, which was reversed by the overexpression of SRSF2 [126]. An intronic sequence element (In100) in intron 9 includes a PTB binding site which repressed exon 9 inclusion [127, 128] and a ‘decoy’ 3′ ss which is able to form non-productive spliceosomal-like complexes with the exon 9 5′ ss [127, 128]. The inclusion of exon 9, and thus the production

of full-length caspase-2 proteins, is also dependent on the binding of RBM5 to a sequence element in intron 9 [129] and on promoter choice [130], although the latter still requires further investigation [114].

1.3.6.2. Alternative Splicing in the Regulation of Metabolism

In the presence of oxygen, cancer cells expend large amounts of glucose, producing immense quantities of lactate through a process known as aerobic glycolysis or the Warburg effect [114]. In this process, pyruvate is shunted from the mitochondria to the cytoplasm, where it is converted to lactate in a reaction catalysed by lactate dehydrogenase (LDH) [114]. An increase in the production of LDH-A, promoted by the oncogenic transcription factor c-Myc [131-133], is essential for the completion of the final step of the Warburg effect, where lactate is produced from pyruvate [134]. Pyruvate, the substrate for aerobic glycolysis, is produced through the enzymatic activity of pyruvate kinase (PK), which is coded for by the *PKM* gene [135]. This gene can produce either PKM1 (adult form) or PKM2 (embryonic version) through mutually exclusive alternative splicing events, resulting in the inclusion of either exon 9 (E9) or exon 10 (E10), respectively [114]. Replacing PKM2 expression with that of PKM1 results in a reduction of lactate production and an increase in oxidative phosphorylation, suggesting that PKM2 is a promoter of the Warburg effect [136]. The splicing repressors PTB, hnRNP A1 and hnRNP A2 bind sequence elements located up and downstream of E9 and promote the inclusion of E10 as well as the formation of the PKM2 isoform [137]. This splicing pattern was reversed by the small interfering RNA (siRNA)-mediated downregulation of these proteins [138]. Reducing the expression of these splicing repressor proteins in a glioblastoma cell line resulted in a decrease in the production of lactate [138], highlighting their role in the metabolism of cancer cells. Lastly, chromatin immunoprecipitation (ChIP) and sequencing (ChIP-seq) data have revealed that the promoter regions of PTB, hnRNP A1 and hnRNP A2 are bound by c-Myc [139], suggesting that their transcription may be activated by this transcription factor.

1.3.6.3. Alternative Splicing in Invasion and Metastasis

Alternative splicing is involved in the regulation of a number of genes that promote invasiveness and epithelial-to-mesenchymal transition in cancer cells [114].

The alternative splicing of *CD44* gives rise to specific variants of the CD44 transmembrane protein [140]. Some of these variants are associated with metastasis – significantly increased levels of CD44 v4-7 and CD44 v6-7 was found expressed in a metastasizing pancreatic cell line compared to the parental tumour [140]. The alternative splicing mechanism of CD44 involves 10 variant exons that are either included individually or in combination in the final transcript [141]. Epithelial tissues typically include CD44 variant exons 8-10 [142] while metastatic tissues include the variant exon 6 [143]. CD44 v6 is necessary for the assembly of a ternary complex made up of itself, Met and the hepatocyte growth factor (HGF) [144] and is strongly linked to the acquisition of metastatic properties by cancer cells [145]. Additionally, the siRNA-mediated downregulation of CD44 v5 in HeLa cells significantly reduced the invasion of these cells, further substantiating the importance of this protein and its isoforms in the metastatic behaviour of these cells [146].

Alternatively spliced transcripts of the *Fibroblast Growth Factor Receptor* (*FGFR*) *2* gene are implicated in epithelial-to-mesenchymal transition in prostate [147] and bladder cancers [148]. Mutually exclusive alternative splicing of the *FGFR2* pre-mRNA involves the choice between the *FGFR2 IIIb* and *FGFR2 IIIc* exons and is cell type-specific (*FGFR2 IIIb* and *FGFR2 IIIc* are preferentially included in epithelial and mesenchymal cells, respectively) with nearly complete switching occurring during EMT [149]. The mechanisms of this alternative splicing event will be discussed in the next section. Genome-wide association studies have revealed an association between 5 single nucleotide polymorphisms (SNPs) located within intron 2 of the *FGFR2* gene and an increased breast cancer risk [150, 151], however, the mechanisms of carcinogenesis are still to be elucidated.

1.4. Fibroblast Growth Factors and Receptors

Fibroblast growth factors (FGFs) are a family of 22 growth factors that play key roles in cellular proliferation and differentiation [152]. Most FGFs contain amino-terminal signal peptides that cause them to be secreted extracellularly where they bind with varying degrees of specificity to fibroblast growth factor receptors (FGFRs) [152]. Once the ligand is bound to the receptor, a signal cascade is initiated which ultimately succeeds in bringing about internal cellular changes [152].

Four signalling FGFRs have been discovered (FGFR1-4), which bind FGFs extracellularly with scaffolding assistance provided by heparin sulphate proteoglycans (HSPG) [152]. These receptors contain a cytoplasmic domain, a single transmembrane domain and three extracellular immunoglobulin (Ig) domains (I-III) [153]. The cytoplasmic domain contains a protein tyrosine kinase core in addition to a number of regulatory sequences [153]. The first two extracellular Ig domains are separated by an acidic region rich in serine residues (called the acid box), which is suggested to be important in FGFR/N-cadherin interactions [154]. The second and third extracellular Ig domains form the ligand-binding pocket and have distinct regions which bind both FGFs and HSPGs [155]. Splicing of the third extracellular Ig domain (Ig-III) results in the first half of Ig-III being formed by exon 8 (*FGFR2 llla*), which is itself alternatively spliced [156], while the second half of the domain being formed by either exon 9 (*FGFR2 lllb*) or exon 10 (*FGFR2 lllc*) (Figure 1.8) [155]. As discussed in section 1.3.6.3, *FGFR2 lllb* and *FGFR2 lllc* are spliced in a mutually exclusive manner and their inclusion is controlled cell-type specifically; *FGFR2 IIIb* and *FGFR2 IIIc* are preferentially included in epithelial and mesenchymal tissues, respectively [155]. It has been suggested that, during EMT, the preferential inclusion of *FGFR2 IIIb* (epithelial) is lost and is preferentially replaced with *FGFR2 IIIc* (mesenchymal); this is often a critical event in the progression of cancer. The specific ligands that bind *FGFR2 IIIb* and *FGFR2 IIIc* solely activate the epithelial and mesenchymal isoforms, respectively.

The ligand-binding domain of the receptor arises from Ig-III, which is alternatively spliced, so the inclusion of either *FGFR2 lllb* or *FGFR2 lllc* alters

ligand specificity e.g. The receptor containing *FGFR2 IIIb* specifically binds FGF1, -3, -7, -10 and -22 while the receptor containing *FGFR2 IIIc* precisely binds FGF1, -2, -4, -6, -9, -16 and -20 [157, 158]. The binding of a particular FGF to its receptor causes specific downstream effects, e.g. FGF-2 promotes skin wound healing while FGF-10 is involved in lung development [159]. Thus, since alternative splicing of the receptor dictates ligand binding, the regulation of this process is of great importance and significance in the cell.

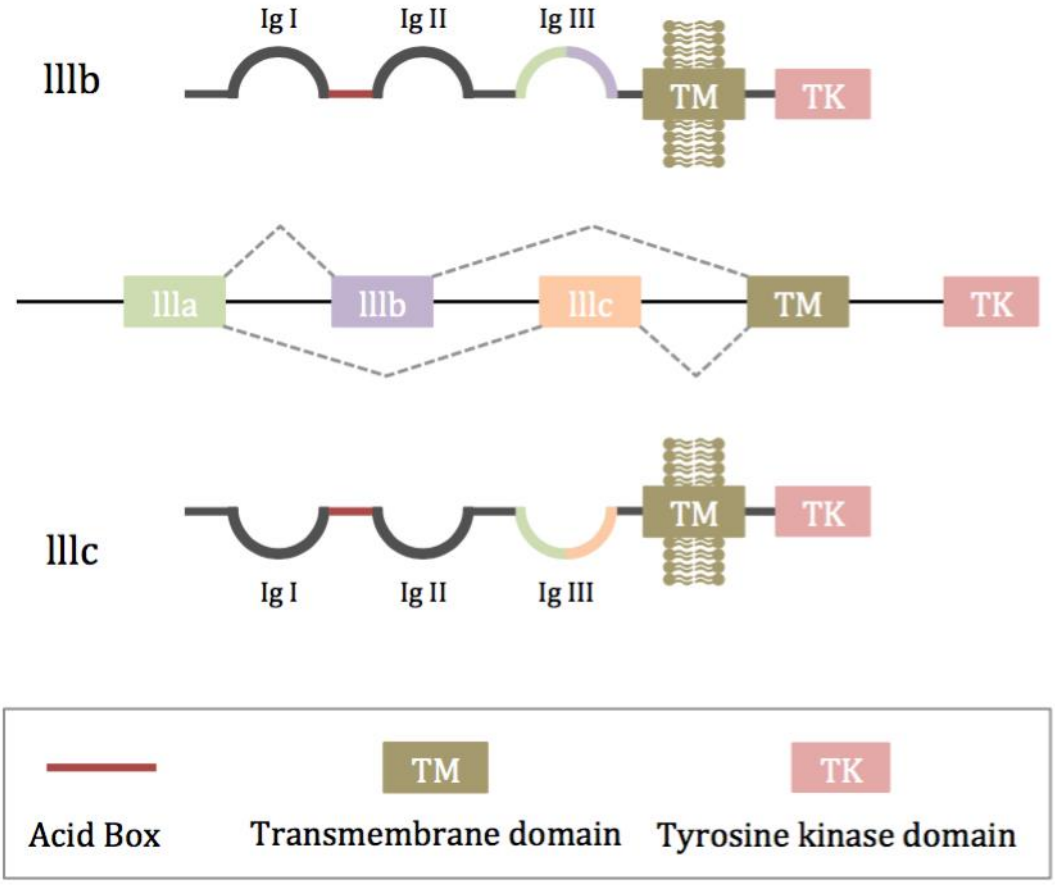

Figure 1.8 – Alternative splicing of the *FGFR* gene causes changes in the structure of the receptor [155]. The FGF receptor consists of an intracellular tyrosine kinase domain, a transmembrane domain and three extracellular Ig domains (Ig I-III). Ig III is responsible for ligand binding and corresponds to *FGFR2 IIIa* and either *FGFR2 IIIb* or *FGFR2 IIIc*. *FGFR2 IIIb* and *FGFR2 IIIc* are alternatively spliced in a mutually exclusive manner and the differential inclusion alters ligand specificity.

1.4.1. Mechanisms Controlling the Alternative Splicing of *FGFR2*

The human *FGFR2* gene is located on chromosome 10q26 and is made up of 21 exons [160]. The two isoforms produced from this gene differ in the inclusion of either the 147-nucleotide (nt) exon 9 (*FGFR2 IIIb*) or the 144-nt exon 10 (*FGFR2 IIIc*) [161]. *FGFR2 IIIb* and *FGFR2 IIIc* form part of the third Ig-like domain of the receptor [162], as discussed above. Much of the research into the mutually exclusive alternative splicing mechanism of *FGFR2 IIIb* and *FGFR2 IIIc* has been undertaken in rat cell lines [163], since these sequences share a high level of homology with those found in humans [161]. The mutually exclusive splicing pattern observed in the *FGFR2* gene is a tightly regulated process, involving *cis*-acting elements, located in the pre-mRNA transcript, as well as the *trans*-acting elements that bind to them [163]. For *FGFR2 IIIb* to be included, the activation of *FGFR2 IIIb* combined with the silencing of *FGFR2 IIIc* is required [163]. Similarly, for *FGFR2 IIIc* to be included, the activation of *FGFR2 IIIc* combined with the silencing of *FGFR2 IIIb* is required [163].

The *cis*-acting elements in the mRNA of this gene are present in both epithelial and mesenchymal cells, however, the binding pattern of *trans*-acting factors differ between these cell types, thus facilitating the splicing differences. It has been suggested that the splicing of *FGFR2 IIIc* is the 'default' splicing pathway and that the splicing of *FGFR2 IIIb* (accompanied by *FGFR2 IIIc* splicing repression) is either activated or repressed depending on the cell type [164].

1.4.1.1. *FGFR2* Splicing in Epithelial Cells

In epithelial cells, *FGFR2 IIIb* is included and *FGFR2 IIIc* is spliced. The control of this splicing pattern is dependent on *cis*-acting factors located in the pre-mRNA transcript as well as *trans*-acting factors that bind to them. Figure 1.9 illustrates the known *FGFR2* splicing mechanisms in epithelial cells.

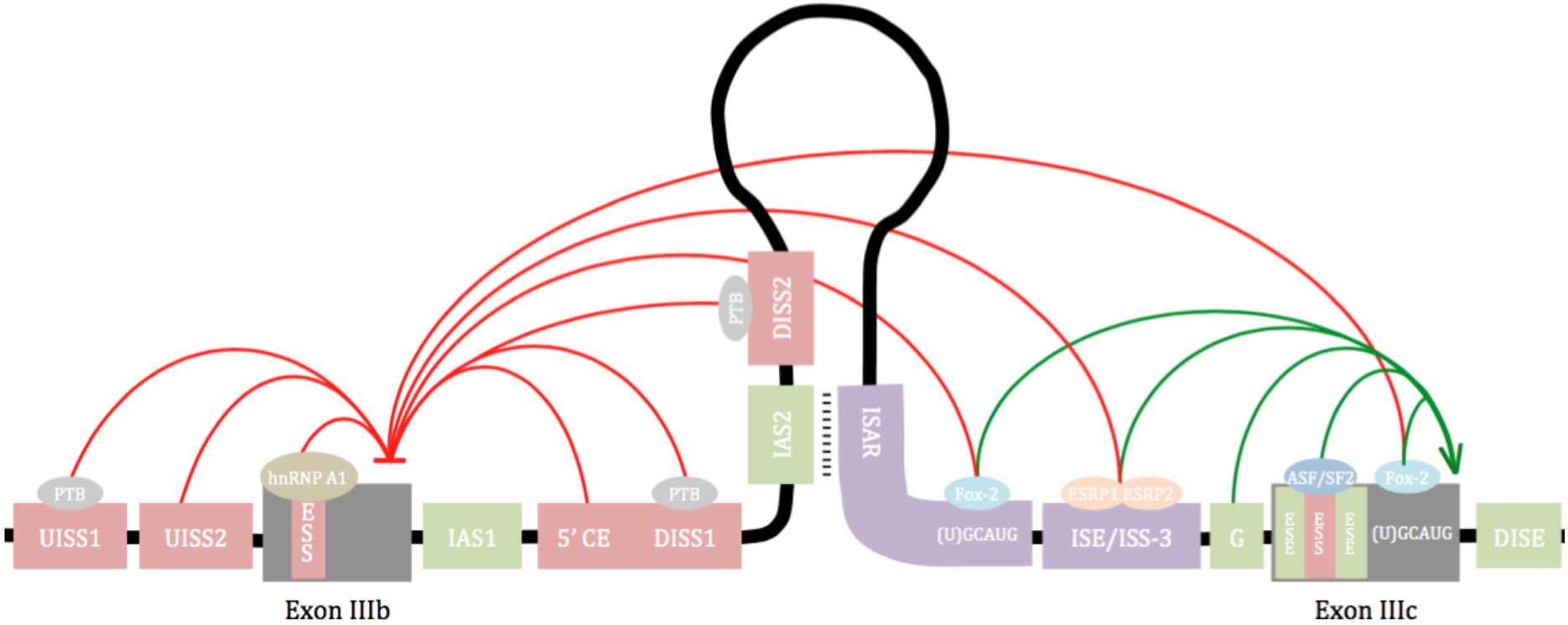

Figure 1.9 – *FGFR2* splicing mechanism in epithelial cells [160-173]. Red and green boxes indicate *cis*-acting splicing silencers and enhancers, respectively. Purple boxes indicate *cis*-acting elements that function to both silence and enhance splicing. Known *trans*-acting factors are illustrated bound to the appropriate *cis*-acting elements. Red and green lines indicate splicing silencing and activation, respectively, at the appropriate exon.

1.4.1.1.1. *FGFR2 IIIb* Inclusion

The exon splicing silencer (ESS) located within *FGFR2 IIIb* represses splicing, specifically, the 5′-TAGGGCAGGC-3′ sequence (termed the S10) positioned in the ESS inhibits the splicing of IIIb [167], thus promoting its inclusion in the final mRNA transcript. Since this sequence is related to a consensus sequence suggested to bind hnRNP A1 with high affinity, a mechanism of splicing repression, where hnRNP A1 binds to this sequence element, has been proposed [167]. In epithelial cells, the binding of hnRNP A1 to the *FGFR2 IIIb* sequence element hinders communication between the exon's 5′ and 3′ splice sites, leading to a block in the splicing of *FGFR2 IIIb* [167]. However, additional research investigating this mechanism is necessary to confirm this. Further investigation into the S10 sequence element revealed that the four initial nucleotide residues, 5′-TAGG-3′, are the functional part of the sequence and that the 5′-AG-3′ dinucleotide is of particular importance to accomplish splicing repression [168]. When mutations that increase the strength of the *FGFR2 IIIb* splice sites (e.g. by decreasing the distance between the 5′ and 3′ splice sites) were introduced into the pre-mRNA transcript, the 5′-TAGG-3′ sequence was unable to repress splicing, suggesting that this four nucleotide sequence is only capable of repressing the splicing of exons with weak splice sites [168].

Intronic splicing silencers (ISS) located up (UISS) and downstream (DISS) of *FGFR2 IIIb* are essential for silencing the splicing of this exon [164, 172]. The UISS is made up of two regions, UISS1 and UISS2, both of which are necessary for the activity of the UISS [164]. UISS1 contains a pyrimidine-rich sequence that readily cross-links with PTB, suggesting that PTB binding is the mechanism by which *FGFR2 IIIb* splicing is repressed [163]. An 8-nucleotide sequence (5′-GCAGCACC-3′) that is required for the silencing of *FGFR2 IIIb* splicing is located at the 3′ end of the UISS2 element [163]. The DISS contains a 5′-conserved sub-element (5′ CE) and two additional regions (named DISS1 and DISS2) that contain multiple PTB binding sites [163]. PTB-binding sites in the DISS are essential for the complete repression of *FGFR2 IIIb* splicing; however, the majority of the silencing activity has been mapped to the conserved octamer

(5′-CUCGGUGC-3′) located in the 5′ CE. Mutations in any of these 8 nucleotides resulted in the reduction of *FGFR2 IIIb* splicing repression [163].

In epithelial cells, two *cis*-acting sequence elements – namely the intronic activating sequence (IAS) 2 and the intronic splicing activator and repressor (ISAR) – play a role in the inclusion of *FGFR2 IIIb* [161, 169]. When a 5′-(U)GCAUG-3′ sequence element located downstream of the ISAR is brought into close proximity with the DISS through the formation of a stem that is formed between the IAS2 and a portion of ISAR, *FGFR2 IIIb* is included [166, 169, 174-176]. In epithelial tissues, Fox-2 binding to 5′-(U)GCAUG-3′ promotes the inclusion of *FGFR2 IIIb*, thereby repressing the splicing of this exon [166]. This sequence element is also located within *FGFR2 IIIc*, and through Fox-2 binding, is an additional promoter of *FGFR2 IIIb* inclusion [165].

Another sequence element, known as the intronic splicing enhancer/intronic splicing silencer-3 (ISE/ISS-3), located downstream of the initial 5′-(U)GCAUG-3′ sequence [173], is required for *FGFR2 IIIb* inclusion. It regulates the splicing of FGFR in a cell-type-specific manner in the absence of other *cis*-elements that have previously been described to regulate *FGFR2* alternative splicing [170]. *FGFR2 IIIb* inclusion in epithelial cells is mediated by the binding of the Epithelial Splicing Regulatory Protein (ESRP) 1 and 2 to the ISE/ISS-3 sequence element [173].

1.4.1.1.2. *FGFR2 IIIc* Splicing

In epithelial tissues, IAS2 and ISAR can function to enhance *FGFR2 IIIc* splicing [161, 177] and the 5′-(U)GCAUG-3′ sequence element, located downstream from the ISAR core, plays a cell-type-specific role in the exclusion of *FGFR2 IIIc* [166]. In epithelial cells, binding of the Fox-2 protein to the 5′-(U)GCAUG-3′ sequence downstream of the ISE/ISS-3 [166] as well as within *FGFR2 IIIc* [165] inhibits the inclusion of this exon in the final mRNA transcript, thus splicing it. ISE/ISS-3 itself also mediates *FGFR2 IIIb* inclusion and *FGFR2 IIIc* exclusion in epithelial cells by the binding of ESRP1 and 2 to this sequence element [173]. ISE/ISS-3 makes use of a suboptimal branch point sequence located in the intronic sequence upstream of *FGFR2 IIIc*. Instead of an A residue, a G residue is used as

the primary branch nucleotide in the initial splicing step [170], repressing *FGFR2 IIIc* inclusion and thereby splicing the exon.

An exonic splicing enhancer (ESE) sequence (5′-CUGGGGA-3′), located within *FGFR2 IIIc* and overlapping the exon splicing silencer (ESS) sequence, binds the SR protein ASF/SF2 and functions to suppress *FGFR2 IIIc* inclusion [171].

1.4.1.2. *FGFR2* Splicing in Mesenchymal Cells

In mesenchymal cells, *FGFR2 IIIb* is spliced and *FGFR2 IIIc* is included. The control of this splicing pattern is dependent on *cis*-acting factors located in the pre-mRNA transcript as well as the *trans*-acting factors that bind them. Figure 1.10 illustrates the known *FGFR2* splicing mechanisms in mesenchymal cells.

1.4.1.2.1. *FGFR2 IIIb* Splicing

Deletion of the IAS1 sequence element, a 20-nucleotide pyrimidine-rich sequence located 10 nucleotides downstream of the *FGFR2 IIIb* 5′ ss [169], completely blocks splicing of this exon and is thus suggested to play a very important role in promoting splicing of this exon [167]. In mesenchymal cells, TIA-1 (an RNA-binding protein) binds to the IAS1 element, inhibiting hnRNP A1-mediated repression of *FGFR2 IIIb* splicing, thereby splicing *FGFR2 IIIb*. TIA-1 accomplishes this either by overcoming the effect of ESS bound hnRNP A1 or by preventing the binding of hnRNP A1 to the ESS located in *FGFR2 IIIb* [178].

1.4.1.2.2. *FGFR2 IIIc* Inclusion

An exonic splicing silencer (ESS) located within *FGFR2 IIIc*, consisting of 5′-GGG-3′ repeats and partially embedded within an exon splicing enhancer (ESE) sequence, facilitates exon inclusion, and therefore, splicing repression, through the binding of either hnRNP H or hnRNP F proteins [171]. The downstream intronic splicing enhancer (DISE) is located immediately downstream of *FGFR2 IIIc* and is necessary for *FGFR2 IIIc* inclusion in mesenchymal tissues [179]. This element must be located close to the 5′ ss of the exon it regulates to function, and promotes U1 snRNP binding, thus facilitating exon inclusion. This element is functionally replaceable by the IAS1 sequence [179].

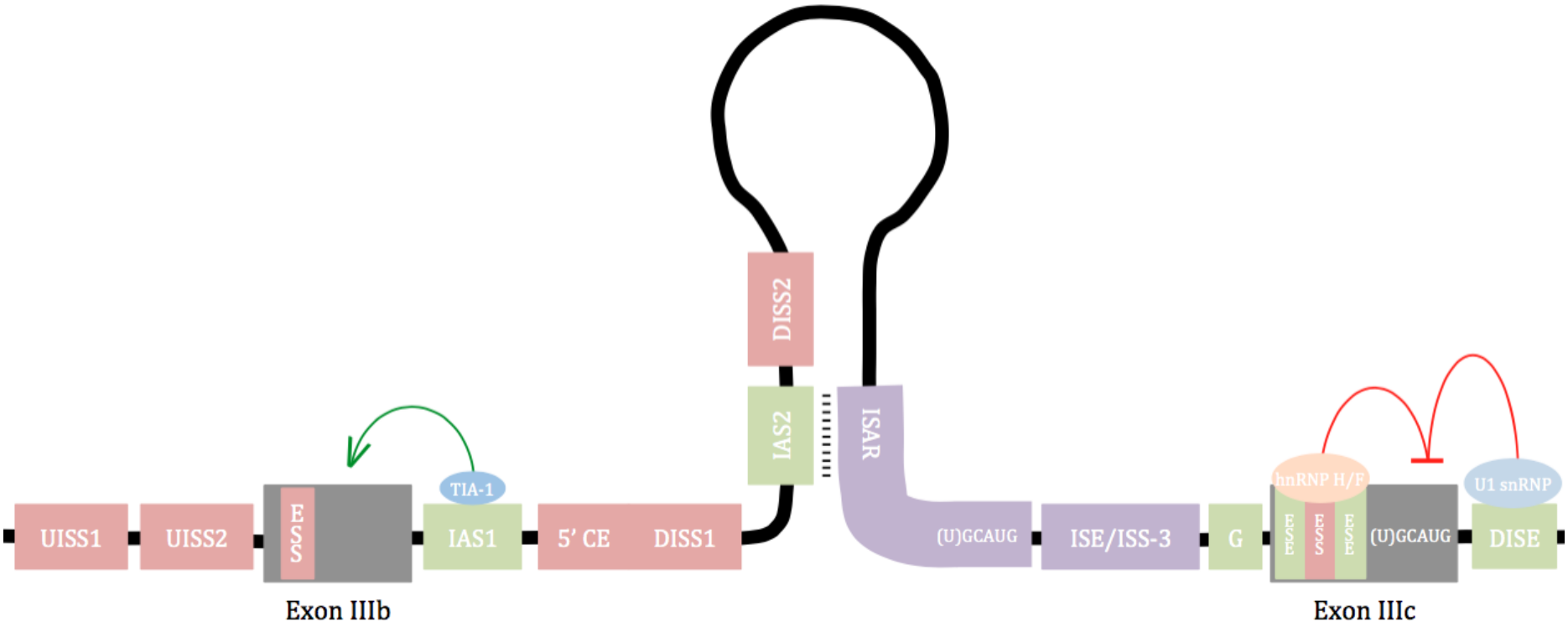

Figure 1.10 – *FGFR2* splicing mechanism in mesenchymal cells [167, 169, 171, 178-180]. Red and green boxes indicate *cis*-acting splicing silencers and enhancers, respectively. Purple boxes indicate *cis*-acting elements that function to both silence and enhance splicing. Known *trans*-acting factors are illustrated bound to the appropriate *cis*-acting elements. Red and green lines indicate splicing silencing and activation, respectively, at the appropriate exon.

1.4.2. Misregulation of *FGFR2* in Disease

The misregulation of *FGFR2* and *FGFR2* splicing is known to be the cause of numerous cancerous and non-cancerous diseases.

1.4.2.1. Misregulation of FGFR2 in Non-Cancerous Diseases

Congenital disorders such as Beare-Stevenson, Pfeiffer, Apert, Crouzon and Jackson-Weiss syndromes, all contain missense activating *FGFR2* gene mutations [181]. These mutations cause the abnormal induction of FGFR2 signal activation during skeletal development causing skeletal disorders such as craniosynostosis [181]. An SNP (rs17101921) located in the 3′-flanking region of the *FGFR2* gene has also been reported to be associated with schizophrenia, although only 10 cases were investigated [182].

1.4.2.2. Misregulation of FGFR2 in Cancerous Diseases

Missense mutations in the *FGFR2* gene occur in ovarian, breast, endometrial uterus gastric and lung cancers [183-185]. Eight SNPs found within the *FGFR2* intron 2 sequence have been associated with an increased risk of breast cancer [150]. The inclusion of the *FGFR2 IIIc* isoform instead of the *FGFR2 IIIb* isoform occurs during the progression of prostate and bladder cancers [148]. Additionally, where *FGFR2 IIIb* had been knocked out in the skin epidermis of mice, an increased occurrence of squamous cell carcinoma was observed after these mice were treated with 7,12-Dimethylbenz[a]anthracene (DMBA) and Tissue plasminogen activator (TPA) [186]. These findings indicate that *FGFR2 IIIb* is protective against chemical carcinogenesis [186].

1.5. The KH-Type Splicing Regulatory Protein

The KH-type splicing regulatory protein (KSRP), also known as the Far Upstream Element-Binding Protein 2 (FUBP2), is a single-stranded RNA-binding protein that was discovered independently by the Levens [187] and Black [188] laboratories. KSRP is ubiquitous and its cellular location (nuclear or cytoplasmic) varies in different cell types [189]. The variation in cellular location is regulated dynamically in response to cellular stimuli [189]. KSRP functions in the control of gene expression and the modulation of cellular processes [190]. Biological activities modulated by KSRP include mRNA degradation, translational control, micro RNA (miRNA) maturation, mRNA localisation, mRNA editing, gene transcription and pre-mRNA splicing [189].

1.5.1. The Structure of KSRP

The KSRP protein is composed of 711 amino acids, which are ordered into three distinct regions – an Amino-terminal (N-terminal) domain, a central region and a Carboxyl-Terminal (C-terminal) domain (Figure 1.11) [189]. The N- and C-terminal domains contain low levels of sequence complexity and include protein-interaction motifs [191]. The central region of KSRP is structured, containing four hnRNPK-homology (KH) domains (Figure 1.11), which function to bind RNA. The modular nature of this protein provides it with binding flexibility, making interactions with multiple targets possible [191]. Post-translational phosphorylation of KSRP by AKT (at Serine 193), ATM (at Serine 132, 274 and 670) and MAPK p38 (at Threonine 692) (Figure 1.11) further increases the functional flexibility of this protein [192-194].

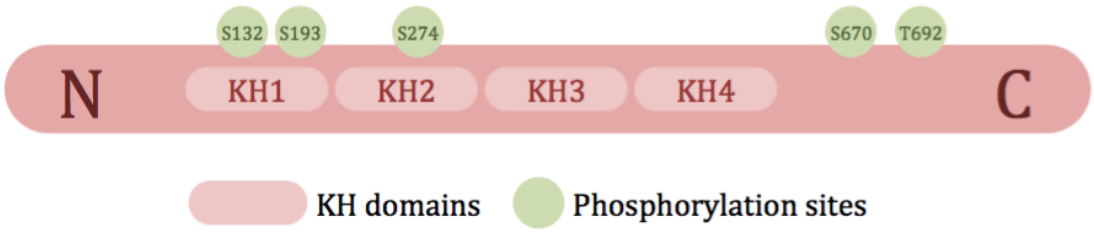

Figure 1.11 – The structure of KSRP [189]. KSRP contains N- and C-terminal domains flanking four KH domains. This protein is post-translationally phosphorylated at Serine 132, 193, 274 and 670 as well as Threonine 692.

1.5.2. The Role of KSRP in mRNA Decay

The modulation of mRNA decay is an important checkpoint in the control of protein expression [195]. In mammalian cells, the presence of adenylate-uridylate-rich elements (AREs) in the 3′ untranslated regions (UTRs) of short-lived transcripts is essential for their decay [196, 197]. AREs are bound by numerous proteins, known as ARE-binding proteins (ARE-BP), with KSRP being one such ARE-BP [196]. Once bound to the ARE, KSRP recruits enzymatic complexes essential for mRNA decay [198-200].

1.5.3. Mediation of miRNA Maturation by KSRP

Almost every cellular function is regulated through the action of short non-coding RNAs known as micro RNAs (miRNAs). In the nucleus, primary micro RNAs (pri-miRNAs) are first transcribed and then cleaved by a ribonuclease Drosha-containing complex to produce precursor micro RNAs (pre-miRNAs) that have a stem-loop-structure [189]. These pre-miRNAs are transported from the nucleus to the cytoplasm where they are again cleaved, this time by the ribonuclease Dicer-containing complex, producing short miRNA duplexes [201]. One strand of this miRNA duplex becomes incorporated into the RNA-induced silencing complex (RISC) where it inhibits translation and favours mRNA decay [201]. KSRP binds to the terminal loop (TL) region of several miRNAs and also interacts with Drosha and Dicer, bringing about the promotion of miRNA maturation [202]. KSRP also regulates the maturation of distinct sets of miRNAs in specific cell lines [203, 204] through its interaction with proteins involved in the regulation of gene expression as well as cell-type specific competition with proteins involved in the regulation of miRNA biogenesis [205, 206].

1.5.4. The Function of KSRP in the Immune Response

Cytokines and chemokines are proteins involved in the immune response. The expression of these proteins is strictly regulated as their overexpression or downregulation can either cause or exacerbate autoimmune diseases, neurodegenerative diseases and cancers [207]. The regulation of these proteins is accomplished at both the transcriptional and the post-transcriptional level. Post-transcriptional regulation involves specific RNA elements that control mRNA translation and/or decay as well as miRNA-mediated gene silencing [207].

Since KSRP functions at both of these levels, it is responsible for controlling the expression of a number of immune modulators [207].

1.5.5. KSRPs Role in Pre-mRNA Splicing

KSRP forms part of a multi-protein complex that binds to the G and U-rich intronic splicing enhancer element [188]. This element is located downstream of the neuron-specific SCR N1 exon, and its presence is essential for the proper splicing of this exon [188]. The *in vitro* addition of KSRP specific antibodies causes the inhibition of NI exon splicing and the splicing of this exon can be rescued with the addition of purified KSRP [188]. It has been suggested that KSRP may regulate the splicing of numerous exons through its interaction with intronic splicing enhancer elements [188].

1.5.6. KSRPs Role in Cancer

The siRNA-mediated loss of KSRP expression causes an increase in the migratory capacity of glioblastoma multiforme (GBM) cells and induces the formation of multi focal GBM *in vivo* [208]. High expression levels of KSRP are observed in GBM patients who survive for a long time after surgery, suggesting that this protein may be a useful novel prognostic marker in the aforementioned patients [208]. The higher overall survival of GBM patients in response to increased KSRP expression levels suggests that this protein causes a better response to GBM therapeutic measures [209]. In contrast, decreased expression of KSRP in hepatocellular carcinoma cells represses the migratory capacity of these cells, retarding the progression of this cancer [210].

These findings indicate that differences in the expression of KSRP will not necessarily have the same effect in all human cancers [207]. The effect of altered KSRP expression on human cancers could depend on the distinct role of KSRP in multi-protein complexes as well as its ability to interact with particular targets in particular cells or tissues [207]. These interesting findings necessitate further research into the mechanistic action of KSRP.

Chapter 2

2. HYPOTHESIS, AIMS & OBJECTIVES

2.1. Hypothesis

The incidence of breast cancer, especially in developing countries, is a serious cause for alarm. The higher incidence of the more aggressive breast cancer subtype, triple-negative breast cancer, in African populations warrants further research. There are a number of subtypes of TNBC, and in this study, cell line representatives of the basal/epithelial (MDA-MB-468) and mesenchymal-like (MDA-MB-436) were used. These cell lines splice *FGFR2* pre-mRNA differently – the epithelial cell line preferentially includes *FGFR2 IIIb*, while the mesenchymal-like cell line includes *FGFR2 IIIc* preferentially. A comparison of the nuclear proteomes of MDA-MB-436 and MDA-MB-468 cells revealed a number of proteins that are differentially expressed. Among these was the KH-type splicing regulatory protein (KSRP), a protein involved in transcription, mRNA localisation and alternative pre-mRNA splicing [199]. This protein was overexpressed in the epithelial cell line compared to the mesenchymal cell line.

KSRP is known to be involved in alternative splicing and we hypothesise that if it is involved in the alternative splicing of *FGFR2*, it may be involved in the progression of triple-negative breast cancers from an epithelial phenotype to a mesenchymal one. Moreover, we seek to identify genome-wide changes in gene expression as a consequence of KSRP knockdown.

2.2. Aims

In this study, we aim to investigate the role of KSRP in the *FGFR2* splicing mechanism in the context of triple-negative breast cancer progression using epithelial and mesenchymal cell line models. Additionally, we aim to discover the genome-wide consequences of KSRP knockdown.

2.3. Objectives

2.3.1. Confirm the Epithelial and Mesenchymal Phenotype, Preferential *FGFR2* Isoform Inclusion, Differential KSRP Expression and Alteration of *FGFR2* Isoform Expression in MDA-MB-436 and MDA-MB-468 Cells

Confirmation of the mesenchymal and epithelial phenotypes of MDA-MB-436 and MDA-MB-468 cells, respectively, will be accomplished by fluorescently visualising the epithelial marker, Cytokeratin 19, and the mesenchymal marker, Vimentin on these cells. Confirming the preferential *FGFR2* isoform inclusion in MDA-MB-436 and MDA-MB-468 cells will be accomplished using polymerase chain reaction (PCR) and semi-quantification of the resultant bands will be completed using ImageJ. In addition, *FGFR2 IIIb* and *FGFR2 IIIc* expression levels in MDA-MD-436 and MDA-MD-468 cells will be quantified using Quantitative Reverse-transcriptase Polymerase Chain Reaction (qRT-PCR). The protein expression level of KSRP in MDA-MB-436 and MDA-MB-468 cells will be confirmed using western blotting and quantification of the resultant bands will be completed using ImageJ. To show that the expression of *FGFR2 IIIb* and *FGFR2 IIIc* could be altered, ESRP1 and ESRP2 (known regulators of *FGFR2* splicing) will be downregulated in MDA-MB-436 and MDA-MB-468 cells, and the effect of this knockdown on *FGFR2 IIIb* and *FGFR2 IIIc* expression determined using qRT-PCR.

2.3.2. Determine the Effect of KSRP Knockdown and KSRP Overexpression on *FGFR2 IIIb* and *FGFR2 IIIc* Expression and the Epithelial and Mesenchymal Phenotype of MDA-MB-436 and MDA-MB-468 Cells

KSRP expression will be downregulated using siRNA and overexpressed by transfection with a plasmid containing full-length KSRP tagged to Green Fluorescent Protein (GFP). KSRP knockdown and overexpression will be confirmed using qRT-PCR and western blotting. The effect of KSRP knockdown and overexpression on *FGFR2 IIIb* and *FGFR2 IIIc* expression will be determined using qRT-PCR. The effect of KSRP overexpression on the mesenchymal and epithelial phenotypes of MDA-MB-436 and MDA-MB-468 cells, respectively, will

be determined by the fluorescent visualisation of the epithelial marker, Cytokeratin 19, and the mesenchymal marker, Vimentin in these cells.

2.3.3. Investigate Possible Direct Binding of KSRP to *FGFR2* mRNA in MDA-MB-468 Cells

A UV cross-linking and immunoprecipitation (CLIP) assay will be used to determine the possible binding of KSRP to *FGFR2* mRNA in MDA-MB-468 cells.

2.3.4. Identify Genome-Wide Gene Expression Changes in Response to KSRP Knockdown in MDA-MB-468 Cells

Genome-wide gene expression changes in response to KSRP knockdown in MDA-MB-468 cells will be analysed using the Affymetrix GeneChip® Human Transcriptome Array 2.0. Targets of interest, whose gene expression is significantly altered in response to KSRP knockdown, will be chosen and the observed gene expression alterations will be validated using qRT-PCR. The potential interaction and co-localisation of KSRP with the selected targets will be predicted using the Search Tool for the Retrieval of Interacting Genes/Proteins (STRING) and determined using confocal fluorescent microscopy, respectively.

Chapter 3

3. MATERIALS & METHODS

3.1. Cell Lines and Cell Culture Maintenance

3.1.1. Cell Lines

The following cell lines were used in this study:

- MDA-MB-436 (ATTC® HTB-130™) – This cell line originated from the metastatic site of the mammary gland/breast of a 43-year-old female with adenocarcinoma. The cells are adherent and pleomorphic in morphology with multinucleated component cells.
- MDA-MB-468 (ATTC® HTB-132™) – This cell line originated from the metastatic site of the mammary gland/breast of a 51-year-old female with adenocarcinoma. The cells are adherent and epithelial in morphology.

3.1.2. Cell Culture Maintenance

- MDA-MB-436 (ATTC® HTB-130™) – Cells were grown in Leibovitz's L-15 medium with Glutamax-1 (Gibco®) supplemented with 10 μg/mL insulin (Gibco®), 10% (v/v) fetal bovine serum (Gibco®) and 1% (v/v) penicillin/streptomycin (Gibco®) in a humidified incubator, without CO_2, at 37 °C.
- MDA-MB-436 (ATTC® HTB-132™) – Cells were grown in Leibovitz's L-15 medium (Gibco®) supplemented with 10% (v/v) fetal bovine serum (Gibco®) and 1% (v/v) penicillin/streptomycin (Gibco®) in a humidified incubator, without CO_2, at 37 °C.

3.2. Plasmids and Plasmid Amplification

3.2.1. Plasmids

The following plasmids were used in this study:

- pEGFP-N1 – encodes for the green fluorescent protein and was acquired from Clontech.

- pEGFPC$_1$-6xHis-FLKSRP – encodes a full-length KSRP with enhanced green fluorescent protein (eGFP) and a polyhistidine tags. This plasmid was a generous donation from the Black laboratory (University of California, Los Angeles).

Plasmid maps can be found in appendix A – Figure 8.1.

3.2.2. Plasmid Amplification

3.2.2.1. Transformation and Bacterial Growth

100 ng of plasmid DNA was added to 50 μL of *E. coli* Stbl3 competent cells (Invitrogen™) that had been thawed on ice for approximately 20 min. The solution was gently mixed and incubated on ice for 20 min. Following the incubation, the solution was heat shocked at 42 °C for 45 s and placed on ice for 2 min. 500 μL LB (appendix A – 8.1) was added and the solution was grown at 37 °C in a shaking incubator for 45 min. After the growth, 100 μL of the transformation solution was plated on pre-warmed (37 °C) LB-kanamycin Agar plates (appendix A – 8.2) and incubated at 37 °C overnight. The following day, a single colony was picked, resuspended in 5 mL LB (appendix A – 8.1) and grown at 37 °C in a shaking incubator overnight.

3.2.2.2. Plasmid DNA Purification Using the QIAprep Spin Miniprep Kit

The bacterial culture (from section 3.2.2.1) was centrifuged (Boeco U320R centrifuge, 8000 x rpm, RT, 3 min) and the supernatant discarded. The bacterial pellet was resuspended in 250 μL of Buffer P1 (appendix A – 8.3) and the solution transferred to a microcentrifuge tube. 250 μL of Buffer P2 (appendix A – 8.4) was added and the solution thoroughly mixed by inversion (6 times). 350 μL of Buffer N3 (appendix A – 8.5) was added, the solution immediately mixed by inversion (6 times) and centrifuged (Boeco M-24A centrifuge, 13000 x rpm, RT, 10 min). The supernatant was added to the QIAprep spin column, the column centrifuged (Boeco M-24A centrifuge, 13000 rpm, RT, 1 min) and the flow-through discarded. 500 μL of Buffer PB (appendix A – 8.6) was added to the column, the column centrifuged (Boeco M-24A centrifuge, 13000 rpm, RT, 1 min) and the flow-through discarded. 750 uL of Buffer PE (appendix A – 8.7) was

added to the column, the column centrifuged (Boeco M-24A centrifuge, 13000 rpm, RT, 1 min) and the flow-through discarded. The column was then centrifuged (Boeco M-24A centrifuge, full speed, RT, 1 min) and placed in a clean 1,5 mL microcentrifuge tube. The DNA was eluted by adding 50 μL of Buffer EB (appendix A – 8.8) directly to the membrane of the column; this was incubated for 1 min at RT and centrifuged (Boeco M-24A centrifuge, 13000 x rpm, RT, 1 min). The plasmid DNA was stored at -20 °C.

3.3. Primers

Primers were designed using the Primer3Plus online bioinformatics tool (http://www.bioinformatics.nl/cgi-bin/primer3plus/primer3plus.cgi/) using sequences acquired from Exonmine (http://www.imm.fm.ul.pt/exonmine/) and were synthesised by Integrated DNA Technologies (IDT) (http://eu.idtdna.com/pages/products/dna-rna/custom-dna-oligos). The names, sequences, melting temperatures and experiments the primer pairs were used in is detailed in Table 3.1.

Table 3.1 – Table of Primer Information

Experiment	Name	Forward Sequence	Reverse Sequence	Melting Temp
semi-qPCR	FGFR2_e8e11	5′-CCT TTC ACT CTG CAT GGT TG-3′	5′-CAT GAC CAC TTG CCC AAA G-3′	60 °C
qRT-PCR (Reference genes)	GAPDH	5′-TGC ACC ACC AAC TGC TTA GC-3′	5′-GGC ATG GAC TGT GGT CAT GAG-3′	60 °C
qRT-PCR (Reference genes)	SDHA	5′-TGG GAA CAA GAG GGC ATC TG-3′	5′-CCA CCA CTG CAT CAA ATT CAT G-3′	60 °C
qRT-PCR (Reference genes)	HPRT1	5′-TGA CAC TGG CAA AAC AAT GCA-3′	5′-GGT CCT TTT CAC CAG CAA GCT-3′	60 °C
qRT-PCR	ESRP1	5′-GGTGCAGCACTTTGTCTGAA-3′	5′-AATATACCGGGTCCCCATGT-3′	60 °C
qRT-PCR	ESRP2	5′-GCTCCCCGACATGTTCTTCT-3′	5′-CATGGTGGCCACAGTGAG-3′	60 °C
qRT-PCR	KSRP	5′-TGC CAC GAC AGT GAA TAA CAG CAC-3′	5′-AGC TTC TTG CTC TCC GGT TGA TCT-3′	60 °C
qRT-PCR	FGFR2_lllb	5′-AGA AGT GCT GGC TCT GTT C-3′	5′-GGC CTG CCC TAT ATA ATT GGA G-3′	60 °C
qRT-PCR	FGFR2_lllc	5′-TGT AAC TTT TGA GGA CGC TGG-3′	5′-GTC AAC CAT GCA GAG TGA AAG-3′	60 °C
qRT-PCR	CCND3	5′-GAC TGG GAG GTG CTG GTC-3′	5′-TGT AGC ACA GAG GGC CAA AA-3′	60 °C
qRT-PCR	DKK1	5′-TGC GCA GAG GAC GAG GAG-3′	5′-TTT TGC AGT AAT TCC CGG GG-3′	60 °C
qRT-PCR	PPP2R1B	5′-GAT TCA GTG CGC CTC CTT G-3′	5′-CTG AAA ATC TGT CAG CCA CCA-3′	60 °C
qRT-PCR (UV-CLIP)	FGFR2_i81	5′-TGC TGT TGC TGC TGA GAG TT-3′	5′-TTA GGC ACC ACA GAA TGC AG-3′	-
qRT-PCR (UV-CLIP)	FGFR2_i82	5′-TCA CCA AAA CTT TTT CAG ACC A-3′	5′-ACG ATG CCC ACT TTT GTT TC-3′	-
qRT-PCR (UV-CLIP)	FGFR2_i83	5′-GAA ACA AAA GTG GGC ATC GT-3′	5′-GTT GAC ACC CAG TTG CAC AG-3′	-
qRT-PCR (UV-CLIP)	FGFR2_i8e9	5′-GCG TCA GTC TGG TGT GCT AA-3′	5′-TAC GTT TGG TCA GCT TGT GC-3′	62 °C
qRT-PCR (UV-CLIP)	FGFR2_e9	5′-CAG CTT CCC CAG ACT ACC TG-3′	5′-TAC GTT TGG TCA GCT TGT GC-3′	62 °C
qRT-PCR (UV-CLIP)	FGFR2_i9	5′-AGC CAG CTT GTG GAT CTT GT-3′	5′-GGG GAT TTG CCT CCA GTT AT-3′	62 °C

3.4. Antibodies

Table 3.2 – Table of Antibody Information

Section	Application	Name	Dilution	Supplier	Catalogue number	Concentration	Data Sheet
3.14.1	Primary KSRP detection	polyclonal rabbit anti-KSRP	1 in 2000	Bethyl Laboratories Inc	A302-021A	0,2 mg/mL	http://www.bethyl.com/product/pdf/A302-021A.pdf
	Primary Histone-3 (H3) detection	polyclonal rabbit anti-Histone H3	1 in 5000	Abcam®	ab1791	0,5 mg/mL	http://www.abcam.com/histone-h3-antibody-nuclear-loading-control-and-chip-grade-ab1791.html.
	Primary IgG detection	monoclonal rabbit anti-Human IgG	1 in 1000	Abcam®	ab109489	0,015 mg/mL	http://www.abcam.com/human-igg-antibody-epr4421-ab109489.html.
	Primary U2AF65 detection	polyclonal rabbit anti-U2AF65	1 in 5000	Abcam®	ab37530	0,9 mg/mL	http://www.abcam.com/u2af65-antibody-ab37530.html.
	Secondary KSRP, H3, IgG and U2AF65 detection	polyclonal goat anti-Rabbit IgG peroxidase conjugate	1 in 5000	Sigma-Aldrich	A0545-1ML	4 mg/mL	http://www.sigmaaldrich.com/content/dam/sigma-aldrich/docs/Sigma/Datasheet/6/a0545dat.pdf.
3.15.2.1	Primary Cytokeratin 19 detection	monoclonal rabbit anti-Cytokeratin 19	1 in 200	Abcam®	ab52625	0,808 mg/mL	http://www.abcam.com/cytokeratin-19-antibody-ep1580y-ab52625.html.
	Primary Vimentin detection	monoclonal mouse anti-Vimentin	1 in 200	Abcam®	ab8978	1 mg/mL	http://www.abcam.com/vimentin-antibody-rv202-ab8978.html.
	Secondary Cytokeratin 19 detection	polyclonal goat anti-Rabbit IgG (H+L) Rhodamine Red™ conjugate	1 in 200	Invitrogen	R-6394	2 mg/mL	https://www.thermofisher.com/order/genome-database/generatePdf?productName=Rabbit%20IgG%20(H+L)&assayType=PRANT&productId=R-6394&detailed=true.
	Secondary Vimentin detection	polyclonal goat anti-Mouse IgG DyLight™ 649 conjugate	1 in 200	BioLegend®	405312	0,5 mg/mL	http://www.biolegend.com/pop_pdf.php?id=5689.
3.16.2.1.1	IgG immunoprecipitation	monoclonal rabbit anti-Human IgG antibody		Abcam®	ab109489	0,015 mg/mL	http://www.abcam.com/human-igg-antibody-epr4421-ab109489.html.
	KSRP immunoprecipitation	polyclonal rabbit anti-KHSRP		Novus Biologicals	NBP1-18911	1 mg/mL	http://www.novusbio.com/PDFs/NBP1-18911.pdf
3.17.2.1	Primary KSRP detection	polyclonal rabbit anti-KSRP antibody	1 in 200	Bethyl Laboratories Inc	A302-022A	1 mg/mL	http://www.bethyl.com/product/pdf/A302-022A.pdf.
	Primary CCND3 detection	monoclonal rabbit anti-Cyclin D3	1 in 100	Abcam®	ab52598	0,039 mg/mL	http://www.abcam.com/cyclin-d3-antibody-ep463e-ab52598.html.
	Primary DKK1 detection	monoclonal rabbit anti-DKK1 antibody	1 in 100	Abcam®	ab109416	1,077 mg/mL	http://www.abcam.com/dkk1-antibody-epr4759-ab109416.html.
	Primary PPP2R1B detection	monoclonal rabbit anti-PPP2R1b antibody	1 in 100	Abcam®	ab154815	0,663 mg/mL	http://www.abcam.com/ppp2r1b-antibody-epr10158-ab154815.html.
	Secondary KSRP, CCND3, DKK1 and PPP2R1B detection	polyclonal goat anti-Rabbit IgG (H+L) Rhodamine Red™ conjugate	1 in 200	Invitrogen	R-6394	2 mg/mL	https://www.thermofisher.com/order/genome-database/generatePdf?productName=Rabbit%20IgG%20(H+L)&assayType=PRANT&productId=R-6394&detailed=true.

3.5. Knockdown and Overexpression of Proteins

3.5.1. Knockdown of ESRP1, ESRP2 and KSRP

0,3 x 10^6 MDA-MB-436 and 0,75 x 10^6 MDA-MB-468 cells were seeded into the wells of a 6 well plate. 24 hrs. later, 5 nM siRNA directed to ESRP1 (catalogue number 4392420, ID s29571) and ESRP2 (catalogue number 4392420, ID s36796), KSRP (catalogue number 4390824, ID s16323) or Scrambled (catalogue 4390843), purchased from Ambion®, and 9 μL of Lipofectamine® RNAiMAX transfection reagent (Invitrogen™) were each diluted in 150 μL Opti-MEM (Gibco®) and allowed to incubate at RT for 5 min. Following this incubation, the diluted siRNA was added to the diluted transfection reagent, and 250 μL of the solution added dropwise directly to the cells. The cells were grown in a humidified incubator in the absence of CO_2, at 37 °C for 6 hrs. The medium was replaced with fresh medium, and the cells grown in same conditions for a further 66 hrs.

3.5.2. Overexpression of KSRP

0,3 x 10^6 MDA-MB-436 and 0,75 x 10^6 MDA-MB-468 cells were seeded either directly into the wells of a 6 well plate or on microscope cover slips in the wells of a 6 well plate. 24 hrs. later, 1000 ng of plasmid DNA (either pEGFP-N1 or pEGFPC1-6xHis-FLKSRP) and 0,2 μL of P3000™ transfection reagent (Invitrogen™) was diluted in 125 μL Opti-MEM (Gibco®) medium and incubated at RT for 5 min. Simultaneously, 2,5 μL of Lipofectamine® 3000 (Invitrogen™) transfection reagent was diluted in 125 μL Opti-MEM (Gibco®) medium and incubated at RT for 5 min. The diluted DNA was added to the diluted transfection reagent and 240 μL of this solution added dropwise directly to the cells. The cells were grown in a humidified incubator in the absence of CO_2, at 37 °C for 6 hrs. The medium was replaced with fresh medium, and the cells grown in same conditions for a further 66 hrs.

3.6. RNA Extractions

Total RNA was extracted from transfected or untransfected MDA-MB-436 and MDA-MB-468 cells using the RNeasy Mini Kit (Qiagen). Extraction of Total RNA Using the RNeasy Mini Kit.

Cells were harvested by trypsinization, pelleted by centrifugation (Boeco U-320R centrifuge, 4000 rpm, 4 °C, 10 min), washed in 1X Phosphate Buffered Saline (PBS) (appendix A – 8.9) and lysed completely in 350 μL RTL buffer (appendix A – 8.10). One volume of 70% ethanol was added to the lysate and this solution mixed well. 700 μL of this solution was then transferred to the RNeasy spin column placed in a collection tube, centrifuged (Boeco M-24A centrifuge, >8000 x g, RT, 15 s) and the flow-through discarded. 500 μL of RPE buffer (appendix A – 8.11) was added to the RNeasy spin column, centrifuged (Boeco M-24A centrifuge, >8000 x g, RT, 15 s) and the flow-through discarded. 500 μL of RPE buffer (appendix A – 8.11) was added to the RNeasy spin column, centrifuged (Boeco M-24A centrifuge, >8000 x g, RT, 2 min) and the flow-through discarded. The RNeasy spin column was then placed in a clean collection tube and centrifuged (Boeco M-24A centrifuge, full speed, RT, 1 min) to fully dry the column. The RNeasy spin column was placed in a clean 1,5 mL collection tube, 30 μL of RNase-free water added directly to the membrane and the column centrifuged (Boeco M-24A centrifuge, >8000 x g, RT, 1 min) to elute the RNA. A DNase 1 solution (consisting of 10 μL 10x buffer, 2 μL DNase 1, and 58 μL H_20) was added to the eluted RNA and this solution incubated at 37 °C for 10 min. 1 μL of 0,5 M Ethylenediaminetetraacetic Acid (EDTA) (appendix A –8.12) was then added and the solution incubated at 75 °C for 10 min. 250 μL of 100% ethanol was added and the solution mixed well by pipetting. The solution was then transferred to a new RNeasy spin column, centrifuged (Boeco M-24A centrifuge, >8000 x g, RT, 15 s) and the flow-through discarded. 500 μL of the RPE buffer (appendix A – 8.11) was added to the column, centrifuged (Boeco M-24A centrifuge, >8000 x g, RT, 15 s) and the flow-through discarded. 500 μL of the RPE buffer (appendix A – 8.11) was added to the column, centrifuged (Boeco M-24A centrifuge, >8000 x g, RT, 2 min) and the flow-through discarded. The RNeasy spin column was placed in a clean collection tube and centrifuged (Boeco M-24A centrifuge, full speed, RT, 1 min) to fully dry the column. The RNeasy spin column was then placed in a clean 1,5 mL collection tube, 40 μL RNase-free water added directly to the membrane and the column centrifuged (Boeco M-24A centrifuge, 8000 x g, RT, 1 min) to elute the RNA. The

quality and concentration of the eluted RNA were determined using a NanoDrop 2000 Ultra Violet-visible (UV-Vis) spectrophotometer (Thermo Scientific™) and the RNA stored at -80 °C until required.

3.7. Complementary DNA Synthesis

Complementary DNA (cDNA) synthesis was performed using the High-Capacity cDNA Reverse Transcription Kit (Applied Biosystems™). 500 ng of RNA in a final volume of 10 μL was added to the reverse transcriptase master mix consisting of 2 μL 10x Buffer, 0,8 μL 25x Deoxynucleotide Triphosphate (dNTP) mix, 2 μL of either 10x RT Random Primers (used when amplifying exonic regions) or Random Hexamers (used when amplifying intronic regions), 1 μL MultiScribe™ Reverse Transcriptase and 4,2 μL Nuclease-free H_20. This solution was briefly centrifuged and placed in a thermocycler programmed with the following cycling conditions:

	Step 1	Step 2	Step 3	Step 4
Temperature (°C)	25	37	85	4
Time (min)	10	120	5	∞

The cDNA was stored at –20 °C until required.

3.8. Semi-Quantitative Polymerase Chain Reaction

0,5 uL of undiluted cDNA was added to a PCR master mix containing 3,5 μL H_20, 5 μL Phusion Flash High-Fidelity PCR Master Mix (Thermo Scientific™), 0,5 μL forward primer (10 μM) and 0,5 μL reverse primer (10 μM). The FGFR2_e8e11, FGFR2_i81, FGFR2_i82, FGFR2_i83, FGFR2_i8e9, FGFR2_e9 and FGFR2_i9 primer pairs were used for these experiments (see Table 3.1). This solution was briefly centrifuged and placed in a thermocycler programmed with the following cycling conditions:

		30 cycles				
	Step 1	Step 2	Step 3	Step 4	Step 5	Step 6
Temperature (°C)	98	98	*	72	72	4
Time (s)	10	1	5	10	60	∞

* For conventional PCR, the melting temperature was calculated for each primer pair using the Thermo Scientific™ Tm calculator. For gradient PCR, 11 melting temperatures ranging from 55 °C and 70 °C – namely 55 °C, 55,4 °C, 56,3 °C, 57,5 °C, 59,2 °C, 61,4 °C, 63,9 °C, 66,1 °C, 67,7 °C, 68,9 °C, 69,7 °C – were used.

3.9. Polyacrylamide Gel Electrophoresis to Resolve DNA

100bp and/or 1Kb GeneRuler™ DNA ladders (Thermo Scientific™) as well as the PCR product (DNA) was resolved on a 10% polyacrylamide gel (appendix A – 8.16) at 180 V for 2,5 h. After the DNA was electrophoresed, the gel was stained with a 1:1000 dilution of Ethidium Bromide (Promega) in 1x Tris/Borate/EDTA (TBE) (appendix A – 8.17) for 5 min with gentle shaking and visualised using a Gel Doc™ EZ Imager (Bio-Rad).

3.10. Quantitative Real-Time Polymerase Chain Reaction

Two methods of qRT-PCR were used, namely relative and absolute quantification. Relative quantification involves the comparison of target and reference gene Ct values while absolute quantification involves the determination of the amount of target gene expression using a calibration/standard curve, which is produced using cDNA amplified from known amounts of RNA. Using the geNorm algorithm (https://genorm.cmgg.be/), the optimal number of control genes for normalisation and the average expression stability values of a number of control genes used routinely in the laboratory were determined for the MDA-MB-436 and MDA-MB-468 cells. The use of three control genes was found to be optimal. *Glyceraldehyde-3-Phosphate Dehydrogenase* (*GAPDH)*, *Succinate Dehydrogenase Complex, Subunit A (SDHA)* and *Hypoxanthine Phosphoribosyltransferase 1 (HPRT1)* were found to have the most stable expression in MDA-MB-436 and MDA-MB-468 cells and were thus used for normalisation. Relative and absolute qRT-PCR experiments were prepared according to the following protocol:

2 µL of a 1:20 cDNA dilution in H_2O (relative quantification experiments) or 2 µL of an appropriate cDNA dilution (absolute quantification experiments), was added to a qRT-PCR master mix containing 5 µL SYBR (iTaq™ Universal SYBR® Green Supermix), 2,2 µL H_20, 0,4 µL forward primer (10 µM) and 0,4 µL reverse primer (10 µM). The ESRP1, ESRP2, KSRP, FGFR2_lllb, FGFR2_lllc, CCND3, DKK1, and PPP2R1B primer pairs were used for these experiments (see Table 3.1). This solution was carefully pipetted in triplicate into the wells of a white 96 well Piko® PCR Plate (Thermo Scientific™) and the plate sealed with the Adhesive Sealing Film (Thermo Scientific™). The qRT-PCR was completed using the

PikoReal® Real-Time instrument programmed with the following cycling conditions:

		40 cycles			Melt Curve	
	Step 1	Step 2	Step 3	Step 4	Step 5	Step 6
Temperature	95 °C	95 °C	60 °C *	60 °C	60 °C;95 °C *	20 °C
Time	7 min	15 s	30 s	30 s		10 s

* Data collection points

Relatively quantified qRT-PCR data was analysed using the Livak and Schmittgen method [211] according to the Minimum Information for Publication of Quantitative Real-Time PCR Experiments (MIQE) guidelines [212] and absolutely quantified qRT-PCR data was analysed using a calibration/standard curve.

3.11. Total Protein Extraction

Cells were harvested by trypsinization, pelleted by centrifugation (Boeco U-320R centrifuge, 4000 x rpm, 4 °C, 15 min) and the pellet washed in 1X PBS. The pellet was lysed in RIPA buffer (appendix A – 8.13) and incubated on ice for 20 min (vortexing at 5 min intervals). The lysate was centrifuged (Eppendorf 5402 centrifuge, 14000 x rpm, 4 °C, 20 min) and the supernatant stored at –20 °C until required.

3.12. Protein Quantification

The concentration of the extracted proteins was determined using the Micro BCA™ Assay Kit (Thermo Scientific™) according to the following protocol:

10 µL of Bovine Serum Albumin (BSA) standards (125, 250, 500, 750, 1000 and 2000 µg/mL) and unknown protein samples were individually incubated with 10 µL of the Micro BCA working reagent (25 parts Micro BCA reagent MA, 24 parts Micro BCA reagent MB and 1 part Micro BCA reagent MC) for 1 h at 37 °C. The absorbance of the standards and unknown samples were determined using the NanoDrop 2000 spectrophotometer at 562 nm. The concentrations of the unknown samples were extrapolated from a standard curve constructed from the absorbance values of the standards.

3.13. Sodium Dodecyl Sulphate Polyacrylamide Gel Electrophoresis to Resolve Proteins

5 μg of protein was mixed with an appropriate volume of 6x loading dye (appendix A – 8.20) and incubated at 95 °C for 5 min. Following this, 5 μL of the Precision Plus Protein™ Dual Colour Standards (Bio-Rad) as well as the protein samples were stacked on a 5% stacking gel (appendix A – 8.21.2) at 40 V for ~20 min and resolved on a 10% separating gel (appendix A – 8.21.1) at 100 V for ~90 min or until the dye front reached ~1 cm from the bottom of the gel.

3.14. Transfer of Proteins From the Resolved Gel to Membrane

The resolved gel, 0,2 μm Polyvinylidene Difluoride (PVDF) membrane (activated in 70% ethanol) and filter paper were soaked in cold transfer buffer (appendix A – 8.23) for 5 min at RT. The gel was placed above the PVDF membrane and these were sandwiched between filter paper with the gel facing the cathode. The sandwich was placed in the transfer tank filled with cold transfer buffer and 250 mA of constant current applied for 1,5 hrs.

3.15. Immunodectection

After transfer, the PVDF membrane (now containing the proteins transferred from the gel) was removed from the sandwich and blocked in 5% non-fat milk in 1X PBS-Tween (appendix A – 8.25) for 1 h at RT with gentle shaking. Following blocking, the membrane was incubated with the appropriate primary antibody (diluted in 5% non-fat milk in 1X PBS-Tween) overnight at 4 °C with gentle shaking. The membrane was then washed 3 times (10 min each) in 1X PBS-Tween (appendix A – 8.24) at RT with gentle shaking, following which, the membrane was incubated with the appropriate secondary antibody (diluted in 5% non-fat milk in 1X PBS-Tween) for 1 h at RT with gentle shaking. The membrane was washed 3 times (10 min each) in 1X PBS-Tween at RT with gentle shaking. The expression of the protein of interest was detected using the SuperSignal® West Pico Chemiluminescent Substrate (Thermo Scientific™) mixed in a 1:1 ratio. The resultant bands were visualised by exposing the membrane for 1-10 min to CL-XPosure™ film (Thermo Scientific™), which was subsequently developed and fixed using the Konica SRX-101A machine.

3.15.1. Antibodies

The polyclonal rabbit anti-KSRP, polyclonal rabbit anti-Histone H3, monoclonal rabbit anti-Human IgG, polyclonal rabbit anti-U2AF65 and polyclonal goat anti-Rabbit IgG peroxidase conjugate antibodies were used (see Table 3.2).

3.16. Confocal Fluorescence Microscopy

In conventional (or wide-field) fluorescence microscopy, the entire specimen in the optical path is flooded with light from the light source, and thus, all areas are excited at the same time. This creates a large unfocused background, which diminishes the optical resolution of the image. The elimination of this out-of-focus background is achieved in confocal fluorescence microscopy through the use of point illumination and a pinhole in an optically conjugate plane in front of the detector. Only fluorescent light near the focal plane can be detected and thus, the optical resolution of the image is increased.

3.16.1. Preparation of Cells

Microscope cover slips were soaked in 100% ethanol, passed through a flame to sterilise and placed in the wells of a cell culture dish (6 or 12 well). Approximately 0,5 x 10^5 and 1 x 10^5 MDA-MB-436 and MDA-MB-468 cells, respectively, were seeded directly on the microscope cover slips in minimal medium and the well filled with medium 6 hrs. later. If necessary, cells were transfected 24 h later with plasmid DNA (pEGFP-N1 or pEGFPC1-6xHis-FLKSRP), the medium changed 6 hrs. after transfection and the cells incubated for a further 66 hrs.

3.16.2. Fixing, Staining and Mounting of Cells Grown on Microscope Cover Slips

After incubation (if necessary), the cell culture medium was removed and the microscope cover slips washed thrice in 1X PBS-Tween (appendix A – 8.24). The microscope cover slips were fixed in 100% methanol (at –20 °C) in a – 20 °C freezer for 5 min. Following fixation, the microscope cover slips were washed thrice in 1X PBS-Tween and incubated in the primary antibody solution diluted in 1X PBS-Tween for 1 h at RT in the dark. After primary antibody staining, the microscope cover slips were washed thrice in 1X PBS-Tween and incubated in

the secondary antibody solution diluted in 1X PBS-Tween for 1 h at RT in the dark. After secondary antibody staining, the microscope cover slips were washed thrice in 1X PBS-Tween, stained with the nuclear stain 4′,6-diamidino-2-phenylindole (DAPI) (1:1000 dilution in 1X PBS-Tween) for 5 min at RT and washed thrice in 1X PBS-Tween. The microscope cover slips were then rinsed in distilled water (dH_2O), mounted (cell side down) on microscope slides in Fluorescence Mounting Medium (Dako), allowed to dry at RT for 1 h in the dark and finally stored in the dark at 4 °C until viewed using the 60x objective on the Olympus IX71 Fluorescence Microscope.

3.16.2.1. Antibodies

The monoclonal rabbit anti-Cytokeratin 19, monoclonal mouse anti-Vimentin, polyclonal goat anti-Rabbit IgG (H+L) Rhodamine Red™ conjugate and polyclonal goat anti-Mouse IgG DyLight™ 649 conjugate antibodies were used (see Table 3.2).

3.17. Ultra Violet Cross-Linking and Immunoprecipitation

This technique is used to identify pre-mRNA sequences bound to specific RNA-binding proteins.

3.17.1. Ultra Violet Cross-Linking

The medium from confluent MDA-MB-468 cells grown in six 10 cm cell culture dishes (Nunc™) was removed, 6 mL ice-cold 1X PBS (appendix A – 8.9) added to each plate and the cells placed on ice. The cells were irradiated with 150 mJ/cm^2 energy transferred at 254 nm in a Stratalinker 2400, scraped using cell scrapers and the cell suspensions transferred to 3 centrifuge tubes. These tubes were centrifuged (Eppendorf 5402 centrifuge, 514 x g, 4 °C, 1 min) to pellet the cells, the supernatant discarded and the pellets snap-frozen in liquid nitrogen. The pellets were stored at –80 °C until needed.

3.17.2. Immunoprecipitation

3.17.2.1. Magnetic Bead Preparation

100 μL of magnetic protein A Dynabeads (Invitrogen) per experiment were placed in microcentrifuge tubes and washed twice with 900 μL lysis buffer

without the protease inhibitor cocktail (appendix A – 8.26). The magnetic beads were resuspended in 100 μL lysis buffer with 10 μg antibody (either control or experimental) per experiment, the tubes rotated for 60 min at RT and the magnetic beads washed 3 times with 900 μL lysis buffer.

3.17.2.1.1. Antibodies

The monoclonal rabbit anti-Human IgG and polyclonal rabbit anti-KHSRP antibodies were used (see Table 3.2).

3.17.2.2. Cell Lysis and Partial RNA Digestion

The cell pellet from section 3.17.1 was resuspended in 1 mL lysis buffer with 1:100 Protease Inhibitor Cocktail Set III (appendix A – 8.26) and transferred into a 1,5 mL microcentrifuge tube. The pellet was lysed using the Bioruptor plus for 5 cycles with alternating 30 s on/30 s off at low intensity. A 1:1000 dilution of RNase 1 (Thermo Scientific ™) in 1X PBS was prepared; 10 μL of this RNase 1 solution with 2 μL Turbo DNase (Thermo Scientific™) was added to the cell lysate and the solution immediately placed at 37 °C for 3 min with rotation at 1100 rpm. Following this incubation, the solution was immediately placed on ice for >3 min, centrifuged (Eppendorf 5402 centrifuge, 22000 x g, 4 °C, 10 min) and the supernatant transferred to a clean microcentrifuge tube, preventing carry-over. An aliquot of the supernatant taken before immunoprecipitation was retained for downstream western blot analysis.

3.17.2.3. Immunoprecipitation

The supernatant (from section 3.17.2.2) was added to the prepared magnetic beads (from section 3.17.2.1) and this solution was rotated (overnight; 4 °C; 1100 rpm). Following incubation, the solution was placed on a magnet, and after an aliquot of the supernatant was retained for downstream western blot analysis, the remainder was discarded. The magnetic beads were washed once with high-salt wash buffer (appendix A – 8.27), washed for a second time with the same buffer, rotated for 1 min at 4 °C and the wash discarded. The magnetic beads were then washed twice with PNK buffer (appendix A – 8.28) and finally resuspended in 1 mL of this same buffer.

3.17.2.4. Extraction of RNA Bound to Immunoprecipitated KSRP

RNA bound to the immunoprecipitated protein (KSRP) was extracted using TRIzol® Reagent (Thermo Scientific™). Immunoprecipitated samples (magnetic beads with bound KSRP and RNA) were incubated with 1 mL of TRIzol® Reagent for 5 min at RT. 200 μL chloroform was added to the TRIzol® solution, the solution mixed vigorously by hand for 25 s and incubated at RT for 3 min. This solution was centrifuged (Eppendorf 5402 centrifuge, 12000 x g, 4 °C, 15 min) and the aqueous phase (colourless upper phase) transferred to a clean microcentrifuge tube. 0,5 mL of 100% isopropanol was added to the aqueous phase, the solution incubated at RT for 10 min, centrifuged (Eppendorf 5402 centrifuge, 12000 x g, 4 °C, 10 min) and the supernatant discarded. The pellet was washed in 1 mL of 75% ethanol, the solution vortexed (Cleaver Scientific Ltd), centrifuged (Eppendorf 5402 centrifuge, 7500 x g, 4 °C, 5 min) and the supernatant discarded. The pellet (containing the RNA) was air dried, resuspended in 30 μL of RNase-free water and incubated at 55 °C for 10 min. The quality and concentration of the RNA were determined using a NanoDrop 2000 UV-Vis spectrophotometer (Thermo Scientific™) and the RNA stored at –80 °C until required.

3.17.2.5. cDNA Synthesis and qRT-PCR

cDNA was synthesised using random hexamers and absolute quantification qRT-PCR was performed as detailed in sections 3.7 and 3.10, respectively. The FGFR2_i81, FGFR2_i82, FGFR2_i83, FGFR2_i8e9, FGFR2_e9 and FGFR2_i9 primer pairs were used for this experiment (see Table 3.1).

3.17.2.6. Western Blotting

Control and experimental pre-IP and post-IP samples were probed for the presence of KSRP or α-U2AF65 (loading control) according to protocols detailed in 3.11, 3.12, 3.13, 3.14 and 3.15.

3.18. Affymetrix GeneChip® Human Transcriptome Array 2.0

Total RNA was extracted (section 3.6) from the following samples:

MDA-MB-436 – 5 biological repeats

MDA-MB-468 – 5 biological repeats

MDA-MB-468 transfection control (siScr) cells – 4 biological repeats

MDA-MB-468 KSRP knockdown (siKSRP) cells – 4 biological repeats

Post-extraction, RNA is extremely susceptible to degradation due to the presence of RNases in the environment and the more degraded the RNA, the poorer its quality. The RNA quality requirements differ between applications, and these requirements are based on the resultant amplicon size e.g. a lower quality RNA can be used for qRT-PCR assays but microarray experiments often require higher-quality RNA. Using microfluidics and sample specific chips, the 2100 Bioanalyzer (Agilent Technologies) analyses RNA integrity and reports this as an RNA Integrity Number (RIN). This RIN is a measure of the electrophoretic trace of the RNA as well as the 28S/18S rRNA ratios. RINs range from 0-10, with 10 indicating the maximum RNA integrity. The integrity quality of the extracted RNA was determined using the 2100 Bioanalyzer (Agilent Technologies), and for each sample, the three biological repeats exhibiting the highest RINs were selected for further analysis (appendix B – 9.1).

The gene expression profiles and transcript isoforms of these samples were determined using the Affymetrix GeneChip® Human Transcriptome Array 2.0. This array contains >6 million distinct probes that cover both the coding and non-coding transcripts. 70% of the probes are designed to cover the coding transcripts and the remaining 30% are designed to cover both the exon-exon splice site junctions and the non-coding transcripts. In this array, each exon has approximately ten probes per exon and four probes are designed per exon-exon splice site. The probes are arranged into probe sets that aid in summarising the data at the gene-level, exon-level and splice junction. The Affymetrix® Transcriptome Analysis Console (TAC) Software assists in the visualisation of the data, the changes in expression at the gene and exon level as well as the alternatively spliced exons. Using this assay, KSRP knockdown MDA-MB-468 cells (MDA-MB-468 cells transfected with siKSRP) were compared to MDA-MB-468 transfection control cells (MDA-MB-468 cells transfected with siScr). Venn diagrams summarising the resultant data were drawn using Venny [Oliveros, J.C. (2007-2015) Venny. An Interactive tool for comparing lists with Venn's diagrams http://bioinfogp.cnb.csic.es/tools/venny/index.html].

3.18.1. Selection and Validation of Targets of Interest

From the results of the Affymetrix GeneChip® Human Transcriptome Array 2.0, targets of interest were selected and the changes in gene expression of these targets upon KSRP knockdown in MDA-MB-468 cells validated using qRT-PCR, (primers used are detailed in Table 3.1).

3.18.2. Prediction of KSRP Interaction and Determination of KSRP Co-Localisation With Selected Targets of Interest

Prediction of KSRP interaction with the selected targets was determined using the Search Tool for the Retrieval of Interacting Genes/Proteins (STRING) – http://string-db.org/. Protein sequences were acquired from UniProt – http://www.uniprot.org/.

MDA-MB-468 cells were seeded on microscope cover slips in the wells of a 6 well plate and transfected with 1000 ng plasmid DNA (either pEGFP-N1 or pEGFPC1-6xHis-FLKSRP) as described in section 3.5.2. 24h after transfection, the cells were fixed, stained and mounted as described in section 3.16.2 and stored at 4 °C until viewed on the Olympus IX71 Fluorescence Microscope. The 2 dimensional (2D) intensity histograms and Pearson's R-values for each potential co-localisation event were acquired using Fiji Is Just ImageJ (FIJI) software.

3.18.2.1. Antibodies

The polyclonal rabbit anti-KSRP, monoclonal rabbit anti-Cyclin D3, monoclonal rabbit anti-DKK1, monoclonal rabbit anti-PPP2R1b and polyclonal goat anti-Rabbit IgG (H+L) Rhodamine Red™ conjugate antibodies were used (see Table 3.2).

3.19. ImageJ Analysis

ImageJ is a program useful for the processing of scientific multidimensional images [213]. This program was used to quantify band intensities in the semi-quantitative PCR (semi-qPCR) and western blot experiments, and to generate 2D intensity histograms and Pearson's R-values in the co-localisation experiments.

3.19.1. Quantification of Band Intensities

16-bit .tiff digital image of the gel (section 3.8) or western blot x-ray films (section 3.15) were uploaded into ImageJ and the intensity of each band (surrounded by a box of equal area) determined.

3.19.2. Generation of 2D Intensity Histograms

A 'batteries included' distribution of ImageJ, known as FIJI (FIJI is just ImageJ) [214], with the Coloc 2 plugin, was used to generate 2D intensity histograms from fluorescent co-localisation images (section 3.16). To generate the 2D intensity histograms, the merged co-localisation images were uploaded into the program and the colour channels (red, green and blue) split. Two colour channels were chosen for comparison (e.g. red and green) and the exact section of the image that the analysis should be completed on (e.g. a specific cell) was identified. Coloc 2 calculated and plotted the intensity values for each pixel in each channel against each other. Positive correlation created a 'cloud' in the centre of the 2D intensity histogram, which is fitted to a linear regression.

3.19.3. Calculation of Pearson's R-Value

A 'batteries included' distribution of ImageJ, was used to calculate Pearson's R-values from fluorescent co-localisation images (section 3.16). To calculate Pearson's R-values, the merged co-localisation images were uploaded into the program and the colour channels (red, green and blue) split. Two colour channels for comparison (e.g. red and green) were chosen and the exact section of the image that the analysis should be completed on (e.g. a specific cell) was selected. Coloc 2 then performed pixel intensity correlation and outputted the Pearson's R-values.

3.20. Statistical Analysis

All statistics were acquired using the STATA version 13 Data Analysis and Statistical Software (STATS Inc., Texas). One and two tailed t-Tests were performed; ns ($p > 0{,}005$), * ($p \leq 0{,}05$), ** ($p \leq 0{,}01$), *** ($p \leq 0{,}001$).

Chapter 4

4. RESULTS

4.1. Hypothesis-Based Approach

The first section of this study adopted a hypothesis-based approach to determine whether the splicing-associated protein, KSRP, is involved in the alternative splicing mechanism of *FGFR2* mRNA. Its potential involvement in the splicing of this gene may impact the ratio of *FGFR2 IIIb* and *FGFR2 IIIc* inclusion in MDA-MB-436 and MDA-MB-468 cells, and thus altering their mesenchymal and epithelial phenotype, respectively.

4.1.1. Confirmation of the Epithelial and Mesenchymal Phenotype, Preferential *FGFR2* Isoform Inclusion, Differential KSRP Expression and Alteration of *FGFR2* Isoform Expression in MDA-MB-436 and MDA-MB-468 Cells

The hypothesis-based section of this study is founded upon the preferential inclusion of *FGFR2 IIIb* and *FGFR2 IIIc* in epithelial and mesenchymal cells, respectively, which corresponds to the phenotype. Thus, we sought to confirm that MDA-MB-468 and MDA-MB-436 cells indeed represent epithelial and mesenchymal phenotypes, respectively, and that there is preferential *FGFR2 IIIb* and *FGFR2 IIIc* inclusion and differential KSRP expression in MDA-MB-436 and MDA-MB-468 cells. Lastly, the ability to alter *FGFR2 IIIb* and *FGFR2 IIIc* expression in MDA-MB-436 and MDA-MB-468 was examined.

4.1.1.1. Confirmation of the Epithelial and Mesenchymal Phenotype in MDA-MB-436 and MDA-MB-468 Cells Using Confocal Fluorescence Microscopy

MDA-MB-436 and MDA-MB-468 cells seeded on microscope cover slips were fixed and stained with primary antibodies specific to either Cytokeratin 19 (an epithelial-specific marker) or Vimentin (a mesenchymal-specific marker) and visualised using the Olympus IX71 Fluorescence Microscope (section 3.16). To prevent manipulation of the images, the gains (exposure) on the red channel (used to capture Cytokeratin 19 and Vimentin staining) were kept constant between cell lines when the fluorescence images were captured.

The epithelial marker, Cytokeratin 19, was not visible in MDA-MB-436 cells (Figure 4.1 A) but the mesenchymal marker, Vimentin, was seen in these cells (Figure 4.1 B). In contrast, the epithelial marker, Cytokeratin 19, was visible in MDA-MB-468 cells (Figure 4.2 A) but the mesenchymal marker, Vimentin, was not (Figure 4.2 B).

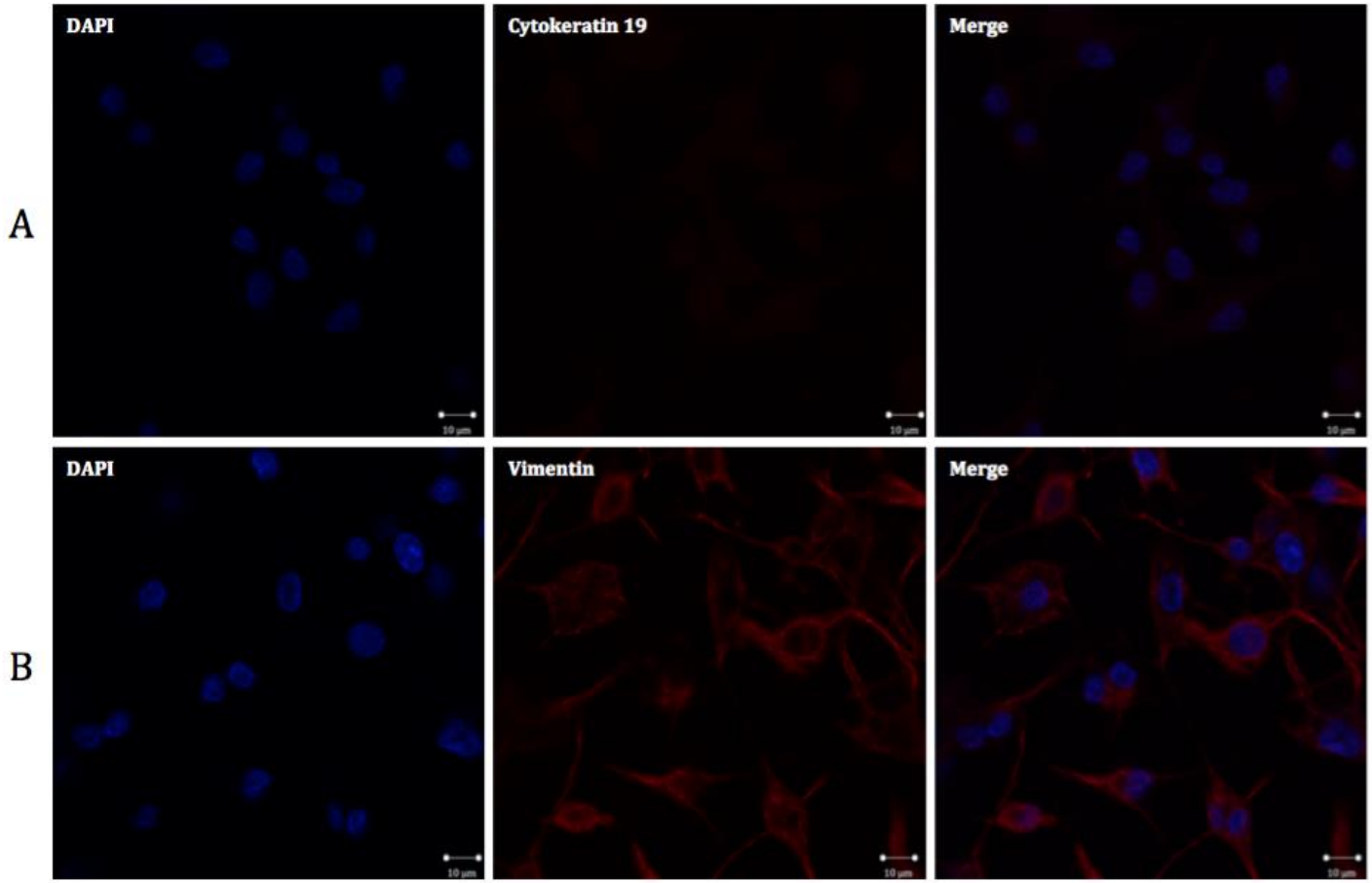

Figure 4.1 – Visualisation of epithelial and mesenchymal markers present in MDA-MB-436 cells. A) The epithelial marker, Cytokeratin 19, was not visible in MDA-MB-436 cells. B) The mesenchymal marker, Vimentin, was visible in MDA-MB-436 cells. The monoclonal rabbit anti-Cytokeratin 19 and monoclonal mouse anti-Vimentin primary antibodies as well as polyclonal goat anti-Rabbit IgG (H+L) Rhodamine Red and polyclonal goat anti-Mouse IgG DyLight 649 secondary antibodies were used. Images were captured using the Olympus IX71 Fluorescence Microscope. Included images are representative of similar ones obtained; n = 3.

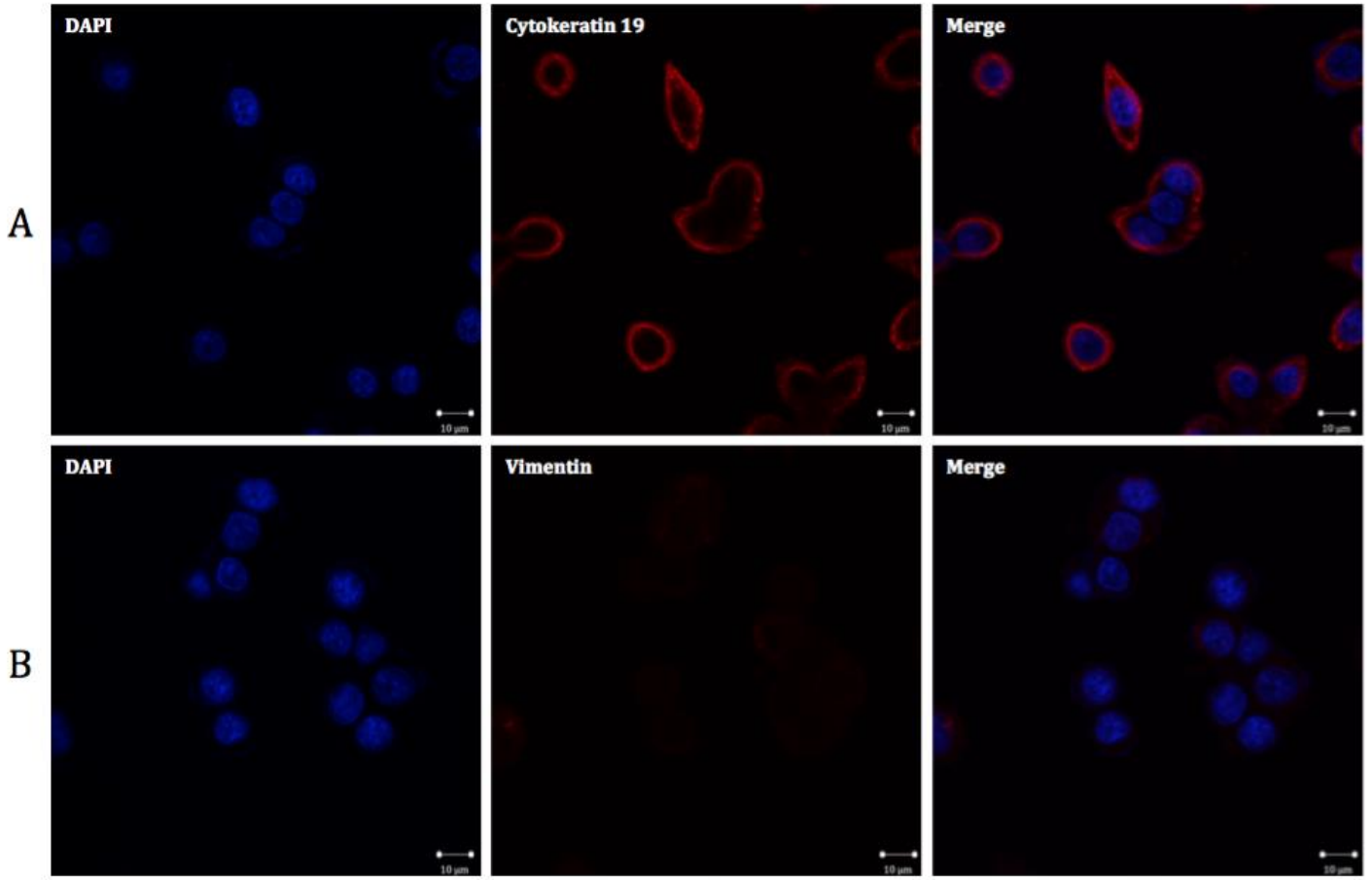

Figure 4.2 - Visualisation of epithelial and mesenchymal markers present in MDA-MB-468 cells. A) The epithelial marker, Cytokeratin 19, was visible in MDA-MB-468 cells. B) The mesenchymal marker, Vimentin, was not visible in MDA-MB-468 cells. The monoclonal rabbit anti-Cytokeratin 19 and monoclonal mouse anti-Vimentin primary antibodies as well as polyclonal goat anti-Rabbit IgG (H+L) Rhodamine Red and polyclonal goat anti-Mouse IgG DyLight 649 secondary antibodies were used. Images were captured using the Olympus IX71 Fluorescence Microscope. Included images are representative of similar ones obtained; n = 3.

4.1.1.2. Confirmation of Preferential *FGFR2* Isoform Inclusion in MDA-MB-436 and MDA-MB-468 Cells Using Semi-qPCR and qRT-PCR

Semi-qPCR (section 3.8) was used to confirm the preferential inclusion of the *FGFR2* isoforms in MDA-MB-436 and MDA-MB-468 cells using cDNA (section 3.7) reverse transcribed from RNA extracted from MDA-MB-436 and MDA-MB-468 cells (section 0). This semi-qPCR was accomplished using a single primer pair (FGFR2_e8e11 – Table 3.1) designed to amplify *FGFR2 IIIb* and *FGFR2 IIIc* in the same reaction. The forward and reverse primers bind to *FGFR2* exon 8 and *FGFR2* exon 11, respectively, flanking the *FGFR2 IIIb* and *FGFR2 IIIc* exons (Figure 4.3). Either exon 9 (*FGFR2 IIIb*) or exon 10 (*FGFR2 IIIc*) is always included in the final transcript after mutually exclusive alternative splicing of the *FGFR2* gene (Figure 4.3). The *FGFR2 IIIb* (exons 8, 9 and 11) transcript (412 bp) is distinguishable from the *FGFR2 IIIc* (exons 8, 10 and 11) (464 bp) transcript when the PCR product is resolved on a gel because of the differential size of the centrally located exon.

The resolved PCR product resulted in two distinct bands of amplified DNA, corresponding to *FGFR2 IIIc* (top) and *FGFR2 IIIb* (bottom) (Figure 4.4 A). Using ImageJ, the *FGFR2 IIIb* and *FGFR2 IIIc* band intensities in each sample (MDA-MB-436 and MDA-MB-468) were determined (section 3.19.1) and the ratio of *FGFR2 IIIb* and *FGFR2 IIIc* inclusion expressed as a percentage of the total. In MDA-MB-436 cells, the *FGFR2* isoforms consisted of 17% IIIb and 83% IIIc while in MDA-MB-468 cells, *FGFR2* isoforms consisted of 67% IIIb and 33% IIIc (Figure 4.4 B).

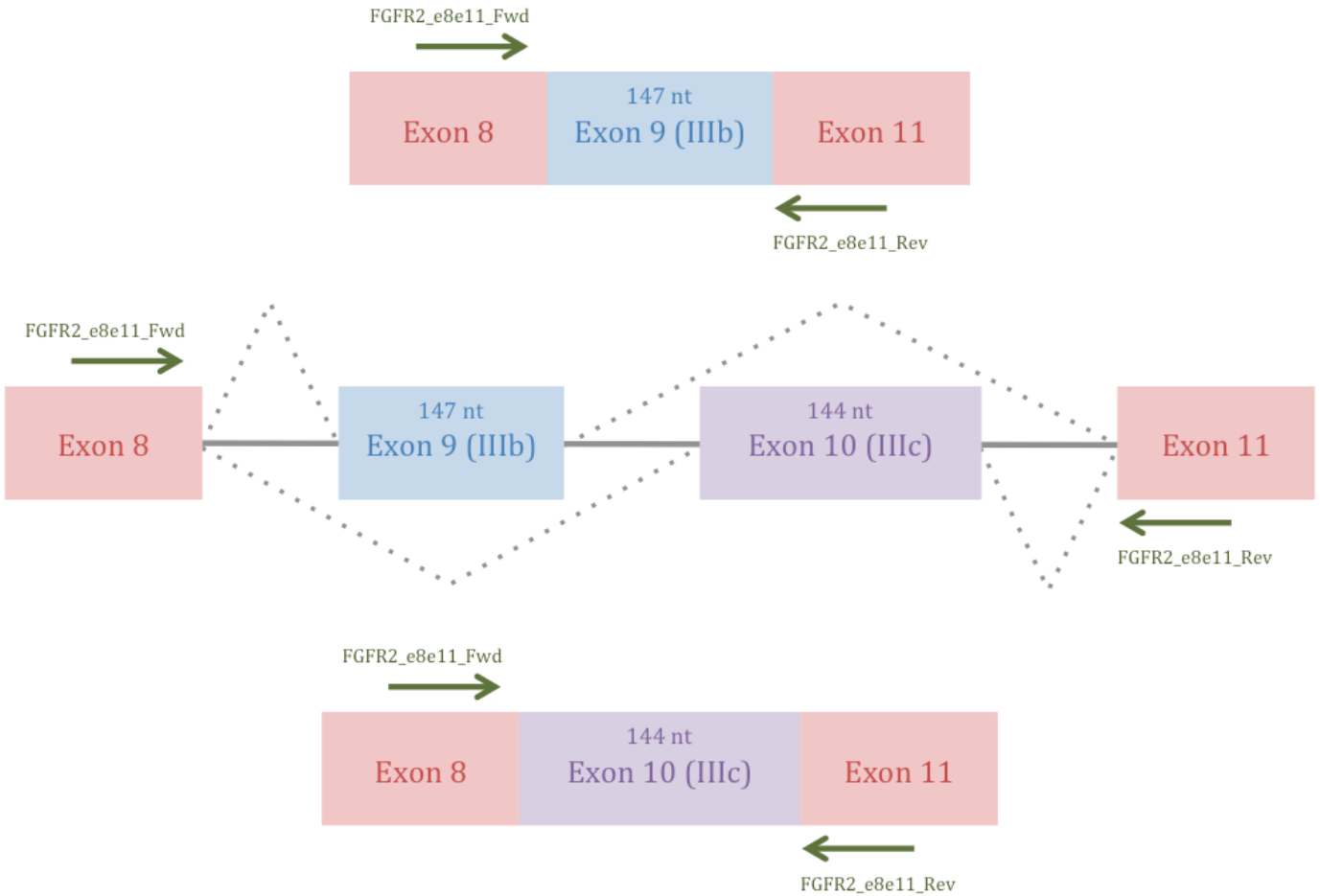

Figure 4.3 - Semi-qPCR primer design. One primer pair (FGFR2_e8e11) was designed to bind to either exon 8 (Fwd) or exon 11 (Rev). Because of the mutually exclusive inclusion of exon 9 (IIIb) and exon 10 (IIIc), and the differential sizes of these exons (IIIb – 147 nt and IIIc –144 nt), the resultant PCR products have distinct sizes.

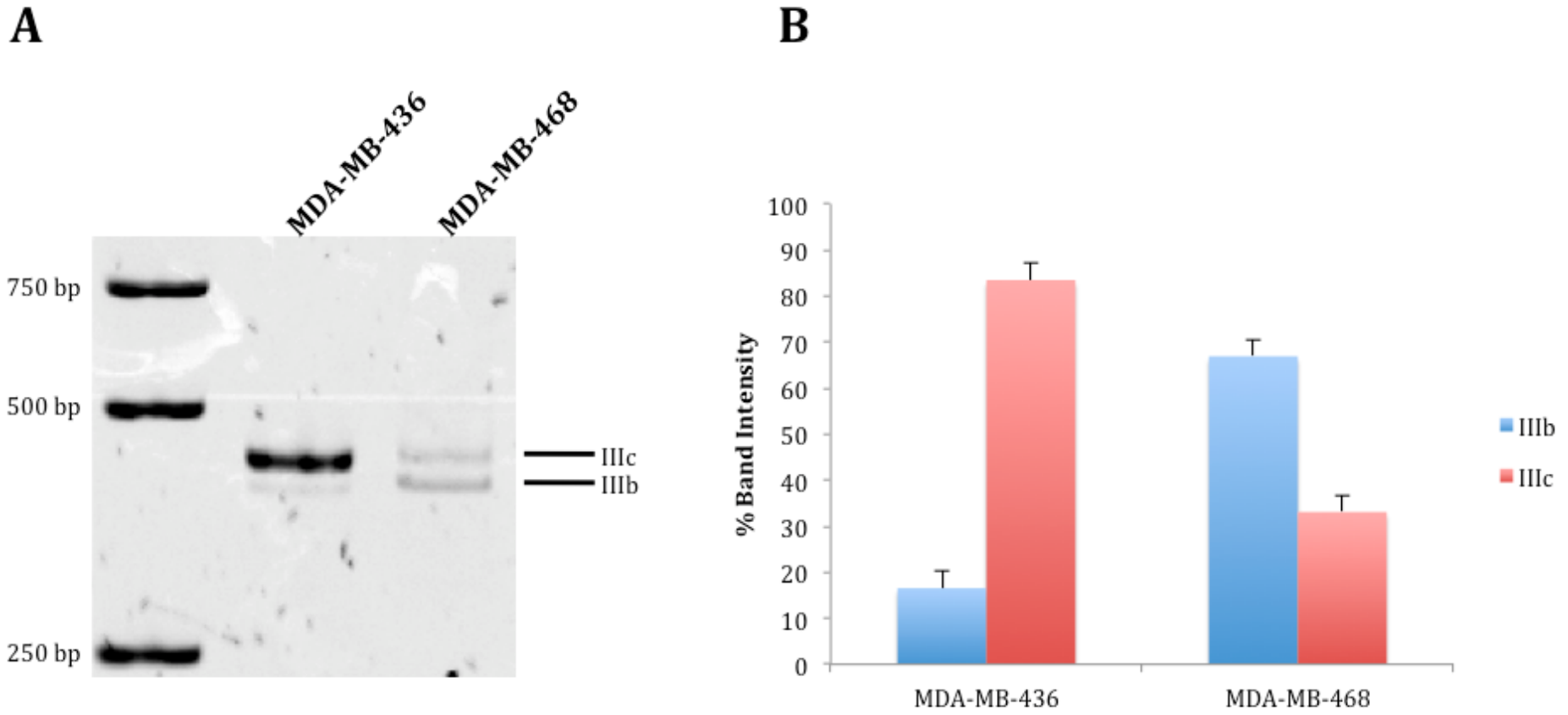

Figure 4.4 – Semi-quantitative analysis of preferential *FGFR2 IIIb* (IIIb) and *FGFR2 IIIc* (IIIc) inclusion in MDA-MB-436 and MDA-MB-468 cells. The *FGFR2 IIIb* transcript (exon 8, 9 and 11) is 412 bp while the *FGFR2 IIIc* transcript (exon 8, 10 and 11) is 464 bp. A) PCR product from each cell line resolved on a 10% polyacrylamide gel representing *FGFR2 IIIc* (top band) and *FGFR2 IIIb* (bottom band). B) ImageJ was used to quantify the intensity of the bands and this showed preferential expression of IIIc and IIIb in MDA-MB-436 and MDA-MB-468 cells, respectively. In MDA-MB-436 cells, the *FGFR2* isoforms consisted of 17% IIIb and 83% IIIc while in MDA-MB-468 cells, *FGFR2* isoforms consisted of 67% IIIb and 33% IIIc. Included image is representative of similar ones obtained; n = 3; standard deviations are shown.

Absolute qRT-PCR (section 3.10) was used to confirm the RNA expression levels of *FGFR2 IIIb* and *FGFR2 IIIc* in MDA-MB-436 and MDA-MB-468 cells. In MDA-MB-436 cells, the *FGFR2* isoforms consisted of 3% *FGFR2 IIIb* and 97% *FGFR2 IIIc*, while in MDA-MB-468 cells, the *FGFR2* isoforms consisted of 66% *FGFR2 IIIb* and 34% *FGFR2 IIIc* (Figure 4.5). In MDA-MB-436 cells, the preferential inclusion of *FGFR2 IIIc* is very clear, however, in MDA-MB-468 cells, this preferential inclusion of *FGFR2 IIIb* is less distinct.

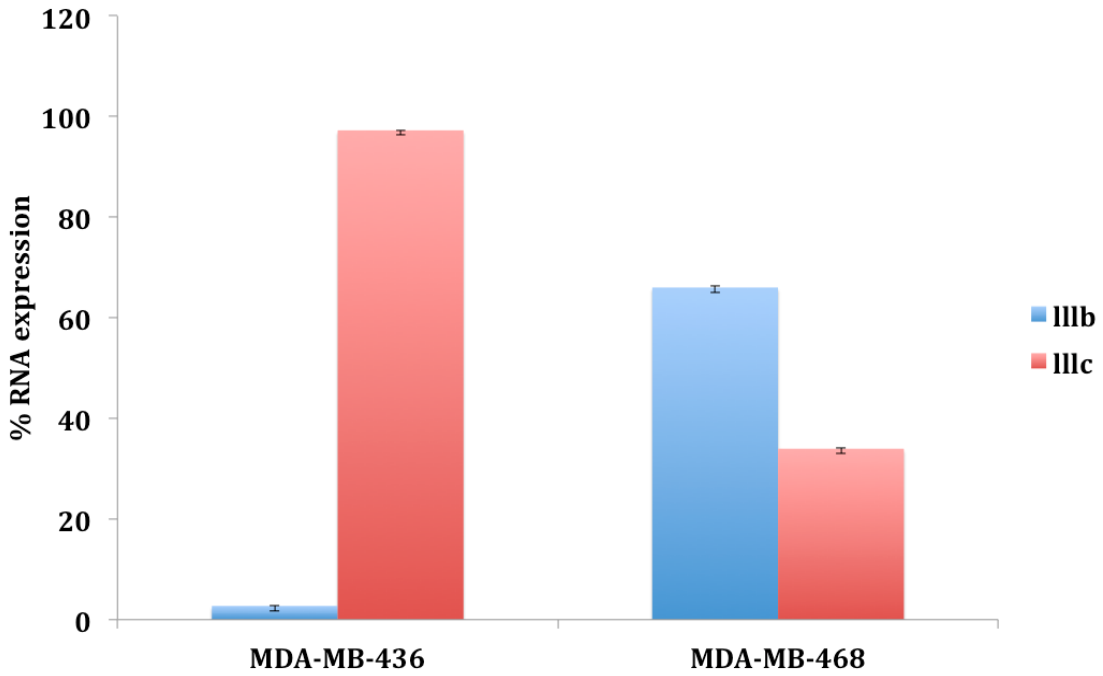

Figure 4.5 – *FGFR2 lllb* (IIIb) and *FGFR2 lllc* (IIIc) expression in MDA-MB-436 and MDA-MB-468. RNA expression levels of lllb and lllc were determined using absolute qRT-PCR quantification. The RNA levels of lllb and lllc in each cell line were expressed as a percentage of total *FGFR2* isoforms. In MDA-MB-436 cells, the *FGFR2* isoforms consisted of 3% *FGFR2 IIIb* and 97% *FGFR2 IIIc*, while in MDA-MB-468 cells, the *FGFR2* isoforms consisted of 66% *FGFR2 IIIb* and 34% *FGFR2 IIIc*. n = 3; standard deviations are shown.

4.1.1.3. Confirmation of Differential KSRP Expression in MDA-MB-436 and MDA-MB-468 Cells Using Western Blotting

KSRP protein expression in MDA-436 and MDA-MB-468 cells was determined by western blotting using Histone-3 protein expression as a loading control (section 3.11-3.15). The amount of protein present in a sample is directly proportional to the intensity of the resultant band on the X-ray film. KSRP bands appeared more intense in MDA-MB-468 cells compared to MDA-MB-436 cells (Figure 4.6 A). Below the KSRP band, a faint secondary band was observed in both cell line samples, which may be a KSRP variant. The primary KSRP band intensities were quantified using ImageJ (section 3.19.1), showing that KSRP protein expression was 14% higher in MDA-MB-468 cells compared to MDA-MB-436 cells (Figure 4.6 B).

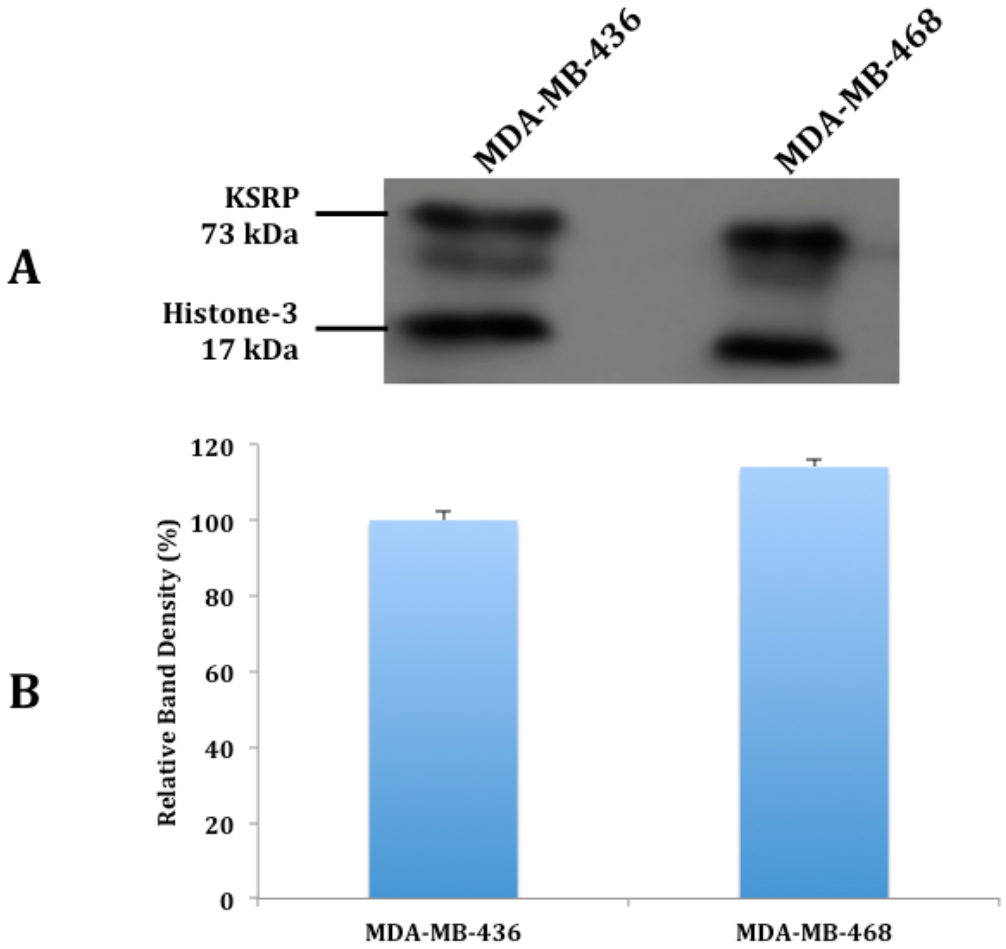

Figure 4.6 – KSRP protein expression level in MDA-MB-436 and MDA-MB-468 cells. A) Composite image of the western blot detection of KSRP and Histone-3 (loading control). B) ImageJ analysis of KSRP band density. KSRP band density in MDA-MB-468 cells was reported relative to KSRP band density in MDA-MB-436 cells, which was set at 100%. KSRP protein expression in MDA-MB-468 cells was 14% higher than KSRP protein expression in MDA-MB-436 cells. Included image is representative of similar ones obtained; n = 2; standard deviations are shown.

4.1.1.4. Confirmation of the Alteration of *FGFR2* Isoform Expression in MDA-MB-436 and MDA-MB-468 Cells

To confirm that the levels of *FGFR2 IIIb* and *FGFR2 IIIc* inclusion, determined by alternative splicing, is dependent on the expression of specific regulatory genes, the splicing regulatory proteins ESRP1 and ESRP2 were downregulated in MDA-MB-436 and MDA-MB-468 cells using siRNA (section 3.5.1). ESRP1 and ESRP2 knockdown was confirmed using qRT-PCR (section 3.10) and the effect of this downregulation on *FGFR2 IIIb* and *FGFR2 IIIc* inclusion levels was also analysed using this technique. ESRP1 and ESRP2 were successfully downregulated in MDA-MB-436 and MDA-MB-468 cells, and in response to this downregulation, *FGFR2 IIIb* inclusion was reduced and *FGFR2 IIIc* inclusion was increased in both cell lines (Figure 4.7).

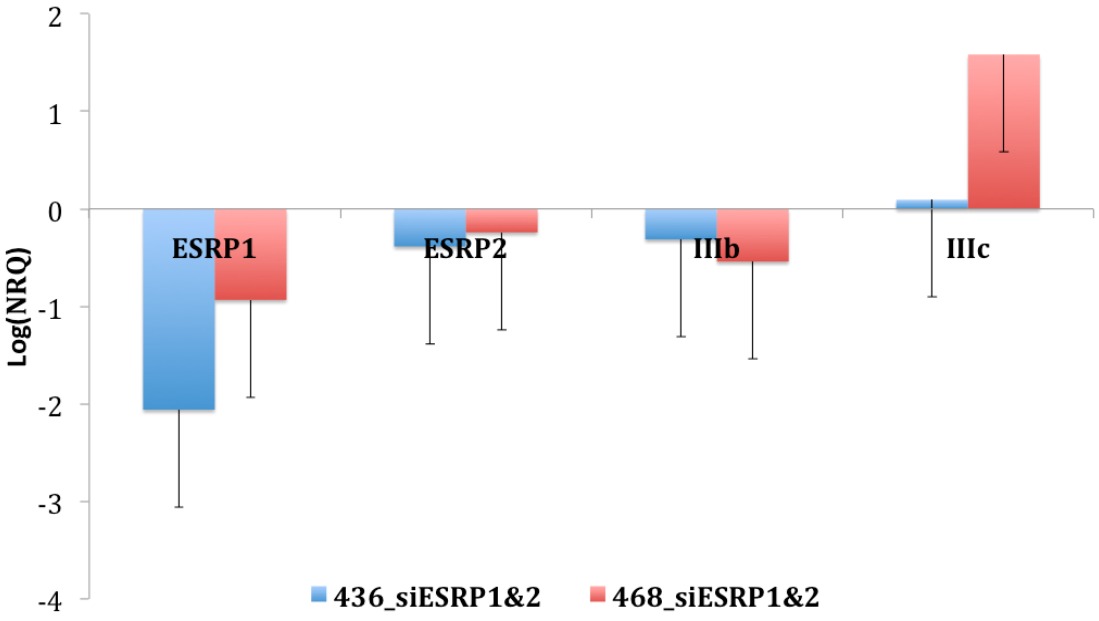

Figure 4.7 – *FGFR2 IIIb* (IIIb) and *FGFR2 IIIc* (IIIc) expression is affected by ESRP1 and ESRP2 knockdown in MDA-MB-436 (436) and MDA-MB-468 (468) cells. mRNA expression levels of ESRP1, ESRP2, IIIb and IIIc in ESRP1&2 knockdown cells (siESRP1&2) were expressed relative to the mRNA expression levels of these genes in the transfection control cells (siScr). ESRP1 and ESRP2 were successfully downregulated in 436 and 468 cells and this downregulation resulted in decreases and increases in the expression of IIIb and IIIc, respectively. n = 3; standard deviations are shown.

4.1.2. Determination of the Effect of the Modification of KSRP Expression on *FGFR2* Isoform Expression and the Epithelial and Mesenchymal Phenotype in MDA-MB-436 and MDA-MB-468 Cells

The role of KSRP in *FGFR2* splicing is an important aspect of this project. Thus, we sought to determine if increasing or decreasing the expression levels of this protein would affect *FGFR2 IIIb* and *FGFR2 IIIc* expression. We also sought to establish if changes in the mRNA expression levels of *FGFR2 IIIb* and *FGFR2 IIIc* as a consequence of altered KSRP expression would result in visible alterations in the mesenchymal and epithelial phenotypes of MDA-MB-436 and MDA-MB-468 cells, respectively. This was determined by the visualisation of the epithelial marker, Cytokeratin 19 and the mesenchymal marker, Vimentin in the aforementioned cells.

4.1.2.1. Confirmation of KSRP Knockdown and KSRP Overexpression in MDA-MB-436 and MDA-MB-468 Cells

KSRP downregulation was achieved by transfection of cells with an siRNA directed against *KSRP* mRNA (labelled siKSRP) (section 3.5.1). Cells were transfected with a non-targeting siRNA (labelled siScr) as a transfection control (section 3.5.1). *KSRP* overexpression was achieved by transfection of cells with the pEGFPC1-6XHis-FLKSRP plasmid (labelled pKSRP), which encodes for the full-length KSRP protein (section 3.5.2). Cells were transfected with the pEGFP-N1 plasmid (pGFP), which encodes for the GFP protein, as a transfection control (section 3.5.2).

Following downregulation or overexpression of *KSRP*, the mRNA expression levels of *KSRP* were determined using qRT-PCR (section 3.10). Levels of *KSRP* expression when down- (siKSRP) or upregulated (pKSRP) were expressed relative to the expression levels of the *KSRP* knockdown (siScr) and overexpression (pGFP) transfection controls, respectively. When *KSRP* was downregulated, there was a significant decrease in the mRNA expression levels of *KSRP* in both MDA-MB-436 ($p \leq 0,01$) and MDA-MB-468 ($p \leq 0,001$) cells (Figure 4.8). This decrease in the RNA expression levels was significantly different in MDA-MB-436 and MDA-MB-468 cells ($p \leq 0,01$). When *KSRP* was overexpressed, there was a significant increase in the mRNA expression levels of

KSRP in MDA-MB-436 ($p \leq 0{,}001$) and MDA-MB-468 ($p \leq 0{,}001$) cells (Figure 4.8). This increase in the mRNA expression levels of this protein is significantly different in MDA-MB-436 and MDA-MB-468 cells ($p \leq 0{,}001$).

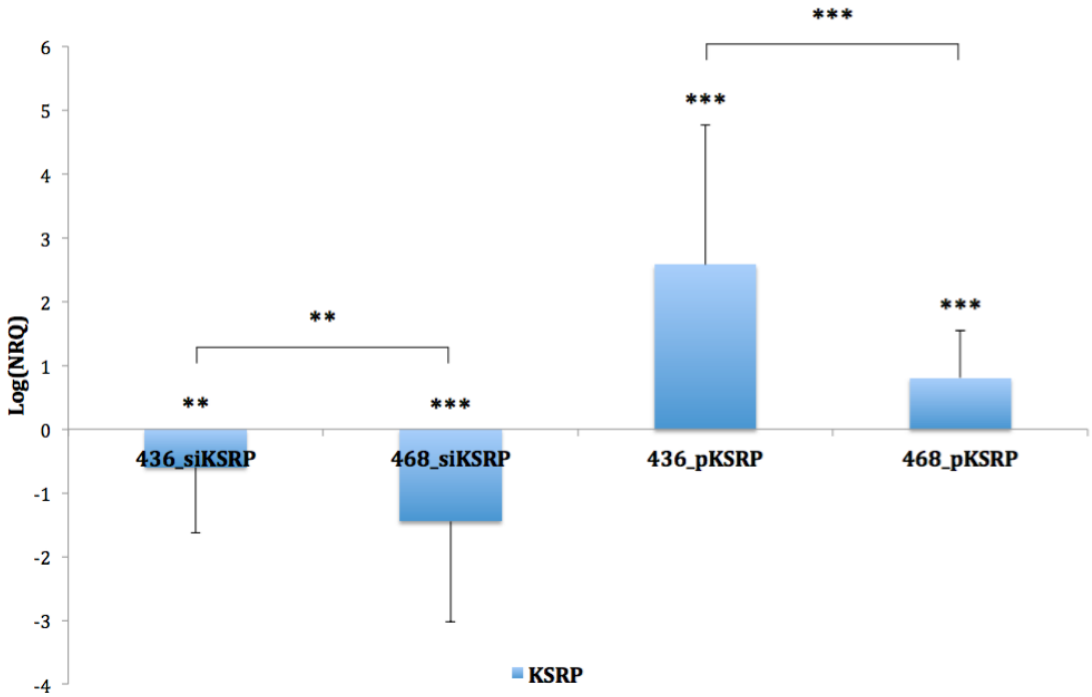

Figure 4.8 – KSRP knockdown (siKSRP) and overexpression (pKSRP) at the mRNA level in MDA-MB-436 (436) and MDA-MB-468 (468) cells. The mRNA expression levels of KSRP when it was down- (siKSRP) or upregulated (pGFP) were expressed relative to the mRNA expression levels of KSRP in the knockdown (siScr) and overexpression (pGFP) transfection controls, respectively. n = 9; standard errors are shown; ** $p \leq 0{,}01$; *** $p \leq 0{,}001$.

MDA-MB-436 and MDA-MB-468 cells were transfected with siScr and siKSRP to confirm KSRP downregulation at the protein level using western blotting analysis (section 3.11-3.15 and Figure 4.9 A). Histone-3 protein expression was used as a loading control. ImageJ was used to analyse KSRP band intensity, and thus quantify the reduction in KSRP protein expression (section 3.19.1). When KSRP was downregulated, the expression levels of this protein were reduced by 100% and 99% in MDA-MB-436 (436) and MDA-MB-468 (468) cells, respectively (Figure 4.9 B). Multiple repeats of this experiment yielded similar results.

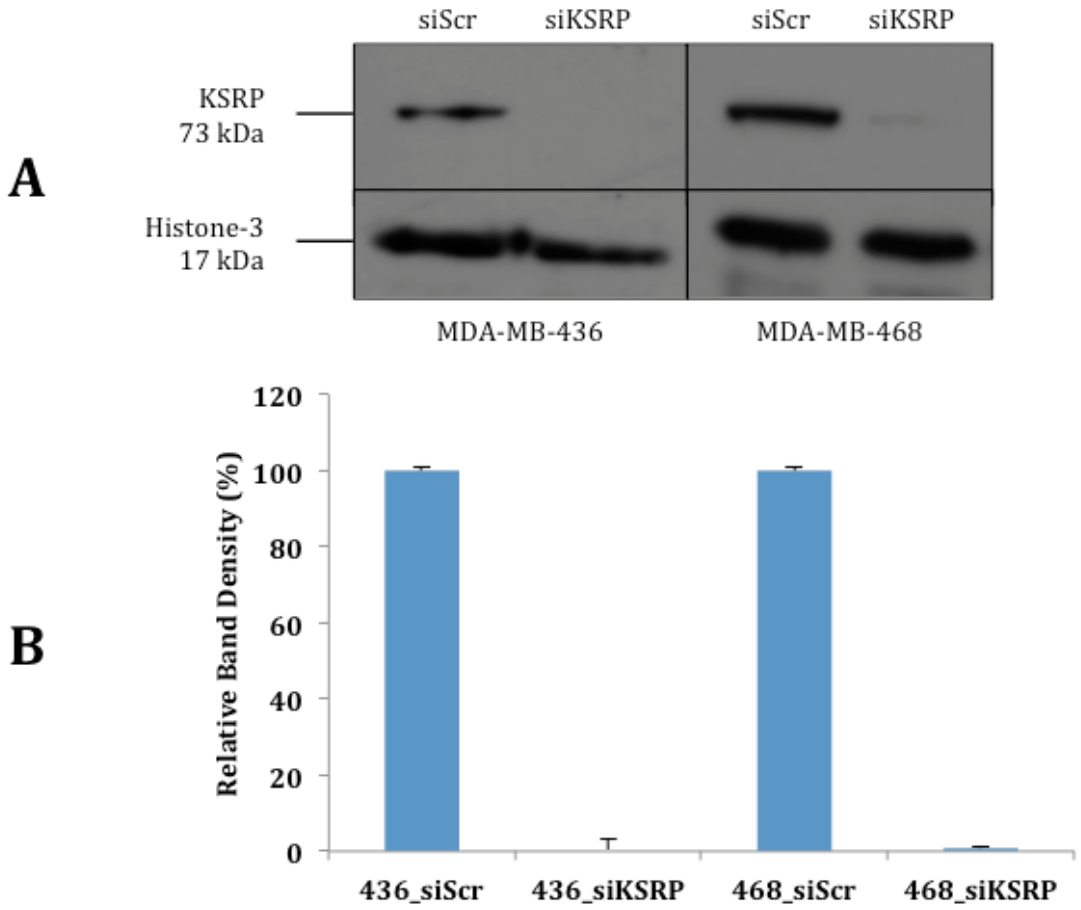

Figure 4.9 – Confirmation of KSRP knockdown at the protein level in MDA-MB-436 (436) and MDA-MB-468 (468) cells. A) Western blots detecting KSRP and Histone-3 (loading control). B) ImageJ analysis of KSRP band density. For each cell line, siKSRP band density was reported as a percentage of siScr band density, which was set at 100%. In MDA-MB-436 KSRP knockdown cells, KSRP protein expression was decreased by 100% and in MDA-MB-468 KSRP knockdown cells, KSRP protein expression was decreased by 98%. Included image is representative of similar ones obtained; n = 3; standard deviations are shown.

MDA-MB-436 cells were transfected with pGFP and pKSRP to confirm KSRP overexpression at the protein level using western blotting analysis (section 3.11-3.15 and Figure 4.10 A). Histone-3 protein expression was used as a loading control. ImageJ was used to analyse KSRP band intensity, and thus quantify the increase in KSRP protein expression (section 3.19.1). When KSRP was overexpressed, expression levels increased by 578% and 256% in MDA-MB-436 (436) and MDA-MB-468 (468) cells, respectively (Figure 4.10 B). Multiple repeats of this experiment yielded similar results.

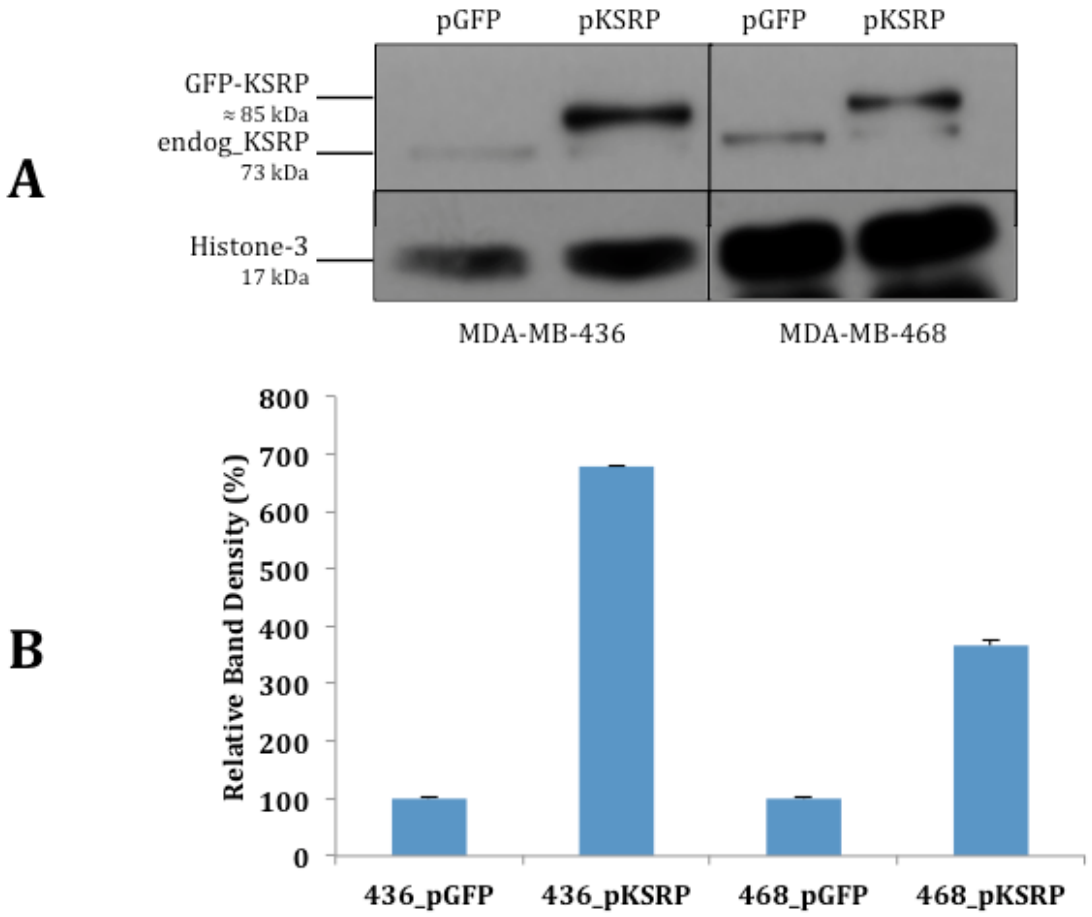

Figure 4.10 – Confirmation of KSRP overexpression at the protein level in MDA-MB-436 (436) and MDA-MB-468 (468) cells. A) Western blots detecting KSRP and Histone-3 (loading control). B) ImageJ analysis of KSRP band density. For each cell line, pKSRP band density was reported as a percentage of pGFP band density, which was set at 100%. In MDA-MB-436 KSRP overexpressed cells, KSRP protein expression was increased by 578% and in MDA-MB-468 KSRP overexpressed cells, KSRP protein expression was increased by 256%. Included image is representative of similar ones obtained; n = 3, standard deviations are shown.

4.1.2.2. Determination of the Effect of KSRP Knockdown and KSRP Overexpression on *FGFR2 IIIb* and *FGFR2 IIIc* Expression in MDA-MB-436 and MDA-MB-468 Cells

RNA from *KSRP* knockdown control (siScr), *KSRP* knockdown (siKSRP), *KSRP* overexpression control (pGFP) and *KSRP* overexpression (pKSRP) treatments was extracted and reverse transcribed into cDNA. This cDNA was analysed using qRT-PCR to determine the relative mRNA expression levels of *KSRP*, *FGFR2 lllb* and *FGFR2 lllc* using the reference genes *GAPDH*, *SDHA* and *HPRT1* for normalisation (section 3.10). The mRNA expression levels of *KSRP*, *FGFR2 IIIb* and *FGFR2 IIIc* when *KSRP* was downregulated (siKSRP) or upregulated (pKSRP) were expressed relative to the mRNA expression level of these genes in the knockdown (siScr) and upregulation (pGFP) transfection controls, respectively.

In MDA-MB-436 cell, there was a significant knockdown of *KSRP* at the mRNA level (Figure 4.8), and this knockdown resulted in a significant increase in the expression levels of both *FGFR2 IIIb* ($p \leq 0{,}01$) and *FGFR2 IIIc* ($p \leq 0{,}01$) (Figure 4.11).

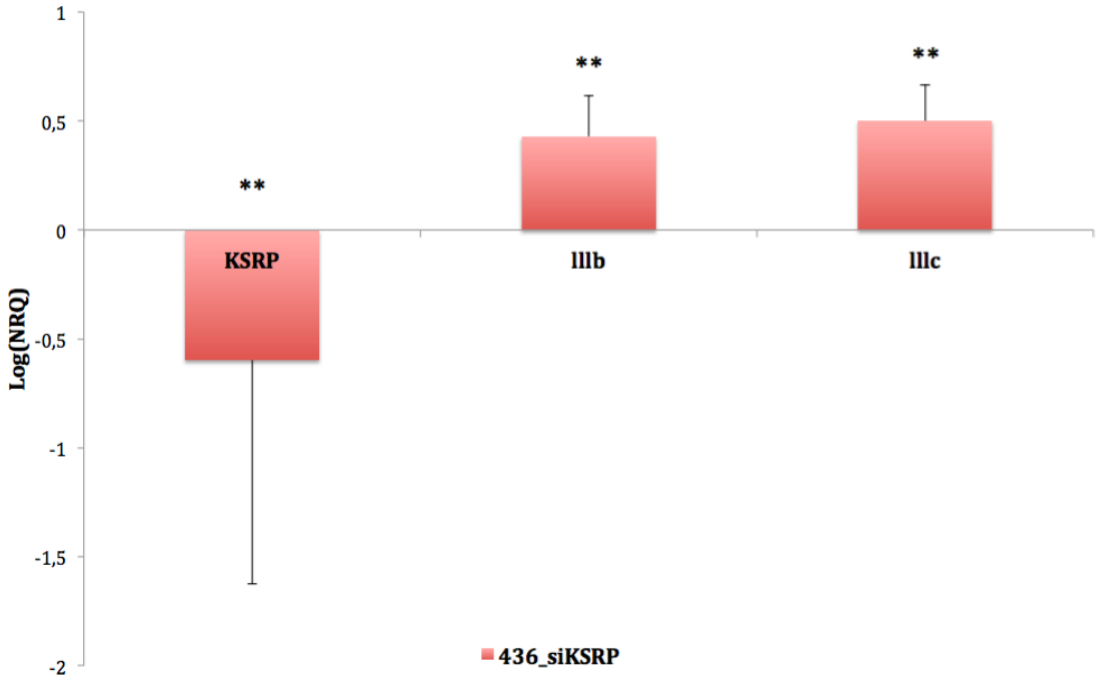

Figure 4.11 – The effect of *KSRP* knockdown (siKSRP) on *FGFR2 IIIb* (IIIb) and *FGFR2 IIIc* (IIIc) mRNA expression levels in MDA-MB-436 (436) cells. The mRNA expression level of *KSRP*, *FGFR2 IIIb* and *FGFR2 IIIc* when *KSRP* was downregulated (siKSRP) were expressed relative to the mRNA expression levels of these genes in the knockdown transfection control (siScr). n = 9; standard errors are shown; ** $p \leq 0{,}01$.

Significant knockdown of *KSRP* at the mRNA level was also achieved in MDA-MB-468 cells (Figure 4.8), which resulted in a significant decrease in the expression levels of both *FGFR2 IIIb* ($p \leq 0{,}001$) and *FGFR2 IIIc* ($p \leq 0{,}05$) (Figure 4.12).

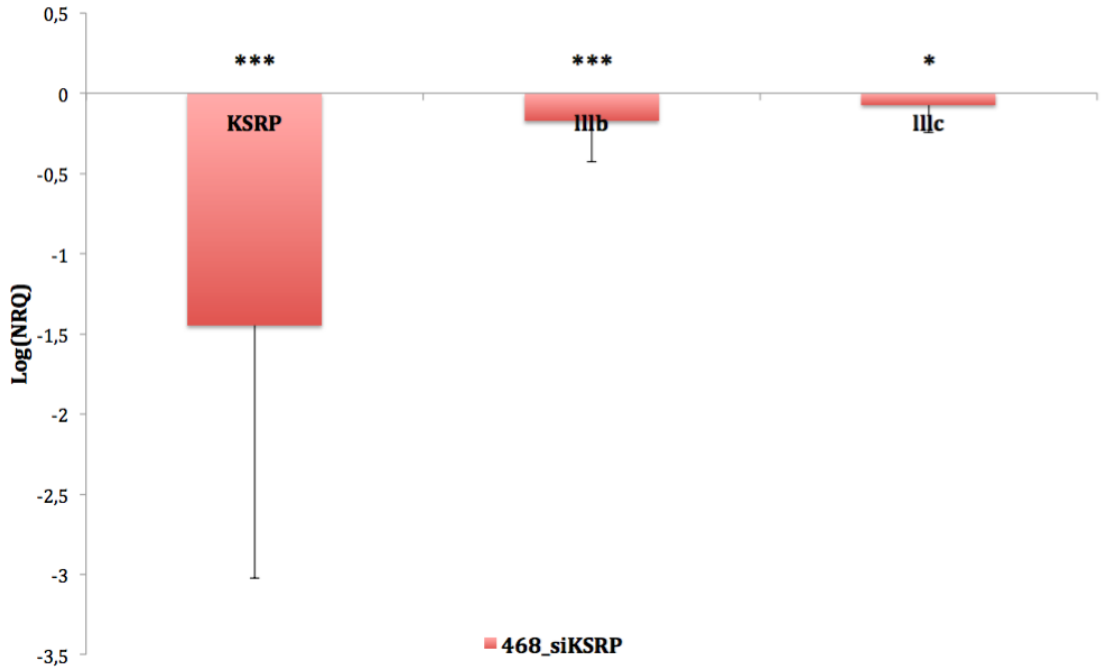

Figure 4.12 – The effect of *KSRP* knockdown (siKSRP) on *FGFR2 IIIb* (IIIb) and *FGFR2 IIIc* (IIIc) mRNA expression levels in MDA-MB-468 (468) cells. The mRNA expression level of *KSRP*, *FGFR2 IIIb* and *FGFR2 IIIc* when *KSRP* was downregulated (siKSRP) were expressed relative to the mRNA expression levels of these genes in the knockdown transfection control (siScr). n = 9; standard errors are shown; *** $p \leq 0{,}001$; * $p \leq 0{,}05$.

Significant overexpression of *KSRP* at the mRNA level in MDA-MB-436 cells (Figure 4.8) resulted in a significant increase in the expression levels of *FGFR2 IIIb* ($p \leq 0,05$) and *FGFR2 IIIc* ($p \leq 0,01$) (Figure 4.13).

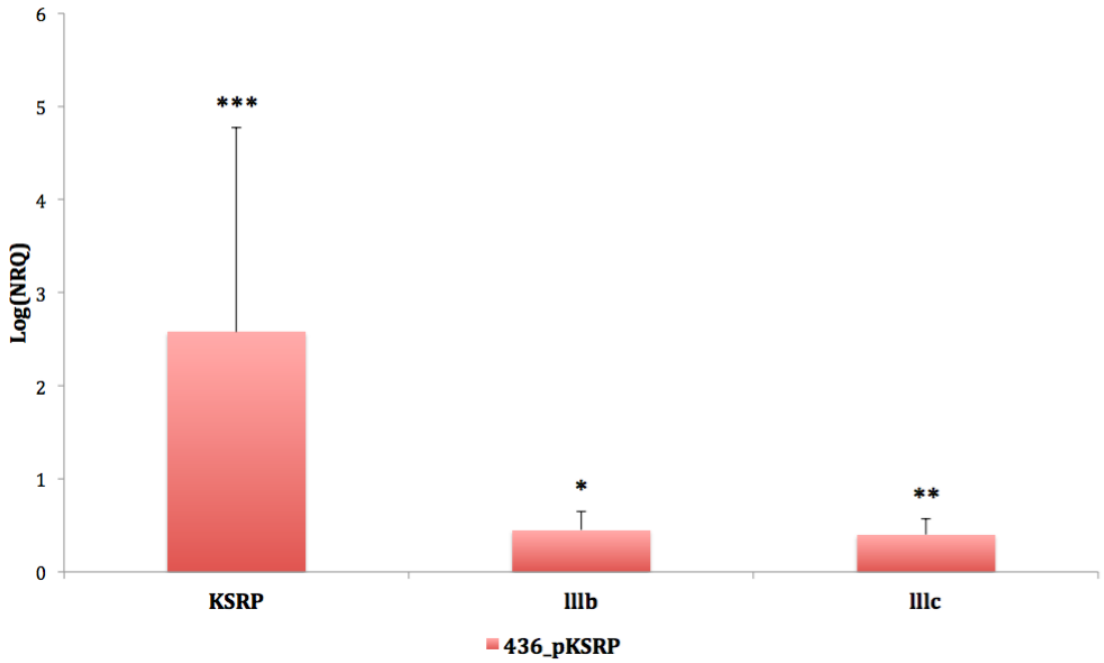

Figure 4.13 – The effect of *KSRP* overexpression (pKSRP) on *FGFR2 IIIb* (IIIb) and *FGFR2 IIIc* (IIIc) mRNA expression levels in MDA-MB-436 (436) cells. The mRNA expression levels of *KSRP*, *FGFR2 IIIb* and *FGFR2 IIIc* when *KSRP* was upregulated (pKSRP) were expressed relative to the mRNA expression levels of these genes in the upregulation transfection control (pGFP). n = 9; standard errors are shown; *** $p \leq 0,001$; ** $p \leq 0,01$; * $p \leq 0,05$.

In contrast, significant overexpression of *KSRP* at the mRNA level in MDA-MB-468 cells (Figure 4.8) resulted in a significant decrease in *FGFR2 IIIb* ($p \leq 0,05$) and *FGFR2 IIIc* ($p \leq 0,001$) expression levels (Figure 4.14).

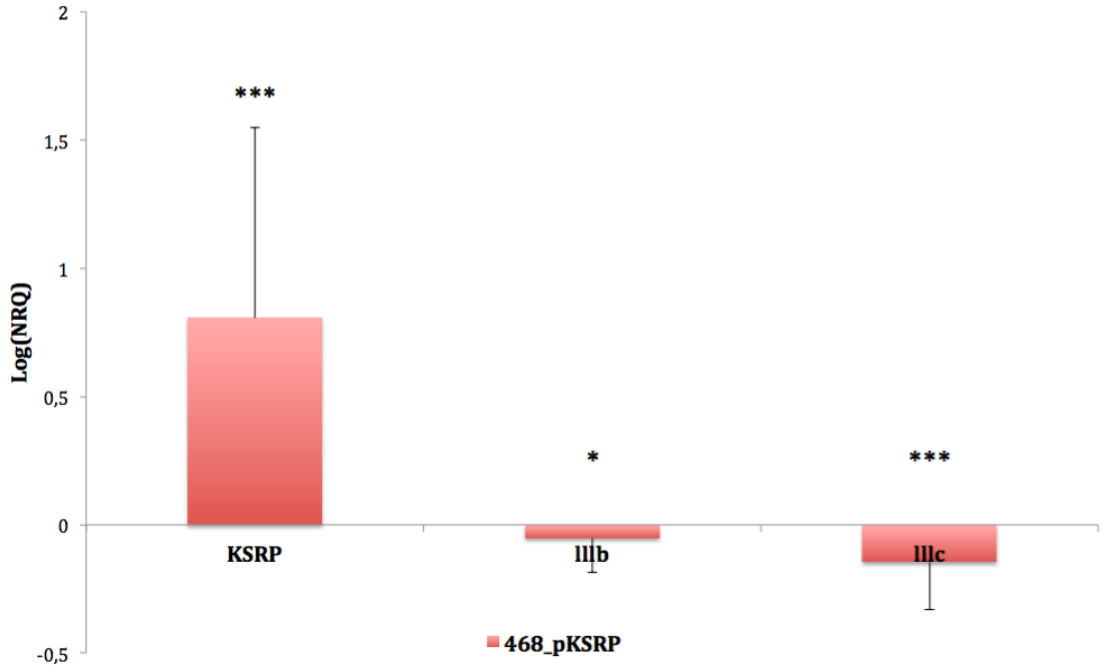

Figure 4.14 – The effect of *KSRP* overexpression (pKSRP) on *FGFR2 IIIb* (IIIb) and *FGFR2 IIIc* (IIIc) mRNA expression levels in MDA-MB-468 (468) cells. The mRNA expression levels of *KSRP*, *FGFR2 IIIb* and *FGFR2 IIIc* when *KSRP* was upregulated (pKSRP) were expressed relative to the mRNA expression levels of these genes in the upregulation transfection control (pGFP). n = 9; standard errors are shown; *** $p \leq 0,001$; * $p \leq 0,05$.

Downregulation of *KSRP* with siKSRP resulted in a decrease in *KSRP* expression at the mRNA level that was significantly different in MDA-MB-436 and MDA-MB-468 cells (Figure 4.8). This decrease in *KSRP* expression in MDA-MB-436 and MDA-MB-468 cells affected the expression of *FGFR2 IIIb* and *FGFR2 IIIc* in opposite ways. *FGFR2 IIIb* and *FGFR2 IIIc* expression was upregulated in MDA-MB-436 cells but downregulated in MDA-MB-468 cells; these changes were significantly different ($p \leq 0{,}001$ for *FGFR2 IIIb* and $p \leq 0{,}01$ for *FGFR2 IIIc*) (Figure 4.15).

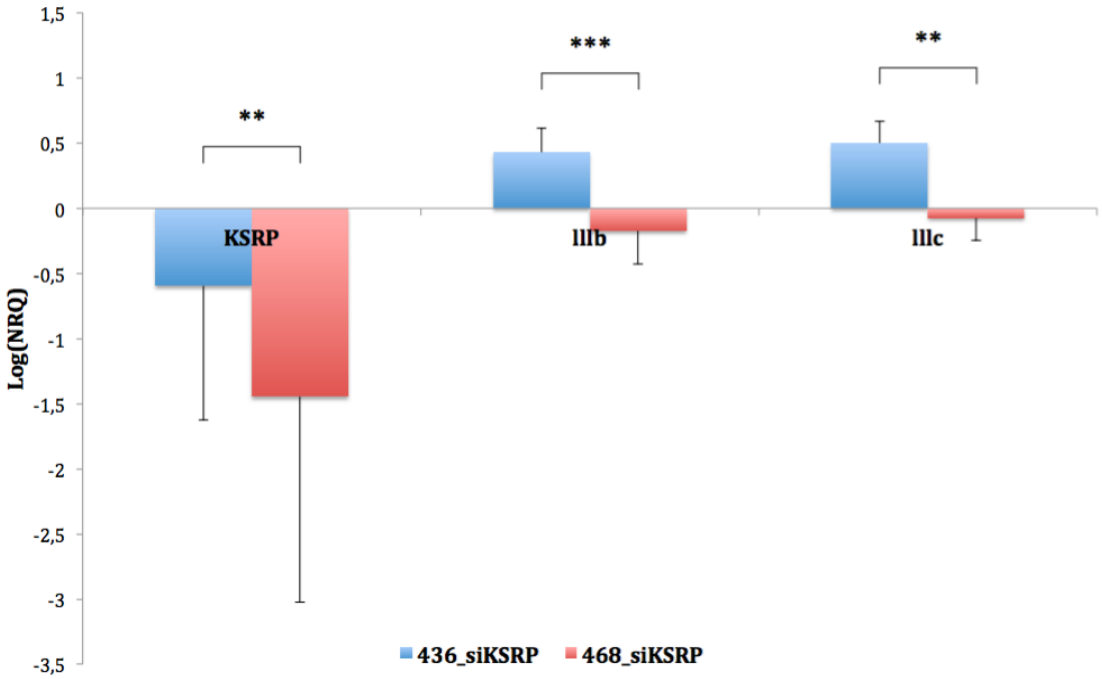

Figure 4.15 – Comparing the effect of *KSRP* knockdown (siKSRP) on *FGFR2 IIIb* (IIIb) and *FGFR2 IIIc* (IIIc) mRNA expression levels between MDA-MB-436 (436) and MDA-MB-468 (468) cells. The mRNA expression levels of *KSRP*, *FGFR2 IIIb* and *FGFR2 IIIc* when *KSRP* was downregulated (siKSRP) were expressed relative to the mRNA expression levels of these genes in the knockdown transfection control (siScr). n = 9; standard errors are shown; ** $p \leq 0{,}01$; *** $p \leq 0{,}001$.

When *KSRP* was upregulated (using pKSRP), the increase in *KSRP* expression at the mRNA level was significantly different in MDA-MB-436 and MDA-MB-468 cells (Figure 4.8). The increase in *KSRP* expression in MDA-MB-436 and MDA-MB-468 cells again affected the expression of *FGFR2 IIIb* and *FGFR2 IIIc* in opposite ways. *FGFR2 IIIb* and *FGFR2 IIIc* expression was upregulated in MDA-MB-436 cells but downregulated in MDA-MB-468 cells; these changes were significantly different ($p \leq 0{,}01$ for *FGFR2 IIIb* and $p \leq 0{,}001$ for *FGFR2 IIIc*) (Figure 4.16).

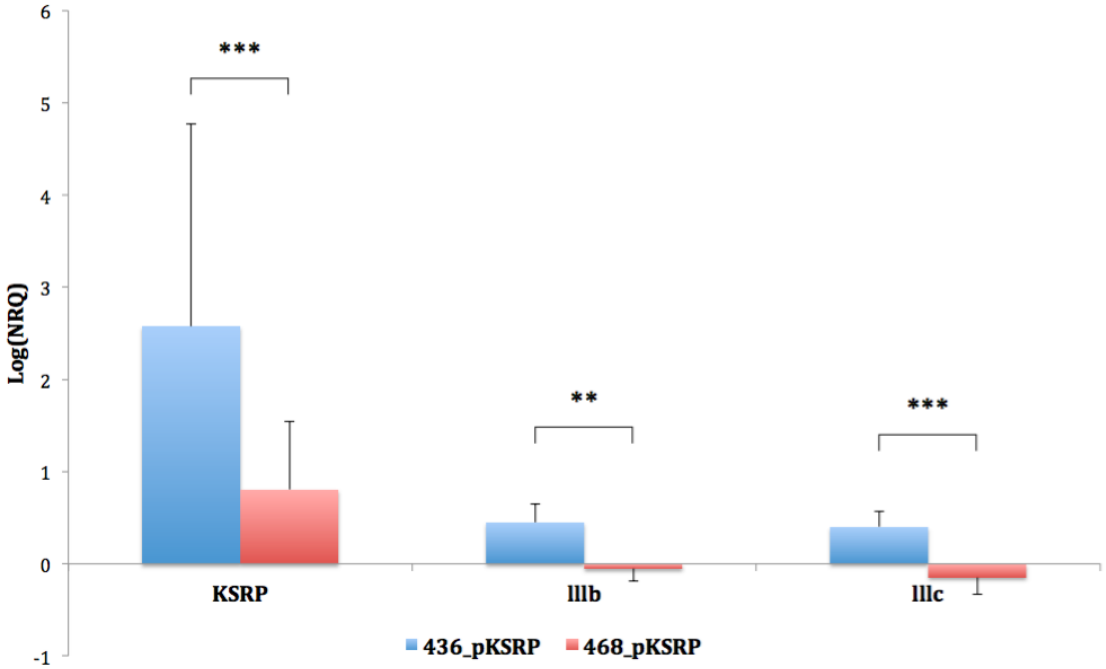

Figure 4.16 – Comparing the effect of *KSRP* overexpression (pKSRP) on *FGFR2 IIIb* (IIIb) and *FGFR2 IIIc* (IIIc) mRNA expression levels between MDA-MB-436 (436) and MDA-MB-468 (468) cells. The mRNA expression levels of *KSRP*, *FGFR2 IIIb* and *FGFR2 IIIc* when *KSRP* was upregulated (pKSRP) were expressed relative to the mRNA expression levels of these genes in the upregulation transfection control (pGFP). n = 9; standard errors are shown; ** $p \leq 0{,}01$; *** $p \leq 0{,}001$.

The decrease and increase in *KSRP* expression in MDA-MB-436 cells when this protein was downregulated (siKSRP) and upregulated (pKSRP), respectively, was significantly different ($p \leq 0{,}001$), as expected. The resultant increases in *FGFR2 IIIb* expression was not significantly different between siKSRP and pKSRP treated samples and neither were the increases in the expression of *FGFR2 IIIc* ($p > 0{,}05$), however, differences in the expression levels were observed (Figure 4.17).

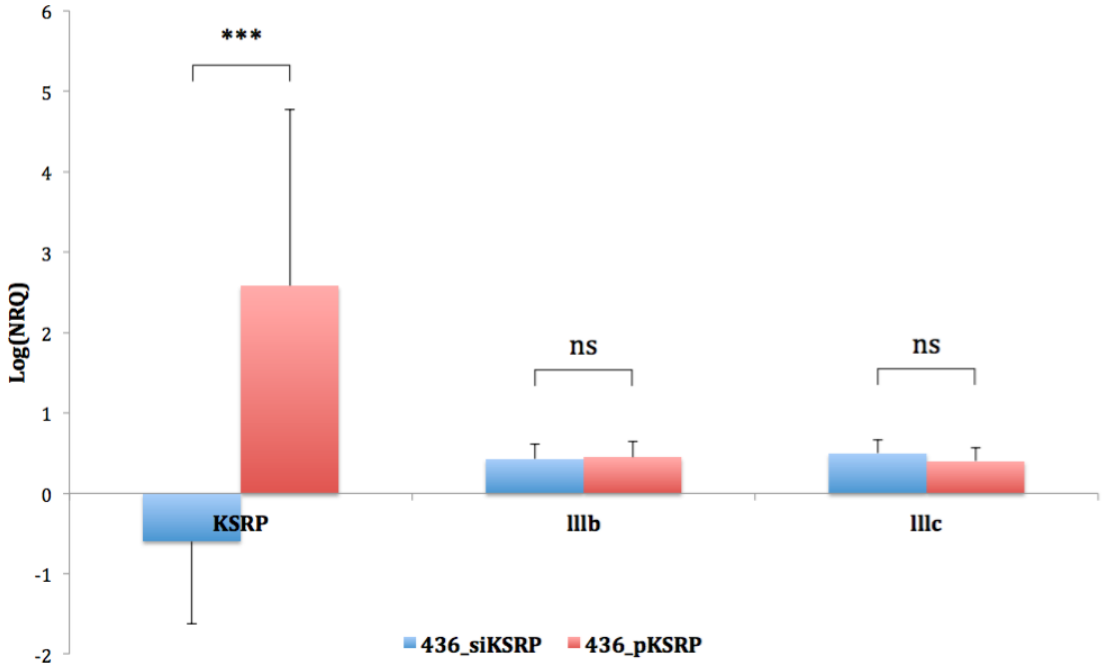

Figure 4.17 – Comparing the effect of *KSRP* knockdown (siKSRP) to the effect of *KSRP* overexpression (pKSRP) on the mRNA expression levels of *FGFR2 IIIb* (IIIb) and *FGFR2 IIIc* (IIIc) in MDA-MB-436 (436) cells. The mRNA expression levels of *KSRP*, *FGFR2 IIIb* and *FGFR2 IIIc* when *KSRP* was downregulated (siKSRP) and upregulated (pKSRP) were expressed relative to the mRNA expression levels of these genes in the knockdown (siScr) and upregulation (pGFP) transfection controls, respectively. n = 9; standard errors are shown; ns $p > 0{,}05$; *** $p \leq 0{,}001$.

In MDA-MB-468 cells, the decrease and increase in *KSRP* expression when this protein was downregulated (siKSRP) and upregulated (pKSRP), respectively, was significantly different ($p \leq 0{,}001$), as expected. The decrease in *FGFR2 IIIb* expression was significantly different between the siKSRP and pKSRP samples ($p \leq 0{,}05$). The decrease in *FGFR2 IIIc* expression was also significantly different between the siKSRP and pKSRP samples ($p \leq 0{,}05$) (Figure 4.18).

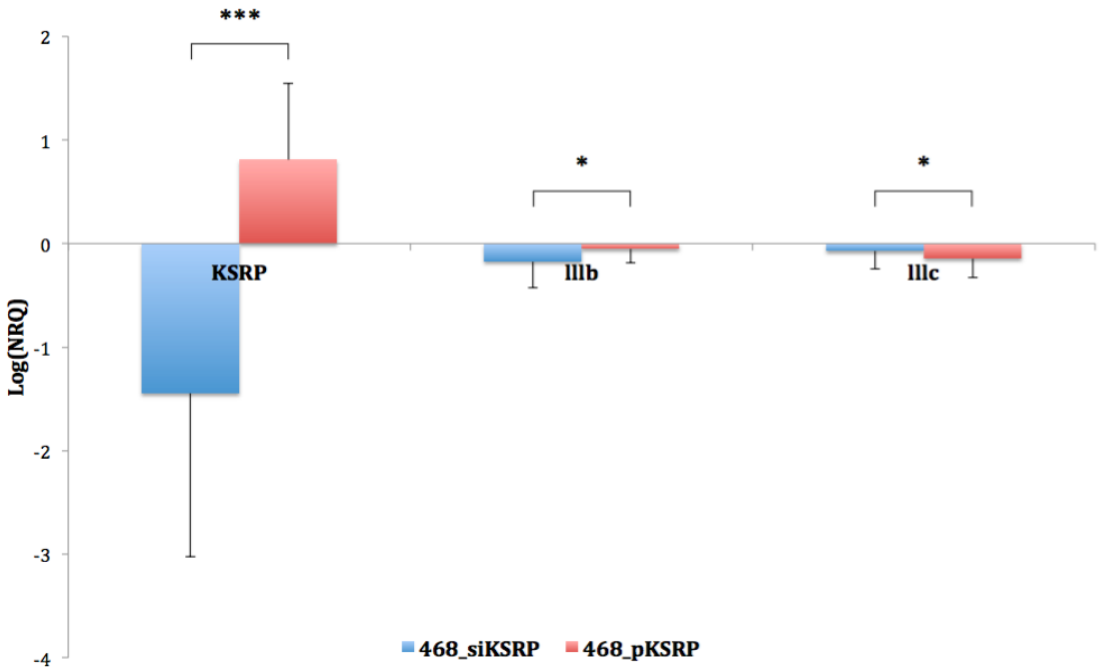

Figure 4.18 – Comparing the effect of *KSRP* knockdown (siKSRP) to the effect of *KSRP* overexpression (pKSRP) on the mRNA expression levels of *FGFR2 IIIb* (IIIb) and *FGFR2 IIIc* (IIIc) in MDA-MB-468 (468) cells. The mRNA expression levels of *KSRP*, *FGFR2 IIIb* and *FGFR2 IIIc* when *KSRP* was downregulated (siKSRP) and upregulated (pKSRP) were expressed relative to the mRNA expression levels of these genes in the knockdown (siScr) and upregulation (pGFP) transfection controls, respectively. n = 9; standard errors are shown; *** $p \leq 0{,}001$; * $p \leq 0{,}05$.

4.1.2.3. Determination of the Effect of KSRP Overexpression on the Epithelial and Mesenchymal Phenotype of MDA-MB-436 and MDA-MB-468 Cells

The effect of KSRP overexpression on the mesenchymal and epithelial phenotype of MDA-MB-436 and MDA-MB-468 cells, respectively, was assessed through the visualisation of the epithelial marker, Cytokeratin 19, and the mesenchymal marker, Vimentin, using an Olympus IX71 Fluorescence Microscope (section 3.16). MDA-MB-436 and MDA-MB-468 were transfected with either the pEGFPC1-6XHis-FLKSRP plasmid (labelled GFP-KSRP) or the control pEGFP-N1 plasmid (labelled GFP) (section 3.5.2). The phenotypes of the MDA-MB-436 and MDA-MB-468 cells transfected with GFP-KSRP were compared to the phenotypes of the respective transfection control (GFP) cells.

In MDA-MB-436 cells, Cytokeratin 19 was not visible in either the GFP expressing cells (Figure 4.19 A) or the GFP-KSRP expressing cells (Figure 4.19 B). Vimentin was visible in both GFP expressing (Figure 4.20 A) and GFP-KSRP expressing (Figure 4.20 B) MDA-MB-436 cells, indicative of their mesenchymal phenotype. In MDA-MB-468 cells, Cytokeratin 19 was visible in both GFP expressing (Figure 4.21 A) and GFP-KSRP expressing (Figure 4.21 B) cells, indicative of their epithelial phenotype. Vimentin, however, was not seen in either GFP expressing (Figure 4.22 A) or GFP-KSRP expressing (Figure 4.22 B) MDA-MB-468 cells.

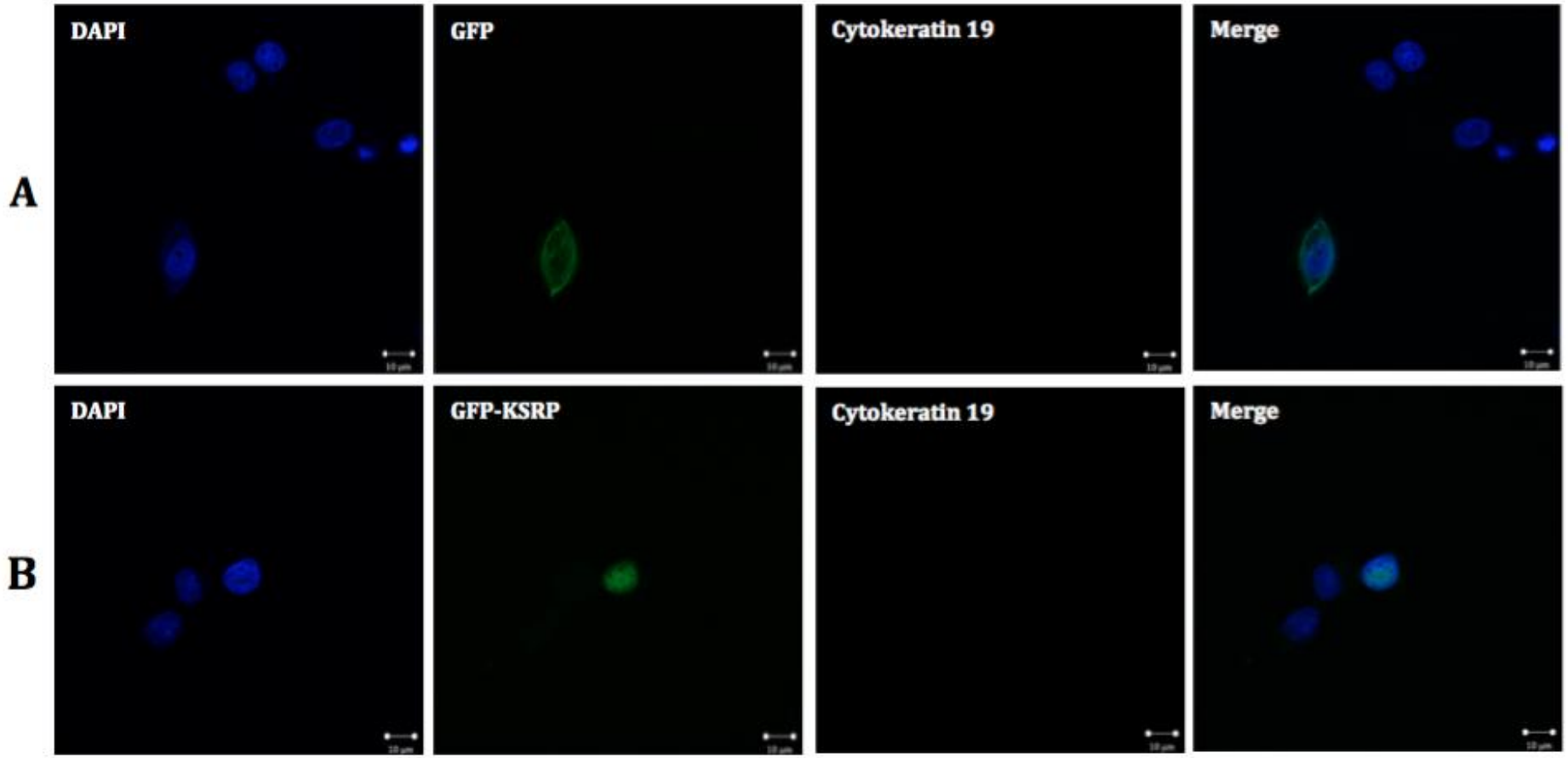

Figure 4.19 – Cytokeratin 19 visualisation in MDA-MB-436 cells expressing pEGFP-N1 (GFP) or pEGFPC1-6XHis-FLKSRP (GFP-KSRP). A) Cytokeratin 19 was not visible in MDA-MB-436 cells expressing GFP. B) Cytokeratin 19 was not visible in MDA-MB-436 cells expressing GFP-KSRP. The monoclonal rabbit anti-Cytokeratin 19 primary and polyclonal goat anti-Rabbit IgG (H+L) Rhodamine Red secondary antibodies were used. Images were captured using the Olympus IX71 Fluorescence Microscope. Included images are representative of similar ones obtained; n = 3.

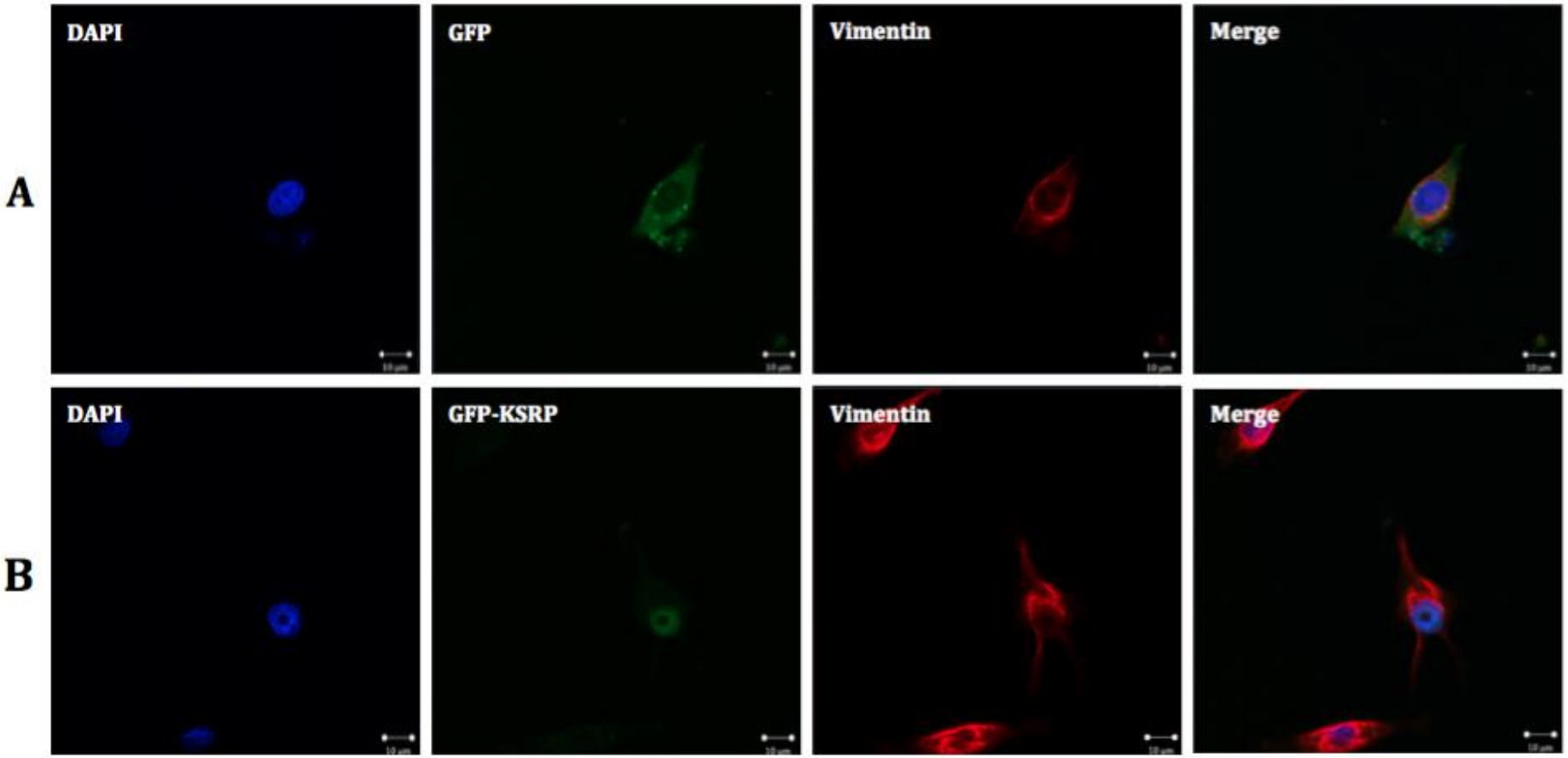

Figure 4.20 – Vimentin visualisation in MDA-MB-436 cells expressing pEGFP-N1 (GFP) or pEGFPC1-6XHis-FLKSRP (GFP-KSRP). A) Vimentin was visible in MDA-MB-436 cells expressing GFP. B) Vimentin was visible in MDA-MB-436 cells expressing GFP-KSRP. The monoclonal mouse anti-Vimentin primary and polyclonal goat anti-Mouse IgG DyLight 649 secondary antibodies were used. Images were captured using the Olympus IX71 Fluorescence Microscope. Included images are representative of similar ones obtained; n = 3.

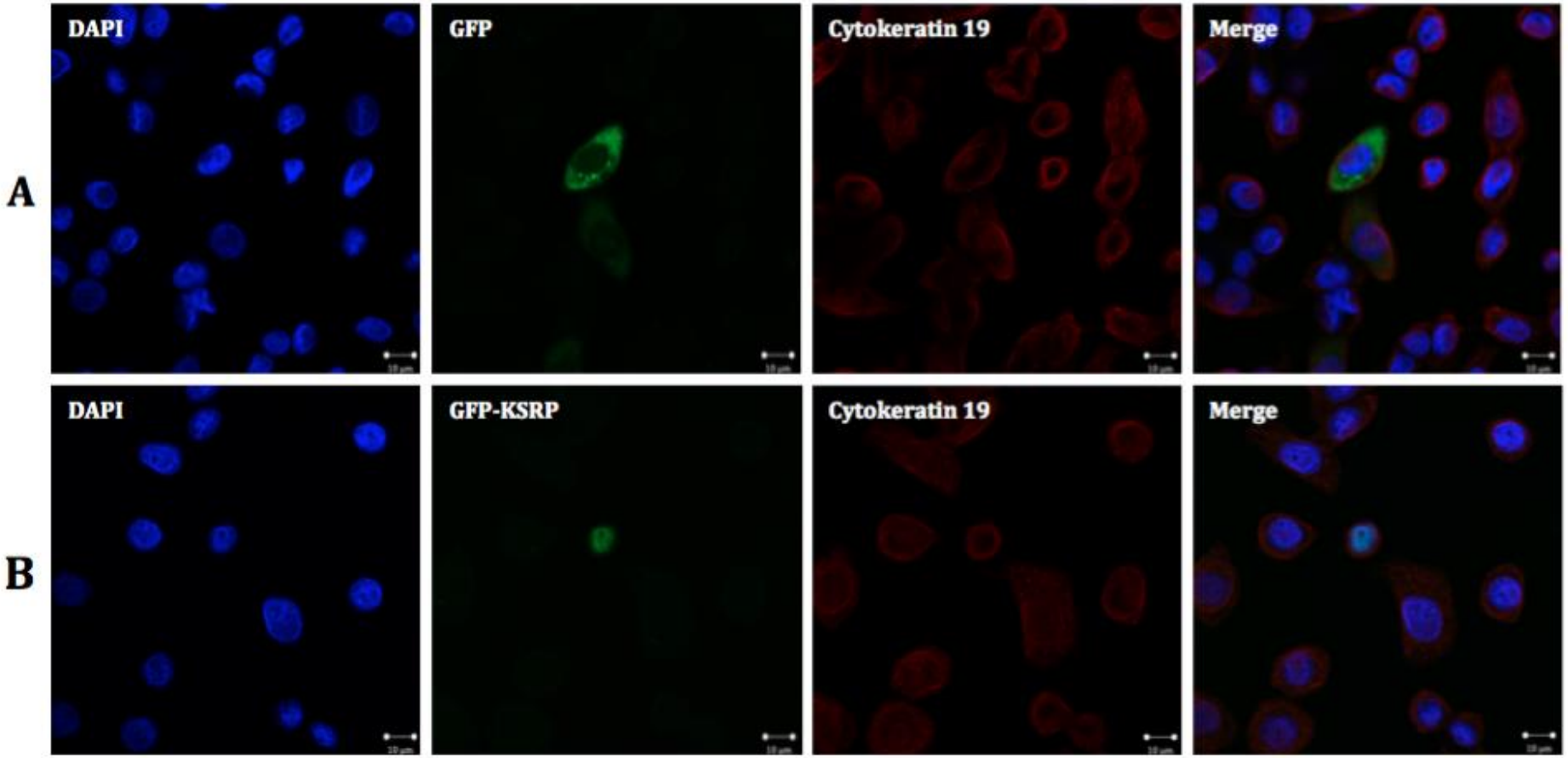

Figure 4.21 – Cytokeratin 19 visualisation in MDA-MB-468 cells expressing pEGFP-N1 (GFP) or pEGFPC1-6XHis-FLKSRP (GFP-KSRP). A) Cytokeratin 19 was visible in MDA-MB-468 cells expressing GFP. B) Cytokeratin 19 was visible in MDA-MB-468 cells expressing GFP-KSRP. The monoclonal rabbit anti-Cytokeratin 19 primary and polyclonal goat anti-Rabbit IgG (H+L) Rhodamine Red secondary antibodies were used. Images were captured using the Olympus IX71 Fluorescence Microscope. Included images are representative of similar ones obtained; n = 3.

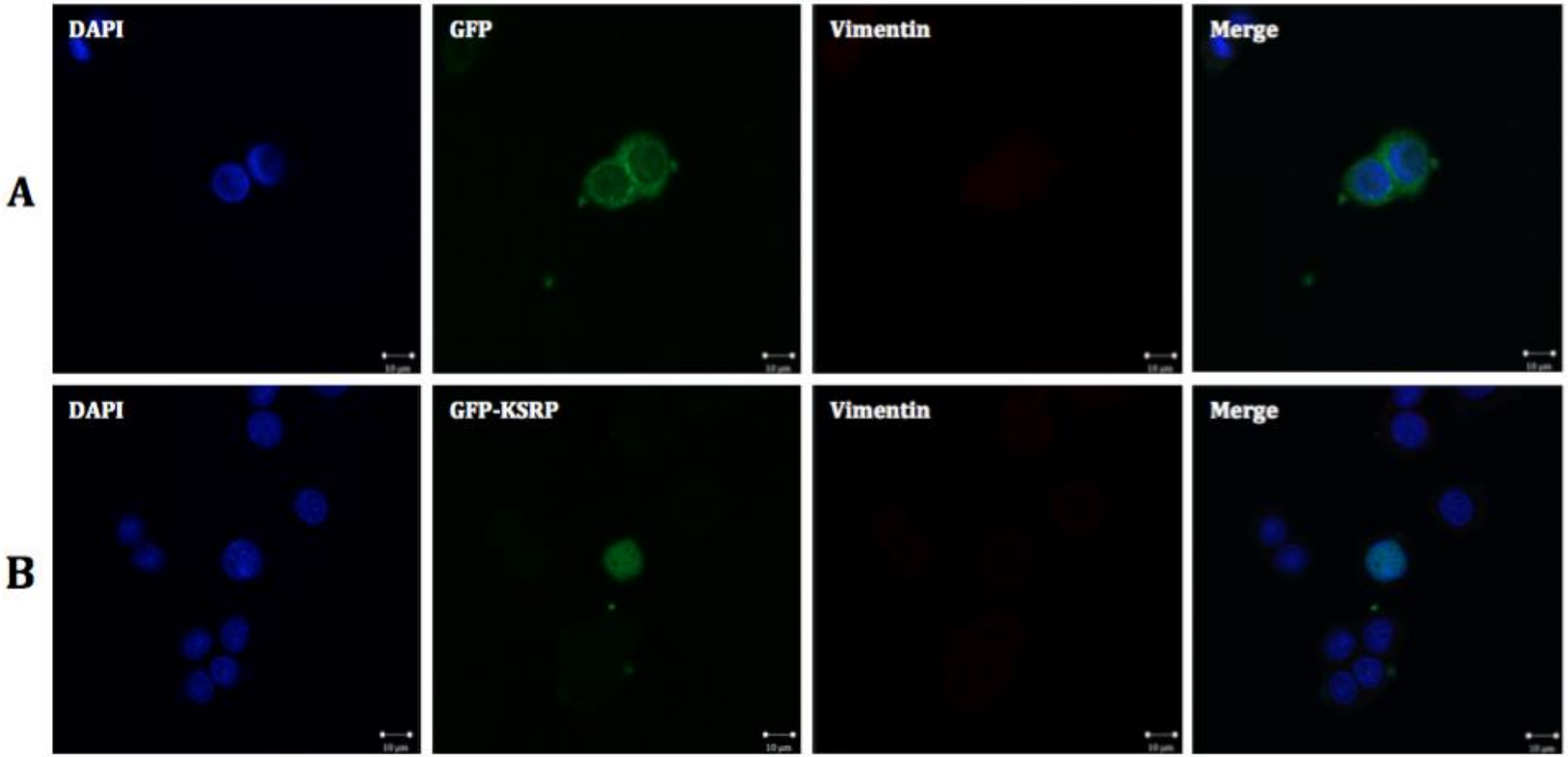

Figure 4.22 – Vimentin visualisation in MDA-MB-468 cells expressing pEGFP-N1 (GFP) or pEGFPC1-6XHis-FLKSRP (GFP-KSRP). A) Vimentin was not visible in MDA-MB-468 cells expressing GFP. B) Vimentin was not visible in MDA-MB-468 cells expressing GFP-KSRP. The monoclonal mouse anti-Vimentin primary and polyclonal goat anti-Mouse IgG DyLight 649 secondary antibodies were used. Images were captured using the Olympus IX71 Fluorescence Microscope. Included images are representative of similar ones obtained; n = 3.

4.1.3. Investigation of the Possible Direct Binding of KSRP to *FGFR2* mRNA in MDA-MB-468 Cells

The possible binding of KSRP to *FGFR2* mRNA was assessed using the ultra-violet cross-linking and immunoprecipitation (UV-CLIP) technique. KSRP was covalently linked to the RNA it was bound to in the cell to using UV cross-linking. KSRP was then immunoprecipitated and the bound RNA extracted, reverse transcribed and analysed by qRT-PCR. Successful amplification of cDNA would provide evidence for the direct binding of KSRP to the region of gene that the primers were designed to. Binding of KSRP to *FGFR2* mRNA would strongly suggest a role for this protein in the *FGFR2* splicing mechanism.

Six primer pairs were designed for this qRT-PCR analysis (Table 3.1) and the exact sequences that would be amplified and their binding positions on the *FGFR2* mRNA are illustrated in Figure 4.23. A gradient semi-qPCR (section 3.8) was used to determine the optimal melting temperature (ranging from 55 °C to 70 °C) for each of the six primer pairs designed for this experiment (Figure 4.24). When primer pair 1 (FGFR2_i81) was used, PCR product was obtained in reactions using melting temperatures between 55 °C and 66,1 °C; non-specific amplification was detected in reactions using melting temperatures between 55 °C and 56,3 °C (Figure 4.24 A). When primer pair 2 (FGFR2_i82) was used, PCR product was obtained in reactions using melting temperatures between 55 °C and 61,4 °C; no non-specific amplification was observed (Figure 4.24 B). When primer pair 3 (FGFR2_i83) was used, PCR product was obtained in reactions using melting temperatures between 55 °C and 66,1 °C; non-specific amplification was observed in reactions using melting temperatures between 55 °C and 59,2 °C (Figure 4.24 C). When primer pair 4 (FGFR2_i8e9) was used, PCR product was obtained in reactions using melting temperatures between 55 °C and 69,7 °C; non-specific amplification was observed in reactions using melting temperatures between 55 °C and 57,5 °C (Figure 4.24 D). When primer pair 5 (FGFR2_e9) was used, PCR product was obtained in reactions using melting temperatures between 55 °C and 69,7 °C; non-specific amplification was observed in reactions using melting temperatures between 55 °C and 59,2 °C (Figure 4.24 E). When primer pair 6 (FGFR2_i9) was used, PCR product was

obtained in reactions using melting temperatures between 55 °C and 66,1 °C; no non-specific amplification was observed (Figure 4.24 F). Primer pairs 4, 5 and 6 (FGFR2_i8e9, FGFR2_e9 and FGFR2_i9, respectively) were chosen for qRT-PCR analysis.

Western blotting analysis (sections 3.11-3.15) confirmed the presence KSRP in both the input (In) and flow-through (FT) fractions of the control and KSRP samples (Figure 4.25 A). When the KSRP antibody was used for immunoprecipitation (in the KSRP samples), the immunoprecipitate (IP) fraction contained KSRP, however, when the control antibody (targeting IgG) was used for immunoprecipitation (in the control samples), the IP fraction did not contain KSRP (Figure 4.25 A).

RNA extracted from the control IP and KSRP IP fractions was reverse transcribed to cDNA, and this cDNA was used for absolute qRT-PCR analysis (section 3.10) using the three primer pairs selected previously. All three primer pairs successfully amplified the cDNA from the control IP fraction; however, only the primer pair designed to amplify *FGFR2* exon 9 (primer pair 5) amplified cDNA from the KSRP IP fraction. When comparing the amount of cDNA amplified from the KSRP IP fraction to the amount of cDNA amplified from the control IP fraction using the *FGFR2* exon 9 primer pair, 41% of the mRNA bound to immunoprecipitated KSRP belonged to *FGFR2* exon 9 (Figure 4.25 B).



Figure 4.23 – UV-CLIP primers. The binding positions of the six designed UV-CLIP primers on *FGFR2* mRNA are illustrated on the top image. The primer sequences and the sequences of *FGFR2* mRNA they amplify are shown in the bottom image.

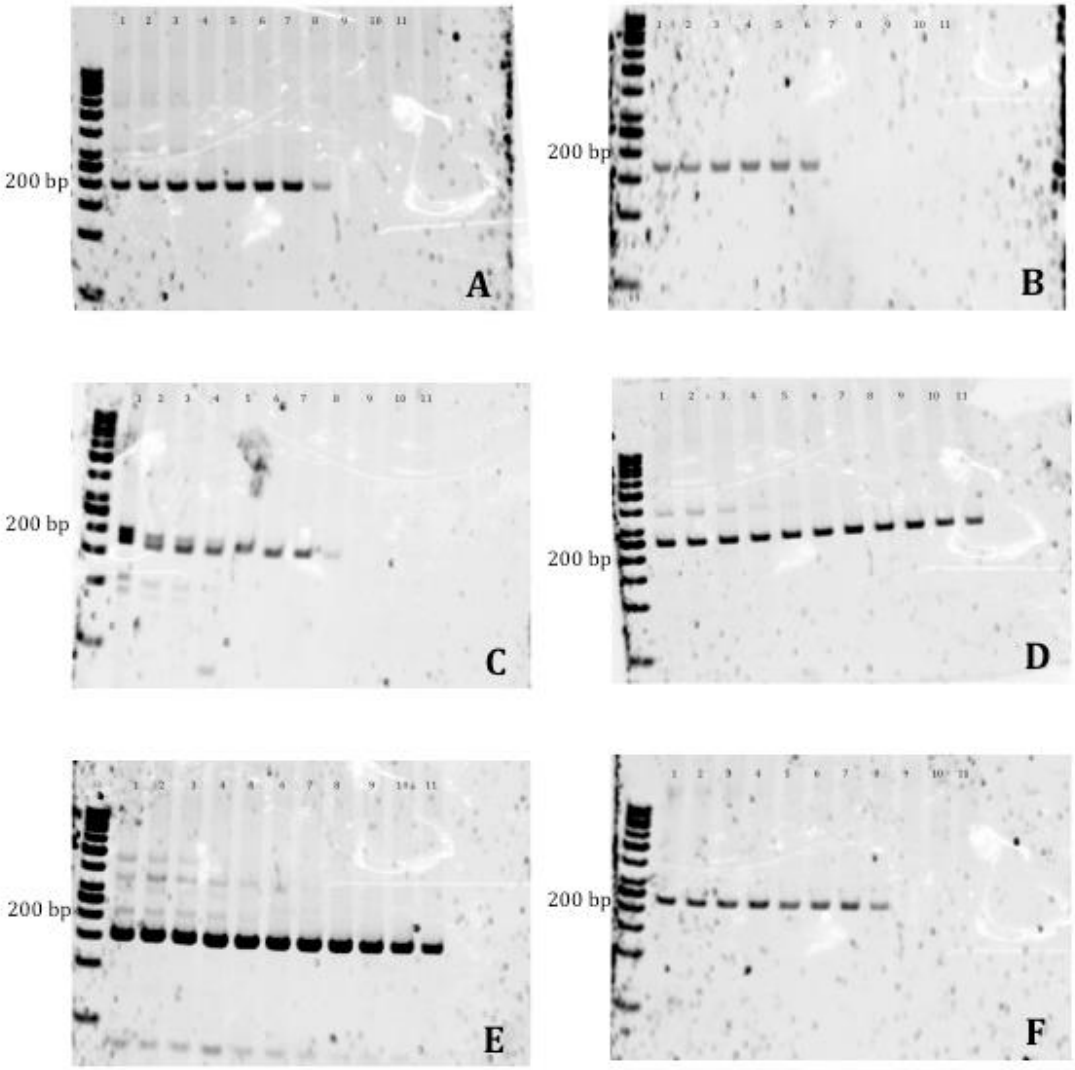

Figure 4.24 – Gradient semi-qPCR analysis used to determine the optimal melting temperature of the six UV-CLIP primer pairs. Gradient semi-qPCR using A) FGFR2_i81 (primer pair 1) yielded a 195 bp PCR product; B) FGFR2_i82 (primer pair 2) yielded a 163 bp PCR product; c) FGFR2_i83 (primer pair 3) yielded a 166 bp PCR product; D) FGFR2_i8e9 (primer pair 4) yielded a 247 bp PCR product; E) FGFR2_e9 (primer pair 5) yielded a 197 bp PCR product; F) FGFR2_i9 (primer pair 6) yielded a 238 bp PCR product. A gradient of melting temperatures was used: lane 1) 55 °C; 2) 55,4 °C; 3) 56,3 °C; 4) 57,5 °C; 5) 59,2 °C; 6) 61,4 °C; 7) 63,9 °C; 8) 66,1 °C; 9) 67,7 °C; 10) 68,9 °C; 11) 69,7 °C.

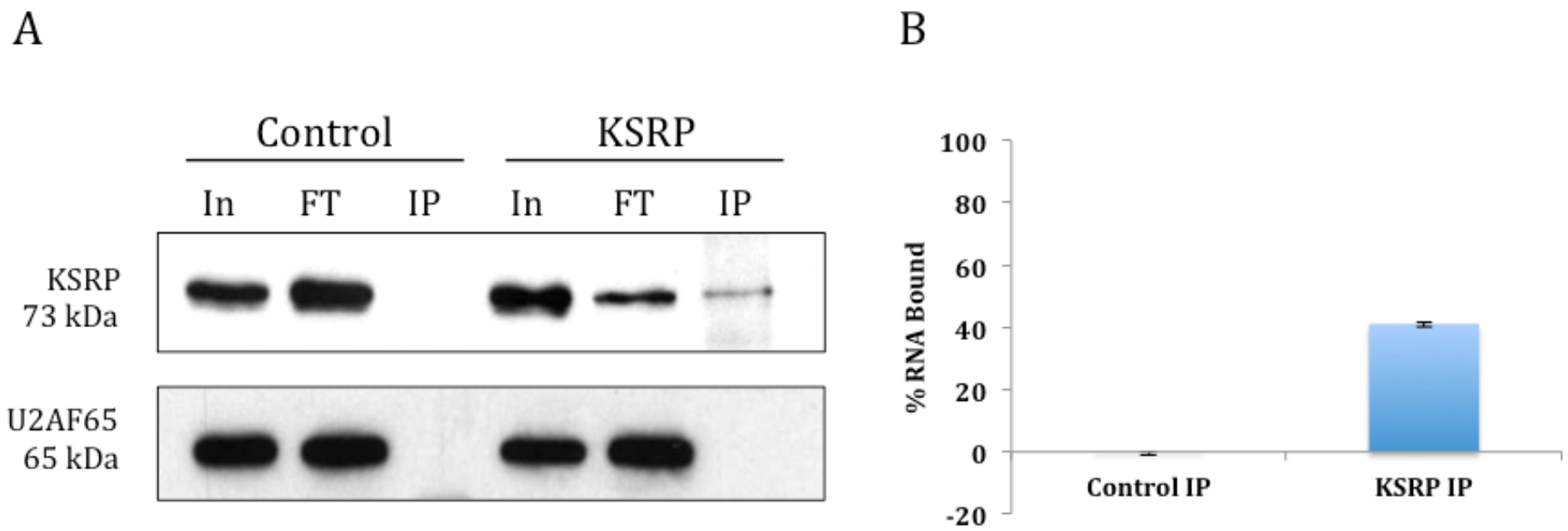

Figure 4.25 – UV cross-linking and immunoprecipitation of KSRP in MDA-MB-468 cells. MDA-MB-468 cells were UV cross-linked, lysed, the lysate incubated with an anti-KSRP antibody bound to magnetic beads (an anti-IgG antibody was used as a control), and the anti-KSRP antibody (with bound RNA) eluted. An aliquot of the input lysate (In), the flow-through (FT) and the elution (IP) was analysed using western blotting. The RNA bound to the eluted KSRP and IgG was extracted, reverse transcribed into cDNA and used for absolute qRT-PCR quantification. A) In the control samples, western blot analysis confirmed the presence of KSRP in the input (In) and flow-through (FT) fractions but the absence of KSRP in the immunoprecipitation (IP) fraction. In the KSRP samples, western blot analysis confirmed the presence of KSRP in the In, FT and IP fractions; U2AF65 was used as a loading control. B) 41% the mRNA bound to immunoprecipitated KSRP from the KSRP IP fraction belonged to *FGFR2* exon 9 (this was calculated relative to the amount of *FGFR2* exon 9 amplified in the control IP fraction). n = 3; standard deviations shown.

4.2. Discovery-Based Approach

A discovery-based approach was taken to profile changes in gene expression in MDA-MB-468 cells when KSRP is downregulated. This was accomplished using the Affymetrix GeneChip® Human Transcriptome Array 2.0.

4.2.1. Identification of Genome-Wide Gene Expression Changes in Response to KSRP Knockdown in MDA-MB-468 Cells

The results from the Affymetrix GeneChip® Human Transcriptome Array 2.0 comparing KSRP knockdown (siKSRP) to the transfection control (siScr) in MDA-MB-468 cells (section 3.18) were hierarchically clustered by gene intensity (Figure 4.26 A) and also by distance to mean (Figure 4.26 B).

49 genes, which had a fold change ≥ 1,5 and a p-value ≤ 0,05, were identified and are detailed in Table 4.1. These 49 genes were considered "regulated" upon KSRP knockdown in MDA-MB-468 cells; 33 were upregulated and 16 were downregulated (Table 4.1). The regulated genes were subjected to Kyoto Encyclopedia of Genes and Genomes (KEGG) pathway analysis, and the Wnt signalling pathway was identified as being regulated upon KSRP knockdown (Table 4.2). Three genes that function in this pathway were upregulated upon KSRP knockdown, namely Cyclin D3 (*CCND3*), Dickkopf WNT Signaling Pathway Inhibitor 1 (*DKK1*) and Protein Phosphatase 2, Regulatory Subunit A, Beta (*PPP2R1B*).

1624 transcription factors were identified as being regulated upon KSRP knockdown, however, only 8 have a fold change ≥ 1,5 (Figure 4.27 A and Table 4.3). 289 splicing factors were identified as being regulated upon KSRP knockdown but none were found have a fold change ≥ 1,5 (Figure 4.27 B). Additionally, 7 differentially regulated exons from 4 distinct genes were identified, one of which had a fold change ≥ 1,5 (Figure 4.27 C and Table 4.4). Finally, 190 differentially regulated alternative splicing patterns from 149 distinct genes were altered when KSRP was downregulated, 4 of which had a fold change ≥ 1,5 (Figure 4.27 D and Table 4.5).

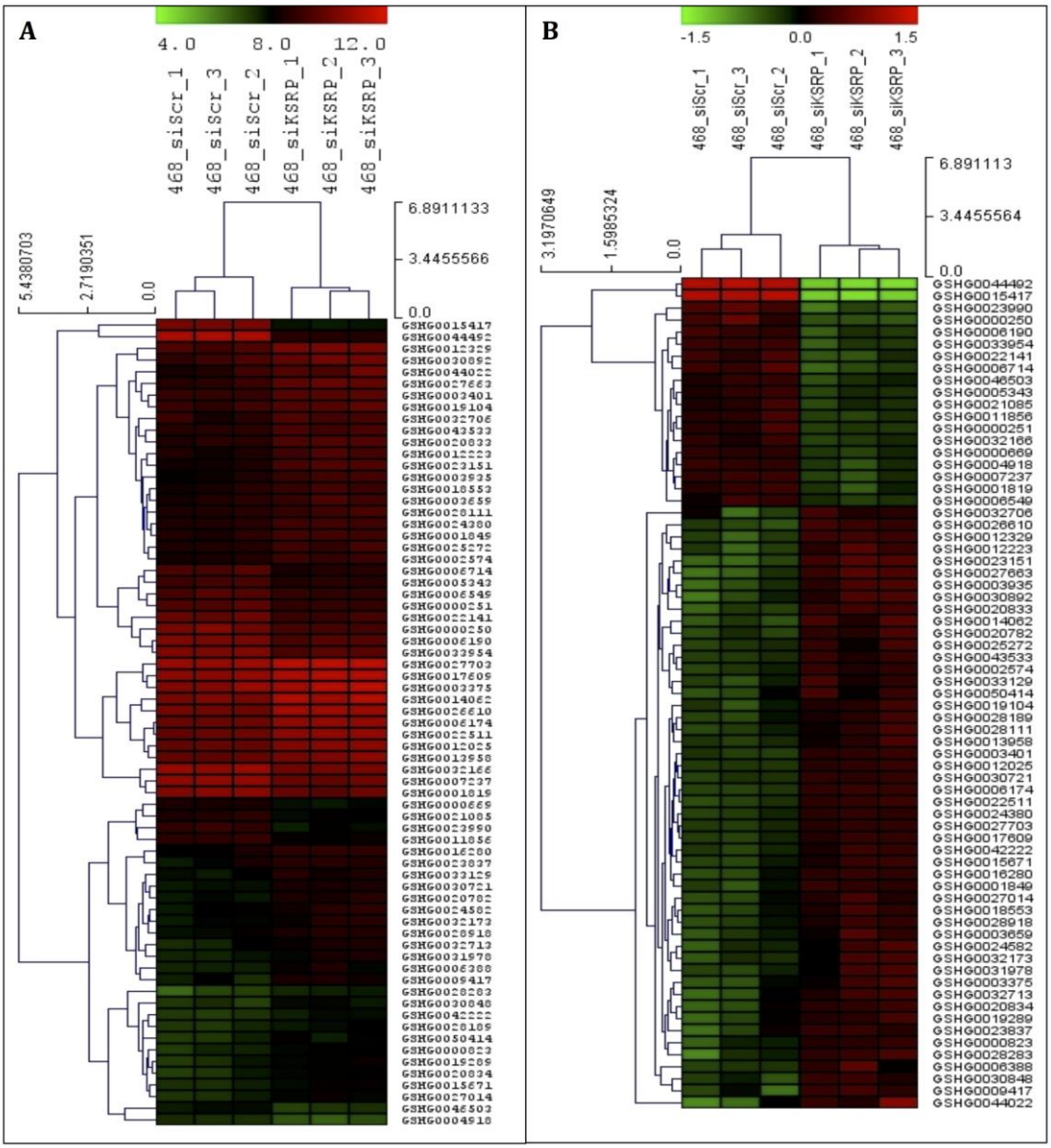

Figure 4.26 – Hierarchical clustering of genes regulated in KSRP downregulated (siKSRP) MDA-MB-468 (468) cells compared to transfection control (siScr) 468 cells. Each row represents the relative expression levels of a single gene and each column represents the gene expression levels in a specific sample. Green and red colours represent relatively low and high gene expression, respectively. Hierarchical clustering was reported by A) Gene intensities and B) Distance to mean. n = 3.

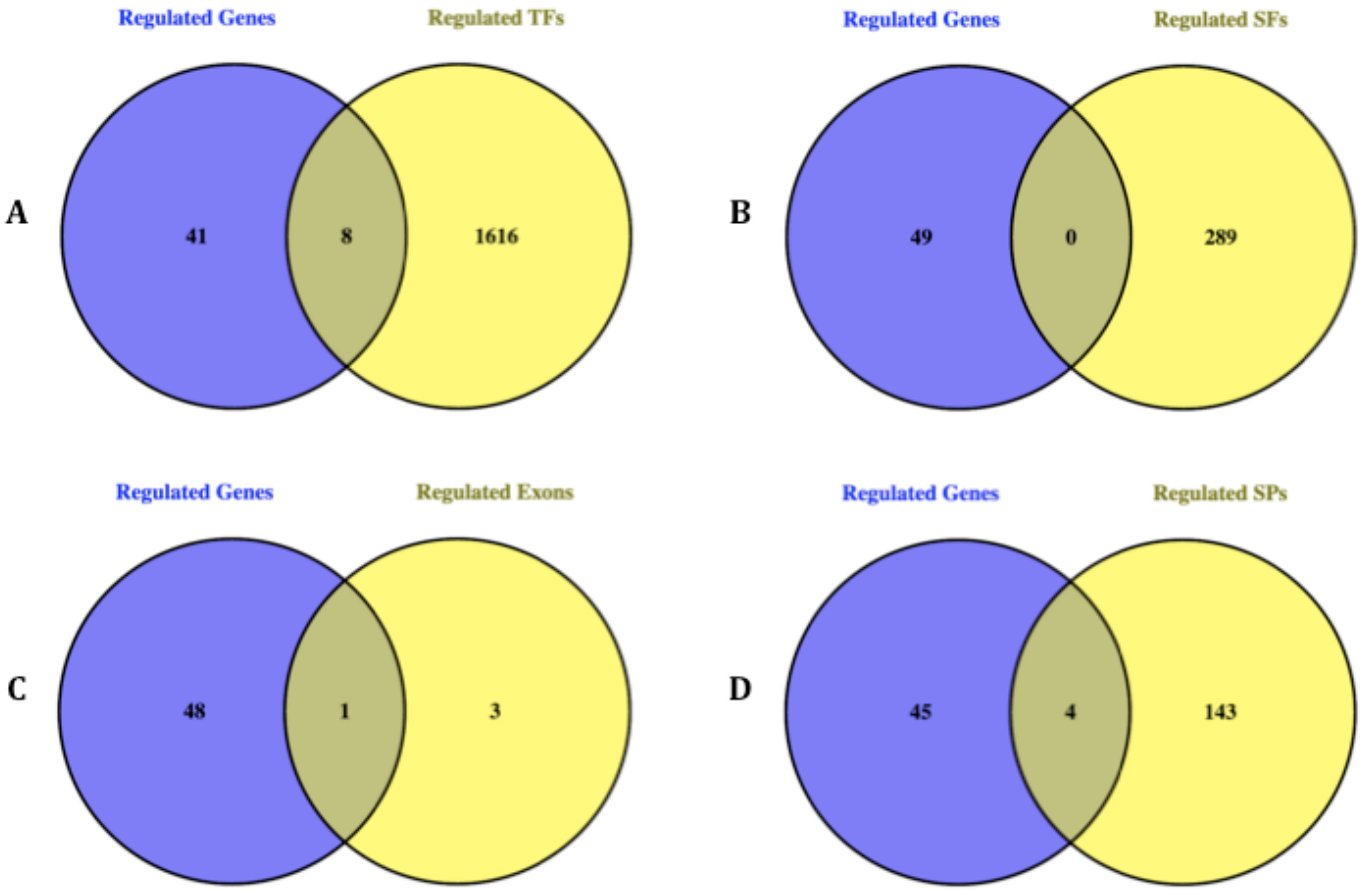

Figure 4.27 – Venn diagrams summarising Affymetrix GeneChip® Human Transcriptome Array 2.0 data comparing MDA-MB-436 KSRP knockdown (siKSRP) cells to MDA-MB-468 transfection control (siScr) cells. A) Regulated genes overlapping regulated transcription factors with a fold change ≥ 1,5. B) No regulated genes overlapped regulated splicing factors with a fold change ≥ 1,5. C) Regulated genes that have regulated exons with a fold change ≥ 1,5. D) Regulated genes that also have regulated splicing patterns with a fold change ≥ 1,5.

Table 4.1 – Regulated Genes. The 49 genes identified as being regulated with a fold change ≥ 1,5 upon KSRP knockdown.

Fast DB Stable ID	Gene Symbol	Regulation	Fold-Change	P-Value	Gene Name
GSHG0023151	TAPT1	up	2.14	2.63E-04	transmembrane anterior posterior transformation 1
GSHG0027663	MET	up	2.04	2.38E-03	met proto-oncogene
GSHG0044022	MIR1244-3	up	1.97	4.17E-02	microRNA 1244-3
GSHG0003935	PIP4K2A	up	1.88	3.44E-03	phosphatidylinositol-5-phosphate 4-kinase, type II, alpha
GSHG0030892	RFK	up	1.85	1.16E-02	riboflavin kinase
GSHG0014062	BOD1L2	up	1.85	2.62E-03	biorientation of chromosomes in cell division 1-like 2
GSHG0012329	WSB1	up	1.84	6.97E-04	WD repeat and SOCS box containing 1
GSHG0020833	RAD54L2	up	1.82	7.96E-04	RAD54-like 2 (S. cerevisiae)
GSHG0012223	NTN1	up	1.81	3.92E-03	netrin 1
GSHG0026610	CCND3	up	1.78	2.24E-04	cyclin D3
GSHG0028283	GATSL2	up	1.74	2.12E-02	GATS protein-like 2
GSHG0022511	RBPJ	up	1.66	2.76E-04	recombination signal binding protein for immunoglobulin kappa J region
GSHG0006174	PPP2R1B	up	1.66	4.23E-05	protein phosphatase 2, regulatory subunit A, beta
GSHG0003375	DKK1	up	1.63	3.15E-02	dickkopf WNT signaling pathway inhibitor 1
GSHG0032173	MAP2K4P1	up	1.59	2.38E-02	mitogen-activated protein kinase kinase 4 pseudogene 1
GSHG0003401	NRBF2	up	1.59	8.17E-05	nuclear receptor binding factor 2
GSHG0031978	TRAPPC2	up	1.58	2.37E-02	trafficking protein particle complex 2
GSHG0018553	CRLS1	up	1.57	1.51E-02	cardiolipin synthase 1
GSHG0016280	RHOB	up	1.57	7.54E-03	ras homolog family member B

GSHG0012025	MBTPS1	up	1.57	9.89E-05	membrane-bound transcription factor peptidase, site 1
GSHG0003659	INA	up	1.57	2.69E-02	internexin neuronal intermediate filament protein, alpha
GSHG0001849	E2F2	up	1.56	3.93E-02	E2F transcription factor 2
GSHG0030848	PGM5P2	up	1.56	7.06E-03	phosphoglucomutase 5 pseudogene 2
GSHG0030721	MIR31HG	up	1.56	8.17E-05	MIR31 host gene (non-protein coding)
GSHG0017609	MCFD2	up	1.54	1.32E-03	multiple coagulation factor deficiency 2
GSHG0028111	RP9	up	1.53	1.53E-02	retinitis pigmentosa 9 (autosomal dominant)
GSHG0025272	BOD1	up	1.53	1.01E-02	biorientation of chromosomes in cell division 1
GSHG0024380	SLC36A1	up	1.53	6.85E-04	solute carrier family 36 (proton/amino acid symporter), member 1
GSHG0042222	CEP170P1	up	1.53	3.84E-03	centrosomal protein 170kDa pseudogene 1
GSHG0019104	PDRG1	up	1.53	1.31E-02	p53 and DNA-damage regulated 1
GSHG0027703	CALU	up	1.52	3.00E-04	calumenin
GSHG0002574	PYGO2	up	1.50	3.30E-03	pygopus homolog 2 (Drosophila)
GSHG0013958	GATA6	up	1.50	1.13E-02	GATA binding protein 6
GSHG0015417	KHSRP	down	5.71	1.28E-07	KH-type splicing regulatory protein
GSHG0023990	MRPS36	down	2.17	7.56E-04	mitochondrial ribosomal protein S36
GSHG0000250	RCAN3	down	1.99	1.80E-02	RCAN family member 3
GSHG0006714	MUCL1	down	1.91	1.22E-03	mucin-like 1
GSHG0022141	CP	down	1.78	2.68E-03	ceruloplasmin (ferroxidase)
GSHG0033954	ATP5E	down	1.76	9.19E-04	ATP synthase, H+ transporting, mitochondrial F1 complex, epsilon subunit
GSHG0006190	USP28	down	1.72	1.54E-03	ubiquitin specific peptidase 28
GSHG0007237	A2M	down	1.68	1.06E-03	alpha-2-macroglobulin

GSHG0011856	CES1	down	1.61	1.40E-03	carboxylesterase 1
GSHG0004918	SCGB2A2	down	1.61	1.78E-03	secretoglobin, family 2A, member 2
GSHG0001819	PLA2G2A	down	1.58	7.34E-03	phospholipase A2, group IIA (platelets, synovial fluid)
GSHG0032166	HDAC8	down	1.54	2.34E-03	histone deacetylase 8
GSHG0021085	SLC15A2	down	1.52	6.60E-03	solute carrier family 15 (oligopeptide transporter), member 2
GSHG0000669	CLCA2	down	1.52	5.36E-04	chloride channel accessory 2
GSHG0005343	GRAMD1B	down	1.52	2.38E-03	GRAM domain containing 1B
GSHG0006549	SSPN	down	1.50	6.90E-03	sarcospan

Table 4.2 – Regulated genes involved in the Wnt signalling pathway. The three genes identified as being involved in the Wnt Signalling pathway and are upregulated with a fold change of ≥ 1,5 upon KSRP knockdown.

Fast DB Stable ID	Pathway Description (KEGG)	Gene Symbol	Gene Name	Regulation	Fold-Change	P-Value
GSHG0026610	Wnt signaling pathway	CCND3	cyclin D3	up	1.78	2.24E-04
GSHG0006174	Wnt signaling pathway	PPP2R1B	protein phosphatase 2, regulatory subunit A, beta	up	1.66	4.22E-05
GSHG0003375	Wnt signaling pathway	DKK1	dickkopf WNT signaling pathway inhibitor 1	up	1.63	3.15E-02

Table 4.3 – Regulated genes that are transcription factors. The 8 transcription factors identified as being regulated with a fold change ≥ 1,5 upon KSRP knockdown.

Fast DB Stable ID	Gene Symbol	Regulation	Fold-Change	P-Value	Gene Name
GSHG0001849	E2F2	up	1.56	3.93E-02	E2F transcription factor 2
GSHG0003375	DKK1	up	1.63	3.15E-02	dickkopf homolog 1 (Xenopus laevis)
GSHG0003401	NRBF2	up	1.59	8.17E-05	nuclear receptor binding factor 2
GSHG0013958	GATA6	up	1.50	1.13E-02	GATA binding protein 6
GSHG0020833	RAD54L2	up	1.82	7.96E-04	RAD54-like 2 (S. cerevisiae)
GSHG0022511	RBPJ	up	1.66	2.76E-04	recombination signal binding protein for immunoglobulin kappa J region
GSHG0031978	TRAPPC2	up	1.58	2.37E-02	trafficking protein particle complex 2
GSHG0032166	HDAC8	down	1.54	2.34E-03	histone deacetylase 8

Table 4.4 – Regulated genes that have regulated exons. The one regulated exon identified as being regulated with a fold change ≥ 1,5 upon KSRP knockdown.

Fast DB Stable ID	Detected Exon	Known Alternative Event	Gene Symbol	Regulation Splicing Index	Fold-Change Splicing Index	P-Value Splicing Index	Gene Name	Regulation Gene	Fold-Change Gene	P-value Gene
GSHG0026610	e1	alternative_first_exon	CCND3	down	2.23	5.52E-05	cyclin D3	up	1.78	2.24E-04

Table 4.5 – Regulated genes that have regulated splicing patterns. The 4 regulated splicing patterns identified as being regulated with a fold change ≥ 1,5 upon KSRP knockdown.

Fast DB Stable ID	Gene Symbol	Alternative Event Type	Involved exon(s)	Regulation Splicing Index	Average Splicing-Index Fold-Change	Max Splicing-Index Fold-Change	Min Splicing-Index P-Value	Gene Name
GSHG0012329	WSB1	Complex	e6-7	down	1.40	1.69	8.44E-03	WD repeat and SOCS box containing 1
GSHG0024380	SLC36A1	Alter. First Exon	e1/e3	down (e1)	1.40	1.43	2.83E-02	solute carrier family 36 (proton/amino acid symporter), member 1
GSHG0023151	TAPT1	Exon Cassette	e2	up	1.20	1.39	4.86E-03	transmembrane anterior posterior transformation 1
GSHG0000250	RCAN3	Exon Cassette	e5	down	1.28	1.52	2.28E-02	RCAN family member 3

4.2.1.1. Selection and Validation of Affymetrix GeneChip® Human Transcriptome Array 2.0 Targets in MDA-MB-468 Cells

The results of the Affymetrix GeneChip® Human Transcriptome Array 2.0 identified three genes involved in the Wnt pathway – namely Cyclin D3 (*CCND3*), Dickkopf WNT Signaling Pathway Inhibitor 1 (*DKK1*) and Protein Phosphatase 2, Regulatory Subunit A, Beta (*PPP2R1B*) – as being significantly upregulated in MDA-MB-468 cells when KSRP is downregulated. Figure 4.28 shows the locations of CCND3 and DKK1 in the Wnt pathway (bordered in red), a pathway annotation adopted from KEGG. PPP2R1B forms part of the Wnt pathway but is sub-classified as part of the TGF-β signalling pathway (bordered in blue in Figure 4.28), which directly feeds into the Wnt signalling pathway by regulating SMAD3. The location of PPP2R1B in the TGF-β, and thus Wnt, pathway is bordered in red (Figure 4.29; a pathway annotation adopted from KEGG).

The upregulation in the expression levels of *CCND3*, *DKK1* and *PPP2R1B* in *KSRP* downregulated MDA-MB-468 cells was confirmed by qRT-PCR (section 3.10). The mRNA expression levels of *KSRP*, *CCND3*, *DKK1* and *PPP2R1B* in MDA-MB-468 cells when KSRP was downregulated (siKSRP) was expressed relative to the mRNA expression levels of these genes in the knockdown transfection control (siScr). The results indicate that a significant decrease in the mRNA expression levels of *KSRP* ($p \leq 0{,}001$) causes a significant increase in the mRNA expression levels of *CCND3*, *DKK1* and *PPP2R1B* ($p \leq 0{,}001$) (Figure 4.30), validating the Affymetrix GeneChip® Human Transcriptome Array 2.0 findings.

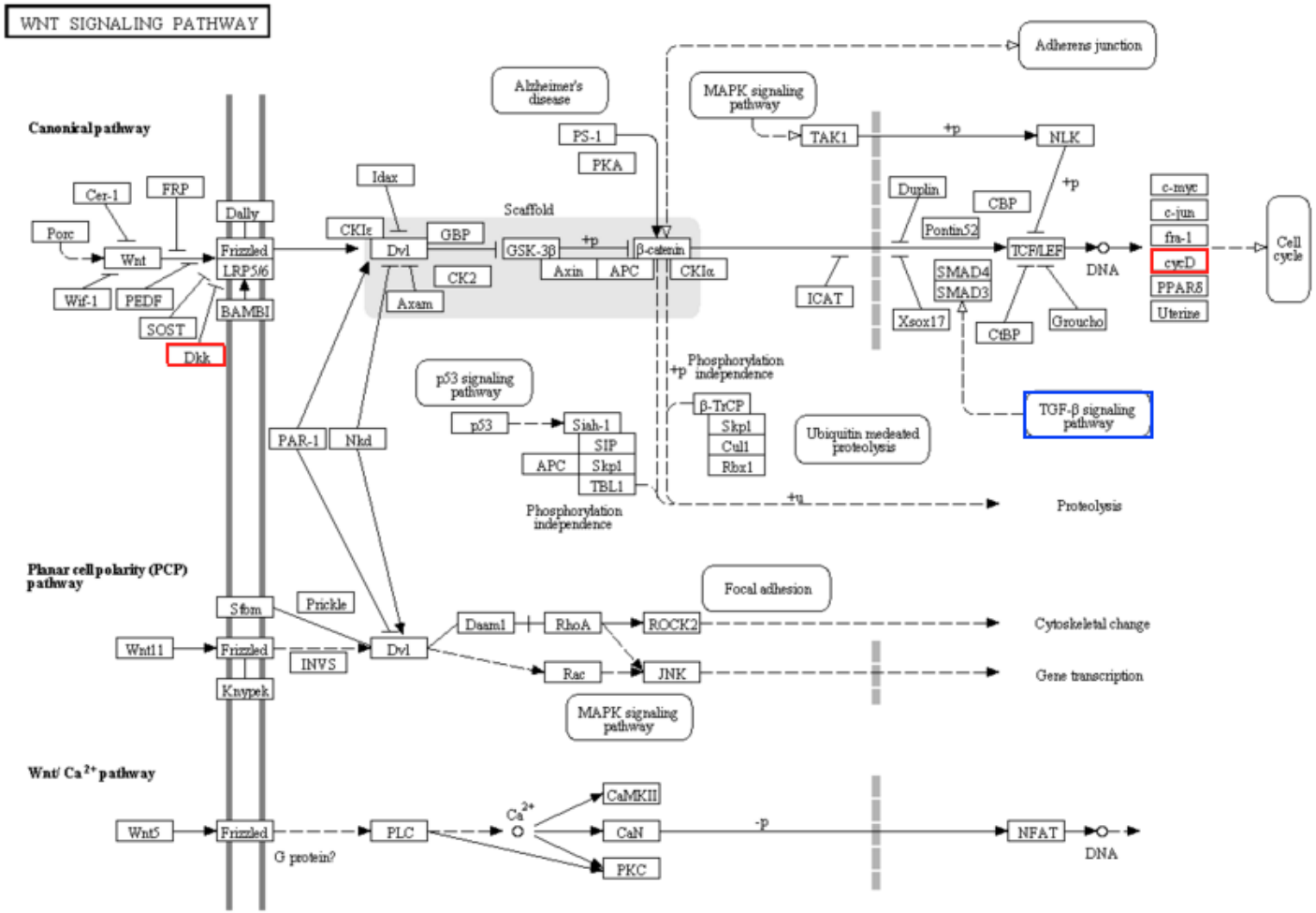

Figure 4.28 – Wnt pathway adapted from KEGG. The positions of DKK (DKK1) and cyD (CCND3) – proteins regulated by KSRP – in the Wnt signalling pathway are bordered in red. The location of the TGF-β signalling pathway is bordered in blue.

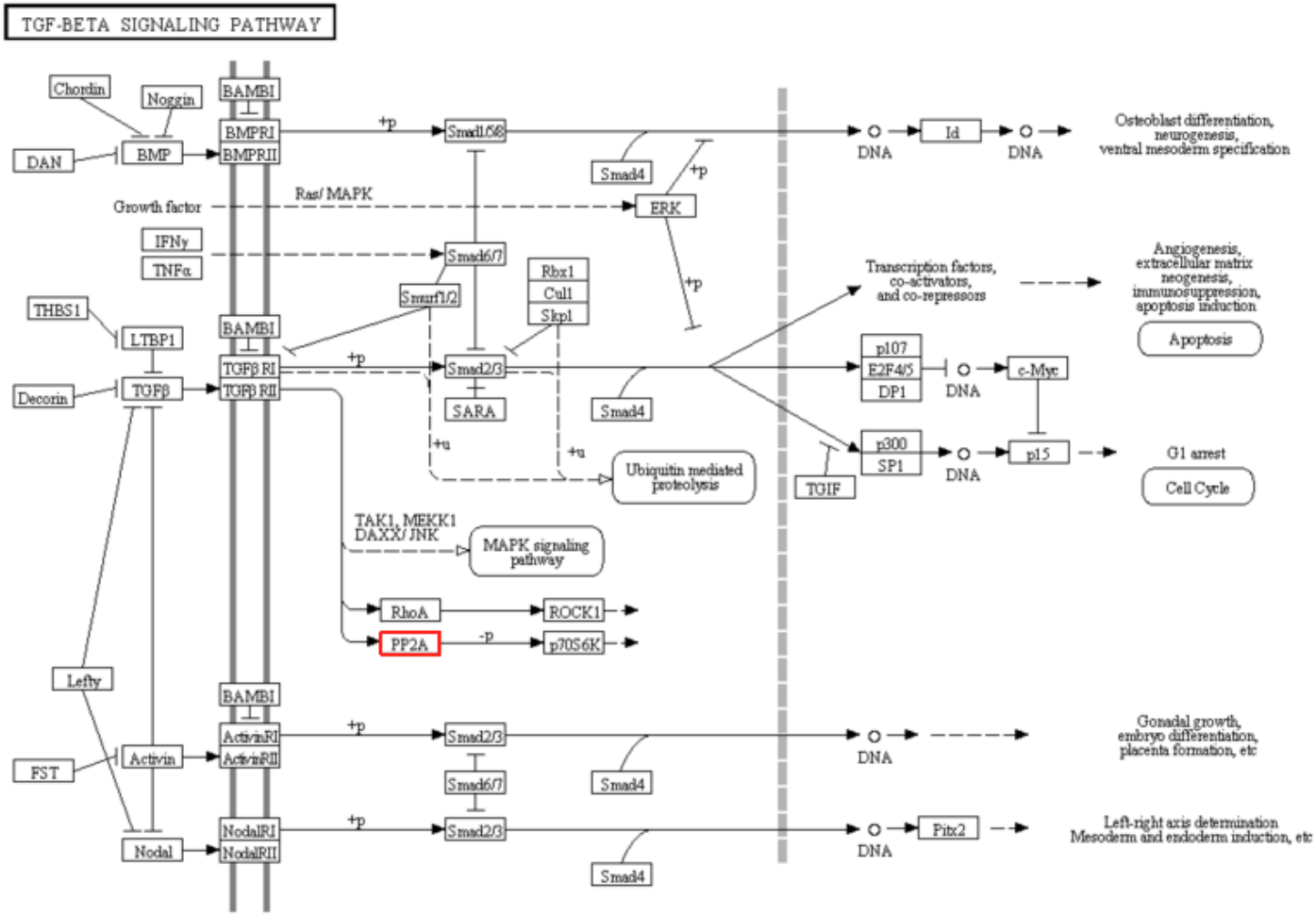

Figure 4.29 – TGF-β pathway adapted from KEGG. The position of PP2A (PPP2R1B) – a protein regulated by KSRP – in the TGF-β pathway is bordered in red.

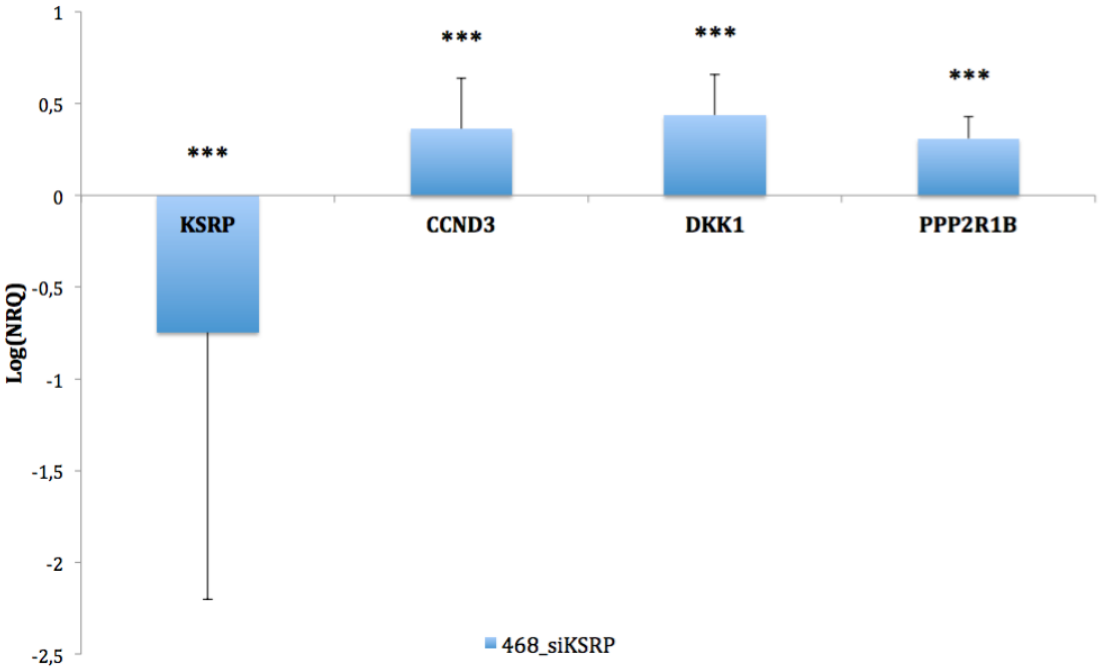

Figure 4.30 – Validation of the effect of *KSRP* knockdown (siKSRP) on *CCND3*, *DKK1* and *PPP2R1B* mRNA expression levels in MDA-MB-468 (468) cells. The mRNA expression levels of *KSRP*, *CCND3*, *DKK1* and *PPP2R1B* in MDA-MB-468 cells when *KSRP* was downregulated (siKSRP) were expressed relative to the mRNA expression levels of these genes in the knockdown transfection control (siScr). n = 9; standard errors are shown; *** $p \leq 0{,}001$.

4.2.2. Prediction of KSRP Interaction and Determination of KSRP Co-Localisation With Selected Affymetrix GeneChip® Human Transcriptome Array 2.0 Targets in MDA-MB-468 Cells

To investigate possible interactions of KSRP with the selected Affymetrix GeneChip® Human Transcriptome Array 2.0 targets, a prediction database was used and co-localisation experiments conducted.

4.2.2.1. Prediction of KSRP Interaction with Selected Affymetrix GeneChip® Human Transcriptome Array 2.0 Targets in MDA-MB-468 Cells

STRING (Search Tool for the Retrieval of Interacting Genes/Proteins), a biological database of known and predicted protein-protein interactions was used to explore the possible direct interactions between KSRP and CCND3, KSRP and DKK1 as well as KSRP and PPP2R1B. The results of the STRING analysis revealed no connecting lines between KSRP and CCND3 (Figure 4.31 A), KSRP and DKK1 (Figure 4.31 B) or KSRP and PPP2R1B (Figure 4.31 C).

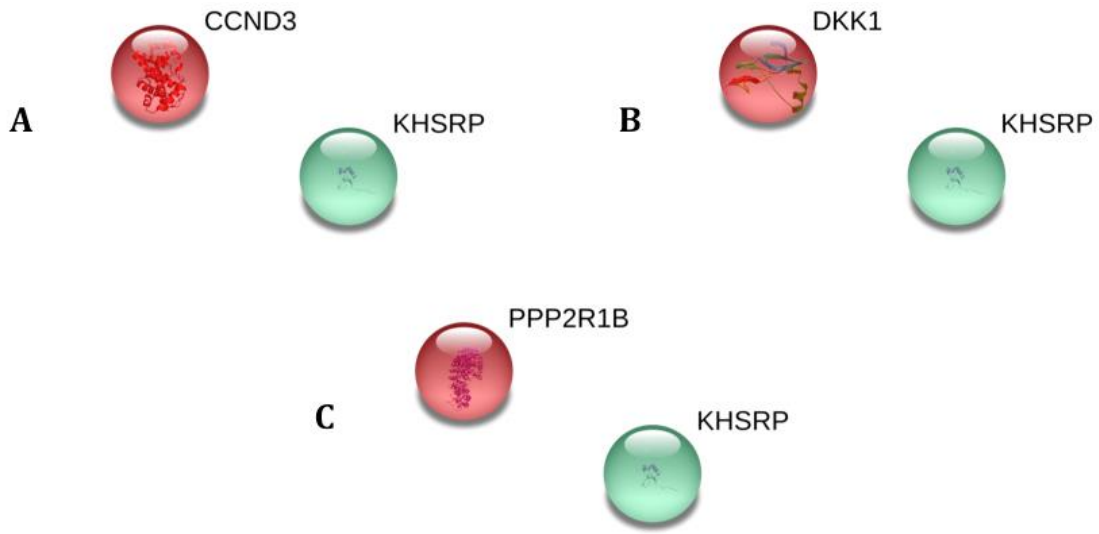

Figure 4.31 – STRING analysis of the possible interactions of A) KSRP and CCND3, B) KSRP and DKK1 as well as C) KSRP and PPP2R1B. No connection lines were observed in A, B or C, suggesting no direct interaction between these proteins.

The STRING database and tool was also used to determine possible indirect interactions between these proteins by investigating the protein interaction networks involving KSRP and CCND3, KSRP and DKK1 as well as KSRP and PPP2R1B. The analysis showed indirect interactions between KSRP and CCND3 (Figure 4.32 A), KSRP and DKK1 (Figure 4.32 B) and KSRP and PPP2R1B (Figure 4.32 C).

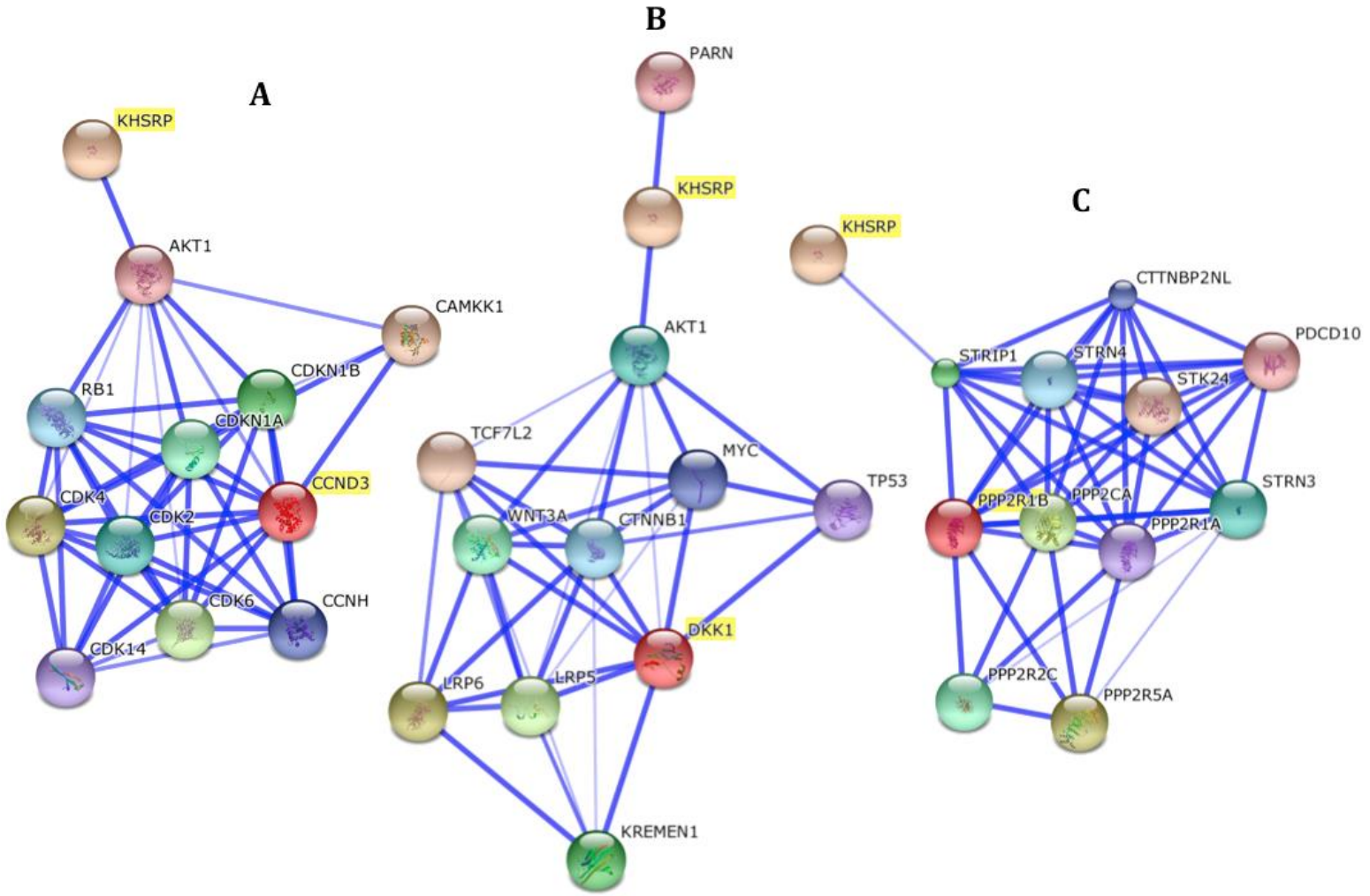

Figure 4.32 – STRING analysis predictions of protein interaction networks involving A) KSRP and CCND3, B) KSRP and DKK1 and C) KSRP and PPP2R1B. The proteins of interest are highlighted in yellow.

4.2.2.2. Determination of KSRP Co-Localisation With Selected Affymetrix GeneChip® Human Transcriptome Array 2.0 Targets in MDA-MB-468 Cells

Co-localisation of KSRP with CCND3, DKK1 or PPP2R1B in KSRP overexpressing MDA-MB-468 cells (transfected with pEGFPC$_1$-6xHis-FLKSRP - GFP-KSRP) was compared to the co-localisation of GFP with CCND3, DKK1 or PPP2R1B in MDA-MB-468 cells transfected with the pEGFP-N1 plasmid (GFP) (section 3.18.2).

GFP and KSRP did not seem to co-localise (Figure 4.33 A), however, co-localisation of GFP-KSRP and KSRP was observed (Figure 4.33 B). Neither GFP nor GFP-KSRP seemed to co-localise with CCND3 (Figure 4.34 A & B) or with PPP2R1B (Figure 4.36 A & B). GFP and DKK1 did not co-localise (Figure 4.35 A), however, co-localisation of GFP-KSRP and DKK1 was seen (Figure 4.35 B).

Using FIJI, 2D intensity histograms were plotted for each of the potential co-localisation events (section 3.19.2). The presence of a diagonal scatter pattern on the 2D intensity histogram showed evidence of positive co-localisation; this was observed when the images representing GFP-KSRP and KSRP co-localisation (Figure 4.37 B) as well as GFP-KSRP and DKK1 co-localisation (Figure 4.37 F) were analysed. The intense diagonals were not observed when images representing GFP co-localisation with KSRP (Figure 4.37 A), CCND3 (Figure 4.37 C), DKK1 (Figure 4.37 E) and PPP2R1B (Figure 4.37 G) as well as GFP-KSRP co-localisation with CCND3 (Figure 4.37 D) and PPP2R1B (Figure 4.37 H) were analysed.

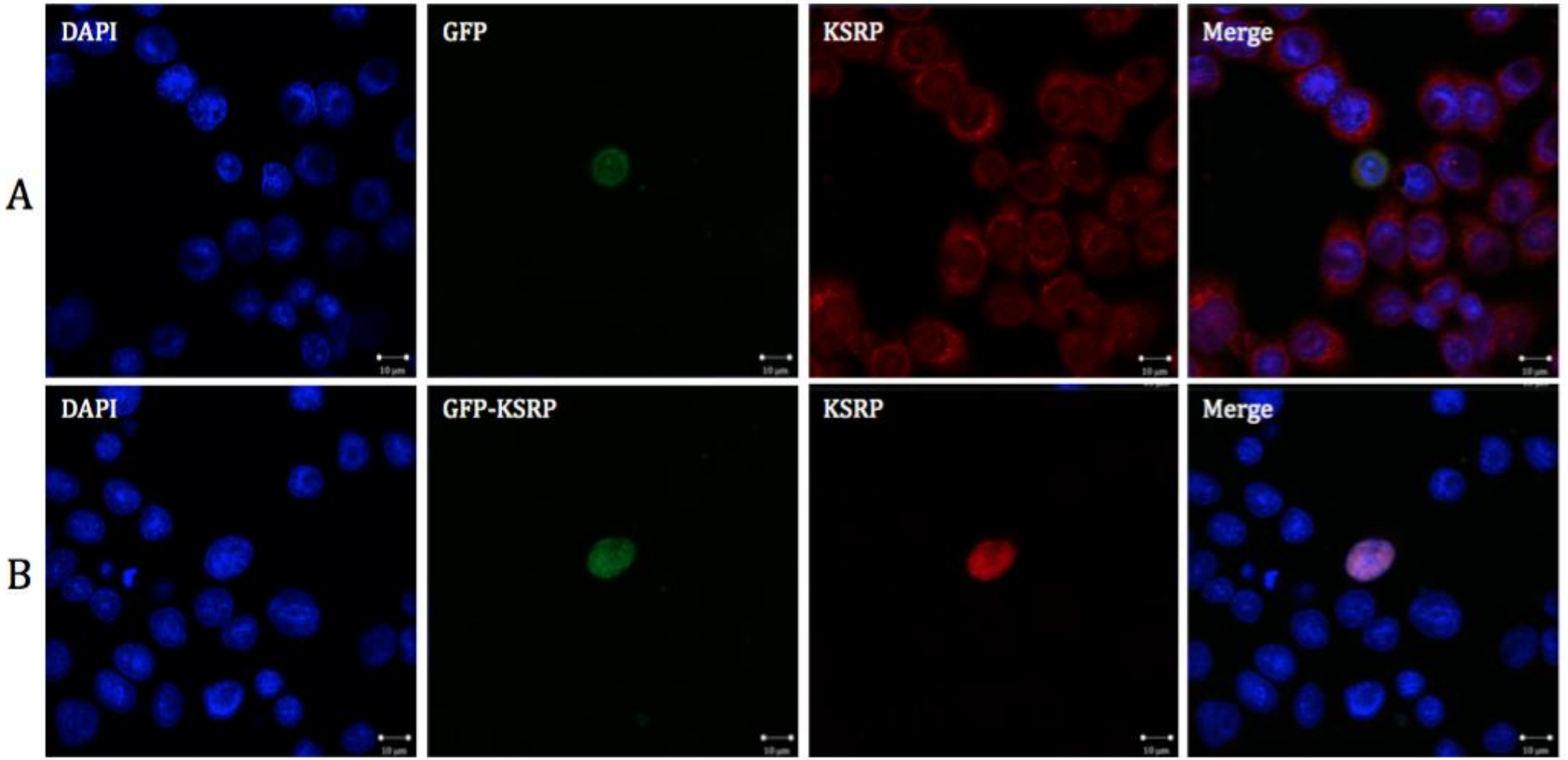

Figure 4.33 – Co-localisation of GFP and KSRP as well as GFP-KSRP and KSRP in MDA-MB-468 cells expressing A) pEGFP-N1 and B) pEGFPC1-6xHis-FLKSRP. A) GFP did not co-localise with KSRP. B) GFP-KSRP co-localised with KSRP. The polyclonal rabbit anti-KSRP primary and polyclonal goat anti-Rabbit IgG (H+L) Rhodamine Red secondary antibodies were used. Images were captured using the Olympus IX71 Fluorescence Microscope. Included images are representative of similar ones obtained; n = 3.

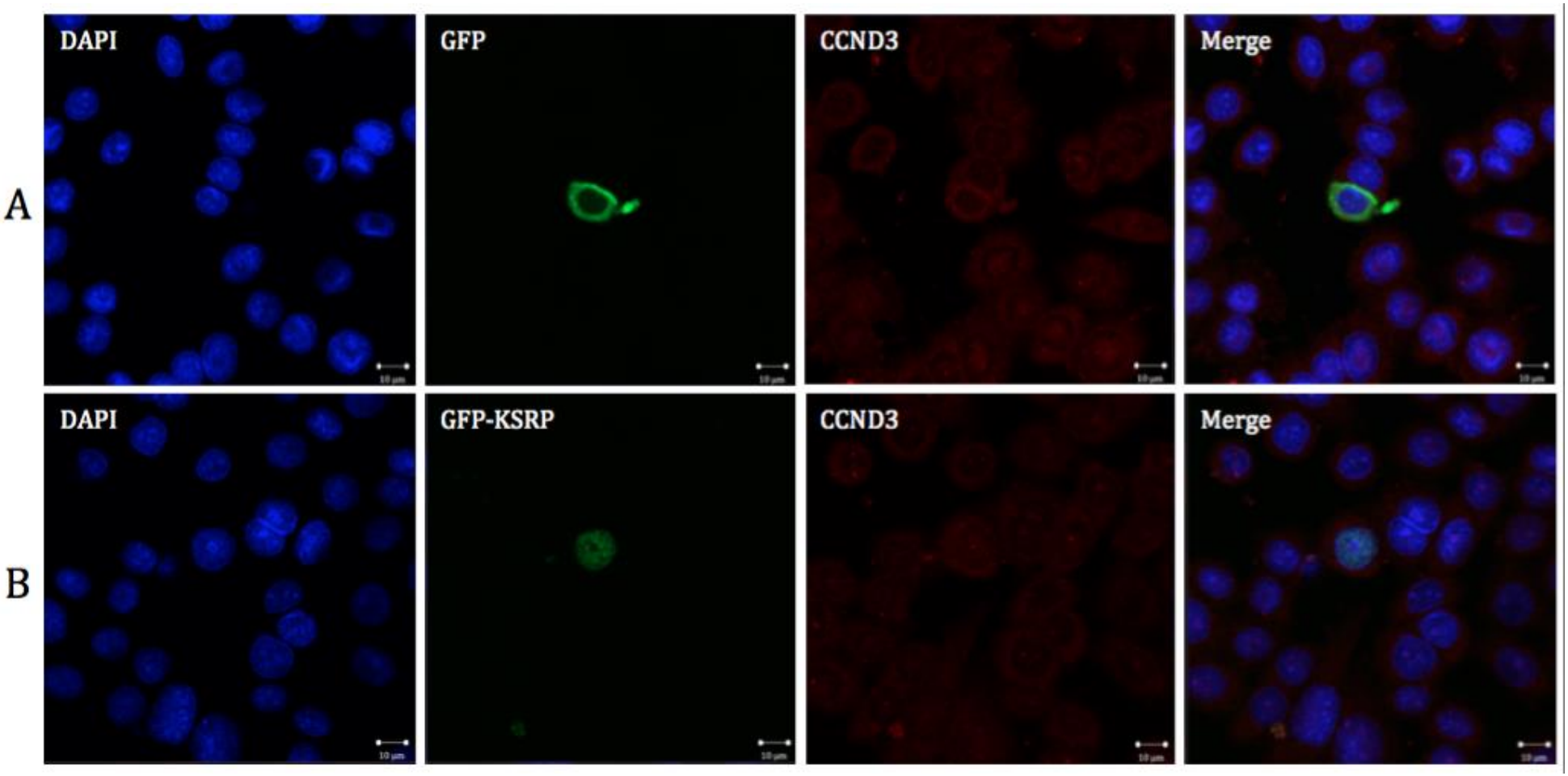

Figure 4.34 – Co-localisation of GFP and CCND3 as well as GFP-KSRP and CCND3 in MDA-MB-468 cells expressing A) pEGFP-N1 and B) pEGFPC1-6xHis-FLKSRP. A) GFP did not co-localise with CCND3. B) GFP-KSRP did not co-localise with CCND3. The monoclonal rabbit anti-Cyclin D3 primary and polyclonal goat anti-Rabbit IgG (H+L) Rhodamine Red secondary antibodies were used. Images were captured using the Olympus IX71 Fluorescence Microscope. Included images are representative of similar ones obtained; n = 3.

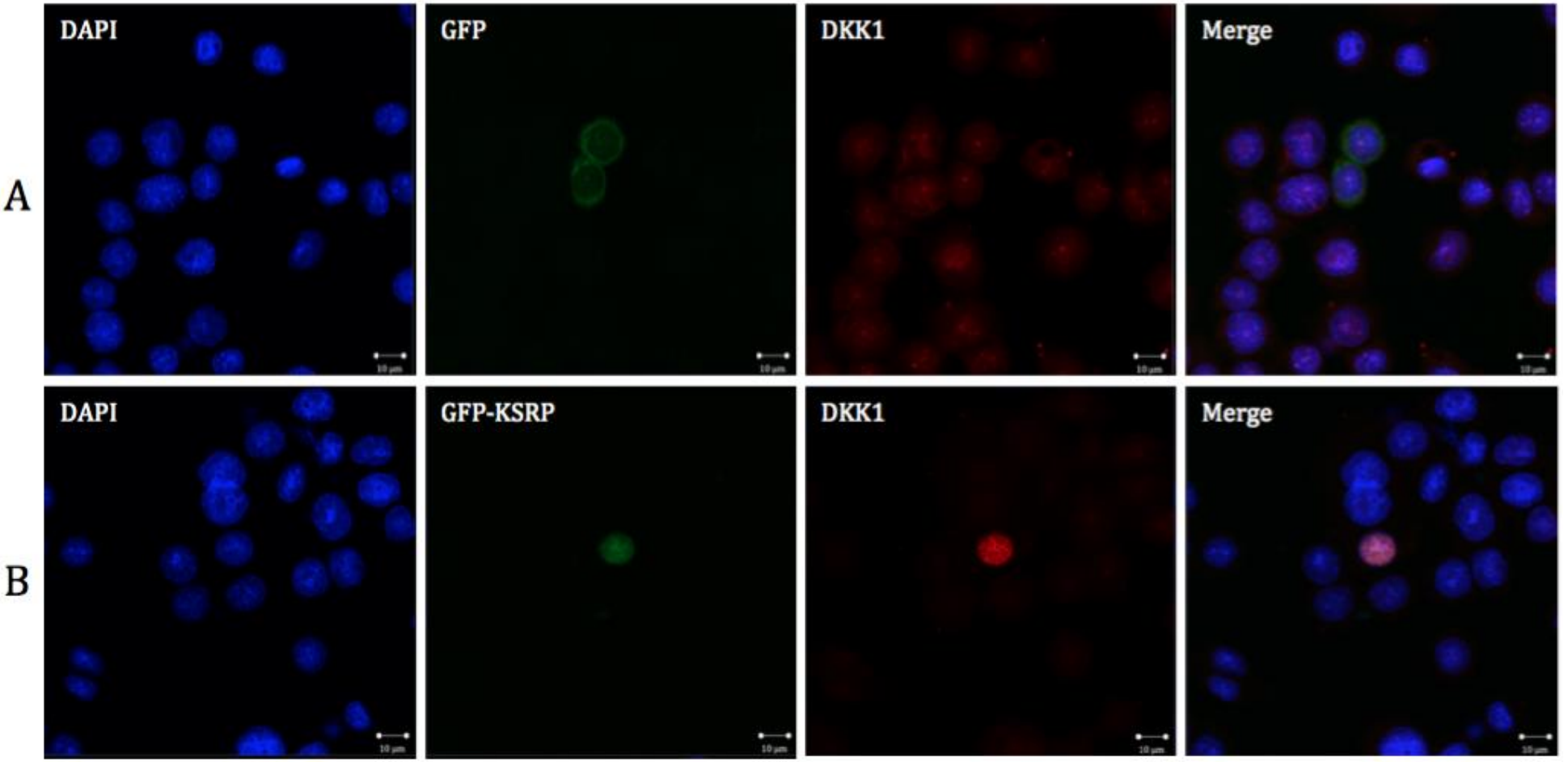

Figure 4.35 – Co-localisation of GFP and DKK1 as well as GFP-KSRP and DKK1 in MDA-MB-468 cells expressing A) pEGFP-N1 and B) pEGFPC1-6xHis-FLKSRP. A) GFP did not co-localise with DKK1. B) GFP-KSRP co-localised with DKK1. The monoclonal rabbit anti-DKK1 primary and polyclonal goat anti-Rabbit IgG (H+L) Rhodamine Red secondary antibodies were used. Images were captured using the Olympus IX71 Fluorescence Microscope. Included images are representative of similar ones obtained; n = 3.

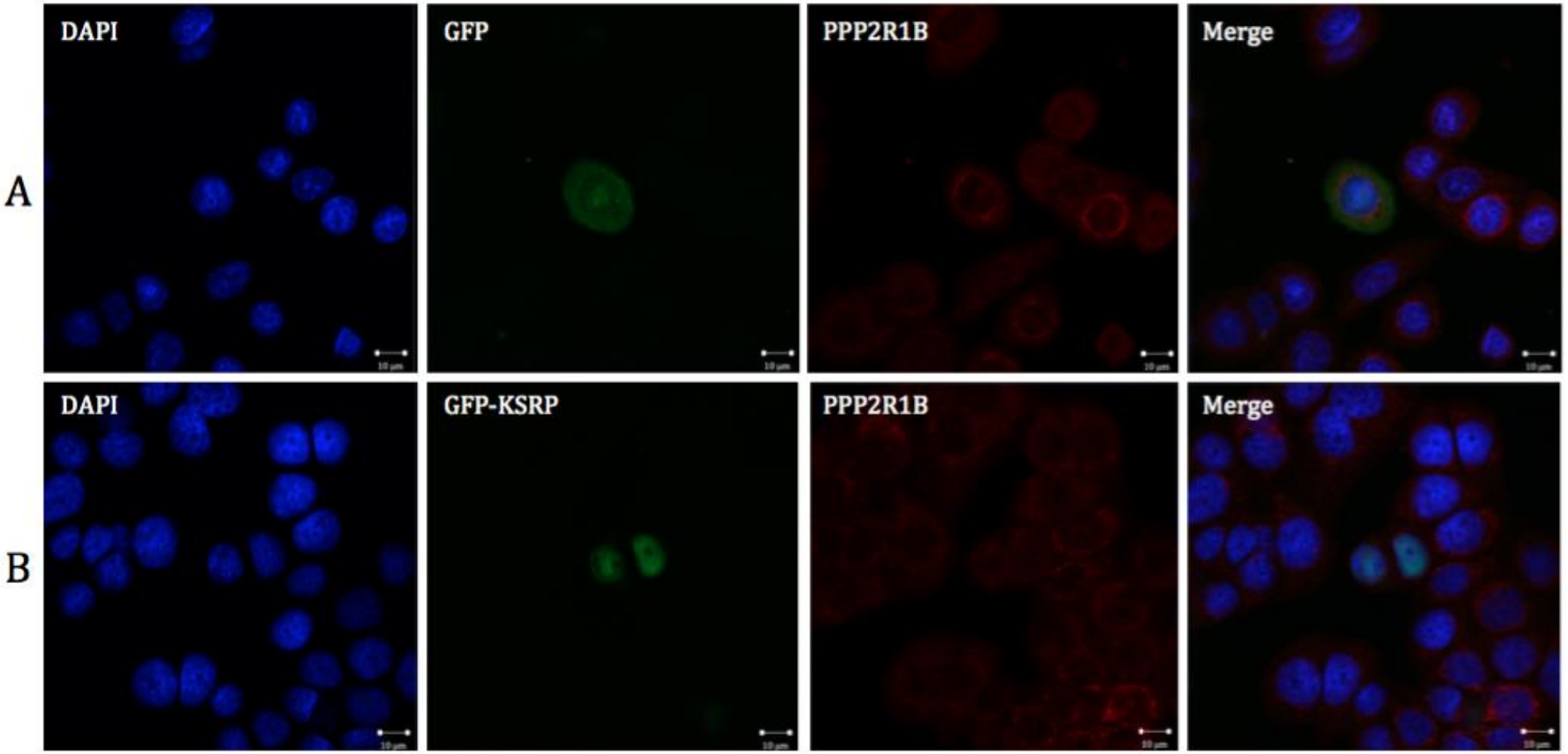

Figure 4.36 – Co-localisation of GFP and PPP2R1B as well as GFP-KSRP and PPP2R1B in MDA-MB-468 cells expressing A) pEGFP-N1 and B) pEGFPC1-6xHis-FLKSRP. A) GFP did not co-localise with PPP2R1B. B) GFP-KSRP did not co-localise with PPP2R1B. The monoclonal rabbit anti-PPP2R1B primary and polyclonal goat anti-Rabbit IgG (H+L) Rhodamine Red secondary antibodies were used. Images were captured using the Olympus IX71 Fluorescence Microscope. Included images are representative of similar ones obtained; n = 3.

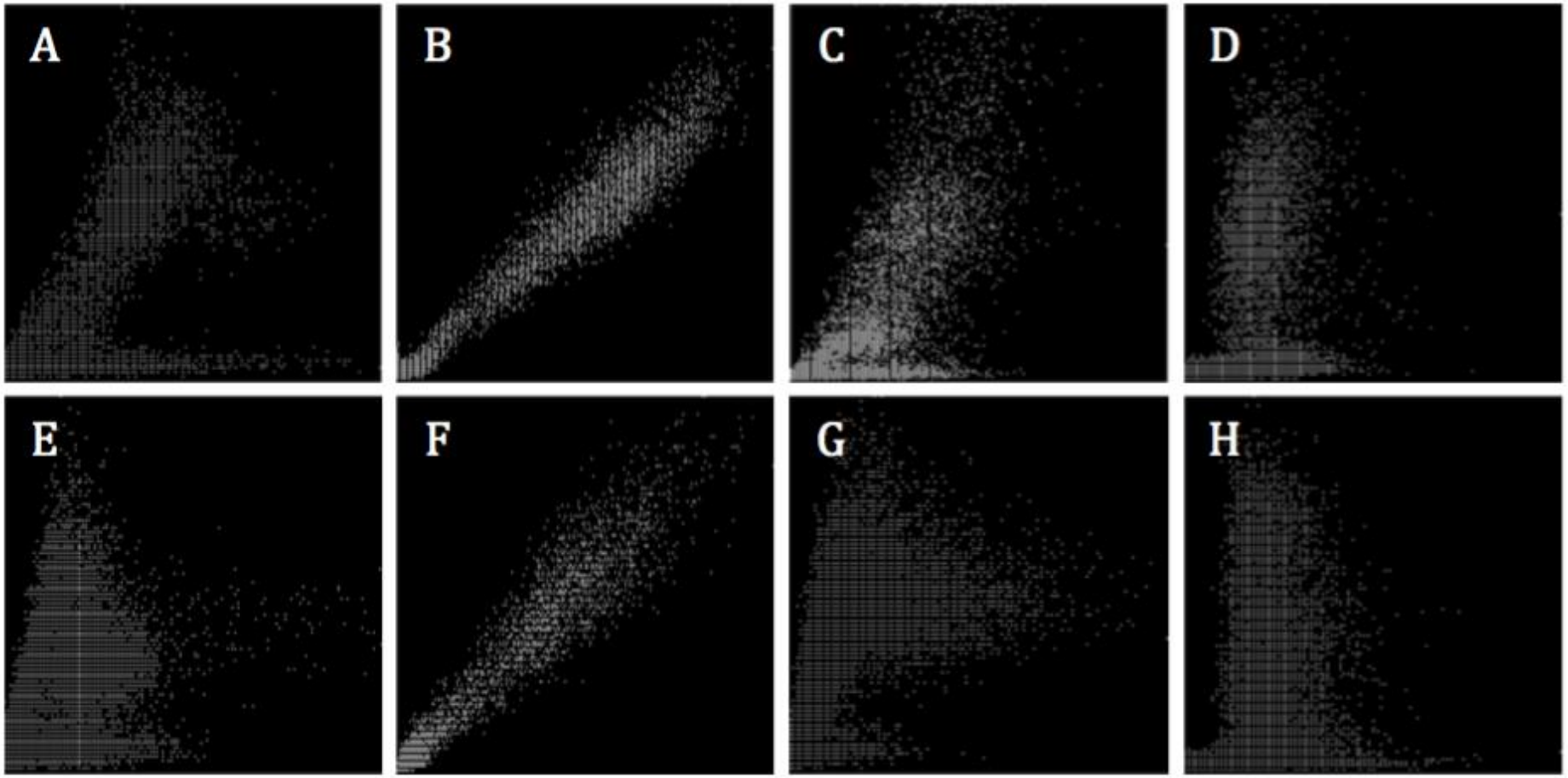

Figure 4.37 – 2D intensity histograms evidencing either positive or negative co-localisation events. Positive co-localisation of targets is indicated by a diagonal scatter pattern on the 2D intensity histogram. Positive co-localisation was seen between B) GFP-KSRP and KSRP and F) GFP-KSRP and DKK1. Negative co-localisation was seen between A) GFP and KSRP, C) GFP and CCND3, D) GFP-KSRP and CCND3, E) GFP and DKK1, G) GFP and PPP2R1B and H) GFP-KSRP and PPP2R1B.

Using FIJI, Pearson's R-values (listed in Table 4.6) were calculated for each potential co-localisation event (section 3.19.3). Pearson's R-values of -1, 0 and 1 represent negative, none and positive correlation, respectively. Pearson's R-values for GFP and KSRP, CCND3, DKK1 and PPP2R1B as well as GFP-KSRP and CCND3 and PPP2R1B corroborate the lack of co-localisation finding of both the co-localisation images and the 2D intensity histograms. Pearson's R-values for GFP-KSRP and KSRP, as well as GFP-KSRP and DKK1 had a value very close to 1, indicating positive correlation and corroborating the findings of the co-localisation images and 2D intensity histograms.

Table 4.6 – Pearson's R Values for potential co-localisation events.

Co-localisation between	Pearson's R Value
GFP and KSRP	0,72
GFP-KSRP and KSRP	0,99
GFP and CCND3	0,73
GFP-KSRP and CCND3	0,3
GFP and DKK1	0,55
GFP-KSRP and DKK1	0,97
GFP and PPP2R1B	0,68
GFP-KSRP and PPP2R1B	0,3

Chapter 5

5. DISCUSSION

5.1. Hypothesis-Based Approach

In the hypothesis-based section of the study, we aimed to determine if KSRP plays a role in epithelial-to-mesenchymal transition of triple-negative breast cancer cells by affecting the expression of *FGFR2 IIIb* and *FGFR2 IIIc* isoforms in MDA-MB-436 and MDA-MB-468 cells. We also aimed to investigate if KSRP directly binds to *FGFR2* mRNA. To accomplish these aims, the epithelial and mesenchymal phenotype, preferential *FGFR2* isoform inclusion, differential KSRP expression and alteration of *FGFR2 IIIb* isoform inclusion in MDA-MB-436 and MDA-MB-468 cells were confirmed. In MDA-MB-436 and MDA-MB-468 cells, KSRP was upregulated by transfection of these cells with a plasmid encoding KSRP (pEGFPC_1-6xHis-FLKSRP) and downregulated by transfection of these cells with siRNA directed against KSRP mRNA (siKSRP). The effect of these changes in KSRP expression on *FGFR2 IIIb* and *FGFR2 IIIc* isoform selection and the epithelial and mesenchymal phenotype of MDA-MB-436 and MDA-MB-468 cells were determined. In addition, direct binding of KSRP to the *FGFR2* mRNA in MDA-MB-468 cells was ascertained.

5.1.1. The Epithelial and Mesenchymal Phenotype, Preferential *FGFR2* Isoform Inclusion, Differential KSRP Expression and Altered *FGFR2* Isoform Expression in MDA-MB-436 and MDA-MB-468 Cells

MDA-MB-436 and MDA-MB-468 cells were chosen for this study because they have been characterised as triple-negative and are genotypically mesenchymal and epithelial, respectively [110]. To determine if the reported genotypes of these cells could be monitored phenotypically, we sought to confirm the presence of epithelial and mesenchymal markers in MDA-MB-436 and MDA-MB-468 cells. There are a number of epithelial and mesenchymal markers commonly used by researchers in the EMT field [64]. In this study, the expression of the epithelial marker, Cytokeratin 19, and the mesenchymal marker, Vimentin, was visualised in the MDA-MB-436 and MDA-MB-468 cells

using fluorescent microscopy. The genotype of MDA-MB-436 cells has been reported to be mesenchymal [110], and this was phenotypically confirmed by the presence of the mesenchymal marker Vimentin and the absence of the epithelial marker Cytokeratin 19. In contrast, MDA-MB-468 cells were reported to be epithelial [110], and this was phenotypically confirmed by the presence of the epithelial marker Cytokeratin 19 and the absence of the mesenchymal marker Vimentin.

The mutually exclusive splicing pattern of the *FGFR2* gene results in the inclusion of either *FGFR2 IIIb* or *FGFR2 IIIc* in the mature mRNA after each splicing reaction. In epithelial tissues, *FGFR2 IIIb* is reported to be the prevalent isoform, while in mesenchymal tissues the prevalent isoform is *FGFR2 IIIc* [164]. This pattern of preferential *FGFR2 IIIb* and *FGFR2 IIIc* inclusion in MDA-MB-436 and MDA-MB-468 cells was confirmed using both semi-qPCR and qRT-PCR. It could be possible that one of the fragments amplified in the semi-qPCR or the qRT-PCR may have been less efficiently amplified than the other because of possible differences in the primer efficiencies. However, the fact that one primer pair was used for the semi-qPCR and two for the qRT-PCR and similar results were obtained gives confidence to the results. Differences in the percentages of *FGFR2 IIIb* and *FGFR2 IIIc* expression when the findings from the semi-qPCR and qRT-PCR methods were compared are negligible and the patterns of *FGFR2* isoform inclusion are indistinguishable. Although the specific percentages of *FGFR2 IIIb* and *FGFR2 IIIc* inclusion differed marginally when the results of the semi-qPCR and qRT-PCR were compared, both techniques similarly illustrate the preferential inclusion of *FGFR2 IIIc* in mesenchymal cells (MDA-MB-436) and *FGFR2 IIIb* in epithelial cells (MDA-MB-468). These results, therefore, corroborate previous findings for the preferential inclusion of these *FGFR2* isoforms in MDA-MB-436 and MDA-MB-468 cells, and thus also mesenchymal and epithelial tissues, respectively [164].

The nuclear proteomes of MDA-MB-436 and MDA-MB-468 cells were previously compared using a proteomic screen, and an upregulation of KSRP in the latter cell line was discovered (unpublished data). To validate this finding, the KSRP protein levels in MDA-MB-436 and MDA-MB-468 cells were determined using western blotting. The presence of a more intense band in the

MDA-MB-468 sample lane compared to the MDA-MB-436 sample lane is indicative of a higher KSRP protein expression level in the former cell line compared to the latter. When assessing the functionality of the primary antibody used here for KSRP detection (polyclonal rabbit anti-KSRP), the suppliers (Bethyl Laboratories Inc.) noticed the presence of secondary band similar to that observed in Figure 4.6. This could suggest the possible existence of a KSRP variant; primarily cytoplasmic 52 kDa KSRP variant, labelled t-KSRP is expressed in a subpopulation of germ cells [215]. This variant was however not observed in Figure 4.9 or Figure 4.10; this could possibly be due to the use of a lesser exposure time for these blots. Quantification of the primary KSRP band intensities revealed that MDA-MB-468 cells express 14% more KSRP than MDA-MB-436 cells, thus confirming the differential expression of KSRP in the aforementioned cells as reported in the proteomic screen. It was surprising that only 14% more KSRP is present in MDA-MB-468 cells compared to MDA-MB-436 cells since a greater differential expression pattern was observed in the results of the proteomic screen. This discrepancy may be due to the fact that the nuclear proteomes of MDA-MB-436 and MDA-MB-468 cells were compared in the proteomic screen while total protein expression (cytoplasmic and nuclear) was compared in this study. Our experiments should ideally therefore have employed the fractionation technique to specifically isolate and investigate nuclear KSRP. The primary localisation of KSRP in MDA-MB-436 and MDA-MB-468 cells has not been reported previously.

Knockdown of *ESRP1* and *ESRP2* in MDA-MB-436 and MDA-MB-468 cells resulted in a change in the expression of *FGFR2 IIIb* and *FGFR2 IIIc* – *FGFR2 IIIb* and *FGFR2 IIIc* expression was decreased and increased, respectively, in these cells. ESRP1 and ESRP2 were chosen for this control analysis since these proteins are known regulators of *FGFR2* splicing and have been suggested to co-operate with additional regulatory proteins to bring about the splicing and silencing of FGFR2 IIIb and FGFR2 IIIc, respectively [173]. Compared to MDA-MB-436 cells, the decrease and increase of *FGFR2 IIIb* and *FGFR2 IIIc* expression, respectively, in MDA-MB-468 cells was more effective, and this may be attributed to ESRP1 and ESRP2 being epithelial-specific regulators. This result confirmed that the expression of *FGFR2 IIIb* and *FGFR2 IIIc* could be modulated

in response to changes in the expression of regulatory splicing factors. This technique, however, is not able to differentiate between changes in gene expression and changes in gene splicing and is a limitation in this study. To conclusively state that the observed changes were due to changes in gene splicing, a constitutive FGFR2 exon (not alternatively spliced and therefore stably expressed), should have been used as a gene expression control. If the expression of the constitutive FGFR2 exon was changed in response to ESRP 1 and 2 knockdown, we could conclude that these proteins alter gene expression, and not splicing.

5.1.2. The Effect of KSRP Knockdown and KSRP Overexpression on *FGFR2 IIIb* and *FGFR2 IIIc* Expression and the Effect of KSRP Overexpression on the Epithelial and Mesenchymal Phenotype in MDA-MB-436 and MDA-MB-468 cells

5.1.2.1. KSRP Knockdown and KSRP Overexpression in MDA-MB-436 and MDA-MB-468 cells

At the mRNA level, *KSRP* was significantly upregulated and downregulated in both MDA-MB-436 and MDA-MB-468 cells. The efficiency of *KSRP* knockdown and *KSRP* overexpression was significantly different between these cells – *KSRP* downregulation was more effective in MDA-MB-468 cells compared to MDA-MB-436 cells while *KSRP* upregulation was more effective in MDA-MB-436 cells. Furthermore, KSRP up- and downregulation was also confirmed at the protein level using western blotting. A change in the molecular weight of KSRP was observed in both cell lines when KSRP was upregulated. This was because the plasmid used for expressing KSRP *in vitro* contained the full-length KSRP protein sequence fused to His and GFP tags, thus increasing the size of the transcript. Quantification of band intensity in samples when KSRP was downregulated confirmed KSRP knockdown in both cell lines but did not indicate major differences of knockdown efficiency. Quantification of band intensities in samples when KSRP was upregulated confirmed KSRP overexpression in both cell lines. KSRP overexpression was more efficient in MDA-MB-436 cells compared to MDA-MB-468 cells. These findings at the protein level substantiate those observed at the mRNA level. The high endogenous

expression of KSRP in MDA-MB-468 cells compared to MDA-MB-436 cells (section 4.1.1.3) could explain the increased efficiency of KSRP knockdown in MDA-MB-468 cells. Similarly, the lower endogenous expression of KSRP in MDA-MB-436 cells compared to MDA-MB-468 cells (section 4.1.1.3) could explain the increased efficiency of KSRP overexpression in MDA-MB-436 cells. This differential control of KSRP expression in MDA-MB-436 and MDA-MB-468 cells could indicate a tissue-specific control of this protein, which could be of great importance in the overall control of the epithelial and mesenchymal cell subtypes.

5.1.2.2. The Effect of *KSRP* Knockdown and *KSRP* Overexpression on *FGFR2 IIIb* and *FGFR2 IIIc* Expression in MDA-MB-436 and MDA-MB-468 Cells

qRT-PCR was used to determine the effect of *KSRP* knockdown and *KSRP* overexpression on *FGFR2* isoform expression. Primers designed to specifically amplify *FGFR2* exon 9 (*FGFR2 IIIb*) or *FGFR2* exon 10 (*FGFR2 IIIc*) was used.

In MDA-MB-436 cells, *KSRP* knockdown caused a significant upregulation of both *FGFR2* isoforms; however, the increase in *FGFR2 IIIc* expression was higher than that of *FGFR2 IIIb*. In contrast, in MDA-MB-468 cells, *KSRP* knockdown resulted in a significant downregulation of both *FGFR2* isoforms with *FGFR2 IIIb* more downregulated than that of *FGFR2 IIIc*.

In MDA-MB-436 cells, *KSRP* overexpression resulted in a significant upregulation of both *FGFR2* isoforms, however, the increase in *FGFR2 IIIb* expression was higher than that of *FGFR2 IIIc*. In MDA-MB-468 cells, *KSRP* overexpression was responsible for the significant downregulation of both *FGFR2* isoforms; however, *FGFR2 IIIc* expression is more downregulated than that of *FGFR2 IIIb*. The significant changes in the expression of *FGFR2 IIIb* and *FGFR2 IIIc* isoforms upon *KSRP* knockdown and overexpression in MDA-MB-436 and MDA-MB-468 cells indicated that the expression of *FGFR2 IIIb* and *FGFR2 IIIc* is regulated by *KSRP* in some way. In MDA-MB-436 and MDA-MB-468 cells, the manipulation of *KSRP* expression exhibited opposite effects on the expression of *FGFR2 IIIb* and *FGFR2 IIIc* (upregulation of both isoforms in MDA-MB-436 cells and downregulation of both isoforms in MDA-MB-468 cells). These changes are

significantly different, providing further evidence for the tissue-specific action of *KSRP* and could indicate that the role of *KSRP* in a particular cell or tissue type is not necessarily predictable.

Certainly the upregulation of *FGFR2 IIIb* and *FGFR2 IIIc* expression when *KSRP* is both overexpressed and downregulated in MDA-MB-436 cells was unexpected. Further the observed downregulation of *FGFR2 IIIb* and *FGFR2 IIIc* isoform expression when *KSRP* is both overexpressed and downregulated in MDA-MB-468 cells was also unexpected. In these cells, *FGFR2 IIIb* expression is significantly more negatively affected when *KSRP* is downregulated compared to when *KSRP* is overexpressed. Conversely, *FGFR2 IIIc* expression is significantly more negatively affected when *KSRP* is overexpressed compared to when *KSRP* is downregulated. The significance of these differences indicates that in MDA-MB-468 cells, the specific role of *KSRP* in *FGFR2* splicing may be to regulate the inclusion ratio of *FGFR2 IIIb* and *FGFR2 IIIc*, and this is dependent on the expression level of this protein. These findings may be relevant *in vivo* particularly in the establishment and maintenance of an epithelial or mesenchymal cell subtype. It would be interesting to determine the effect of these treatments on the overall expression levels of *FGFR2*.

5.1.2.3. The Effect of KSRP Overexpression on the Epithelial and Mesenchymal Phenotype in MDA-MB-436 and MDA-MB-468 Cells

It is known that the ratio of *FGFR2 IIIb* and *FGFR2 IIIc* inclusion is linked to the epithelial and mesenchymal nature of tissues [164]. An increase in the expression of *FGFR2 IIIc* coupled with a decrease in the expression of *FGFR2 IIIb* is linked to epithelial-to-mesenchymal transition (EMT) [216]. Conversely, an increase in the expression of *FGFR2 IIIb* coupled with a decrease in the expression of *FGFR2 IIIc* is linked to mesenchymal-to-epithelial transition (MET) [216].

Since the expression of *FGFR2 IIIb* and *FGFR2 IIIc* are significantly altered in response to alterations in *KSRP* expression, and because changes in the inclusion ratio of these *FGFR2* isoforms control both EMT and MET, the effect of *KSRP* overexpression on the mesenchymal and epithelial phenotype of

MDA-MB-436 and MDA-MB-468 cells, respectively, was investigated. In MDA-MB-436 cells, downregulation and overexpression of *KSRP* expression both resulted in a significant increase in the expression of *FGFR2 IIIb* and *FGFR2 IIIc*. In MDA-MB-468 cells, the downregulation and overexpression of *KSRP* both resulted in a significant decrease in the expression of the *FGFR2* isoforms. Since either *KSRP* down- or upregulation had similar effects on *FGFR2 IIIb* and *FGFR2 IIIc* expression, either of these alterations could theoretically be used to investigate whether the observed changes in the expression of these *FGFR2* isoforms would visually affect the mesenchymal and epithelial phenotype of the selected cells.

KSRP overexpression was achieved by transfecting MDA-MB-436 and MDA-MB-468 cells with the pEGFPC1-6xHis-FLKSRP plasmid, which encodes full-length KSRP tagged to GFP. Visualising GFP in these cells, therefore, permitted the identification of individual cells overexpressing KSRP and consequently allowed for the visualisation of potential changes in the visualisation of the epithelial and mesenchymal markers.

The increase in the expression of *FGFR2 IIIb* and *FGFR2 IIIc* mRNA in MDA-MB-436 cells when KSRP is overexpressed did not result in a change in the phenotype of these cells; this is evidenced by the lack of increase in the visualisation of Cytokeratin 19 or Vimentin. The decrease in the expression of *FGFR2 IIIb* and *FGFR2 IIIc* mRNA in MDA-MB-468 cells when KSRP is overexpressed also did not seem to cause a change in the phenotype of these cells. This was evidenced by the lack of a decrease in the visualisation of Cytokeratin 19. These results suggest that the up- and downregulation of *FGFR2 IIIb* and *FGFR2 IIIc* expression in MDA-MB-436 and MDA-MB-468 cells, respectively, as a consequence of KSRP upregulation does not visually affect the mesenchymal and epithelial phenotypes of these cells.

The changes in the expression of *FGFR2 IIIb* and *FGFR2 IIIc* were dissimilar to those observed when EMT was accomplished; epithelial-to-mesenchymal transition was reported as a consequence of an increase in the expression of *FGFR2 IIIc* combined with a decrease in the expression of *FGFR2 IIIb* [173]. This, therefore, suggests that EMT and MET are accomplished when one *FGFR2* isoform is favoured over the other (IIIc over IIIb

and IIIb over IIIc, respectively), thus, increasing or decreasing the expression of both *FGFR2* isoforms may not result in an alteration of the epithelial or mesenchymal phenotype of these cells.

It is well known that EMT is a tightly regulated process, and involves a large number of proteins. Known transcription factor regulators of EMT (e.g. Snail, TWIST, SIP1 etc.) are regulated by numerous factors (e.g. NF-κB, MAPK, Smad, etc.) and in turn, affect a number of genes (e.g. *E-cadherin*, *Cytokeratin*, *Vimentin*, *Fibronectin* etc.) that ultimately cause EMT [217]. Thus, to efficiently reverse EMT (important to combat cancer progression), major regulators of this process should be targeted, and from the results of this research, we suggest that KSRP does not act as one such regulator. We, therefore, suggest EMT regulators that are high up in the signalling pathway should be targeted for modulation (e.g. decreasing the expression of the protein by siRNA-mediated knockdown), as this should result in the manipulation of a large number of EMT-related proteins, thus efficiently and effectively reversing EMT.

It is possible that a switch in the *FGFR2* isoform inclusion may be a consequence of EMT, rather than the switch in *FGFR2* isoform inclusion a cause of EMT. The possible alteration in *FGFR2* isoform inclusion as a consequence of EMT could explain why the epithelial marker, Cytokeratin 19, and the mesenchymal marker, Vimentin, were unchanged upon changes in *FGFR2 IIIb* and *FGFR2 IIIc* expression. Induction of EMT, e.g. through the expression of TGFβ, and the monitoring of *FGFR2* splicing could have clarified this mechanism. This approach could have provided information about whether targeting *FGFR2* splicing factors altered the EMT phenotype. In addition, the induction of EMT though the expression of TGFβ could have served as a positive control for changes in the visualisation of the EMT markers, Cytokeratin 19 and Vimentin. This approach would however not investigate KSRPs specific role in FGFR2 splicing and EMT.

Another approach to this experiment could have been to transfect MDA-MB-436 and MDA-MB-468 cells with plasmids encoding for either *FGFR2 IIIb* or *FGFR2 IIIc*. The effect on *FGFR2 IIIc* expression when *FGFR2 IIIb* is overexpressed, and vice versa, as well as the impact, if any, on EMT phenotype could have been determined with this experimental approach. However, this

experimental approach would not assist in the investigation of KSRP's impact on *FGFR2* splicing and therefore, its role in EMT.

5.1.3. The Direct Binding of KSRP to *FGFR2* mRNA in MDA-MB-468 Cells

The purpose of this investigation was to determine whether KSRP directly binds to *FGFR2* mRNA. UV-irradiation of MDA-MB-468 cells causes the formation of covalent bonds at protein-RNA interaction sites, thus maintaining the *in vivo* protein-RNA binding pattern. KSRP was immunoprecipitated and any RNA bound to this protein extracted from the precipitate. At this point, this RNA could have been sequenced in order to determine all the mRNA binding partners of the protein of interest. However, the extracted RNA was reverse-transcribed into cDNA, and this cDNA was used in downstream qRT-PCR experiments. Before and after immunoprecipitation in both the control and KSRP samples, an aliquot of the input (In) and flow-through (FT) fractions, respectively, was saved for analysis. Furthermore, the immunoprecipitate (IP) fraction (the protein-RNA complex of interest that was bound to the magnetic beads) was used for analysis. Two antibodies were used for the immunoprecipitation, namely anti-KSRP to immunoprecipitate KSRP (the protein of interest used in the KSRP samples) and anti-IgG (the control protein used in the control samples). The input (In) fraction from the control and KSRP samples both exhibited KSRP protein expression. The flow-through (FT) fraction from the control and KSRP samples both exhibited KSRP protein expression, however, in the KSRP samples, much less KSRP was evident in the FT fraction compared to the In fraction. KSRP present in the In fraction for the KSRP sample would become bound to the anti-KSRP antibody attached to the magnetic beads, thus explaining the decreased prevalence of KSRP in the FT fraction. KSRP protein expression was observed in the KSRP IP fraction and not in the control IP fraction, indicating the successful immunoprecipitation of the protein of interest. U2AF65 protein expression was used as a loading control; this protein was not immunoprecipitated and, therefore, was not present in KSRP IP and control IP fractions. Additional negative controls, such as using KSRP knockout MDA-MB-468 cells, non-cross-linked MDA-MB-468 cells or an antibody that does not bind RNA,

could have been incorporated in this experiment and would have strengthened the validity of the findings.

To determine if KSRP directly binds to *FGFR2* mRNA attention was focussed on the *FGFR2 IIIb* mRNA sequence and the sequences directly surrounding it. This region of *FGFR2* mRNA was selected since this analysis was undertaken in MDA-MB-468 cells with *FGFR2 IIIb* the prevalent isoform in these cells. Six primer pairs, specific to different regions including and surrounding exon 9 (*FGFR2 IIIb*) of *FGFR2* pre-mRNA were designed (Figure 4.23). Primer pairs 1, 2 and 3 were designed to amplify regions of intron 8, primer pair 4 was designed to amplify the intron 8 exon 9 junction, primer pair 5 was designed to amplify exon 9 and primer pair 6 was designed to amplify intron 9. Primer pairs 4, 5 and 6 were used to complete the qRT-PCR analysis because of their ability to effectively amplify the desired sequences at high melting temperatures with minimal non-specific amplification. The RNA extracted from control and KSRP In and IP fractions was used for absolute qRT-PCR analysis and only primer pair 5 (designed to exon 9 of *FGFR2*) was successful in amplifying cDNA from the KSRP IP fraction, thus indicating that KSRP directly binds to this region of *FGFR2* mRNA in MDA-MB-468 cells.

This finding is relevant as it provides further evidence for a role played by KSRP in the regulation of *FGFR2 IIIb* and *FGFR2 IIIc* expression in MDA-MB-468 cells. In addition, this finding has shown that KSRP binds to *FGFR2* mRNA at exon 9, which corresponds to the *FGFR2 IIIb* exon, illustrated in Figure 5.1. The known amplified sequence of exon 9 (*FGFR2 IIIb*), depicted in Figure 5.2, provides an indication of what the exact binding position of KSRP on the *FGFR2 IIIb* exon may be, however, the exact nucleotides to which KSRP binds on FGFR2 mRNA remains to be elucidated.

Recent studies into erythroid development have revealed that KSRP is able to bind an exonic splicing silencer (ESS16) only by associating with hnRNP A1, additionally, this study reported that the loss of KSRP expression did not affect the splicing of the exon in question [218]. As discussed in section 1.4.1.1, the *FGFR2 IIIb* exon contains an ESS, which becomes bound by the RNA-binding protein hnRNP A1 in epithelial cells, and there it functions to suppress the splicing of this exon. Since it is known that *FGFR2 IIIb* contains an ESS and binds

hnRNP A1, it could be possible that KSRP binds to exon 9 (*FGFR2 IIIb*) by associating with hnRNP A1, as in the erythroid study. Nevertheless, KSRP binding to *FGFR2 IIIb* in the absence of hnRNP A1 will first have to be investigated before this can be conclusively stated.

In MDA-MB-468 cells, KSRP binding to *FGFR2 IIIb* might be necessary for the decrease in the expression of this exon. Since no primers were designed to potentially amplify *FGFR2* exon 10 (*FGFR2 IIIc*), KSRP binding to this exon in MDA-MB-468 cells was not determined. In addition, KSRP binding to either *FGFR2 IIIb* or *FGFR2 IIIc* in MDA-MB-436 cells was not determined.

Interestingly, in mesenchymal cells, hnRNP H and F, members of the hnRNP family, bind the ESS located in *FGFR2 IIIc*. This observation could provide initial evidence that KSRP could bind to this exon at the ESS site again by associating with either of these proteins.

As reviewed in section 1.4.1, multiple splicing factors e.g. TIA-1, PTB, hnRNPA1, Fox-2, ESRP1, ESRP2, ASF/SF2, hnRNP H/F and U1 snRNP have been shown to bind *FGFR2* mRNA, and it is also possible that KSRP may bind *FGFR2* mRNA through interactions with one or many of these factors.

5.1.3.1. KSRP, hnRNP A1 and PTB binding sites on *FGFR2*

The KSRP protein contains four KH RNA binding domains, and each of these domains is capable of binding different RNA sequences, thus, several RNA-binding sequences for KSRP have been reported. A number of these KSRP binding sequences (GGG [219], UGCAU [43] GGGU [219] and AGGG [219]), are present in the *FGFR2* exon 9 (*FGFR2 IIIb*) sequence and form a potential 'binding zone' (illustrated in Figure 5.2 and highlighted in yellow). The reported hnRNP A1 binding site, UAGGG [220], is also found in the *FGFR2 IIIb* (exon 9) sequence and overlaps the proposed KSRP 'binding zone' (illustrated in Figure 5.2 and bordered in blue). Interestingly, a binding site for PTB, UCUUCUU [221], can also be found in the *FGFR2* exon 9 (*FGFR2 IIIb*) sequence, and slightly overlaps the proposed KSRP binding zone (illustrated in Figure 5.2 and shown in red letters). This close binding proximity of KSRP, PTB and a member of the hnRNP family of proteins (hnRNP H) on a specific sequence element has been previously reported in c-src N1 exon splicing in neuronal cells [43].

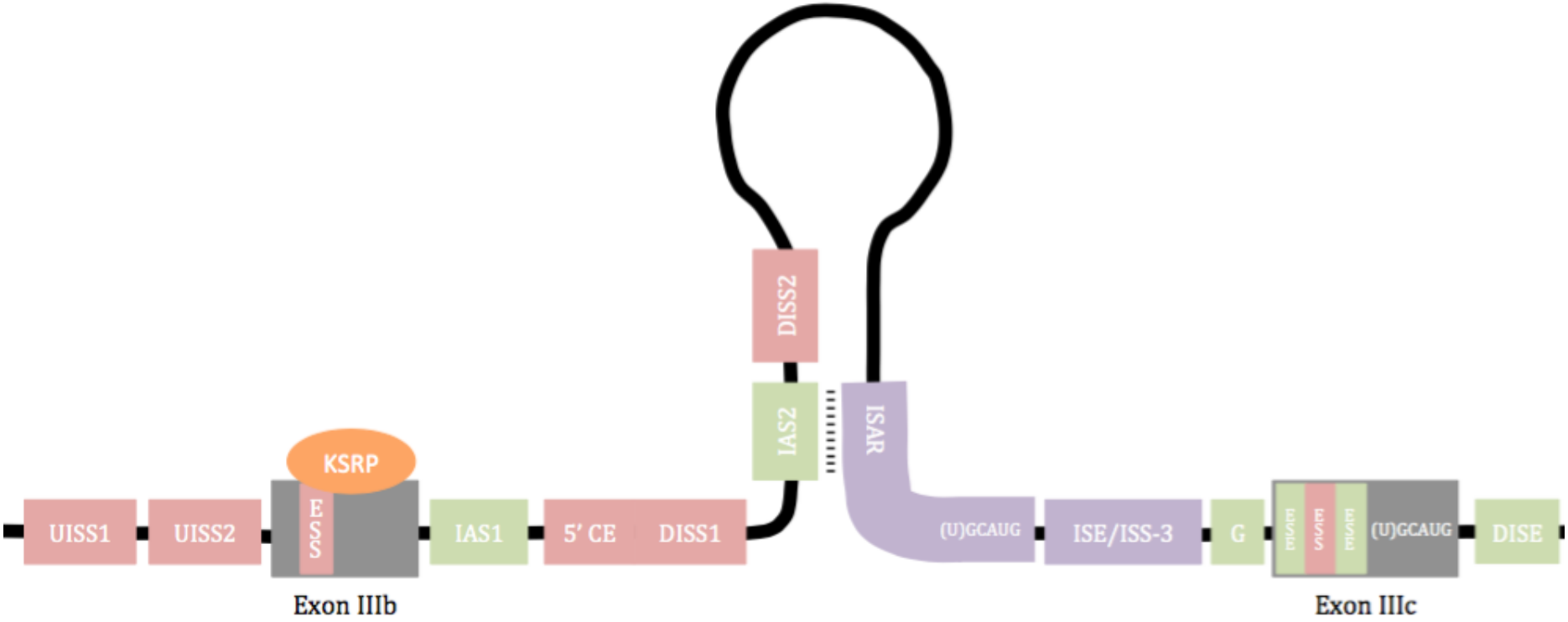

Figure 5.1 – *FGFR2* pre-mRNA illustrating the positions of *cis*-acting elements and indicating the position of KSRP binding in MDA-MB-468 cells. UV-CLIP findings revealed that KSRP directly binds to *FGFR2* pre-mRNA at exon 9 (*FGFR2 IIIb*) in MDA-MB-468 cells.



Figure 5.2 – Known amplified *FGFR2* exon 9 (IIIb) sequence, indicating reported KSRP, hnRNP A1 and PTB binding sites. The reported KSRP binding sites (GGG, UGCAU, GGGU and AGGG) are highlighted in yellow. The reported hnRNP A1 binding site (UAGGG) is bordered in blue. The reported PTB binding site is indicated in red letters.

5.1.3.2. Proposed Mechanism

From the observations thus far, it is proposed that KSRP functions in a tissue-specific manner to bring about the observed changes in *FGFR2 IIIb* and *FGFR2 IIIc* expression. In epithelial cells, KSRPs binding to *FGFR2 IIIb* at the ESS site through association with hnRNP A1 causes a decrease in the expression of both *FGFR2 IIIb* and *FGFR2 IIIc* through this protein-RNA binding and protein-protein interaction. In mesenchymal cells, KSRPs binding to *FGFR2 IIIc* at the ESS site through association with hnRNP H/F causes an increase in the expression of both *FGFR2 IIIb* and *FGFR2 IIIc* through this protein-RNA binding and protein-protein interaction. In addition, we propose that the amount of KSRP binding to *FGFR2 IIIb* in epithelial cells and *FGFR2 IIIc* in mesenchymal cells determines the efficiency of down- or upregulation of these exons, respectively. In epithelial cells, a low amount of KSRP binding to exon 9 (*FGFR2 IIIb*) could be the cause of a more efficient downregulation of *FGFR2 IIIb* and a less efficient downregulation of *FGFR2 IIIc*; conversely, a high amount of KSRP binding to *FGFR2 IIIb* could be the cause of a more efficient downregulation of *FGFR2 IIIc* and a less efficient downregulation of *FGFR2 IIIb*. In mesenchymal cells, a low amount of KSRP binding to *FGFR2 IIIc* could be the cause of a more efficient upregulation of *FGFR2 IIIc* and a less efficient upregulation of *FGFR2 IIIb*; conversely, a high amount of KSRP binding to *FGFR2 IIIc* could be the cause of a more efficient upregulation of *FGFR2 IIIb* and a less efficient upregulation of *FGFR2 IIIc*. We, therefore, propose a threshold mechanism of action for KSRP in both epithelial and mesenchymal cells; the increased binding of KSRP to *FGFR2 IIIb* in epithelial cells or *FGFR2 IIIc* in mesenchymal cells causes an increased exertion of its downregulatory and upregulatory effect, respectively, on the exon it is not bound to. In the same way, we propose that the decreased binding of KSRP to *FGFR2 IIIb* in epithelial cells or *FGFR2 IIIc* in mesenchymal cells causes an increased exertion of its downregulatory and upregulatory effect, respectively, on the exon to which it is bound. This proposed mechanism is illustrated in Figure 5.3.

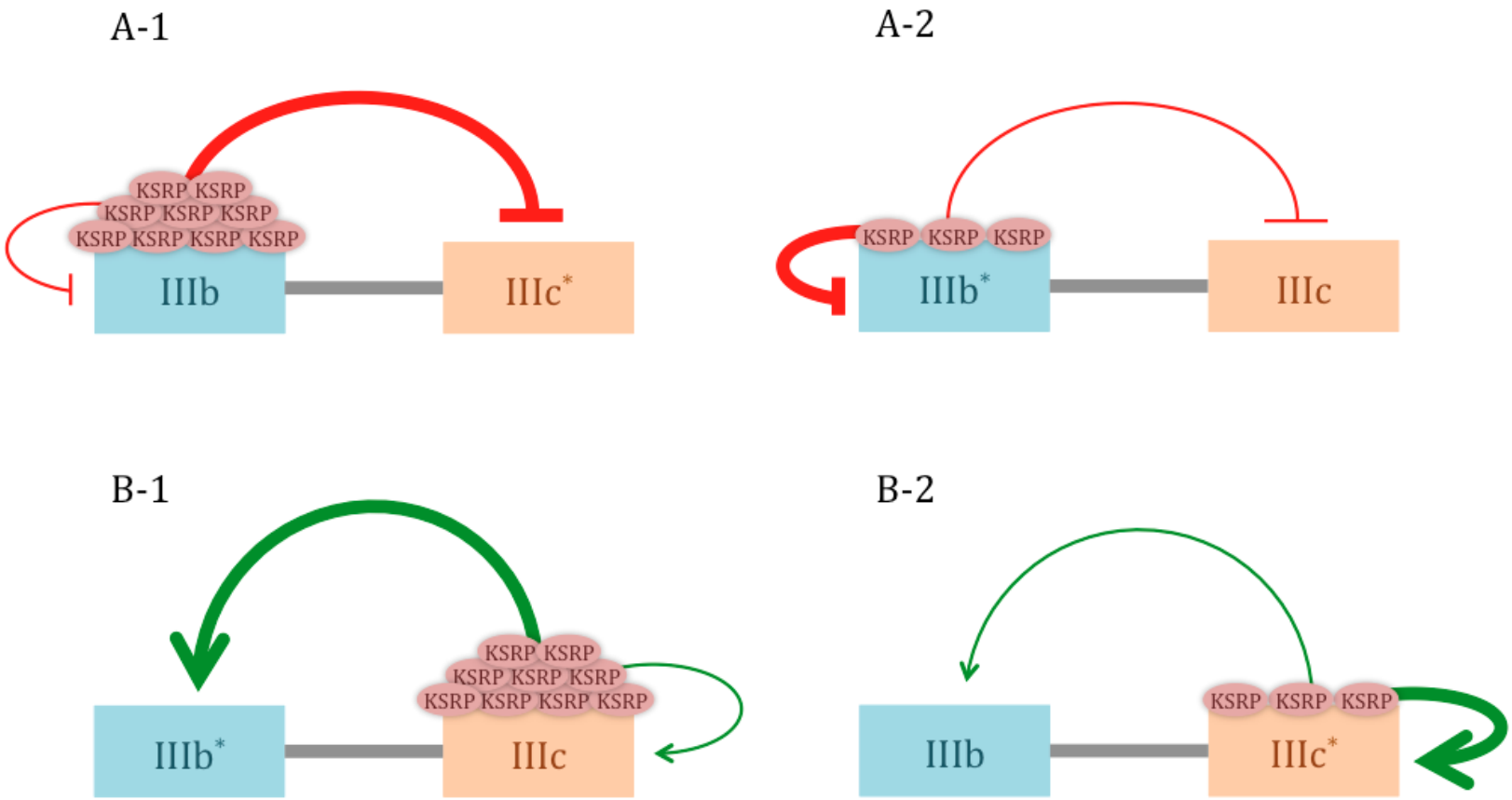

Figure 5.3 – The proposed mechanism of KSRP action on *FGFR2 IIIb* and *FGFR2 IIIc* in epithelial and mesenchymal cells. A-1) in epithelial cells, abundant KSRP binding to *FGFR2 IIIb* causes a more efficient repression of *FGFR2 IIIc* expression compared to *FGFR2 IIIb* expression. A-2) in epithelial cells, scarce KSRP binding to *FGFR2 IIIb* causes a more efficient repression of *FGFR2 IIIb* expression compared to *FGFR2 IIIc* expression. B-1) in mesenchymal cells, abundant KSRP binding to *FGFR2 IIIc* causes a more efficient enhancement of *FGFR2 IIIb* expression compared to *FGFR2 IIIc* expression. B-2) in mesenchymal cells, scarce KSRP binding to *FGFR2 IIIc* causes a more efficient enhancement of *FGFR2 IIIc* expression compared to *FGFR2 IIIb* expression. * Denotes the exon that becomes more efficiently upregulated (in mesenchymal cells - B) or downregulated (in epithelial cells - A) when KSRP is either upregulated (A-1 and B-1) or downregulated (A-2 and B2).

5.1.4. Hypothesis-Based Approach Summary

The first aim of this study was to investigate the role of KSRP in the *FGFR2* splicing mechanism in the context of triple-negative breast cancer progression using cell line models. We have shown that KSRP affects the expression of *FGFR2 IIIb* and *FGFR2 IIIc* in both epithelial and mesenchymal cells, but in opposite ways (down- and upregulation of the isoforms in epithelial and mesenchymal cells, respectively). These findings indicate that the role of KSRP in *FGFR2* splicing involves the tissue-specific control of the expression of *FGFR2 IIIb* and *FGFR2 IIIc*. Additionally, these findings indicate that the level of KSRP expression affects the levels *FGFR2 IIIb* and *FGFR2 IIIc* expression in epithelial and mesenchymal cells. A clear switch in isoform splicing (from either *FGFR2 IIIb* to *FGFR2 IIIc*, or vice versa), in response to manipulation of *KSRP* expression, was not observed in either cell line, indicating that this protein does not control the mutually exclusive splicing nature of this gene. Furthermore, we have discovered that KSRP binds directly to *FGFR2* mRNA (on exon 9 – *FGFR2 IIIb*) in epithelial cells. Binding of KSRP to the mRNA of this gene has not been shown previously and provides strong evidence for a role played by this protein in the control of *FGFR2 IIIb* and *FGFR2 IIIc* expression. Finally, we show that the overexpression of KSRP in MDA-MB-436 and MDA-MB-468 cells did not cause an alteration in the mesenchymal and epithelial phenotype of these cells. These findings indicate that KSRP may not be the controlling factor in the EMT progression of triple-negative breast cancer but may rather play a role in maintaining cell subtype.

5.2. Discovery-Based Approach

The hypothesis-based section of this study revealed that the expression of *FGFR2 IIIb* and *FGFR2 IIIc* were significantly affected in MDA-MB-468 cells in response to alterations in the level of KSRP expression. Differences were also observed in MDA-MB-436 cells, but were not as significant. Analysis of the role played by KSRP was limited to MDA-MB-468 cells.

We aimed to analyse the transcriptome of MDA-MB-468 cells in response to KSRP knockdown by using microarray technology to potentially clarify the cellular and molecular mechanisms that are associated with this protein using the Affymetrix GeneChip® Human Transcriptome Array 2.0. In addition to regulated gene analysis, this array provided pathway, transcription factor, splicing factor, regulated exon and regulated splicing pattern analysis, and thus, this array could be used to suggest if gene regulation was related to exon and splicing pattern regulation.

5.2.1. Genome-Wide Gene Expression Changes in Response to KSRP Knockdown in MDA-MB-468 cells

Hierarchical clustering by distance to the mean exhibited clear differences when the RNA from MDA-MB-468 *KSRP* knockdown (siKSRP) and MDA-MB-468 transfection control (siScr) cells was compared. Analysis of the results of the Affymetrix GeneChip® Human Transcriptome Array 2.0 identified genes, transcription factors, splicing factors, exons and splicing patterns which became regulated in response to *KSRP* knockdown. As expected, *KSRP* was the most significantly downregulated at the gene level, indicating an extremely effective knockdown. Interestingly, *FGFR2* gene expression was not significantly altered when *KSRP* was downregulated. KEGG pathway analysis revealed that three of the regulated genes – namely *CCND3*, *PPP2R1B* and *DKK1* – are involved in the Wnt pathway, and this was the only pathway that was regulated in response to KSRP knockdown.

During embryonic development, the Wnt pathway is critically involved in the regulation of cell fate determination, cell polarity, cell migration, neural patterning and organogenesis [78]. Aberrant activation of the Wnt pathway in healthy cells plays a causative role in several cancers [84]. Furthermore,

signalling of this pathway is associated with metastasis in TBNC [222] and is suggested to be potential therapeutic target for the treatment of this disease [223]. The inhibition Wnt signalling impeded cell proliferation as well as cell migration and induced apoptosis of TNBC cells [180]. The Wnt pathway has been reviewed in section 1.3.3.1.

According to the results from the Affymetrix GeneChip® Human Transcriptome Array 2.0, when *KSRP* is downregulated in MDA-MB-468 cells, *CCND3*, *PPP2R1B* and *DKK1* became significantly upregulated, and this finding was validated using qRT-PCR. Investigations into the signalling locations of these proteins revealed that they are all functional in the canonical Wnt pathway and not in the planar cell polarity pathway or the Wnt/Ca^{2+} pathway. This observation could indicate a specific regulatory role for KSRP in the canonical Wnt pathway.

The Cyclin D3 (*CCND3*) is a gene encoding a protein belonging to the highly conserved cyclin family [224]. This family of proteins are heavily involved in the progression of the cell through the cell cycle and function as regulators for cyclin-dependent kinases (CDKs) [224]. CCND3 binds to and forms a complex with CDK4 or CDK6, functioning as their regulatory subunit [224]. The activity of the CCND3-CDK4 or CCND3-CDK6 complex is required for G1/S transition in the cell [224], a checkpoint that must be overcome for the cells to undergo DNA replication. In addition, CCND3 interacts with and is involved in the phosphorylation of the tumour suppressor protein Rb, which promotes cell cycle progression [225]. The roles of CCND3 in the cell and its inversely proportional relationship with *KSRP* suggest that *KSRP* could function to restrict cell cycle progression through its regulation of *CCND3* expression. This could indicate that *KSRP* functions tumour suppressively.

Dickkopf1 (DKK1) is one of the five members of the Dickkopf (DKK) family of proteins that function as antagonists of Wnt signalling by binding to and sequestering the Wnt co-receptors LRP5/6, thereby inhibiting the signalling of this pathway [226, 227]. The expression levels of *DKK1* are elevated in a number of cancers and many researchers associate *DKK1* expression with the progression of cancer and poor prognosis [228]. Overexpression of DKK1 is observed in multiple myelomas [229], Wilms' tumours [230] and

hormone-resistant breast cancer [231]. Conversely, DKK1 also negatively affects tumour growth [232], and its overexpression suppresses tumour growth [233-237]. Clinical studies researching melanoma [238], breast cancer [239] and colon cancer [240] have reported a loss of DKK1 expression in these tissues. These findings suggest that DKK1 may have tumour suppressive functions and this may be as a consequence of the DKK1-mediated downregulation of Wnt signalling [228]. In addition, reports have suggested an apoptosis inducing role for DKK1 [241-244]. Interestingly, in the TNBC cell line, MDA-MB-231, the ectopic expression of DKK1 not only caused an increased apoptosis sensitivity in these cells but also caused an alteration in the phenotype of these cells [239]. The Wnt signalling pathway plays a vital role the regulation of epithelial plasticity and EMT by its regulation of mesenchymal phenotype promoting transcription factors e.g. Snail [245, 246]. Since DKK1 is a known regulator of the Wnt signalling pathway, it could, therefore, be an additional regulator of EMT. Exogenous expression of DKK1 in the malignant mesenchymal-like breast cancer cell line, SUM1315, caused a significant reduction in the expression of *SLUG* and *TWIST*, EMT promoting factors [235]. In addition, DKK1 downregulation in non-tumorigenic epithelial breast cancer cells, MCF10A, increased the invasive capacity of these cells and caused a decrease in the expression of E-cadherin (important for cell adhesion) [233]. These findings indicate that DKK1 expression could prevent epithelial-to-mesenchymal transition. We have revealed that upon *KSRP* knockdown, *DKK1* becomes overexpressed, and this overexpression is linked to tumour growth suppression, increased apoptosis and the prevention of EMT, we suggest that *KSRP* could promote tumour growth, desensitise cells to apoptosis and stimulate EMT, suggesting a tumour promotive role for KSRP.

Protein phosphatase 2, regulatory subunit A, Beta (*PPP2R1B*) is a gene encoding for the regulatory subunit of protein phosphatase 2, a protein that catalyses the dephosphorylation of specific target proteins [247]. Mutations in *PPP2R1B* are present in breast and colorectal cancers [248], in addition, the loss of heterozygosity of *PPP2R1B* is linked to the formation of certain subtypes of ovarian cancer [249]. The inverse relationship of the expression of *KSRP* and

PPP2R1B and the discussed roles of the latter protein in the cell could suggest that *KSRP* negatively affects cancer progression.

Research into the function of CCND3, DKK1 and PPP2R1B and analysis into the observed regulatory role of KSRP on the expression of these proteins does not indicate a clear tumour suppressive or tumour promotive role for KSRP. We, therefore, suggest that this protein exerts its specific function in the cell regardless of the effect on tumour formation and thus, should not be broadly categorised as either a tumour promoter or a tumour suppressor.

5.2.2. KSRP Interaction and KSRP Co-Localisation With Selected Affymetrix GeneChip® Human Transcriptome Array 2.0 Targets

Protein-protein interactions can either be direct (two proteins physically associate with each other) or indirect (two proteins form part of a multi-protein complex, regulate each other or share a metabolite). Investigation into the nature of these interactions is important as it could provide information concerning the regulation of various cellular pathways, and thus, cellular processes [250].

KSRPs interaction with RNA is well known, however, KSRP also interacts with proteins, e.g. Poly(A)-Specific Ribonuclease (PARN), ARE-directed mRNA turnover [199]. For this reason, direct protein-protein interactions between KSRP and CCND3, KSRP and DKK1 as well as KSRP and PPP2R1B were predicted using STRING.

The STRING database contains a comprehensive collection of known and predicted direct and indirect protein-protein interactions from 2031 different organisms. This information is amassed from four sources, namely genomic context, high-throughput experiments, conserved co-expression and prior knowledge. In the STRING database, a confidence score for each predicted protein-protein interaction is calculated and in the resultant image, the value of the confidence score, and thus the likelihood of the protein-protein interaction, is directly proportional to the thickness of the linkage line between the two proteins. The array data indicated that the removal of KSRP positively affected the expression of *CCND3, DKK1 and PPP2R1B*. The reason for a protein interacting with the protein product of a gene upregulated by its downregulation is unknown but may suggest a regulatory negative-feedback loop.

No direct interaction of KSRP and CCND3, KSRP and DKK1 or KSRP and PPP2R1B was predicted using STRING, however, the protein networks predicted in the same database suggest an indirect associations of the aforementioned proteins. These predictions suggest that the increase in the expression of *CCND3*, *DKK1* and *PPP2R1B* in response to *KSRP* downregulation is not dependent on direct binding protein-protein interactions between these proteins. These predictions further suggest that KSRP and CCND3, KSRP and DKK1 or KSRP and PPP2R1B could share a metabolite or be part of a multi-protein complex.

Bearing these predictions in mind, co-localisation studies were completed to empirically determine whether KSRP directly interacts with CCND3, DKK1 and PPP2R1B. Co-localisation in the context of fluorescence microscopy refers to the spatial overlap of two or more fluorescent labels. When these fluorescent labels are linked to molecules of interest in the cell, co-localisation provides evidence for a direct biological interaction between these proteins; thus, co-localisation of KSRP and CCND3, KSRP and DKK1 or KSRP and PPP2R1B was assessed. Visually, GFP-KSRP appeared to co-localise with KSRP (as expected) as well as with DKK1, but not with CCND3 or PPP2R1B. Untransfected KSRP cells do not appear in Figure 4.33 B as they do in Figure 4.33 A due to the strong GFP-KSRP signal.

2D intensity histograms are scatter plots where the intensity of the pixels from the first channel (e.g. green in the case of GFP and GFP-KSRP) is plotted on the x-axis and the intensity of the pixels from the second channel (e.g. red in the case of KSRP, CCND3, DKK1 and PPP2R1B) is plotted on the y-axis. Pixels with equal intensities on both channels (positive co-localisation) present on the 2D intensity histogram along a 45° angle passing through the origin [251], thus appearing as a diagonal. Pearson's R-values are an additional measure of co-localisation; values of -1, 0 and 1 are indicative of negative, none and positive correlation, respectively [252]. The 2D intensity histograms positively confirmed co-localisation of GFP-KSRP and KSRP, as well as GFP-KSRP and DKK1. Moreover, the Pearson's R-values obtained when analysing the potential co-localisation events between GFP-KSRP and KSRP as well as GFP-KSRP and DKK1 strongly indicate perfect correlation, and, therefore, co-localisation of these proteins. The visual image, 2D intensity histogram and Pearson's R-value findings are corroboratory and provide strong evidence that KSRP and DKK1

interact with each other at the protein level. These results indicate that the KSRP-DKK1 protein relationship is direct and further suggests that the upregulation of *DKK1* upon *KSRP* knockdown could be directly mediated by KSRP binding to DKK1. The suggested direct interaction between KSRP and DKK1 is unexpected due to the predominant cellular localizations of these proteins. KSRP is mainly nuclear, but is also located in the cytoplasm and can be exported extracellularly while DKK1 is mainly extracellular but has also been found in the nucleus, albeit to a lesser extent. These proteins could therefore share a cellular or extracellular location for a short period of time. The evidence of a possible direct interaction between KSRP and DKK1 is contradictory to the STRING prediction and may suggest a previously unpredicted interaction pattern of these proteins.

The microarray findings and validations have shown that DKK1 expression is upregulated when KSRP is downregulated in MDA-MB-468 cells. We would therefore expect that when KSRP is upregulated in these cells, DKK1 expression would decrease. However, comparison of GFP-KSRP and DKK1 co-localisation image (Figure 4.35 B) to the GFP and DKK1 co-localisation image (Figure 4.35 A) indicated that when KSRP was overexpressed, so was DKK1. The reasons for this are unknown and require further investigation e.g. the determination of mRNA levels of DKK1 when KSRP is overexpressed using qRT-PCR and the determination of protein expression levels of DKK1 when KSRP is overexpressed using western blotting.

Positive correlation between GFP-KSRP and CCND3 as well as GFP-KSRP and PPP2R1B was not observed, which could indicate an indirect relationship between KSRP-CCND3 and KSRP-PPP2R1B. Additionally, the lack of co-localisation of these proteins may suggest that the observed upregulation of CCND3 and PPP2R1B upon KSRP knockdown is not directly mediated by the direct binding of KSRP to these proteins. The lack of evidence for a direct interaction between KSRP and CCND3 and KSRP and PPP2R1B supports the STRING prediction, further suggesting that their interaction is indirect and may be as a consequence of the proteins sharing a metabolite or being part of a multi-protein complex. In addition, numerous reports have suggested that CCND3 and PPP2R1B are regulated by microRNAs [253-257]. Since KSRP

functions in the regulation of microRNAs [191, 202], the regulation of *CCND3* and *PPP2R1B* by *KSRP* could be mediated by KSRP's regulation of specific microRNAs.

5.2.3. Discovery-Based Approach Summary

The second aim of this study was to discover the genome-wide consequences of KSRP knockdown in epithelial cells. Using the Affymetrix GeneChip® Human Transcriptome Array 2.0, numerous significant changes in gene expression in response to *KSRP* knockdown were identified. In particular, three genes involved in the Wnt pathway – namely *CCND3*, *DKK1* and *PPP2R1B* – were upregulated in response to *KSRP* downregulation, suggesting a regulatory role of *KSRP* in this pathway. In addition, KSRP co-localises with DKK1, suggesting that a direct interaction of these proteins exists and that KSRP could antagonise Wnt signalling. This link between *KSRP*, *DKK1* and the Wnt pathway was previously unknown.

Chapter 6

6. FINDINGS, CONCLUSIONS & FUTURE WORK

6.1. Findings and Conclusions

MDA-MB-436 and MDA-MB-468 cells are phenotypically mesenchymal and epithelial, respectively. *FGFR2 IIIc* is the preferentially included isoform in MDA-MB-436 cells and MDA-MB-468 cells preferentially include *FGFR2 IIIb*. *FGFR2 IIIb* and *FGFR2 IIIc* expression can be altered in response to the downregulation of the splicing regulators, ESRP1 and ESRP2, in MDA-MB-436 and MDA-MB-468 cells. The preferential inclusion of *FGFR2 IIIc* in MDA-MB-436 cells corresponds to their mesenchymal nature and the preferential inclusion of *FGFR2 IIIb* in MDA-MB-468 cells corresponds to their epithelial nature. It is possible to alter the expression of *FGFR2 IIIb* and *FGFR2 IIIc* in MDA-MB-436 and MDA-MB-468 cells.

MDA-MB-468 cells exhibit an increased endogenous KSRP expression compared to MDA-MB-436 cells. KSRP knockdown is more efficient in MDA-MB-468 cells compared to MDA-MB-436 cells, and KSRP overexpression is more efficient in MDA-MB-436 cells compared to MDA-MB-468 cells indicating that the expression of KSRP is controlled in a cell-specific manner. The efficiency of up- or downregulation of KSRP expression is dependent on the endogenous expression level of this protein in either mesenchymal or epithelial tissues.

Manipulation of *KSRP* expression (either up- or downregulation) in MDA-MB-436 cells causes a significant increase in *FGFR2 IIIb* and *FGFR2 IIIc* expression. Manipulation of *KSRP* expression (either up- or downregulation) in MDA-MB-468 cells causes significant decreases in *FGFR2 IIIb* and *FGFR2 IIIc* expression. In MDA-MB-468 cells, *FGFR2 IIIb* expression is more reduced when *KSRP* is downregulated compared to when *KSRP* is overexpressed and *FGFR2 IIIc* expression is more reduced when *KSRP* is overexpressed compared to when *KSRP* is downregulated, and these differences are significant. KSRP directly binds to *FGFR2* mRNA at exon 9 (*FGFR2 IIIb*) in MDA-MB-468 (epithelial) cells and could possibly bind to *FGFR2* exon 10 (*FGFR2 IIIc*) in MDA-MB-436

(mesenchymal) cells. The binding of KSRP to *FGFR2 IIIb* in epithelial cells could cause the downregulation of *FGFR2 IIIb* and *FGFR2 IIIc*. The proposed binding of KSRP to *FGFR2 IIIc* in mesenchymal cells could cause the upregulation of *FGFR2 IIIb* and *FGFR2 IIIc*. In epithelial and mesenchymal tissue types, KSRP's abundant presence and binding could cause the increased exertion of its effect (downregulation of *FGFR2* isoforms in epithelial cells and upregulation of *FGFR2* isoforms in mesenchymal cells) on the exon it is not bound to (*FGFR2 IIIc* in epithelial cells and *FGFR2 IIIb* in mesenchymal cells). In epithelial and mesenchymal tissue types, KSRP's limited presence and binding could cause an increased exertion of its effect (downregulation of *FGFR2* isoforms in epithelial cells and upregulation of *FGFR2* isoforms in mesenchymal cells) on the exon it is bound to (*FGFR2 IIIb* in epithelial cells and *FGFR2 IIIc* in mesenchymal cells).

These observed alterations in *FGFR2 IIIb* and *FGFR2 IIIc* expression in response to *KSRP* overexpression in MDA-MB-436 and MDA-MB-468 cells does not alter the mesenchymal and epithelial nature of these cells, respectively. While *KSRP* alters *FGFR2 IIIb* and *FGFR2 IIIc* expression in MDA-MB-436 and MDA-MB-468 cells, these changes do not translate to changes in the mesenchymal and epithelial phenotypes of these cells, thus suggesting that KSRP does not act as a master regulator of EMT or MET.

The expression of *CCND3*, *DKK1* and *PPP2R1B* (three proteins involved in the Wnt signalling pathway) is upregulated upon *KSRP* downregulation. KSRP and DKK1 co-localise, however, KSRP and CCND3, as well as KSRP and PPP2R1B, do not co-localise. KSRP could be involved in the regulation of the canonical Wnt pathway through its regulation of *CCND3*, *DKK1* and *PPP2R1B*. Additionally, KSRP and DKK1 interact directly, and therefore, KSRP could antagonise Wnt signalling.

6.2. Future Work

To further this research, the following additional experiments are proposed:

Conclusively determine if KSRP binds to *FGFR2 IIIc* in MDA-MB-468 cells and if KSRP binds to *FGFR2 IIIb* and *FGFR2 IIIc* in MDA-MB-436 cells using UV-CLIP experiments as successfully completed within this thesis. These results would provide a more thorough picture of KSRP's binding patterns in epithelial

and mesenchymal tissue types. Additionally, these results could either corroborate or refute the proposed mechanism of action.

Use an inducible protein expression system, e.g. GeneSwitch™ (Thermo Scientific™) to control KSRP expression and further investigate the dose dependent effect of KSRP expression on the expression *FGFR2 IIIb* and *FGFR2 IIIc*. KSRP expression will be dose-dependently induced and the expression of *FGFR2 IIIb* and *FGFR2 IIIc* investigated using qRT-PCR at various KSRP concentrations.

Create a KSRP knock out cell line, which could be beneficial in the investigation of the *FGFR2* splicing mechanism in the complete absence of KSRP binding. To accomplish this, shRNA directed against KSRP will be stably transfected into MDA-MB-436 and MDA-MB-468 cells and UV-CLIP of KSRP and FGFR2 mRNA will be completed.

Utilise qRT-PCR to determine if the modulation of *KSRP* expression alters the expression of *Cytokeratin 19* and *Vimentin* at the mRNA level and determine whether the expression of other markers of EMT become altered. This will be accomplished using RNA extracted from KSRP downregulated MDA-MB-436 and MDA-MB-468 cells for qRT-PCR.

Determine the effect of *KSRP* overexpression on the expression of *DKK1* and use co-immunoprecipitation experiments to further investigate the direct interaction of KSRP with DKK1. To accomplish this, MDA-MB-436 and MDA-MB-468 cell lysates will be passed through a column containing a bound anti-KSRP specific antibody. Once the column has been washed, the bound antibody-protein complexes will be eluted and the elution subjected to western blot analysis. The confirmed presence of DKK1 in the western blot would provide evidence for a direct interaction of KSRP and DKK1. Additionally, whether KSRP binds to *DKK1* mRNA could be investigated using UV-CLIP experiments.

In addition, monitoring cell growth in response to *KSRP* mediated *DKK1* overexpression and downregulation could provide insight into the role of *KSRP* in Wnt signalling. This could be accomplished by either using cell viability assays at a certain time point after KSRP overexpression or through the use of the XCELLigence cell monitoring system directly after the cells have been transfected with the KSRP expressing plasmid.

Chapter 7

7. REFERENCES

1. Crick, F., *Central dogma of molecular biology.* Nature, 1970. **227**(5258): p. 561-3.
2. Alberts, B., Johnson, A., Lewis, J., Raff, M., Roberts, K., Walter., *Molecular Biology of the Cell*. 4th Edition ed. 2002, New York: Garland Science.
3. Hanahan, D. and R.A. Weinberg, *Hallmarks of cancer: the next generation.* Cell, 2011. **144**(5): p. 646-74.
4. Lewis, J.D. and E. Izaurralde, *The role of the cap structure in RNA processing and nuclear export.* European Journal of Biochemistry, 1997. **247**(2): p. 461-9.
5. Shatkin, A.J., *Capping of eucaryotic mRNAs.* Cell, 1976. **9**(4 PT 2): p. 645-53.
6. Konarska, M.M., R.A. Padgett, and P.A. Sharp, *Recognition of cap structure in splicing in vitro of mRNA precursors.* Cell, 1984. **38**(3): p. 731-6.
7. Millevoi, S. and S. Vagner, *Molecular mechanisms of eukaryotic pre-mRNA 3′ end processing regulation.* Nucleic acids research, 2010. **38**(9): p. 2757-74.
8. Balbo, P.B. and A. Bohm, *Mechanism of poly(A) polymerase: structure of the enzyme-MgATP-RNA ternary complex and kinetic analysis.* Structure, 2007. **15**(9): p. 1117-31.
9. Wahle, E., *Poly(A) tail length control is caused by termination of processive synthesis.* The Journal of biological chemistry, 1995. **270**(6): p. 2800-8.
10. Matera, A.G. and Z. Wang, *A day in the life of the spliceosome.* Nature reviews. Molecular cell biology, 2014. **15**(2): p. 108-21.
11. Aebi, M., H. Hornig, and C. Weissmann, *5′ cleavage site in eukaryotic pre-mRNA splicing is determined by the overall 5′ splice region, not by the conserved 5′ GU.* Cell, 1987. **50**(2): p. 237-46.
12. Cieply, B. and R.P. Carstens, *Functional roles of alternative splicing factors in human disease.* Wiley interdisciplinary reviews. RNA, 2015. **6**(3): p. 311-26.
13. Pan, K., et al., *Coupling and coordination in gene expression processes with pre-mRNA splicing.* International Journal of Molecular Sciences, 2015. **16**(3): p. 5682-96.
14. Baralle, D. and M. Baralle, *Splicing in action: assessing disease causing sequence changes.* Journal of medical genetics, 2005. **42**(10): p. 737-48.
15. Will, C.L. and R. Luhrmann, *Spliceosome structure and function.* Cold Spring Harbor perspectives in biology, 2011. **3**(7).
16. Jurica, M.S. and M.J. Moore, *Pre-mRNA splicing: awash in a sea of proteins.* Molecular cell, 2003. **12**(1): p. 5-14.
17. Staknis, D. and R. Reed, *SR proteins promote the first specific recognition of Pre-mRNA and are present together with the U1 small nuclear ribonucleoprotein particle in a general splicing enhancer complex.* Molecular and cellular biology, 1994. **14**(11): p. 7670-82.

18. Cho, S., et al., *Interaction between the RNA binding domains of Ser-Arg splicing factor 1 and U1-70K snRNP protein determines early spliceosome assembly.* Proceedings of the National Academy of Sciences of the United States of America, 2011. **108**(20): p. 8233-8.
19. Pabis, M., et al., *The nuclear cap-binding complex interacts with the U4/U6.U5 tri-snRNP and promotes spliceosome assembly in mammalian cells.* RNA, 2013. **19**(8): p. 1054-63.
20. Sun, J.S. and J.L. Manley, *A novel U2-U6 snRNA structure is necessary for mammalian mRNA splicing.* Genes & development, 1995. **9**(7): p. 843-54.
21. Yang, F., et al., *Splicing proofreading at 5′ splice sites by ATPase Prp28p.* Nucleic acids research, 2013. **41**(8): p. 4660-70.
22. Kohler, A. and E. Hurt, *Exporting RNA from the nucleus to the cytoplasm.* Nature reviews. Molecular cell biology, 2007. **8**(10): p. 761-73.
23. Cole, C.N. and J.J. Scarcelli, *Transport of messenger RNA from the nucleus to the cytoplasm.* Current opinion in cell biology, 2006. **18**(3): p. 299-306.
24. Kelemen, O., et al., *Function of alternative splicing.* Gene, 2013. **514**(1): p. 1-30.
25. Rajan, P., et al., *Alternative splicing and biological heterogeneity in prostate cancer.* Nature reviews. Urology, 2009. **6**(8): p. 454-60.
26. Matlin, A.J., F. Clark, and C.W. Smith, *Understanding alternative splicing: towards a cellular code.* Nature reviews. Molecular cell biology, 2005. **6**(5): p. 386-98.
27. Caceres, J.F. and A.R. Kornblihtt, *Alternative splicing: multiple control mechanisms and involvement in human disease.* Trends in genetics : TIG, 2002. **18**(4): p. 186-93.
28. House, A.E. and K.W. Lynch, *Regulation of alternative splicing: more than just the ABCs.* The Journal of biological chemistry, 2008. **283**(3): p. 1217-21.
29. Hertel, K.J., *Combinatorial control of exon recognition.* The Journal of biological chemistry, 2008. **283**(3): p. 1211-5.
30. Buratti, E., et al., *RNA folding affects the recruitment of SR proteins by mouse and human polypurinic enhancer elements in the fibronectin EDA exon.* Molecular and cellular biology, 2004. **24**(3): p. 1387-400.
31. Singh, N.N., R.N. Singh, and E.J. Androphy, *Modulating role of RNA structure in alternative splicing of a critical exon in the spinal muscular atrophy genes.* Nucleic acids research, 2007. **35**(2): p. 371-89.
32. Graveley, B.R., *Mutually exclusive splicing of the insect Dscam pre-mRNA directed by competing intronic RNA secondary structures.* Cell, 2005. **123**(1): p. 65-73.
33. Black, D.L., *Mechanisms of alternative pre-messenger RNA splicing.* Annual review of biochemistry, 2003. **72**: p. 291-336.
34. Zahler, A.M., et al., *SC35 and heterogeneous nuclear ribonucleoprotein A/B proteins bind to a juxtaposed exonic splicing enhancer/exonic splicing silencer element to regulate HIV-1 tat exon 2 splicing.* The Journal of biological chemistry, 2004. **279**(11): p. 10077-84.
35. Hastings, M.L., C.M. Wilson, and S.H. Munroe, *A purine-rich intronic element enhances alternative splicing of thyroid hormone receptor mRNA.* RNA, 2001. **7**(6): p. 859-74.

36. Gallego, M.E., et al., *The SR splicing factors ASF/SF2 and SC35 have antagonistic effects on intronic enhancer-dependent splicing of the beta-tropomyosin alternative exon 6A.* The EMBO journal, 1997. **16**(7): p. 1772-84.
37. Forch, P., et al., *The apoptosis-promoting factor TIA-1 is a regulator of alternative pre-mRNA splicing.* Molecular cell, 2000. **6**(5): p. 1089-98.
38. Del Gatto-Konczak, F., et al., *The RNA-binding protein TIA-1 is a novel mammalian splicing regulator acting through intron sequences adjacent to a 5' splice site.* Molecular and cellular biology, 2000. **20**(17): p. 6287-99.
39. Huh, G.S. and R.O. Hynes, *Regulation of alternative pre-mRNA splicing by a novel repeated hexanucleotide element.* Genes & development, 1994. **8**(13): p. 1561-74.
40. Modafferi, E.F. and D.L. Black, *A complex intronic splicing enhancer from the c-src pre-mRNA activates inclusion of a heterologous exon.* Molecular and cellular biology, 1997. **17**(11): p. 6537-45.
41. Lim, L.P. and P.A. Sharp, *Alternative splicing of the fibronectin EIIIB exon depends on specific TGCATG repeats.* Molecular and cellular biology, 1998. **18**(7): p. 3900-6.
42. Chan, R.C. and D.L. Black, *The polypyrimidine tract binding protein binds upstream of neural cell-specific c-src exon N1 to repress the splicing of the intron downstream.* Molecular and cellular biology, 1997. **17**(8): p. 4667-76.
43. Markovtsov, V., et al., *Cooperative assembly of an hnRNP complex induced by a tissue-specific homolog of polypyrimidine tract binding protein.* Molecular and cellular biology, 2000. **20**(20): p. 7463-79.
44. Wang, Z. and C.B. Burge, *Splicing regulation: from a parts list of regulatory elements to an integrated splicing code.* RNA, 2008. **14**(5): p. 802-13.
45. Dhir, A. and E. Buratti, *Alternative splicing: role of pseudoexons in human disease and potential therapeutic strategies.* The Federation of European Biochemical Societies Journal, 2010. **277**(4): p. 841-55.
46. Wang, G.S. and T.A. Cooper, *Splicing in disease: disruption of the splicing code and the decoding machinery.* Nature reviews. Genetics, 2007. **8**(10): p. 749-61.
47. Green, R.E., et al., *Widespread predicted nonsense-mediated mRNA decay of alternatively-spliced transcripts of human normal and disease genes.* Bioinformatics, 2003. **19 Suppl 1**: p. i118-21.
48. Sterne-Weiler, T., et al., *Loss of exon identity is a common mechanism of human inherited disease.* Genome research, 2011. **21**(10): p. 1563-71.
49. Faustino, N.A. and T.A. Cooper, *Pre-mRNA splicing and human disease.* Genes & development, 2003. **17**(4): p. 419-37.
50. Singh, R.K. and T.A. Cooper, *Pre-mRNA splicing in disease and therapeutics.* Trends in molecular medicine, 2012. **18**(8): p. 472-82.
51. Edery, P., et al., *Association of TALS developmental disorder with defect in minor splicing component U4atac snRNA.* Science, 2011. **332**(6026): p. 240-3.
52. He, H., et al., *Mutations in U4atac snRNA, a component of the minor spliceosome, in the developmental disorder MOPD I.* Science, 2011. **332**(6026): p. 238-40.

53. Papaemmanuil, E., et al., *Somatic SF3B1 mutation in myelodysplasia with ring sideroblasts.* The New England journal of medicine, 2011. **365**(15): p. 1384-95.
54. Yoshida, K., et al., *Frequent pathway mutations of splicing machinery in myelodysplasia.* Nature, 2011. **478**(7367): p. 64-9.
55. Wang, L., et al., *SF3B1 and other novel cancer genes in chronic lymphocytic leukemia.* The New England journal of medicine, 2011. **365**(26): p. 2497-506.
56. Quesada, V., et al., *Exome sequencing identifies recurrent mutations of the splicing factor SF3B1 gene in chronic lymphocytic leukemia.* Nature genetics, 2012. **44**(1): p. 47-52.
57. Graubert, T.A., et al., *Recurrent mutations in the U2AF1 splicing factor in myelodysplastic syndromes.* Nature genetics, 2012. **44**(1): p. 53-7.
58. Makishima, H., et al., *Mutations in the spliceosome machinery, a novel and ubiquitous pathway in leukemogenesis.* Blood, 2012. **119**(14): p. 3203-10.
59. WHO. *Cancer*. 2015 February 2015; Available from: http://www.who.int/mediacentre/factsheets/fs297/en/.
60. WHO. *South Africa: WHO statistical profile*. 2015 January 2015; Available from: http://www.who.int/gho/countries/zaf.pdf?ua=1.
61. Hanahan, D. and R.A. Weinberg, *The hallmarks of cancer.* Cell, 2000. **100**(1): p. 57-70.
62. Negrini, S., V.G. Gorgoulis, and T.D. Halazonetis, *Genomic instability--an evolving hallmark of cancer.* Nature reviews. Molecular cell biology, 2010. **11**(3): p. 220-8.
63. Salk, J.J., E.J. Fox, and L.A. Loeb, *Mutational heterogeneity in human cancers: origin and consequences.* Annual review of pathology, 2010. **5**: p. 51-75.
64. Kalluri, R. and R.A. Weinberg, *The basics of epithelial-mesenchymal transition.* The Journal of clinical investigation, 2009. **119**(6): p. 1420-8.
65. Kalluri, R. and E.G. Neilson, *Epithelial-mesenchymal transition and its implications for fibrosis.* The Journal of clinical investigation, 2003. **112**(12): p. 1776-84.
66. Thiery, J.P., *Epithelial-mesenchymal transitions in tumour progression.* Nature reviews. Cancer, 2002. **2**(6): p. 442-54.
67. Fidler, I.J. and G. Poste, *The "seed and soil" hypothesis revisited.* The Lancet. Oncology, 2008. **9**(8): p. 808.
68. Brabletz, T., et al., *Variable beta-catenin expression in colorectal cancers indicates tumor progression driven by the tumor environment.* Proceedings of the National Academy of Sciences of the United States of America, 2001. **98**(18): p. 10356-61.
69. Jechlinger, M., S. Grunert, and H. Beug, *Mechanisms in epithelial plasticity and metastasis: insights from 3D cultures and expression profiling.* Journal of mammary gland biology and neoplasia, 2002. **7**(4): p. 415-32.
70. Shi, Y. and J. Massague, *Mechanisms of TGF-beta signaling from cell membrane to the nucleus.* Cell, 2003. **113**(6): p. 685-700.
71. Niessen, K., et al., *Slug is a direct Notch target required for initiation of cardiac cushion cellularization.* The Journal of cell biology, 2008. **182**(2): p. 315-25.

72. Medici, D., E.D. Hay, and B.R. Olsen, *Snail and Slug promote epithelial-mesenchymal transition through beta-catenin-T-cell factor-4-dependent expression of transforming growth factor-beta3.* Molecular biology of the cell, 2008. **19**(11): p. 4875-87.
73. Kokudo, T., et al., *Snail is required for TGFbeta-induced endothelial-mesenchymal transition of embryonic stem cell-derived endothelial cells.* Journal of cell science, 2008. **121**(Pt 20): p. 3317-24.
74. Tse, J.C. and R. Kalluri, *Mechanisms of metastasis: epithelial-to-mesenchymal transition and contribution of tumor microenvironment.* Journal of cellular biochemistry, 2007. **101**(4): p. 816-29.
75. Yang, J. and R.A. Weinberg, *Epithelial-mesenchymal transition: at the crossroads of development and tumor metastasis.* Developmental cell, 2008. **14**(6): p. 818-29.
76. Noda, M., et al., *Multiple signal transduction pathways mediated by 5-HT receptors.* Molecular Neurobiology, 2004. **29**(1): p. 31-9.
77. Vogelstein, B. and K.W. Kinzler, *Cancer genes and the pathways they control.* Nature Medicine, 2004. **10**(8): p. 789-99.
78. Komiya, Y. and R. Habas, *Wnt signal transduction pathways.* Organogenesis, 2008. **4**(2): p. 68-75.
79. Welters, H.J. and R.N. Kulkarni, *Wnt signaling: relevance to beta-cell biology and diabetes.* Trends Endocrinol Metab, 2008. **19**(10): p. 349-55.
80. Logan, C.Y. and R. Nusse, *The Wnt signaling pathway in development and disease.* Annual Review of Cell and Developmental Biology 2004. **20**: p. 781-810.
81. Smolich, B.D., et al., *Wnt family proteins are secreted and associated with the cell surface.* Molecular Biology of the Cell, 1993. **4**(12): p. 1267-75.
82. Willert, K., et al., *Wnt proteins are lipid-modified and can act as stem cell growth factors.* Nature, 2003. **423**(6938): p. 448-52.
83. Lin, X., *Functions of heparan sulfate proteoglycans in cell signaling during development.* Development, 2004. **131**(24): p. 6009-21.
84. Nusse, R., *Wnt signaling in disease and in development.* Cell Research, 2005. **15**(1): p. 28-32.
85. Kinzler, K.W., et al., *Identification of FAP locus genes from chromosome 5q21.* Science, 1991. **253**(5020): p. 661-5.
86. Nishisho, I., et al., *Mutations of chromosome 5q21 genes in FAP and colorectal cancer patients.* Science, 1991. **253**(5020): p. 665-9.
87. Giles, R.H., J.H. van Es, and H. Clevers, *Caught up in a Wnt storm: Wnt signaling in cancer.* Biochimica et Biophysica Acta, 2003. **1653**(1): p. 1-24.
88. Satoh, S., et al., *AXIN1 mutations in hepatocellular carcinomas, and growth suppression in cancer cells by virus-mediated transfer of AXIN1.* Nature Genetics, 2000. **24**(3): p. 245-50.
89. Korinek, V., et al., *Depletion of epithelial stem-cell compartments in the small intestine of mice lacking Tcf-4.* Nature Genetics, 1998. **19**(4): p. 379-83.
90. Pinto, D., et al., *Canonical Wnt signals are essential for homeostasis of the intestinal epithelium.* Genes & Development, 2003. **17**(14): p. 1709-13.
91. Kuhnert, F., et al., *Essential requirement for Wnt signaling in proliferation of adult small intestine and colon revealed by adenoviral expression of*

Dickkopf-1. Proceedings of the National Academy of Sciences of the United States of America, 2004. **101**(1): p. 266-71.
92. Taipale, J. and P.A. Beachy, *The Hedgehog and Wnt signalling pathways in cancer.* Nature, 2001. **411**(6835): p. 349-54.
93. Ferlay, J., et al., *Estimates of worldwide burden of cancer in 2008: GLOBOCAN 2008.* International journal of cancer. Journal international du cancer, 2010. **127**(12): p. 2893-917.
94. Shulman, L.N., et al., *Breast cancer in developing countries: opportunities for improved survival.* Journal of oncology, 2010. **2010**: p. 595167.
95. Carey, L.A., et al., *The triple negative paradox: primary tumor chemosensitivity of breast cancer subtypes.* Clinical cancer research : an official journal of the American Association for Cancer Research, 2007. **13**(8): p. 2329-34.
96. Brenton, J.D., et al., *Molecular classification and molecular forecasting of breast cancer: ready for clinical application?* Journal of clinical oncology : official journal of the American Society of Clinical Oncology, 2005. **23**(29): p. 7350-60.
97. Hudis, C.A. and L. Gianni, *Triple-negative breast cancer: an unmet medical need.* The oncologist, 2011. **16 Suppl 1**: p. 1-11.
98. Brewster, A.M., M. Chavez-MacGregor, and P. Brown, *Epidemiology, biology, and treatment of triple-negative breast cancer in women of African ancestry.* The Lancet. Oncology, 2014. **15**(13): p. e625-34.
99. Bauer, K.R., et al., *Descriptive analysis of estrogen receptor (ER)-negative, progesterone receptor (PR)-negative, and HER2-negative invasive breast cancer, the so-called triple-negative phenotype: a population-based study from the California cancer Registry.* Cancer, 2007. **109**(9): p. 1721-8.
100. Carey, L.A., et al., *Race, breast cancer subtypes, and survival in the Carolina Breast Cancer Study.* Journal of the American Medical Association, 2006. **295**(21): p. 2492-502.
101. Cubasch, H., et al., *Breast cancer characteristics and HIV among 1,092 women in Soweto, South Africa.* Breast cancer research and treatment, 2013. **140**(1): p. 177-86.
102. Sorlie, T., et al., *Gene expression patterns of breast carcinomas distinguish tumor subclasses with clinical implications.* Proceedings of the National Academy of Sciences of the United States of America, 2001. **98**(19): p. 10869-74.
103. Perou, C.M., et al., *Molecular portraits of human breast tumours.* Nature, 2000. **406**(6797): p. 747-52.
104. Thompson, P.A., et al., *Selective genomic copy number imbalances and probability of recurrence in early-stage breast cancer.* PloS one, 2011. **6**(8): p. e23543.
105. Sethi, S., et al., *Molecular markers of epithelial-to-mesenchymal transition are associated with tumor aggressiveness in breast carcinoma.* Translational oncology, 2011. **4**(4): p. 222-6.
106. Beslija, S., et al., *Third consensus on medical treatment of metastatic breast cancer.* Annals of oncology : official journal of the European Society for Medical Oncology / ESMO, 2009. **20**(11): p. 1771-85.
107. Liedtke, C., et al., *Response to neoadjuvant therapy and long-term survival in patients with triple-negative breast cancer.* Journal of clinical oncology :

official journal of the American Society of Clinical Oncology, 2008. **26**(8): p. 1275-81.
108. Tan, D.S., et al., *Triple negative breast cancer: molecular profiling and prognostic impact in adjuvant anthracycline-treated patients.* Breast cancer research and treatment, 2008. **111**(1): p. 27-44.
109. Chacon, R.D. and M.V. Costanzo, *Triple-negative breast cancer.* Breast cancer research : BCR, 2010. **12 Suppl 2**: p. S3.
110. Lehmann, B.D., et al., *Identification of human triple-negative breast cancer subtypes and preclinical models for selection of targeted therapies.* The Journal of clinical investigation, 2011. **121**(7): p. 2750-67.
111. Xu, Q. and C. Lee, *Discovery of novel splice forms and functional analysis of cancer-specific alternative splicing in human expressed sequences.* Nucleic acids research, 2003. **31**(19): p. 5635-43.
112. Hui, L., et al., *Identification of alternatively spliced mRNA variants related to cancers by genome-wide ESTs alignment.* Oncogene, 2004. **23**(17): p. 3013-23.
113. Venables, J.P., et al., *Cancer-associated regulation of alternative splicing.* Nature structural & molecular biology, 2009. **16**(6): p. 670-6.
114. David, C.J. and J.L. Manley, *Alternative pre-mRNA splicing regulation in cancer: pathways and programs unhinged.* Genes & development, 2010. **24**(21): p. 2343-64.
115. Schwerk, C. and K. Schulze-Osthoff, *Regulation of apoptosis by alternative pre-mRNA splicing.* Molecular cell, 2005. **19**(1): p. 1-13.
116. Boise, L.H., et al., *bcl-x, a bcl-2-related gene that functions as a dominant regulator of apoptotic cell death.* Cell, 1993. **74**(4): p. 597-608.
117. Olopade, O.I., et al., *Overexpression of BCL-x protein in primary breast cancer is associated with high tumor grade and nodal metastases.* The cancer journal from Scientific American, 1997. **3**(4): p. 230-7.
118. Takehara, T., et al., *Expression and role of Bcl-xL in human hepatocellular carcinomas.* Hepatology, 2001. **34**(1): p. 55-61.
119. Xerri, L., et al., *Predominant expression of the long isoform of Bcl-x (Bcl-xL) in human lymphomas.* British journal of haematology, 1996. **92**(4): p. 900-6.
120. Mercatante, D.R., J.L. Mohler, and R. Kole, *Cellular response to an antisense-mediated shift of Bcl-x pre-mRNA splicing and antineoplastic agents.* The Journal of biological chemistry, 2002. **277**(51): p. 49374-82.
121. Paronetto, M.P., et al., *The RNA-binding protein Sam68 modulates the alternative splicing of Bcl-x.* The Journal of cell biology, 2007. **176**(7): p. 929-39.
122. Ho, L.H., et al., *A tumor suppressor function for caspase-2.* Proceedings of the National Academy of Sciences of the United States of America, 2009. **106**(13): p. 5336-41.
123. Kumar, S., *Caspase 2 in apoptosis, the DNA damage response and tumour suppression: enigma no more?* Nature reviews. Cancer, 2009. **9**(12): p. 897-903.
124. Wang, L., et al., *Ich-1, an Ice/ced-3-related gene, encodes both positive and negative regulators of programmed cell death.* Cell, 1994. **78**(5): p. 739-50.

125. Solier, S., et al., *Nonsense-mediated mRNA decay among human caspases: the caspase-2S putative protein is encoded by an extremely short-lived mRNA.* Cell death and differentiation, 2005. **12**(6): p. 687-9.
126. Jiang, Z.H., et al., *Regulation of Ich-1 pre-mRNA alternative splicing and apoptosis by mammalian splicing factors.* Proceedings of the National Academy of Sciences of the United States of America, 1998. **95**(16): p. 9155-60.
127. Cote, J., et al., *Caspase-2 pre-mRNA alternative splicing: Identification of an intronic element containing a decoy 3' acceptor site.* Proceedings of the National Academy of Sciences of the United States of America, 2001. **98**(3): p. 938-43.
128. Cote, J., S. Dupuis, and J.Y. Wu, *Polypyrimidine track-binding protein binding downstream of caspase-2 alternative exon 9 represses its inclusion.* The Journal of biological chemistry, 2001. **276**(11): p. 8535-43.
129. Fushimi, K., et al., *Up-regulation of the proapoptotic caspase 2 splicing isoform by a candidate tumor suppressor, RBM5.* Proceedings of the National Academy of Sciences of the United States of America, 2008. **105**(41): p. 15708-13.
130. Logette, E., et al., *The human caspase-2 gene: alternative promoters, pre-mRNA splicing and AUG usage direct isoform-specific expression.* Oncogene, 2003. **22**(6): p. 935-46.
131. Shim, H., et al., *c-Myc transactivation of LDH-A: implications for tumor metabolism and growth.* Proceedings of the National Academy of Sciences of the United States of America, 1997. **94**(13): p. 6658-63.
132. Kim, J.W., et al., *Evaluation of myc E-box phylogenetic footprints in glycolytic genes by chromatin immunoprecipitation assays.* Molecular and cellular biology, 2004. **24**(13): p. 5923-36.
133. Dang, C.V., A. Le, and P. Gao, *MYC-induced cancer cell energy metabolism and therapeutic opportunities.* Clinical cancer research : an official journal of the American Association for Cancer Research, 2009. **15**(21): p. 6479-83.
134. Fantin, V.R., J. St-Pierre, and P. Leder, *Attenuation of LDH-A expression uncovers a link between glycolysis, mitochondrial physiology, and tumor maintenance.* Cancer cell, 2006. **9**(6): p. 425-34.
135. Mazurek, S., et al., *Pyruvate kinase type M2 and its role in tumor growth and spreading.* Seminars in cancer biology, 2005. **15**(4): p. 300-8.
136. Christofk, H.R., et al., *The M2 splice isoform of pyruvate kinase is important for cancer metabolism and tumour growth.* Nature, 2008. **452**(7184): p. 230-3.
137. David, C.J., et al., *HnRNP proteins controlled by c-Myc deregulate pyruvate kinase mRNA splicing in cancer.* Nature, 2010. **463**(7279): p. 364-8.
138. Clower, C.V., et al., *The alternative splicing repressors hnRNP A1/A2 and PTB influence pyruvate kinase isoform expression and cell metabolism.* Proceedings of the National Academy of Sciences of the United States of America, 2010. **107**(5): p. 1894-9.
139. Chen, M., C.J. David, and J.L. Manley, *Tumor metabolism: hnRNP proteins get in on the act.* Cell cycle, 2010. **9**(10): p. 1863-4.
140. Gunthert, U., et al., *A new variant of glycoprotein CD44 confers metastatic potential to rat carcinoma cells.* Cell, 1991. **65**(1): p. 13-24.

141. Ponta, H., L. Sherman, and P.A. Herrlich, *CD44: from adhesion molecules to signalling regulators.* Nature reviews. Molecular cell biology, 2003. **4**(1): p. 33-45.
142. Galiana-Arnoux, D., et al., *The CD44 alternative v9 exon contains a splicing enhancer responsive to the SR proteins 9G8, ASF/SF2, and SRp20.* The Journal of biological chemistry, 2003. **278**(35): p. 32943-53.
143. Arch, R., et al., *Participation in normal immune responses of a metastasis-inducing splice variant of CD44.* Science, 1992. **257**(5070): p. 682-5.
144. Orian-Rousseau, V., et al., *CD44 is required for two consecutive steps in HGF/c-Met signaling.* Genes & development, 2002. **16**(23): p. 3074-86.
145. Cecchi, F., D.C. Rabe, and D.P. Bottaro, *Targeting the HGF/Met signalling pathway in cancer.* European journal of cancer, 2010. **46**(7): p. 1260-70.
146. Cheng, C. and P.A. Sharp, *Regulation of CD44 alternative splicing by SRm160 and its potential role in tumor cell invasion.* Molecular and cellular biology, 2006. **26**(1): p. 362-70.
147. Carstens, R.P., et al., *Alternative splicing of fibroblast growth factor receptor 2 (FGF-R2) in human prostate cancer.* Oncogene, 1997. **15**(25): p. 3059-65.
148. Chaffer, C.L., et al., *Aberrant fibroblast growth factor receptor signaling in bladder and other cancers.* Differentiation; research in biological diversity, 2007. **75**(9): p. 831-42.
149. Yan, G., et al., *Exon switching and activation of stromal and embryonic fibroblast growth factor (FGF)-FGF receptor genes in prostate epithelial cells accompany stromal independence and malignancy.* Molecular and cellular biology, 1993. **13**(8): p. 4513-22.
150. Easton, D.F., et al., *Genome-wide association study identifies novel breast cancer susceptibility loci.* Nature, 2007. **447**(7148): p. 1087-93.
151. Hunter, D.J., et al., *A genome-wide association study identifies alleles in FGFR2 associated with risk of sporadic postmenopausal breast cancer.* Nature genetics, 2007. **39**(7): p. 870-4.
152. Ornitz, D.M. and N. Itoh, *Fibroblast growth factors.* Genome biology, 2001. **2**(3): p. REVIEWS3005.
153. Schlessinger, J., *Cell signaling by receptor tyrosine kinases.* Cell, 2000. **103**(2): p. 211-25.
154. Sanchez-Heras, E., et al., *The fibroblast growth factor receptor acid box is essential for interactions with N-cadherin and all of the major isoforms of neural cell adhesion molecule.* The Journal of biological chemistry, 2006. **281**(46): p. 35208-16.
155. Turner, N. and R. Grose, *Fibroblast growth factor signalling: from development to cancer.* Nature reviews. Cancer, 2010. **10**(2): p. 116-29.
156. Wheldon, L.M., et al., *Identification and characterization of an inhibitory fibroblast growth factor receptor 2 (FGFR2) molecule, up-regulated in an Apert Syndrome mouse model.* Biochemical Journal, 2011. **436**(1): p. 71-81.
157. Ornitz, D.M., et al., *Receptor specificity of the fibroblast growth factor family.* The Journal of biological chemistry, 1996. **271**(25): p. 15292-7.
158. Zhang, X., et al., *Receptor specificity of the fibroblast growth factor family. The complete mammalian FGF family.* The Journal of biological chemistry, 2006. **281**(23): p. 15694-700.

159. Powers, C.J., S.W. McLeskey, and A. Wellstein, *Fibroblast growth factors, their receptors and signaling.* Endocrine-related cancer, 2000. **7**(3): p. 165-97.
160. Katoh, M., *Cancer genomics and genetics of FGFR2 (Review).* International journal of oncology, 2008. **33**(2): p. 233-7.
161. Carstens, R.P., W.L. McKeehan, and M.A. Garcia-Blanco, *An intronic sequence element mediates both activation and repression of rat fibroblast growth factor receptor 2 pre-mRNA splicing.* Molecular and cellular biology, 1998. **18**(4): p. 2205-17.
162. Katoh, M., *FGFR2 and WDR11 are neighboring oncogene and tumor suppressor gene on human chromosome 10q26.* International journal of oncology, 2003. **22**(5): p. 1155-9.
163. Wagner, E.J., et al., *Characterization of the intronic splicing silencers flanking FGFR2 exon IIIb.* The Journal of biological chemistry, 2005. **280**(14): p. 14017-27.
164. Carstens, R.P., E.J. Wagner, and M.A. Garcia-Blanco, *An intronic splicing silencer causes skipping of the IIIb exon of fibroblast growth factor receptor 2 through involvement of polypyrimidine tract binding protein.* Molecular and cellular biology, 2000. **20**(19): p. 7388-400.
165. Baraniak, A.P., J.R. Chen, and M.A. Garcia-Blanco, *Fox-2 mediates epithelial cell-specific fibroblast growth factor receptor 2 exon choice.* Molecular and cellular biology, 2006. **26**(4): p. 1209-22.
166. Baraniak, A.P., et al., *A stem structure in fibroblast growth factor receptor 2 transcripts mediates cell-type-specific splicing by approximating intronic control elements.* Molecular and cellular biology, 2003. **23**(24): p. 9327-37.
167. Del Gatto, F. and R. Breathnach, *Exon and intron sequences, respectively, repress and activate splicing of a fibroblast growth factor receptor 2 alternative exon.* Molecular and cellular biology, 1995. **15**(9): p. 4825-34.
168. Del Gatto, F., M.C. Gesnel, and R. Breathnach, *The exon sequence TAGG can inhibit splicing.* Nucleic acids research, 1996. **24**(11): p. 2017-21.
169. Del Gatto, F., et al., *Multiple interdependent sequence elements control splicing of a fibroblast growth factor receptor 2 alternative exon.* Molecular and cellular biology, 1997. **17**(9): p. 5106-16.
170. Hovhannisyan, R.H. and R.P. Carstens, *A novel intronic cis element, ISE/ISS-3, regulates rat fibroblast growth factor receptor 2 splicing through activation of an upstream exon and repression of a downstream exon containing a noncanonical branch point sequence.* Molecular and cellular biology, 2005. **25**(1): p. 250-63.
171. Mauger, D.M., C. Lin, and M.A. Garcia-Blanco, *hnRNP H and hnRNP F complex with Fox2 to silence fibroblast growth factor receptor 2 exon IIIc.* Molecular and cellular biology, 2008. **28**(17): p. 5403-19.
172. Wagner, E.J. and M.A. Garcia-Blanco, *RNAi-mediated PTB depletion leads to enhanced exon definition.* Molecular cell, 2002. **10**(4): p. 943-9.
173. Warzecha, C.C., et al., *ESRP1 and ESRP2 are epithelial cell-type-specific regulators of FGFR2 splicing.* Molecular cell, 2009. **33**(5): p. 591-601.
174. Jones, R.B., et al., *5′- and 3′-terminal nucleotides in the FGFR2 ISAR splicing element core have overlapping roles in exon IIIb activation and exon IIIc repression.* Nucleic acids research, 2001. **29**(17): p. 3557-65.

175. Muh, S.J., R.H. Hovhannisyan, and R.P. Carstens, *A Non-sequence-specific double-stranded RNA structural element regulates splicing of two mutually exclusive exons of fibroblast growth factor receptor 2 (FGFR2).* The Journal of biological chemistry, 2002. **277**(51): p. 50143-54.
176. Mistry, N., et al., *Of urchins and men: evolution of an alternative splicing unit in fibroblast growth factor receptor genes.* RNA, 2003. **9**(2): p. 209-17.
177. Wagner, E.J., et al., *Imaging alternative splicing in living cells.* Methods in molecular biology, 2004. **257**: p. 29-46.
178. Gesnel, M.C., F. Del Gatto-Konczak, and R. Breathnach, *Combined use of MS2 and PP7 coat fusions shows that TIA-1 dominates hnRNP A1 for K-SAM exon splicing control.* Journal of biomedicine & biotechnology, 2009. **2009**: p. 104853.
179. Seth, P., et al., *Identification of an intronic splicing enhancer essential for the inclusion of FGFR2 exon IIIc.* The Journal of biological chemistry, 2008. **283**(15): p. 10058-67.
180. Bilir, B., O. Kucuk, and C.S. Moreno, *Wnt signaling blockage inhibits cell proliferation and migration, and induces apoptosis in triple-negative breast cancer cells.* Journal of Translational Medicine, 2013. **11**: p. 280.
181. Katoh, Y. and M. Katoh, *FGFR2-related pathogenesis and FGFR2-targeted therapeutics (Review).* Int J Mol Med, 2009. **23**(3): p. 307-11.
182. O'Donovan, M.C., et al., *Analysis of 10 independent samples provides evidence for association between schizophrenia and a SNP flanking fibroblast growth factor receptor 2.* Mol Psychiatry, 2009. **14**(1): p. 30-6.
183. Pollock, P.M., et al., *Frequent activating FGFR2 mutations in endometrial carcinomas parallel germline mutations associated with craniosynostosis and skeletal dysplasia syndromes.* Oncogene, 2007. **26**(50): p. 7158-62.
184. Jang, J.H., K.H. Shin, and J.G. Park, *Mutations in fibroblast growth factor receptor 2 and fibroblast growth factor receptor 3 genes associated with human gastric and colorectal cancers.* Cancer Research, 2001. **61**(9): p. 3541-3.
185. Davies, H., et al., *Somatic mutations of the protein kinase gene family in human lung cancer.* Cancer Research, 2005. **65**(17): p. 7591-5.
186. Grose, R., et al., *The role of fibroblast growth factor receptor 2b in skin homeostasis and cancer development.* European Molecular Biology Organization Journal, 2007. **26**(5): p. 1268-78.
187. Davis-Smyth, T., et al., *The far upstream element-binding proteins comprise an ancient family of single-strand DNA-binding transactivators.* The Journal of Biological Chemistry, 1996. **271**(49): p. 31679-87.
188. Min, H., et al., *A new regulatory protein, KSRP, mediates exon inclusion through an intronic splicing enhancer.* Genes & Development, 1997. **11**(8): p. 1023-36.
189. Briata, P., et al., *Functional and molecular insights into KSRP function in mRNA decay.* Biochim Biophys Acta, 2013. **1829**(6-7): p. 689-94.
190. Gherzi, R., et al., *KSRP controls pleiotropic cellular functions.* Seminars in Cell & Developmental Biology, 2014. **34**: p. 2-8.
191. Gherzi, R., et al., *The role of KSRP in mRNA decay and microRNA precursor maturation.* Wiley Interdisciplinary Reviews RNA, 2010. **1**(2): p. 230-9.

192. Gherzi, R., et al., *The RNA-binding protein KSRP promotes decay of beta-catenin mRNA and is inactivated by PI3K-AKT signaling.* PLoS Biology, 2006. **5**(1): p. e5.
193. Zhang, X., et al., *The ATM kinase induces microRNA biogenesis in the DNA damage response.* Molecular Cell, 2011. **41**(4): p. 371-83.
194. Briata, P., et al., *p38-dependent phosphorylation of the mRNA decay-promoting factor KSRP controls the stability of select myogenic transcripts.* Molecular Cell, 2005. **20**(6): p. 891-903.
195. Hao, S. and D. Baltimore, *The stability of mRNA influences the temporal order of the induction of genes encoding inflammatory molecules.* Nature Immunology, 2009. **10**(3): p. 281-8.
196. Gingerich, T.J., J.J. Feige, and J. LaMarre, *AU-rich elements and the control of gene expression through regulated mRNA stability.* Animal Health Research Reviews, 2004. **5**(1): p. 49-63.
197. Wu, X. and G. Brewer, *The regulation of mRNA stability in mammalian cells: 2.0.* Gene, 2012. **500**(1): p. 10-21.
198. Chen, C.Y., et al., *AU binding proteins recruit the exosome to degrade ARE-containing mRNAs.* Cell, 2001. **107**(4): p. 451-64.
199. Gherzi, R., et al., *A KH domain RNA binding protein, KSRP, promotes ARE-directed mRNA turnover by recruiting the degradation machinery.* Molecular cell, 2004. **14**(5): p. 571-83.
200. Chou, C.F., et al., *Tethering KSRP, a decay-promoting AU-rich element-binding protein, to mRNAs elicits mRNA decay.* Molecular and cellular biology, 2006. **26**(10): p. 3695-706.
201. Krol, J., I. Loedige, and W. Filipowicz, *The widespread regulation of microRNA biogenesis, function and decay.* Nature Reviews Genetics, 2010. **11**(9): p. 597-610.
202. Trabucchi, M., et al., *The RNA-binding protein KSRP promotes the biogenesis of a subset of microRNAs.* Nature, 2009. **459**(7249): p. 1010-4.
203. Liu, Y. and Q. Liu, *ATM signals miRNA biogenesis through KSRP.* Molecular Cell, 2011. **41**(4): p. 367-8.
204. Michlewski, G. and J.F. Caceres, *Antagonistic role of hnRNP A1 and KSRP in the regulation of let-7a biogenesis.* Nature Structural & Molecular Biology, 2010. **17**(8): p. 1011-8.
205. Trabucchi, M., et al., *How to control miRNA maturation?* RNA Biology, 2009. **6**(5): p. 536-40.
206. Ruegger, S. and H. Grosshans, *MicroRNA turnover: when, how, and why.* Trends in Biochemical Sciences, 2012. **37**(10): p. 436-46.
207. Briata, P., et al., *Diverse roles of the nucleic acid-binding protein KHSRP in cell differentiation and disease.* Wiley Interdiscip Rev RNA, 2015.
208. Yang, J., et al., *Genome-wide RNAi screening identifies genes inhibiting the migration of glioblastoma cells.* PLoS One, 2013. **8**(4): p. e61915.
209. Boucas, J., et al., *Label-Free Protein-RNA Interactome Analysis Identifies Khsrp Signaling Downstream of the p38/Mk2 Kinase Complex as a Critical Modulator of Cell Cycle Progression.* PLoS One, 2015. **10**(5): p. e0125745.
210. Zubaidah, R.M., et al., *2-D DIGE profiling of hepatocellular carcinoma tissues identified isoforms of far upstream binding protein (FUBP) as novel candidates in liver carcinogenesis.* Proteomics, 2008. **8**(23-24): p. 5086-96.

211. Livak, K.J. and T.D. Schmittgen, *Analysis of relative gene expression data using real-time quantitative PCR and the 2(-Delta Delta C(T)) Method.* Methods, 2001. **25**(4): p. 402-8.
212. Bustin, S.A., et al., *The MIQE guidelines: minimum information for publication of quantitative real-time PCR experiments.* Clinical Chemistry, 2009. **55**(4): p. 611-22.
213. Schneider, C.A., W.S. Rasband, and K.W. Eliceiri, *NIH Image to ImageJ: 25 years of image analysis.* Nature Methods, 2012. **9**(7): p. 671-5.
214. Schindelin, J., et al., *Fiji: an open-source platform for biological-image analysis.* Nature Methods, 2012. **9**(7): p. 676-82.
215. Xu, M., J.R. McCarrey, and N.B. Hecht, *A cytoplasmic variant of the KH-type splicing regulatory protein serves as a decay-promoting factor for phosphoglycerate kinase 2 mRNA in murine male germ cells.* Nucleic Acids Research, 2008. **36**(22): p. 7157-67.
216. Oltean, S., et al., *Alternative inclusion of fibroblast growth factor receptor 2 exon IIIc in Dunning prostate tumors reveals unexpected epithelial mesenchymal plasticity.* Proceedings of the National Academy of Sciences of the United States of America, 2006. **103**(38): p. 14116-21.
217. Kang, Y. and J. Massague, *Epithelial-mesenchymal transitions: twist in development and metastasis.* Cell, 2004. **118**(3): p. 277-9.
218. Douablin, A., et al., *HnRNP A1 tethers KSRP to an exon splicing silencer that inhibits an erythroid-specific splicing event in PU.1-induced erythroleukemia.* American Journal of Cancer Research, 2015. **5**(4): p. 1410-22.
219. Garcia-Mayoral, M.F., et al., *The sequence selectivity of KSRP explains its flexibility in the recognition of the RNA targets.* Nucleic acids research, 2008. **36**(16): p. 5290-6.
220. Burd, C.G. and G. Dreyfuss, *RNA binding specificity of hnRNP A1: significance of hnRNP A1 high-affinity binding sites in pre-mRNA splicing.* The EMBO Journal, 1994. **13**(5): p. 1197-204.
221. Shen, H., et al., *A single polypyrimidine tract binding protein (PTB) binding site mediates splicing inhibition at mouse IgM exons M1 and M2.* RNA, 2004. **10**(5): p. 787-94.
222. Dey, N., et al., *Wnt signaling in triple negative breast cancer is associated with metastasis.* BMC Cancer, 2013. **13**: p. 537.
223. King, T.D., M.J. Suto, and Y. Li, *The Wnt/beta-catenin signaling pathway: a potential therapeutic target in the treatment of triple negative breast cancer.* Journal of Cellular Biochemistry, 2012. **113**(1): p. 13-8.
224. Buschges, R., et al., *Amplification and expression of cyclin D genes (CCND1, CCND2 and CCND3) in human malignant gliomas.* Brain Pathology, 1999. **9**(3): p. 435-42; discussion 432-3.
225. Mao, X., et al., *Cyproheptadine displays preclinical activity in myeloma and leukemia.* Blood, 2008. **112**(3): p. 760-9.
226. Bafico, A., et al., *Novel mechanism of Wnt signalling inhibition mediated by Dickkopf-1 interaction with LRP6/Arrow.* Nature Cell Biology, 2001. **3**(7): p. 683-6.
227. Semenov, M.V., et al., *Head inducer Dickkopf-1 is a ligand for Wnt coreceptor LRP6.* Current biology : CB, 2001. **11**(12): p. 951-61.

228. Menezes, M.E., et al., *Dickkopf1: a tumor suppressor or metastasis promoter?* International journal of cancer. Journal international du cancer, 2012. **130**(7): p. 1477-83.
229. Tian, E., et al., *The role of the Wnt-signaling antagonist DKK1 in the development of osteolytic lesions in multiple myeloma.* The New England journal of medicine, 2003. **349**(26): p. 2483-94.
230. Wirths, O., et al., *Overexpression of human Dickkopf-1, an antagonist of wingless/WNT signaling, in human hepatoblastomas and Wilms' tumors.* Laboratory Investigation, 2003. **83**(3): p. 429-34.
231. Forget, M.A., et al., *The Wnt pathway regulator DKK1 is preferentially expressed in hormone-resistant breast tumours and in some common cancer types.* British Journal of Cancer, 2007. **96**(4): p. 646-53.
232. Qiao, L., et al., *Dkk-1 secreted by mesenchymal stem cells inhibits growth of breast cancer cells via depression of Wnt signalling.* Cancer Letters, 2008. **269**(1): p. 67-77.
233. Mitra, A., et al., *DNAJB6 induces degradation of beta-catenin and causes partial reversal of mesenchymal phenotype.* The Journal of Biological Chemistry, 2010. **285**(32): p. 24686-94.
234. Fillmore, R.A., et al., *Nmi (N-Myc interactor) inhibits Wnt/beta-catenin signaling and retards tumor growth.* International journal of cancer. Journal international du cancer, 2009. **125**(3): p. 556-64.
235. DiMeo, T.A., et al., *A novel lung metastasis signature links Wnt signaling with cancer cell self-renewal and epithelial-mesenchymal transition in basal-like breast cancer.* Cancer Research, 2009. **69**(13): p. 5364-73.
236. Hirata, H., et al., *Wnt antagonist DKK1 acts as a tumor suppressor gene that induces apoptosis and inhibits proliferation in human renal cell carcinoma.* International journal of cancer. Journal international du cancer, 2011. **128**(8): p. 1793-803.
237. Cowling, V.H., et al., *c-Myc transforms human mammary epithelial cells through repression of the Wnt inhibitors DKK1 and SFRP1.* Molecular and cellular biology, 2007. **27**(14): p. 5135-46.
238. Kuphal, S., et al., *Expression of Dickkopf genes is strongly reduced in malignant melanoma.* Oncogene, 2006. **25**(36): p. 5027-36.
239. Mikheev, A.M., et al., *Dickkopf-1 mediated tumor suppression in human breast carcinoma cells.* Breast Cancer Research and Treatment 2008. **112**(2): p. 263-73.
240. Gonzalez-Sancho, J.M., et al., *The Wnt antagonist DICKKOPF-1 gene is a downstream target of beta-catenin/TCF and is downregulated in human colon cancer.* Oncogene, 2005. **24**(6): p. 1098-103.
241. Mikheev, A.M., et al., *A functional genomics approach for the identification of putative tumor suppressor genes: Dickkopf-1 as suppressor of HeLa cell transformation.* Carcinogenesis, 2004. **25**(1): p. 47-59.
242. Lee, A.Y., et al., *Dickkopf-1 antagonizes Wnt signaling independent of beta-catenin in human mesothelioma.* Biochemical and Biophysical Research Communications, 2004. **323**(4): p. 1246-50.
243. Shou, J., et al., *Human Dkk-1, a gene encoding a Wnt antagonist, responds to DNA damage and its overexpression sensitizes brain tumor cells to apoptosis following alkylation damage of DNA.* Oncogene, 2002. **21**(6): p. 878-89.

244. Mikheev, A.M., et al., *Dickkopf-1 activates cell death in MDA-MB435 melanoma cells.* Biochemical and Biophysical Research Communications, 2007. **352**(3): p. 675-80.
245. Micalizzi, D.S., S.M. Farabaugh, and H.L. Ford, *Epithelial-mesenchymal transition in cancer: parallels between normal development and tumor progression.* Journal of Mammary Gland Biology and Neoplasia, 2010. **15**(2): p. 117-34.
246. Yook, J.I., et al., *A Wnt-Axin2-GSK3beta cascade regulates Snail1 activity in breast cancer cells.* Nature Cell Biology, 2006. **8**(12): p. 1398-406.
247. Wang, F., et al., *Infrequent mutations of the PPP2R1A and PPP2R1B genes in patients with ovarian cancer.* Molecular Medicine Reports, 2013. **7**(6): p. 1826-30.
248. Calin, G.A., et al., *Low frequency of alterations of the alpha (PPP2R1A) and beta (PPP2R1B) isoforms of the subunit A of the serine-threonine phosphatase 2A in human neoplasms.* Oncogene, 2000. **19**(9): p. 1191-5.
249. Wu, R., et al., *Somatic mutations of the PPP2R1B candidate tumor suppressor gene at chromosome 11q23 are infrequent in ovarian carcinomas.* Neoplasia, 1999. **1**(4): p. 311-4.
250. von Mering, C., et al., *STRING: a database of predicted functional associations between proteins.* Nucleic Acids Research, 2003. **31**(1): p. 258-61.
251. Agnati, L.F., et al., *New methods to evaluate colocalization of fluorophores in immunocytochemical preparations as exemplified by a study on A2A and D2 receptors in Chinese hamster ovary cells.* Journal of Histochemistry & Cytochemistry, 2005. **53**(8): p. 941-53.
252. Zinchuk, V. and O. Zinchuk, *Quantitative colocalization analysis of confocal fluorescence microscopy images.* Current Protocols in Cell Biology, 2008. **Chapter 4**: p. Unit 4 19.
253. Zhang, Q.Q., et al., *MicroRNA-195 plays a tumor-suppressor role in human glioblastoma cells by targeting signaling pathways involved in cellular proliferation and invasion.* Neuro-Oncology, 2012. **14**(3): p. 278-87.
254. Lal, A., et al., *Capture of microRNA-bound mRNAs identifies the tumor suppressor miR-34a as a regulator of growth factor signaling.* PLoS Genetics, 2011. **7**(11): p. e1002363.
255. Calin, G.A., et al., *Human microRNA genes are frequently located at fragile sites and genomic regions involved in cancers.* Proceedings of the National Academy of Sciences of the United States of America, 2004. **101**(9): p. 2999-3004.
256. Garzon, R., et al., *MicroRNA expression and function in cancer.* Trends in molecular medicine, 2006. **12**(12): p. 580-7.
257. Ma, D., et al., *miR-224 functions as an onco-miRNA in hepatocellular carcinoma cells by activating AKT signaling.* Oncology Letters, 2012. **4**(3): p. 483-488.

Appendices

8. APPENDIX A

8.1. Luria Broth

Dissolve the following ingredients in 800 mL dH_2O:

10 g Bacto-tryptone

5 g Yeast extract

10 g NaCl

Adjust the pH and volume of the solution to 7,5 and 1 L, respectively.

Autoclave to sterilise and store at 4 °C.

8.2. LB-Kanamycin Agar Plates

Place the following ingredients in a flask and add dH_2O up to 500 mL

5 g NaCl

5 g Tryptone

2,5 g Yeast extract

7,5 g Agar

Autoclave to sterilise and add Kanamycin (1:1000 dilution) when the solution has cooled to ~55 °C. Pour ~20 mL into each 10 cm Petri dish and cool until solidified. Once solidified, invert plates and dry overnight. Seal with Parafilm and store at 4 °C.

8.3. Buffer P1

This buffer composed of

50 mM Tris-HCl (pH 8,0)

10 mM EDTA

100 µg/mL RNase A

and is stored at 4 °C after the addition of RNase A.

8.4. Buffer P2

This buffer is composed of

200 mM NaOH

1% SDS

and is stored at RT.

8.5. Buffer N3

This buffer is composed of

4.2 M Gu-HCl

0.9 M Potassium acetate

pH adjusted to 4.8 and is stored at RT.

8.6. Buffer PB

This buffer is composed of

5 M Gu-HCl

30% Isopropanol

And is stored at RT.

8.7. Buffer PE

This buffer is composed of

10 mM Tris-HCl pH 7.5

80% Ethanol

And is stored at RT.

8.8. Buffer EB

This buffer is composed of

10 mM Tris-HCl (pH 8.5)

And is stored at RT.

8.9. 10x PBS

Dissolve the following ingredients in 800 mL dH_2O:

80 g NaCl

2 g KCl

14,4 g Na_2HPO_4

2,4 g KH_2PO_4

Adjust pH to 7,4 and the volume to 1 L with dH_2O.

Autoclave to sterilise and store at RT. Dilute to 1x before use.

8.10. RLT Buffer

The exact composition of this buffer is confidential.

8.11. RPE Buffer

The exact composition of this buffer is confidential.

8.12. 0,5 M EDTA

Dissolve 186,1 g EDTA in 800 mL dH_2O and adjust the pH of the solution to 8.0.

Adjust the volume of the solution to 1 L with dH_2O and store at RT.

8.13. RIPA Buffer

Combine the following components:

5 mL 1 M Tris-HCl PH 7.4

30 mL 5 M NaCl

5 mL 20% NP-40

5 mL 10% Sodium deoxycholate

0.5 mL 20% SDS

Adjust volume to 50 mL with dH_2O and store at 4 °C.

Add Protease Inhibitor Cocktail (1:1000) before use.

8.14. 10% SDS

Dissolve 1 g SDS in 10 mL dH_2O and store at RT.

8.15. 10% APS

Dissolve 1 g APS in 10 mL dH_2O and store at 4 °C.

8.16. 10% Polyacrylamide Gel

Mix the following together:

5 mL	H_20
1 mL	10x TBE
4 mL	30% Acrylamide
100 µL	10% APS
10 µL	TEMED

Immediately pour gel and use once polymerised.

8.17. 10x TBE

Dissolve the following ingredients in 800 mL H_2O:

108 g Tris base

55 g Boric acid

9,3 g EDTA

Adjust the volume to 1 L with distilled dH_2O and store at RT.

Dilute to 1x with distilled water before use.

8.18. Stacking Gel Buffer (0,5 M Tris-HCl)

Dissolve 6,05 g Tris in 70 mL dH_2O and adjust the pH to 6,8 using HCl.

Adjust the volume of the solution to 100 mL and store at RT.

8.19. Separating Gel Buffer (1,5 M Tris-HCl)

Dissolve 18,17 g Tris in 70 mL dH_2O and adjust pH to 8,8 using HCl.

Adjust the volume of the solution to 100 mL and store at RT.

8.20. 6x Loading Dye

Combine the following components:

3,75 mL	1M Tris-HCl (pH 6.8)
6 mL	Glycerol
1,2 g	SDS
0,93 g	DTT
6 mg	Bromophenol blue

Adjust the volume of the solution to 10 mL with dH_2O and store at –20 ˚C in 0,5 mL aliquots.

8.21. Sodium Dodecyl Sulphate Polyacrylamide Gel

8.21.1. 10% Separating Gel

Mix the following together:

3,5 mL	dH_2O
4,15 mL	30% Acrylamide/bis acrylamide
4,725 μL	Separating gel buffer (1,5 M Tris-HCl) (section 8.19)
125 μL	10% SDS (section 8.14)
125 μL	10% APS (section 8.15)
5 μL	TEMED

Pour immediately and allow to polymerise.

8.21.2. 5% Stacking Gel

Mix the following together

3,4 mL	dH_2O
850 μL	30% Acrylamide/bis acrylamide
625 μL	Stacking gel buffer (0,5 M Tris-HCl) (section 8.18)
50 μL	10% SDS (section 8.14)
50 μL	10% APS (section 8.15)
5 μL	TEMED

Immediately pour over separating gel.

8.22. SDS Running Buffer

Dissolve

30 g Tris base

144 g Glycine

10 g SDS

In 1 L dH_2O.

Store at RT and dilute to 1X before use.

8.23. Transfer Buffer

8.23.1. 10x Transfer Buffer

Dissolve

30,3 g Tris base

144,1 g Glycine

In 800 mL dH_2O, adjust the volume of the solution to 1 L with dH_2O and store at RT.

8.23.2. 1x Transfer Buffer

100 mL 10x stock

100 mL Methanol

800 mL dH_2O

Store at 4 °C

8.24. 1X PBS-Tween

Add 1 mL Tween-20 to 1 L of 1X PBS and mix thoroughly and store at RT.

8.25. 5% Non-Fat Milk in 1X PBS-Tween

Dissolve 2,5 g non-fat milk in 1X PBS-Tween and store at 4 °C.

8.26. Lysis Buffer

Combine

50 mM	Tris-HCl (pH 7.4)
100 mM	NaCl
1%	Igepal CA-630
0,1%	SDS
0,5%	Sodium deoxycholate

In dH_2O and store at 4 °C. On the day of use (if necessary), add Protease Inhibitor Cocktail (1:100).

8.27. High-Salt Wash

Combine

0,5 M	NaCl
1 mM	EDTA
1%	Igepal CA-630
0,1%	SDS
0,5%	Sodium deoxycholate

In dH_2O and store at 4 °C

8.28. PNK Buffer

Combine

20 mM	Tris-HCl (pH 7.4)
10 mM	$MgCl_2$
0,2%	Tween-20

In dH_2O and store at 4 °C.

8.29. Plasmid Maps

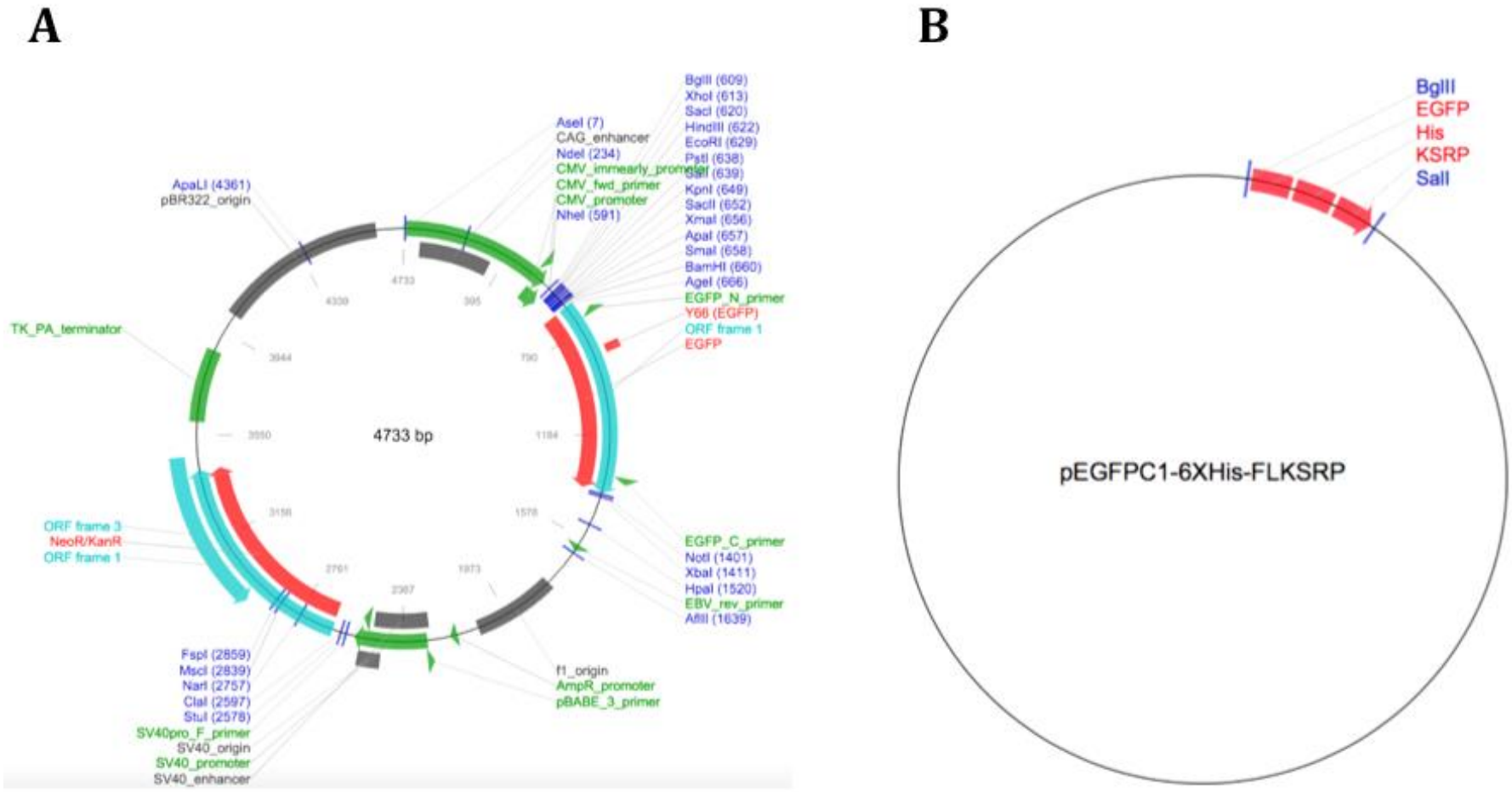

Figure 8.1 – Plasmid maps. A) pEGFP-N1 plasmid map. B) pEGFPC1-6xHis-FLKSRP plasmid map.

9. APPENDIX B

9.1. 2100 Bioanalyzer Results

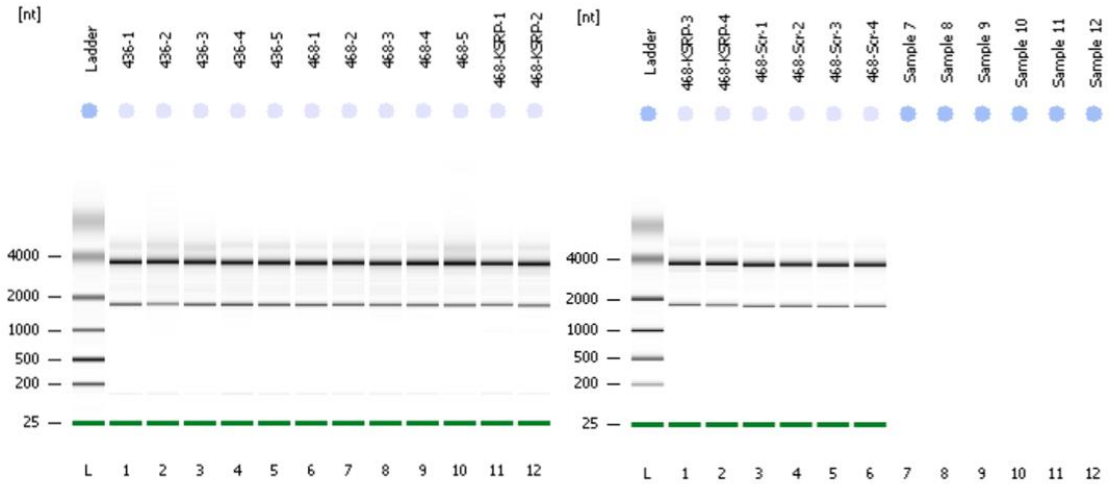

Sample Name	Status	Result Label
436-1	✔	RIN: 9.90
436-2	✔	RIN: 9.40
436-3	✔	RIN: 9.80
436-4	✔	RIN: 9.80
436-5	✔	RIN: 9.80
468-1	✔	RIN:10
468-2	✔	RIN:10
468-3	✔	RIN: 9.70
468-4	✔	RIN: 9.90
468-5	✔	RIN: 9.80
468-KSRP-1	✔	RIN: 9.60
468-KSRP-2	✔	RIN: 9.60
Ladder	✔	All Other Samples

Sample Name	Status	Result Label
468-KSRP-3	✔	RIN:10
468-KSRP-4	✔	RIN:10
468-Scr-1	✔	RIN:10
468-Scr-2	✔	RIN:10
468-Scr-3	✔	RIN:10
468-Scr-4	✔	RIN:10
Sample 7		
Sample 8		
Sample 9		
Sample 10		
Sample 11		
Sample 12		
Ladder	✔	All Other Samples

Figure 9.1 – 2100 Bioanalyzer results. RNA integrity was analysed using the 2100 Bioanalyzer. The top panel illustrates the electrophoretic trace of the 28S and 18S rRNA and the bottom panel displays the RINs for each sample.

10. APPENDIX C

10.1. Ethical Clearance Certificate

HUMAN RESEARCH ETHICS COMMITTEE (MEDICAL)

CLEARANCE CERTIFICATE NO. M130868

NAME: (Principal Investigator)	Ms Kiashanee Moodley
DEPARTMENT:	Department of Internal Medicine Center for Genomic Regulartion (CRG) Spain
PROJECT TITLE:	A Study to Determine Whether the KH Type Splicing Regulatory Protein is a Regulator of Fibroblast Growth Factor Receptor 2 Alternative Splicing in Triple Negative Breast Cacer Cells
DATE CONSIDERED:	Ad oc
DECISION:	Approved unconditionally
CONDITIONS:	
SUPERVISOR:	Dr Raquel Duarte
APPROVED BY:	Professor PE Cleaton-Jones, Chairperson, HREC (Medical)

DATE OF APPROVAL: 11/09/2013

This clearance certificate is valid for 5 years from date of approval. Extension may be applied for.

DECLARATION OF INVESTIGATORS

To be completed in duplicate and **ONE COPY** returned to the Secretary in Room 10004, 10th floor, Senate House, University.

I/we fully understand the conditions under which I am/we are authorized to carry out the above-mentioned research and I/we undertake to ensure compliance with these conditions. Should any departure be contemplated, from the research protocol as approved, I/we undertake to resubmit the application to the Committee. **I agree to submit a yearly progress report**.

Principal Investigator Signature M130868Date

PLEASE QUOTE THE PROTOCOL NUMBER IN ALL ENQUIRIES

11. APPENDIX D

11.1. Turnitin Report

turnitin

Digital Receipt

This receipt acknowledges that Turnitin received your paper. Below you will find the receipt information regarding your submission.

The first page of your submissions is displayed below.

Submission author:	Kiashanee Moodley
Assignment title:	kiashnee
Submission title:	KiashaneeThesis20160318.pdf
File name:	Kiashanee_Moodley_0707149w_K...
File size:	4.37M
Page count:	195
Word count:	47,863
Character count:	265,043
Submission date:	18-Mar-2016 10:41AM
Submission ID:	647025888

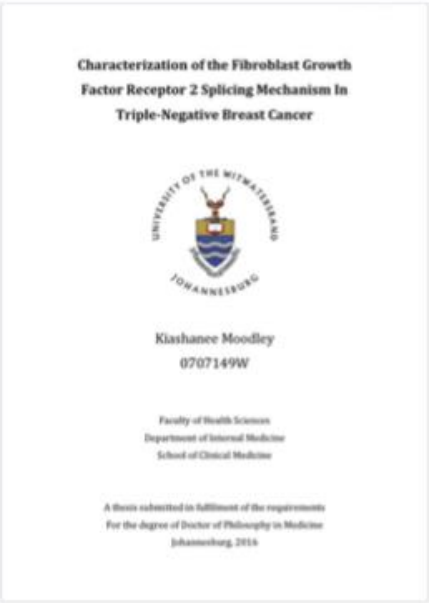

Characterization of the Fibroblast Growth Factor Receptor 2 Splicing Mechanism In Triple-Negative Breast Cancer

Kiashanee Moodley
0707149W

Copyright 2016 Turnitin. All rights reserved.

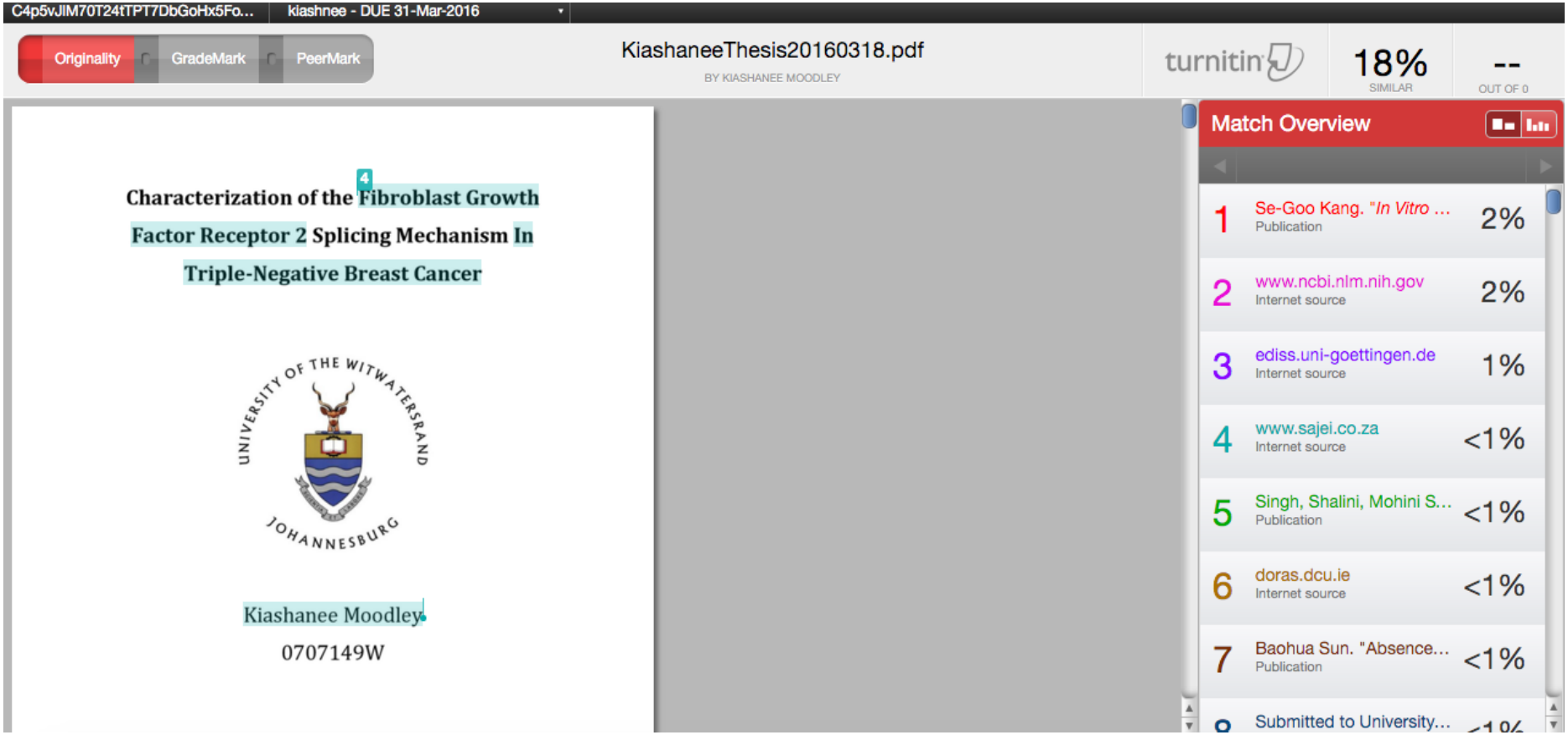
C4p5vJIM70T24tTPT7DbGoHx5Fo...
kiashnee - DUE 31-Mar-2016
Originality
GradeMark
PeerMark
KiashaneeThesis20160318.pdf
BY KIASHANEE MOODLEY
turnitin
18%
SIMILAR
--
OUT OF 0
Characterization of the Fibroblast Growth Factor Receptor 2 Splicing Mechanism In Triple-Negative Breast Cancer
UNIVERSITY OF THE WITWATERSRAND JOHANNESBURG
Kiashanee Moodley
0707149W
Match Overview
1 Se-Goo Kang. "In Vitro ... Publication 2%
2 www.ncbi.nlm.nih.gov Internet source 2%
3 ediss.uni-goettingen.de Internet source 1%
4 www.sajei.co.za Internet source <1%
5 Singh, Shalini, Mohini S... Publication <1%
6 doras.dcu.ie Internet source <1%
7 Baohua Sun. "Absence... Publication <1%
Submitted to University...